Universidad de Cádiz

research group tep243 – molecular sieves and other nanomaterials

Titania-silica composite materials for self-cleaning applications on monumental stones

Luís Pinho

TITANIA-SILICA COMPOSITE MATERIALS FOR SELF-CLEANING APPLICATIONS ON MONUMENTAL STONES

BY

Luís Pinho

A Ph. D. thesis submitted to the Physical Chemistry Department and the University of Cádiz in partial fulfillment of the requirements for the degree of

Doctor of Philosophy in Science

Cádiz, September 2012

UCA Universidad de Cádiz

MARÍA JESÚS MOSQUERA DÍAZ, PROFESORA TITULAR DEL DEPARTAMENTO DE QUÍMICA FÍSICA DE LA UNIVERSIDAD DE CÁDIZ

EN LA CONDICIÓN DE DIRECTORA DE TESIS DOCTORAL

CERTIFICA:

Que la presente memoria titulada "TITANIA-SILICA COMPOSITE MATERIALS FOR SELF-CLEANING APPLICATIONS ON MONUMENTAL STONES", elaborada por el máster en Conservación y Restauración D. Luís Miguel Faria Soares Pinho da Silva ha sido realizada bajo mi dirección en el Departamento de Química Física y que, hallándose concluida, autoriza su presentación a fin de que pueda ser juzgada por el Tribunal correspondiente.

Y para que conste, expido y firmo el presente certificado en Puerto Real (Cádiz) a 14 de Septiembre de 2012.

Dra. María Jesús Mosquera Díaz

Universidade do Porto
Faculdade de Engenharia
FEUP

Departamento de
Engenharia Civil
DEC

Secção de Materiais
de Construção

ARLINDO JORGE SÁ DE BEGONHA, PROFESOR AUXILIAR DEL DEPARTAMENTO DE INGENIERÍA CIVIL DA FACULDADE DE ENGENHARIA DA UNIVERSIDAD DE PORTO

NA CONDIÇÃO DE CO-DIRECTOR DE TESE DE DOUTORAMENTO

CERTIFICA:

Que a presente tese intitulada "TITANIA-SILICA COMPOSITE MATERIALS FOR SELF-CLEANING APPLICATIONS ON MONUMENTAL STONES", elaborada pelo Mestre em Conservação e Restauro, Luís Miguel Faria Soares Pinho da Silva, foi realizada sob a minha orientação no Departamento de Engenharia Civil e que, encontrando-se concluída, autorizo a sua apresentação a fim de que possa ser avaliada pelo Júri correspondente.

E para que conste, expido e assino o presente certificado, em Porto (Portugal) a 30 de Julio de 2012.

Eng. Arlindo Jorge Sá de Begonha

Ph.D Thesis report

Ph.D. Student: Luís Miguel Faria Soares Pinho da Silva

Ph.D. Thesis: TITANIA-SILICA COMPOSITE MATERIALS FOR SELF-CLEANING APPLICATIONS ON MONUMENTAL STONES

Ph.D. Supervisors: María Jesús Mosquera Díaz and Arlindo Jorge Sá de Begonha

European Union researcher providing favorable report: Prof. Pagona Maravelaki. Technical University of Crete.

In this Doctoral Thesis TiO_2-SiO_2 nano-composites were developed and assessed for their self-cleaning and strengthening efficiency when applied to monumental stone. Through a sol-gel route, VOC-free photocatalyst mesoporous materials were obtained, using the surfactant n-octylamine as pore template, as well as TiO_2 nanoparticles of different concentration and particle size. The synthesized products were thoroughly characterized concerning their textural and structural properties, as well as their photocatalytic behavior, the self-cleaning, consolidation, adhesion, hydrophobic properties and resistance to salt crystallization after being applied to monumental stone.

The results demonstrated that the optimal photocatalytic activity was achieved when larger and sharper titania particles with a content of around 4% w/v are integrated into the silica mesoporous gel network. The photocatalysts synthesized have demonstrated: a self-cleaning efficiency on stones, a good adhesion, an increase of the mechanical resistance of stones and a considerable durability in the degradation by salt crystallization.

Overall, in the present Doctoral Thesis mesoporous silica-supported TiO_2 photocatalysts have successfully synthesized, exhibiting self-cleaning properties, enhanced mechanical and salt-decay resistance when applied to monumental building stones.

The quality and innovation of the Doctoral Thesis results are demonstrated by the fact that papers describing the contribution of the Thesis have been published and accepted to the most prestigious journals in the field.

The above considerations lead to a strongly positive opinion and my support to the PhD thesis by Luís Miguel Faria Soares Pinho da Silva that indeed possesses the qualities to be defended.

Monday, September 24, 2012

Pagona Maravelaki,
Assistant Professor, Department of Sciences, Technical University of Crete

Università degli Studi di Firenze
Dipartimento di Chimica "Ugo Schiff

Ph.D Thesis report

Ph.D. Student: Luís Miguel Faria Soares Pinho da Silva

Ph.D. Thesis: TITANIA-SILICA COMPOSITE MATERIALS FOR SELF-CLEANING APPLICATIONS ON MONUMENTAL STONES

Ph.D. Supervisors: María Jesús Mosquera Díaz and Arlindo Jorge Sá de Begonha

European Union researcher providing favorable report: Prof. Piero Frediani, University of Florence.

Dr. Pinho has developed some titania silica composites by mixing silica oligomers with titanium dioxide nanoparticles in the presence of n-octylamine. Different ratios between the two comonomers have been tested and the products have been applied on pure limestone to evaluate the performances.

Some performances such as peeling test to evaluate if the Titania may be easily removed, the self cleaning effectiveness of the coating, the colour change of stone stained with methylene blue and exposed to UV radiation (336 nm), the water uptake of the sample and the DRMS has been evaluated.

The new materials show very interesting properties for their use as consolidating and self-cleaning agent.

The above considerations lead to a positive opinion on the PhD thesis by Luís Miguel Faria Soares Pinho da Silva that indeed possesses the qualities to be defended.

September 24, 2012

Prof. Piero Frediani
Full professor of Industrial Chemistry
University of Florence

Via della Lastruccia, 3-13 50019 Sesto Fiorentino (Fi) piero.frediani@unifi.it
tel. 055/4573522 fax 055/4573531 www.unifi.it/dipchim/

FEUP FACULDADE DE ENGENHARIA
UNIVERSIDADE DO PORTO

DEPARTAMENTO DE ENGENHARIA CIVIL

SECÇÃO DE CONSTRUÇÕES CIVIS

RESEARCH REPORT - Ph.D THESIS

Ph.D. Student: Luís Miguel Faria Soares Pinho da Silva
Ph.D. Thesis: TITANIA-SILICA COMPOSITE MATERIALS FOR SELF-CLEANING APPLICATIONS ON MONUMENTAL STONES
Ph.D. Supervisors: María Jesús Mosquera Díaz and Arlindo Jorge Sá de Begonha

I was a member of this research project and I express my positive opinion regarding the quality of the work and the potential of the technological transfer of this thesis results to the industry. The technology proposed is original with interesting application for historical buildings.
The above considerations lead to a positive opinion on the Ph.D report by ***Luís Miguel Faria Soares Pinho da Silva*** and I believe in his abilities to produce very good results.

Porto, 25th September 2012

Vasco Peixoto de Freitas
Full Professor - FEUP

RUA DR. ROBERTO FRIAS, 4200-465 PORTO - PORTUGAL | TELEFONE +351 225 081 940 | FAX +351 225 081 940 | WWW.FE.UP.PT

Acknowledgements

To my PhD directors, Dr. María Jesús Mosquera and Arlindo Begonha

To the Fundação Ciência e Tecnologia, for the fellowship SFRH/BD/43492/2008

To the members of the research group TEP-243 - Molecular sieves and other nanomaterials

To my family and friends, who have demonstrated their support in the most difficult moments

To all the people who have directly or indirectly helped me in the work of this PhD thesis.

Long live those who seek wisdom, even though they know that the closer they are, the more inaccessible it becomes

To Ana Pedro

Abstract

Atmospheric pollution has an evidently adverse impact on the aesthetics of urban buildings and structures. Thus, the synthesis of photocatalysts capable of removing pollutants deposited on the surface of stone and other building materials is an interesting challenge to researchers. In the work undertaken for the Doctoral Thesis presented, mesoporous TiO_2-SiO_2 composites that have photocatalytic activity have been synthesized by mixing ethoxysilane oligomers and TiO_2 nanoparticles in the presence of a non-ionic surfactant (*n*-octylamine). The products synthesized have a clear practical application on buildings and other monumental heritage structures since they can be applied outdoors by means of a simple and low-cost process. The resulting nanomaterials give self-cleaning properties and create crack-free effective adhesive coatings for exterior stone surfaces. In addition, they improve the mechanical resistance of the stone. Another important advantage of these nanocomposites is that they substantially improve protection against salt crystallization degradation processes.

By using of N_2 physisorption, atomic force microscopy and electron tomography, together with 3D reconstructions, we have been able to conclude that the texture of the nanocomposites synthesized is a key parameter for controlling the photocatalytic activity. Specifically, we find that *n*-octylamine creates a mesoporous SiO_2 structure within which TiO_2 nanoparticles are embedded, and that TiO_2 and SiO_2 are present in separate domains in the bulk of the material. The mesoporous structure enhances the activity of the material by improving the access of light to photoactive sites.

We optimize the effectiveness of these photocatalysts on stone by varying the loading and particle size of TiO_2 in the starting sol. We find that the integration of around 4% w/v content of TiO_2 nanoparticles into the SiO_2 network significantly improves their effectiveness due to a higher availability

of photoactive sites. For higher TiO_2 loadings (10% w/v), photocatalytic activity decreases because the porous volume is drastically reduced and access to photoactive sites is more restricted. Regarding the effect of particle size, we observe that larger and sharper TiO_2 nanoparticles enhance the photocatalytic activity.

Resumen

En la actualidad, la elevada contaminación ambiental que sufren nuestras ciudades está originando un gran impacto en la estética de los monumentos y edificios históricos construidos con materiales pétreos. Por esta razón, presenta gran interés sintetizar nuevos materiales con actividad fotocatalítica específicamente diseñados para eliminar los contaminantes depositados sobre estas superficies pétreas. En la presente Tesis Doctoral, se han desarrollado composites TiO_2-SiO_2 con estructrura mesoporosa, mediante un proceso que consiste en mezclar oligómeros de etoxisilano con nanopartículas de TiO_2 en presencia de un surfactante no iónico (*n*-octilamina). Los materiales desarrollados tienen una aplicación directa en la conservación de monumentos porque se pueden utilizar, directamente, sobre el propio edificio mediante un proceso simple y de bajo coste. Los nanomateriales formados no se fracturan y se adhieren eficazmente al sustrato pétreo, dotándolo de propiedades auto-limpiantes. Adicionalmente, pueden incrementar la resistencia mecánica de las rocas tratadas y su durabilidad frente al deterioro originado por cristalización de sales solubles.

La aplicación de técnicas tan diversas como Fisisorción de N_2, Microscopía de Fuerza Atómica y Tomografía Electrónica, asociadas a reconstrucciones 3D, nos ha permitido concluir que la textura de los nanocomposites sintetizados durante el desarrollo de esta Tesis Doctoral es un parámetro clave para controlar la actividad fotocatalítica. En concreto, hemos demostrado que la *n*-octilamina crea una estructura mesoporosa de SiO_2 en la que se integran las partículas de TiO_2. También, hemos constatado que TiO_2 y SiO_2 forman dominios separados en la estructura del nanocomposite. Finalmente, demostramos que la formación de una estructura mesoporosa incrementa la actividad del material porque facilita la accesibilidad de los contaminantes a los centros fotoactivos.

La eficacia sobre sustratos pétreos de los materiales fotocatalíticos objeto de estudio fue optimizada mediante la modificación de dos variables: el contenido en TiO_2 y su tamaño de partícula. Los resultados obtenidos nos han permitido concluir que un contenido en TiO_2 en torno a un 4% w/v mejora significativamente su eficacia porque facilita el acceso a los centros fotoactivos. Un contenido en TiO_2 más elevado (10% w/v) reduce la actividad fotocatalítica porque disminuye, significativamente, el volumen poroso y en consecuencia la accesibilidad a dichos centros. Con relación al tamaño de partícula, demostramos que las partículas con mayor tamaño y más afiladas incrementan significativamente la fotoactividad.

Resumo

Na actualidade, a elevada poluição atmosférica que sofrem as nossas cidades tem um grande impacto estético sobre a estética dos monumentos e edifícios históricos construídos com materiais pétreos. Por isso, apresenta grande interesse sintetizar novos materiais com actividade fotocatalítica, especialmente desenhados para remover poluentes depositados nestas superfícies pétreas. Na presente Tese de Doutoramento, foram sintetizados compósitos mesoporosos TiO_2-SiO_2 com actividade fotocatalítica, misturando oligómeros de etoxissilano e nanopartículas de TiO_2 na presença de um surfactante não-iónico (*n*-octilamina). Os produtos sintetizados têm uma clara aplicação prática na conservação de monumentos porque podem ser aplicados directamente sobre o edifício, por meio de um processo simples e pouco dispendioso. Os nanomateriais resultantes conferem propiedades auto-laváveis e criam revestimentos aderentes e livres de fractura para pedra. Além disso, podem aumentar a resistência mecânica das pedras tratadas e protegê-las da contra os mecanismos de degradação gerados pela cristalização de sais solúveis.

O uso de técnicas tão diversas como a fisisorção de N_2, microscopia de força atómica e tomografia electrónica, associadas a reconstruções 3D, permite-nos concluir que a textura dos nanocompósitos sintetizados no desenvolvimento desta Tese de Doutoramento, é um parâmetro-chave para controlar a actividade fotocatalítica. Concretamente, demonstrámos que a *n*-octilamina cria uma estrutura mesoporosa de SiO_2 na qual se integram as nanopartículas de TiO_2, e que o TiO_2 e o SiO_2 formam domínios independentes na estrutura do nanocompósito. Finalmente, demonstrámos que a formação de uma estrutura mesoporosa melhora a actividade dos fotocatalizadores porque facilita o acesso dos poluentes aos sítios fotoactivos.

Optimizámos a eficácia dos fotocatalizadores sobre substratos pétreos modificando duas variáveis: a carga de TiO_2 e o seu tamanho de partícula. Os

resultados obtidos permitem-nos conlcuir que a integração de um conteúdo aproximado de 4% p/v de nanopartículas de TiO_2 na rede de SiO_2 melhora significativamente a sua eficácia devido a um melhor acesso aos sítios fotoactivos. Para cargas de TiO_2 mais altas (10% p/v), a actividade fotocatalítica diminui devido a uma redução drástica do volume poroso, acompanhada de um acesso dificultado aos sítios fotoactivos. Considerando o tamanho de partícula, observamos que partículas maiores e mais alongadas melhoram significativamente a actividade fotocatalítica.

Zusammenfassung

Heutzutage hat die hohe Atmosphärenverschmutzung in unseren Staaten eine große Wirkung auf die Ästhetik von historischen Gebäuden aus Stein und die Denkmalpflege. Demzufolge ist die Entwicklung von neuen Materialien mit photokatalytischen Eigenschaften von großem Interesse, die entworfen sind, um die auf der Steinoberfläche liegenden Schmutzstoffe zu entfernen. In dieser Doktorarbeit sind mesoporöse TiO_2-SiO_2-Komposite mit photokatalytischen Eigenschaften entwickelt worden. Die Synthese der Komposite erfolgt durch die Mischung von Ethoxysilane-Oligomere und TiO_2-Nanopartikeln in der Anwesenheit eines nichtionischen Tensides (*n*-octylamine). Die synthetisierten Produkte haben eine offensichtliche, praktische Anwendung in der Denkmalpflege, weil sie auf eine einfache und preiswerte Weise im Freien zum Einsatz gebracht werden können. Die entstandenen Nanomaterialien verleihen dem Stein Selbstreinigungs-Eingenschaften und schaffen feste Beschichtungen, die frei von Rissen sind. Diese können den mechanischen Widerstand des Steins verbessern und seine Dauerhaftigkeit gegen Verwitterung durch Salz-Kristallbildungs-Mechanismen steigern.

Mit Hilfe von unterschiedlichen Methoden, wie N_2-Physisorption, Rasterkraftmikroskop und Elektron-Tomographie, verbunden mit 3D-Rekonstruktionen, können wir schlussfolgern, dass die Textur der synthetisierten Nanokompositen ein Schlüsselparameter ist, um die photokatalytische Aktivität zu kontrollieren. Insbesondere wurde nachgewiesen, dass *n*-octylamine eine mesoporöse SiO_2-Struktur erzeugt, die die TiO_2-Nanopartikel einlagert. Darüber hinaus, wurde festgestellt, dass TiO_2 und SiO_2 in getrennten Domänen der Hauptmasse des Grundmaterials anwesend ist. Schließlich wurde gezeigt, dass die Entstehung einer mesoporösen Struktur die Aktivität des photokatalytischen Materials fördert, indem sie den Zugang der Schadstoffe zu photoaktiven Stellen verbessert.

Die Wirksamkeit des studierten photokatalytischen Materials auf Steinträgern wurde optimiert anhand der Änderung von zwei Variablen: die Konzentration von TiO_2 und die Größe der Partikel. Die gewonnenen Ergebnisse erlauben die Schlussfolgerung, dass eine Konzentration von TiO_2-Nanopartikeln um ca. 4% w/v im SiO_2-Netzwerk ihre Effektivität bedeutsam verbessert, weil die Verfügbarkeit der photoaktiven Stellen aufgestockt wird. Für eine erhöhte Konzentration von TiO_2 (10% w/v) nimmt die photokatalytische Aktivität ab, weil das Volumen der Porosität drastisch reduziert wird und dadurch die photokatalytischen Stellen weniger zugänglich werden. In Bezug auf die Auswirkung des Korngrößen-Effekts wurde festgestellt, dass größere und eckigere TiO_2-Nanopartikeln die Photoaktivität steigern.

Résumé

Actuellement, la forte pollution qui souffrent nos villes a un grand impact sur l'esthétique des monuments et des édifices historiques construits avec des matériaux en pierre. Pour cette raison, il est d'un grand intérêt développer de nouveaux matériaux ayant une activité photocatalytique, spécialement conçu pour éliminer ces contaminants déposés sur la surface de la pierre. Dans cette Thèse de doctorat, des composites de TiO_2-SiO_2 ont été développés avec une structure mésoporeuse. Le procédé de synthèse consiste à mélanger d'oligomères d'éthoxysilanes avec des nanoparticules de TiO_2 en présence d'un surfactant non ionique (*n*-octylamine). Les matériaux développés sont directement applicables à la conservation des monuments et autres édifices car ils peuvent être appliqués grâce à un processus simple et à faible coût. Les nanomatériaux formés ne pas se fracturer et efficacement adhérer au substrat de pierre, offrant des propriétés autonettoyantes. En outre, ils peuvent augmenter la résistance mécanique des roches traitées et sa durabilité contre la détérioration provoquée par la cristallisation des sels solubles.

L'application des techniques aussi diverses que physisorption de N_2, la microscopie à force atomique et la tomographie électronique, associée à des reconstructions 3D, nous a permis de conclure que la texture des nanocomposites synthétisés pendant l'élaboration de cette thèse est un paramètre clé pour contrôler l'activité photocatalytique. En particulier, nous avons montré que la *n*-octylamine crée une structure mésoporeuse de SiO_2 qui intègre des particules de TiO_2. En outre, nous avons constaté que TiO_2 et SiO_2 sont présents dans des domaines séparés dans la structure du nanocomposite. Enfin, nous montrons que la formation d'une structure mésoporeuse augmente l'activité du matériau qui facilite l'accès des contaminants vers les sites photoactives.

L'efficacité des matériaux photocatalytiques sur la pierre a été optimisé grâce à la modification de deux variables: teneur en TiO_2 et sa taille des particules. Les résultats nous ont permis de conclure que la teneur en TiO_2 d'environ 4% p/v améliore considérablement son efficacité, car il facilite l'accès aux sites photoactives. Une teneur en TiO_2 plus élevé (10% p/v) réduit l'activité photocatalytique car diminue, significativement, le volume poreux et donc l'accessibilité pour les sites photoactives. Par rapport à la taille des particules, nous montrons que les particules avec une plus grande taille et plus angulaire augmentent la photoactivité.

Riassunto

Oggigiorno l'elevato tasso di inquianamento atmosferico e ambientale che affligge le nostre città sta generando un enorme impatto sull'estetica di monumenti ed edifici storici costruiti con materiali rocciosi. Per questo motivo è di grande interesse sintetizzare nuovi materiali con attività fotocatalitica specificamente progettati per eliminare gli inquinanti che si depositano su tali superfici rocciose. In questa Tesi di Dottorato si sono sviluppati composti TiO_2-SiO_2 con struttura mesoporosa mediante un processo che consiste nel miscelare oligomeridi etossilati con nanoparticelle di TiO_2 in presenza di surfattanti non ionici (*n*-ottilamina). I materiali sviluppati hanno un'applicazione diretta nel campo della conservazione dei monumenti in quanto si possono applicare direttamente sull'edificio mediante un processo semplice e di basso costo. I nanomateriali formati non si fratturano e aderiscono efficacemente al substrato roccioso, conferendogli proprietà autopulenti. In più sono in grado di aumentare la resistenza meccanica delle rocce trattate e la loro durabilità rispetto al deterioramento causato dalla cristallizzazione dei sali solubili.

L'applicazione di tecniche così diverse, come la Fisisorzione di N_2, la Microscopia a Forza Atomica e la Tomografia Elettronica, associate alla ricostruzione 3D, ci ha permesso di concludere che la trama dei nanocomposti sintetizzati durante lo sviluppo di questa Tesi di Dottorato è un parametro chiave per controllare l'attività fotocatalitica. Concretamente, abbiamo dimostrato che la n-ottilamina crea una struttura mesoporosa di SiO_2 nella quale si integrano le pariticelle di TiO_2. Inoltre, abbiamo constatato que TiO_2 e SiO_2 formano dominii separati dentro la struttura del nanocomposto. Infine, dimostriamo che la formazione di una struttura mesoporosa autenta l'attività del materiale perchè facilita l'accessibilità degli inquinanti ai centri fotoattivi.

L'efficacia su substrati rocciosi dei materiali fotocatalitici oggetto di studio è stata ottimizzata attraverso la variazione di due variabili: il contenuto di TiO_2 e la rispettiva dimensione di particella. I risultati ottenuti ci hanno permeso di concludere che un contenuto di TiO_2 intorno al 4% p/v migliora significativamente la sua efficacia perchè agevola l'accesso ai centri fotoattivi. Un contenuto più elevato (10% p/v) riduce l'attività fotocatalitica perchè diminuisce, in maniera significativa, il volume poroso e di conseguenza l'accessibilità ai suddetti centri. Per quanto riguarda la dimensione della particella, abbiamo dimostrato che particelle di maggiore dimensione e più angolose aumentano significativamente la fotoattività.

Table of contents

1. State of the art critical analysis

This first chapter is divided in two sections. In the first, we describe the fundamentals of light-induced phenomena in TiO_2. We also report the advantages of integrating TiO_2 into a matrix, paying special attention to the support given to the photocatalysts by a silica gel network. Finally, the effect of the structure of these materials on their final properties is considered.

In the second section, there is a brief review of the evolution of the materials applied for conservation of monumental stones across history, especially the alkoxysilanes. The drawbacks of these products associated, mainly, to their cracking during the drying into the pores of the stone are elucidated. After briefly reviewing the process by which these materials crack, we examine the current research carried out with the object of avoiding fractures. Finally, the attempts made to employ TiO_2 as self-cleaning material on stone are explored.

1.1. TiO_2 photocatalysis

TiO_2 photocatalytic effect and related phenomena

The description of an electrochemical photolysis phenomenon in 1972, by Honda and Fujishima is one of the most important milestones in the research field of photocatalysis.[1] The phenomenon, now well-known as Honda-Fujishima effect involves the absorption of photons by TiO_2, and the consequent promotion of an electron to the conduction band of the semiconductor, leaving a hole in its valence band. These electron-hole pairs are then responsible for reactions of oxidation and reduction of several molecules and can be used for numerous applications.

[1] A. Fujishima, K. Honda, Nature 238 (1972) 37.

The photocatalytic effect occurs with the generation of electron-hole pairs on a TiO_2 surface when irradiated by light of an adequate wavelength. Figure 1 illustrates the process and Table 1 gives the main equations that describe it.

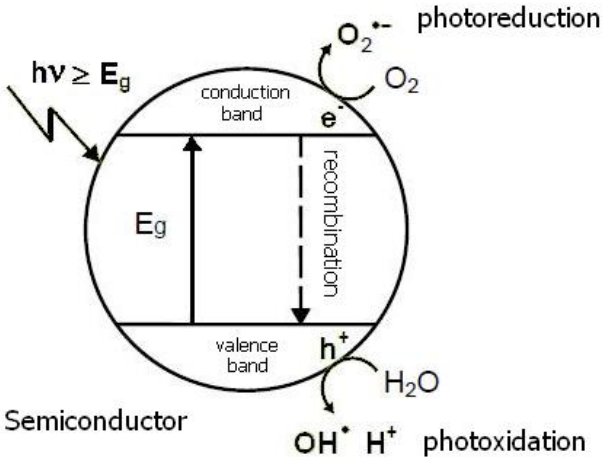

Figure 1. Schematic representation of the photocatalytic process in TiO_2[2]

Table 1. Reactions involved in the photocatalytic process[2]

$MO_x + h\nu \rightarrow h^+ + e^-$ (electron-hole pair generation)	eq. 1
$h^+ + H_2O_{ads} \rightarrow H_2O^{\bullet+}_{ads} \leftrightarrow OH^{\bullet+}_{ads} + H^+$	eq. 2
$h^+ + OH^-_{ads} \rightarrow OH^\bullet_{ads}$	eq. 3
$h^+ + RH_{ads} \rightarrow RH^\bullet_{ads} \leftrightarrow R^\bullet_{ads} + H^+$	eq. 4
$OH^\bullet_{ads} + RH_{ads} \rightarrow R^\bullet_{ads} + H_2O$ (oxidation of organic compounds)	eq. 5
$e^- + O_{2,ads} \rightarrow O^{\bullet-}_{2,ads}$	eq. 6
$O^{\bullet-}_{2,ads} + H^+ \leftrightarrow HO^\bullet_{2,ads}$	eq. 7
$2HO^\bullet_{2,ads} \leftrightarrow H_2O_{2,ads} + O_{2,ads}$	eq. 8
$e^- + H_2O_{2,ads} \rightarrow OH^\bullet_{ads} + OH^-_{ads}$	eq. 9
$h^+ + e^- \rightarrow$ heat/luminescence (recombination)	eq. 10

Specifically, the phenomena occur as follows: when TiO_2 is irradiated with photons more energetic than its band gap ($h\nu \geq E_g$), light absorption displaces electrons from the valence band to the conduction band, generating electron-hole pairs (Table 1, eq. 1).

[2] R. Portela Rodríguez, Eliminación fotocatalítica de H_2S en aire mediante TiO_2 soportado sobre sustratos transparentes en el UV-A, Universidad de Santiago de Compostela: Santiago de Compostela (2008)

If adsorbed species are present on the surface of the semiconductor, the electrons are transferred from the conduction band to the molecular acceptors (with less negative redox potential than e^-) (Table 1, eqs. 6 and 9), while the donors (with less positive redox potential than h^+) (Table 1, eqs. 2, 3 and 4) provide electrons to the holes in the valence band.

If they have not been previously captured, transferred or separated by an electric field, electrons and holes recombine with each other in a time of nanoseconds. This particular phenomenon is the main cause for the decrease in photonic yield of these reactions, since part of the energy provided is dissipated as light or heat. (Table 1, eq. 10).

In oxidative photocatalysis, holes can oxidise adsorbed molecules, either directly or through the formation of the radical $OH^{\bullet}$ (Table 1, eqs. 4, 5, Figure 2) while the electrons are trapped by an oxidant (Table 1, eqs. 6, 9). The steps in such a process are: 1) adsorption of the reagents (acceptors and donors); 2) occurrence of surface photoactivated redox reactions; 3) desorption of products.

One of the unique aspects of TiO_2 is that there are two distinct photo-induced phenomena: one is the photocatalytic effect already referred to, which leads to the breakdown of organic compounds; and the other phenomenon is related to its high surface "wettability". This second phenomenon was discovered by accident during the research carried out at TOTO Inc., in 1995. In short, when a TiO_2 film is prepared with a certain percentage of SiO_2, it shows very low water contact angles after UV illumination. Therefore, films having such properties are known as superhydrophilic.

In this case, the electrons tend to reduce the Ti(IV) cations to the Ti(III) state, and the holes oxidize the O_2^- anions. In the process, oxygen atoms are ejected, creating oxygen vacancies. Water molecules can then occupy these oxygen vacancies, producing adsorbed OH groups, which tend to make the surface hydrophilic (Figure 2). The longer the surface is illuminated with UV light, the smaller the contact angle for water becomes; after about 30 min or so under a

moderate intensity UV light source, the contact angle approaches zero, meaning that water has a tendency to spread perfectly across the surface.[3]

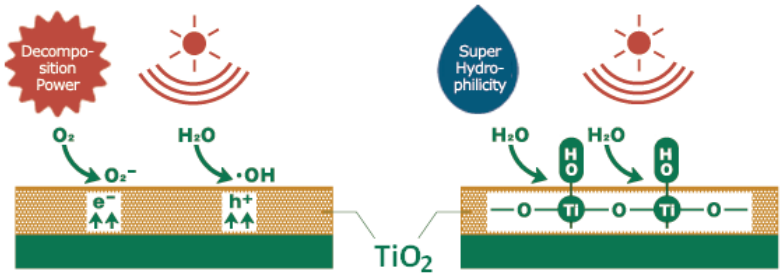

Figure 2 Illustration of the two distinct photo-induced phenomena produced on TiO_2 surfaces.[4]

These two phenomena involving TiO_2 allowed innovative applications to be developed in solar energy conversion, environmental photocatalysis and the production of antifogging surfaces. Moreover, the unique combination of properties in TiO_2 makes it very appropriate for self-cleaning applications. It presents a unique photo-induced efficiency, it is non-toxic, non-soluble in water and it is photo-stable. Its cost is also low. Therefore, TiO_2 is regarded as the most efficient and environmentally-friendly photocatalyst, with the potential to oxidize virtually all organic pollutants[5]. In addition it also finds useful application in photochemical cells, water purification, air cleaning, self-cleaning, sterilization or antitumor activity.[3]

In all these applications, the control of the particle size and spatial structuring of the semiconductor through a physical approach is crucial to improving the photocatalytic activity of TiO_2. Thus, the encapsulation of TiO_2 inside the zeolites or periodic mesoporous materials, is a powerful methodology for improving the photocatalytic efficiency.[6] Another advantage of using a binder

[3] A. Fujishima, T. Rao, D. Tryk, J. Photochem. Photobiol. C 1 (2000) 1.
[4] http://www.toto.co.jp/docs/hyd_patent_en/hydro_img/ill01.gif (25/11/2009)
[5] I. Karatasios, M. S. Katsiotis, V. Likodimos, A. Kontos, G. Papavassiliou, P. Falaras, V. Kilikoglou, Appl. Catal. B 95 (2010) 78.
[6] C. Aprile, A. Corma, H. García, Phys. Chem. Chem. Phys. 10 (2008) 769.

is that TiO_2 immobilization is achieved,[7] with the object of preventing a decrease in its activity and its release to the environment.[8-10]

Moreover, including TiO_2 within such structures may also be beneficial for increasing the cohesion between the photoactive fraction and the supporting matrix of the material through a physical interaction.[11] In this respect, if the matrix is able to act both as a binder and a catalytic support, this would make it an interesting and advantageous alternative material for many applications.[12]

TiO_2-SiO_2 supported photocatalysts

Synthesis routes

Silica is often chosen as matrix because it can bind a range of chemically and physically diverse particles into its tri-dimensional network[11] and can enhance the activity and selectivity of the photocatalyst.[12] Binary TiO_2-SiO_2 oxides are solids that have always attracted attention as advanced materials due their potential as heterogeneous catalysts and catalytic supports. They find good application in acid-catalyzed reactions and selective oxidation; their low coefficients of thermal expansion over a wide temperature range make them very useful for optical applications.[13]

Regarding the possible strategies for synthesising these materials, they include mixing Si and Ti alkoxides[13-17] by sol-gel methods,[18] and grafting pre-

[7] M. Bideau, B. Claudel, C. Dubien, L. Faure, H. Kazouan, J. Photochem. Photobiol. A 91 (1995) 137.
[8] L.Windler, C. Lorenz, N. von Goetz, K. Hungerbühler, M. Amberg, M. Heuberger, B. Nowack, Environ. Sci. Technol. 46 (2012) 8181.
[9] N. T. Boncagni, J. M. Otaegui, E. Warner, T. Curran, J. Ren, M. M. F. Cortalezzi, Environ. Sci. Tecnhol. 43 (2009) 7699.
[10] L. Rejinders, Polym. Degrad. Stabil. 94 (2009) 873.
[11] C. A. Morris, M. L. Anderson, R. M. Stroud, C. I. Merzbacher, D. R. Rolison, Science 284 (1999) 622.
[12] H. Kibombo, R. Peng, S. Rasalingam, R. Koodali, Catal. Sci. Technol. 2 (2012) 1737.
[13] R. J. Davis, Z. Liu, Chem. Mater. 9 (1997) 2311.
[14] J. J. Calvino, M. A. Cauqui, G. Cifredo, L. Esquivias, J. A. Pérez, M. Ramírez del Solar, J. M. Rodríguez-Izquierdo, J. Mater. Sci. 28 (1993) 2191.
[15] S. Gontier, A. Teruel, Zeolites 15 (1995) 601.
[16] W. Zhang, M. Fröba, J. Wang, P. Tanev, J. Wong, T. Pinnavaia, J. Am. Chem. Soc. 118 (1996) 9164.

synthesized silica with Ti alkoxides.[19,20] However, some difficulties arise when Ti and Si alkoxides are mixed together: the Ti alkoxides hydrolyze much faster than the Si in presence of ambient water,[13,21] the TiO_2 loading that can be achieved is quite low; and the formation of TiO_2 photoactive crystals through a calcination process is severely limited by the low heating temperature tolerated by certain substrates such as textiles,[22-25] plastics[26-30] and glasses.[31-35]

Other possible ways to obtain a TiO_2-SiO_2 binary oxide could be considered, such as mixing colloidal silica particles with a Ti alkoxide,[36] or mixing TiO_2 and SiO_2 colloidal particles.[37] However, heating would still be necessary, either to create crystalline photoactive TiO_2 or to promote adhesion of the coating to the substrate. Another possibility would be grafting TiO_2 (from Ti alkoxides) into preformed SiO_2 matrices. However, this process requires a gradual and time-demanding addition of the alkoxides to the silica matrix, in several deposition cycles and it still requires heating.[19]

---

[17] M. Kruk, M. Jaroniec, A. Sayari, Microporous Mater. 9 (1997) 173.
[18] M. A. Cauqui, J. M. Rodríguez-Izquierdo, J. Non-Cryst. Sol. 147 (1992) 724.
[19] K. de Witte, V. Meynen, M. Mertens, O. I. Lebedev, G. Van Tendeloo, A. Sepúlveda-Escribano, F. Rodríguez-Reinoso, E. F. Vansant, P. Cool, Appl. Cat. B, 84 (2008) 125.
[20] E. Beyers, E. Biermans, S. Ribbens, K. de Witte, M. Mertens, V. Meynen, S. Bals, G. Van Tendeloo, E. F. Vansant, P. Cool, Appl. Catal. B 88 (2009) 515.
[21] M. M. Haridas, S. Datta, J. R. Bellare, Ceramics International 25 (1999) 601.
[22] A. Bozzi, T. Yuranova, J. Kiwi, J. Photochem. Photobiol. A 172 (2005) 27.
[23] K. Qi, W. Daoud, J. Xin, C. Mak, W. Tang, W. Cheung, J. Mater. Chem. 16 (2006) 4567.
[24] M. Uddin, F. Cesano, D. Scarano, F. Bonino, G. Agostini, G. Spoto, S. Bordiga, A. Zecchina, J. Photochem. Photobiol. A 199 (2008) 64.
[25] D. Wu, M. Long, ACS Appl. Mater. Interfaces 3 (2011) 4770.
[26] K. Tennakone, C. Tilakaratne, I. Kottegoda, J. Photochem. Photobiol. A 87 (1995) 177.
[27] H. Chen, C. Liang, H. Huang, J. Chen, R. Vittal, C. Lin, K. Wu, K. Ho, Chem. Commun. 47 (2011) 346.
[28] S. Lam, A. Soetanto, R. Amal, J. Nanopart. Res. 11 (2009) 1971.
[29] R. Fatteh, A. Ismail, R. Dillert, D. Bahnemann, J. Phys. Chem. C 115 (2011) 10405.
[30] K. Nakata, M. Sakai M, O. Tsuyoshi, T. Murakami, K. Takagi, A. Fujishima, Langmuir 27 (2011) 3275.
[31] Y. Paz, Z. Luo, L. Rabenberg, A. Heller, J. Mat. Res. 11 (1995) 2842.
[32] T. Watanabe, A. Nakajima, R. Wang R, M. Minabe, S. Koizumi, A. Fujishima, K. Hashimoto, Thin Solid Films 351 (1999) 260.
[33] J. Chen, C. S. Poon, Build. Environ. 44 (2009) 1899.
[34] B. Xi, L. K. Verma, J. Li, C.S. Bathia, A. J. Danner, H. Yang, H. C. Zeng, ACS Appl. Mater. Interfaces 4 (2012) 1093.
[35] A. Pénard, T. Gacoin, J. Boilot, Acc. Chem. Res. 40 (2007) 895.
[36] C. P. Scherer, C. G. Pantano, J. Non-Cryst. Solids 354 (2008) 645.
[37] M. Machida, K. Norimoto, T. Watanabe, K. Hashimoto, A. Fujishima, J. Mater. Sci. 34 (1999) 2569.

Therefore, synthesizing TiO_2-SiO_2 nanocomposites using preformed TiO_2 nanoparticles is an interesting alternative[38-42] for *in-situ* coating processes on porous building materials where, for practical reasons, the deposition method should involve just one single application. This therefore would exclude any additional treatments, such as thermal ones. In addition, silica acts as a "nanoglue",[11] providing molecular access to the TiO_2 phase within the material and giving mechanical reinforcement to the substrate.[43] In this respect, it is essential that the SiO_2 binder does not block the diffusion pathways between the organic species to be degraded and the radicals generated at the surface of the photoactive oxide.[35] Consequently, these nanocomposites must assume a porous configuration such as MCF,[20] zeolite,[41] HMS,[44] MCM,[45] or SBA.[46]

Finally, it should be noted that two fundamental types of interaction between TiO_2 and SiO_2 could occur: one physical (weak van der Wall forces) and the other chemical (with formation of Si-O-Ti linkages). When strong interaction results in chemical bonding, the properties of the mixed oxide are very different from the simple combination of the individual phases. At low TiO_2 contents, the substitution of tetrahedral Si atoms for Ti ones is claimed to be responsible for a bandgap increase, often observed as a blueshift of absorption edges.[43,47]

Structural issues and characterization

TiO_2-SiO_2 photocatalytic activity and sorption properties depend on the optimization of textural parameters such as surface area, pore size and volume,

[38] N. Suzuki, X. Jiang, L. Radhakrishnan, K. Takai, K. Shimasaki, Y. Huang, N. Miyamoto, Y. Yamauchi, Bull. Chem. Soc. Jpn. 84 (2011) 812.
[39] K. Inumaru, M. Yasui, T. Kasahara, K. Yamaguchi, A. Yasuda, S. Yamanaka, J. Mater. Chem. 21 (2011) 12117.
[40] D. Fattakhova-Rohlfing, J. Szeifert, Q. Yu,; V. Kalousek, R. Rathouský, T. Bein, Chem. Mater. 21 (2009) 2410.
[41] M. Alvaro, E. Carbonell, V. Fornés, H. García, Chem. Phys. Chem. 7 (2006) 200.
[42] E. Allain, S. Besson, C. Durand, M. Moreau, T. Gacoin, J. P. Boilot, Adv. Funct. Mater. 17 (2007) 549.
[43] X. Gao, I. E. Wachs, Catal. Today 51 (1999) 233.
[44] Y. Zhang, C. Chen, H. Qing, R. Wu, H. Zou, Chem. Commun. 12 (2010) 2271.
[45] S. Wang, Y. Shi, X. Ma, J. Gong, ACS Appl. Mater. Interfaces, 3 (2011) 2154.
[46] V. Zeleňak, V. Hornebecq, S. Mornet, O. Schäf, P. Llewellyn, Chem. Mater. 18 (2006) 3184.
[47] T. Kamegawa, Y. Masuda, N. Suzuki, Y. Horiuchi, H. Yamashita, Appl. Mater. Interfaces 3 (2011) 4561.

in order to produce effective access to the TiO_2 photocatalyst.[20,35] However, the detailed surface disposition and nanostructure of the TiO_2-SiO_2 system are not completely understood. Conventional electron microscopy images, obtained by means of the detection of secondary, back-scattered or transmitted electrons after interaction with the materials, provide only limited information about the structure of the nanomaterials.[11,39] The images obtained can often be ambiguous because only 2D projections of the objects are recorded. Electron tomography, however, provides 3D projections, and this technique has proved to be a powerful tool that has enabled a more complete 3D characterization of meso-structured materials.[48] In particular, electron tomography has been used successfully to characterize nanomaterials including SiO_2[49,50] and TiO_2[51,52]as well as TiO_2-SiO_2 composites.[20]

The imaging modes based on high angle annular dark field (HAADF) in the scanning transmission electron microscope (STEM) are the modes most suited to reveal the 3D structure of various kinds of nanomaterial because they reduce the contribution of diffraction contrast to image artifacts.[20,49,53-55] Another advantage of this imaging mode is that the HAADF detector captures electrons that undergo high-angle scattering, and the signal is approximately proportional to Z^2, where Z is the atomic number. The contrast provided is sensitive to compositional changes, and allows the identification of components with different atomic numbers in nanocomposite materials.[56]

---

[48] J. C. Hernández-Garrido, K. Yoshida, P. L. Gai, E. D. Boyes, C. H. Christensen, P. A. Midgley, Catal. Today 160 (2011) 165.
[49] P. Linton, J. C. Hernandez-Garrido, P. A. Midgley, H. Wennerström, V. Alfredsson, Phys. Chem. Chem. Phys. 11 (2009) 10973.
[50] E. Doren, P. Temmerman, M. Francisco, J. J. Mast, J. Nanobiotechnol. 9 (2011) 17.
[51] K. Yoshida, M. Makihara, N. Tanaka, S. Ayoagi, E. Nishibori, M. Sakata, E. Boyes, P. Gai, Microsc. Microanal. 12 (2011) 264.
[52] S. Li, C. Chang, C. Lin, Y. Lin, C. Chang, J. Yang, M. Chu, C. Chen, J. Am. Chem. Soc. 133 (2011) 11614.
[53] M. Okuda, M. Takeguchi, Y. Zhu, A. Hashimoto, N. Ogawa, M. Tagaya, S. Chen, N. Hanagata, T. Ikoma, Surf. Interface Anal. 42 (2010) 1548.
[54] S. Sueda, K. Yoshida, N. Tanaka, Ultramicroscopy 110 (2010) 1120.
[55] K. J. Batenburg, S. Bals; J. Sijbers, C. Kübel, P. A. Midgley, J. C. Hernández, U. Kaiser, E. R. Encina, E. A. Coronado, G. Van Tendeloo, Ultramicroscopy 109 (2009) 730.
[56] J.M. Thomas, P.A. Midgley, T.J.V. Yates, J.S. Barnard, R. Raja, I. Arslan, M. Weyland, Angew. Chem. Int. Ed. 43 (2004) 6745.

By using this technique, we can locate very precisely the position of SiO_2 and TiO_2 nanoparticles in the nanocomposite, and identify the interaction between the two oxides.

Another important aid to structural characterization is to obtain high-resolution N_2 physisorption isotherms, so that the NLDFT approach can be used from the isotherm branches. By employing this procedure a pore size distribution can be obtained that integrates micro and mesopores present in the materials under study.[57]

In addition, since the surface morphology of the photocatalysts is important for their activity, 2D and 3D images of the surface can also be obtained using amplitude-modulated atomic force microscopy (AM-AFM). The quality of these images is enhanced by the movement of a probe tip in the vertical Z axis. The analysis of the results provides detailed topographic information of the material's surface such as the profiles and distribution of particle heights, and rugosity, at the nanometric scale.[58,59]

[57] M. Thommes, B. Smarsly, M. Groenewolt, P.I. Ravikovitch, A.V. Neimark, Langmuir 22 (2006) 756.
[58] Y. V. Lim, H. Fan, Z. Shen, C. H. Kang, Y. Feng, S. Wang, Appl. Phys. A 95 (2009) 555.
[59] A. I. Kontos, I. M. Arabatzis, D. S. Tsoukleris, A. G. Kontos, M. C. Bernard, D. E. Petrakis, P. Falaras, Catal. Today 101 (2005) 275.

1.2. Materials for monumental stone conservation

Alkoxysilanes and other commercial products

After synthesizing tetraethoxysilane (TEOS) in 1861, A. W. von Hoffman suggested using it for the preservation of the stone substrate of the Houses of Parliament buildings, in London. This suggestion was not accepted at that time. It was not until 1923 that A. P. Laurie registered his method for preserving stone[60] by using silicic esters (alkoxysilanes) and an acid catalyst. Later, around 1960, Wacker OH (a product containing TEOS and a neutral catalyst) was very successful as a product for consolidating stone. These are the three most important milestones for understanding the historical evolution of alkoxysilanes in stone conservation.

Nowadays, SILRES® BS OH 100 (an evolution of Wacker OH, manufactured by Wacker Silicones) and its most important competitor TEGOVAKON® V100 (Evonik) are very popular solvent-free stone consolidants. SILRES® BS OH 100 is sold in the USA under the designation CONSERVARE® OH 100 (Prosoco). Other similar materials are ESTEL 1000 (CTS) and RC70 (Bluestar silicones). These contain organic solvents in order to increase penetration depth. Thus, the latter types of products tend to excluded from the market due to their incompatibility with current EU rules on the use of volatile organic compounds (VOCs).[61]

Several modifications of the composition of TEOS-based products have been tried: 1) by adding methyltriethoxysilane (Conservare H, Prosoco); 2) by including flexible/hydrophobic segments (RC 80, RC 90, KSE 500 E, KSE 300 E, ESTEL 1100); 3) by adding particles (KSE 500 STE); and 4) by including biocides (BIOESTEL, CTS). Other modifications have been made with the

[60] A. Laurie, Improvements related to the preservation of stone, U.K. Patent Office, 6-9-1923.
[61] Council Directive 1999/13/EC, 11-3-1999

intention of improving adhesion to limestone by including coupling agents between silica and calcium carbonate (KSE 300 HV). Concerning the products containing flexible/hydrophobic segments, RC 80 and RC90 (which include respectively, dimethylsiloxane and phenylsiloxane) were sold by Rhône-Poulenc, at the end of the last century (now sold by Bluestar Silicones). The KSE products (sold by Remmers®) resulted from an innovative research on ORMOSILS by Wendler et al.[62] These were first used as stone consolidants, and a significant reduction in the gel fracture was obtained due to the elastic properties of PDMS. Their commercialization implies a slight change in the "one-product-fits-all" strategy applied by the most of the manufacturers, when developing functional conservation materials.

EP 2101 (Stac) is an epoxy resin and PB72 (from Rohm and Haas, now a DOW Corning company) is an ethylmethacrylate-methylmethacrylate copolymer. Both materials must be dissolved in organic solvents in order to penetrate inside the stone. The most significant drawback of these products is that they form impermeable surface films which reduce the water vapour permeability and so potentially damage the stone surface.

Other stone conservation materials are available in the market for treating stone surfaces. "Nanolimes" are dispersions of calcium hydroxide in alcoholic solvents which deserve serious attention because they have a similar chemical nature to calcium carbonate building stones. NANORESTORE (CTS) and CALOSIL (Ibz Freieberg) are two "nanolime" products. Other particle dispersions can be employed for stone treatments, such as NANOESTEL (SiO_2 in water, from CTS) a E503 (TiO_2 in water, from Nanocer), respectively for stone strengthening and self-cleaning.

Some additional innovations in the field of stone conservation research have been modifying the understanding of stone treatments. Clay-swelling inhibitors,[63] salt crystallization inhibitors[64] have also been proposed as

[62] E. Wendler, D. D. Klemm, R. Snethlage, Proceedings of the 5th International Conference on Durability of Building Materials and Components. Brighton (UK), 1991.
[63] I. J. González, G.W. Scherer, Environ. Geol. 46 (2004) 364.

solutions to prevent stone decay for limestones containing swelling clays and to prevent damage through salt crystallization, respectively. The objective of this technological change seems clear: there is a recognized need to create better functional materials, which can provide a set of treatments aimed at resolving specific problems and outstanding issues of stone conservation.

Advantages and drawbacks of alkoxysilanes

Nowadays, products containing alkoxysilanes are the most popular in the market. They are applied in liquid state, absorbed by capillary suction and they polymerize *in-situ*, inside the pore structure of the disintegrating stone through a classic sol-gel process. Their advantages are well known: their ability to form siloxane bonds, and the low viscosity of alkoxysilanes facilitates their penetration into the inter-granular network of the stone.[65]

Two main reactions take place during the sol-gel transition of Si alkoxides: the first is the hydrolysis of the alkoxy groups to form silanols (eq. 11) and the second is the condensation of silanols (eqs. 12 and 13) to generate the silica polymer network.

$$\equiv Si\text{-}OR + H\text{-}OH \longrightarrow \equiv Si\text{-}OH + R\text{-}OH \quad \text{(eq. 11)}$$

$$\equiv Si\text{-}OH + HO\text{-}Si\equiv \longrightarrow \equiv Si\text{-}O\text{-}Si\equiv + H_2O \quad \text{(eq. 12)}$$

$$\equiv Si\text{-}OH + RO\text{-}Si\equiv \longrightarrow \equiv Si\text{-}O\text{-}Si\equiv + ROH \quad \text{(eq. 13)}$$

The process concludes with the removal of the solvent from the gel pores. After the solvent removal phase, a xerogel is formed. It is well-known that one serious limitation of the sol-gel method is the occurrence of cracking during the drying phase. This limitation has prevented the more widespread use of the sol-gel route for producing monoliths and films.

---

[64] E. Ruiz-Agudo, C. Rodriguez-Navarro, E. Sebastián-Pardo, Crys. Growth Design 6 (2006) 1575.
[65] G. Scherer, G. Wheeler, Key Engineering Materials, 391 (2009) 1.

Two significant drawbacks are associated with TEOS consolidants: (1) the practical impossibility of binding with carbonate stones, and coupling agents [66] such as tartaric acid or aminopropyl-triethoxysilane (APTES)[67] have been tested with a view to solve this drawback; (2) gel cracking during drying.

In order to understand why commercial consolidants crack, we need to consider the drying mechanisms of gels obtained from Si alkoxides. A gel is composed of two phases: the polymer network and the solvent, which is present inside the pores of the network. When the solvent evaporates, a liquid-vapour interface is formed in the pores of the gel. As the solvent wets the internal wall of the pores, a concave meniscus is created. As Scherer reported,[68] gel cracking occurs as a result of stresses caused by the existence of a meniscus at the liquid-vapour interface, which generates a differential capillary pressure within the gel. This makes the network shrink until it becomes stiff enough to resist the stress imposed by the capillary pressure. At this point, the maximum capillary tension is reached inside the network. Its value is given by the Young-Laplace equation, which (assuming cylindrical pores) is:

$$P_C = \frac{2 \cdot \gamma_{LV} \cdot \cos\theta}{r_p} \qquad \text{(eq. 14)}$$

where γ_{LV} is the liquid-vapour tension, θ is the contact angle of liquid to pore wall, and r_p is the pore radius.

According to equation 14, smaller pores are subject to higher pressure than larger pores. Thus, dense gels containing micropores, typically obtained from alkoxysilanes, are susceptible to cracking. In the specific case of stone consolidants, Scherer and Wheeler[69] determined the pore size of wet gels from a commercial consolidant based on alkoxysilanes (Conservare OH from Wacker).

---

[66] I. O Slavid, N. R. Weiss, Method for Consolidating and Protecting Calcareous Materials, United States Patent and Trademark Office, 28-10-1999.
[67] A. F. Pinto, J. Delgado Rodrigues, S. Bracci, B. Sacchi, in João Mimoso, José Delgado Rodrigues (Eds.) Stone consolidation in cultural heritage, research and practice: proceedings of the international conference, Lisbon, 2008, 71.
[68] G.W. Scherer, J. Non-Cryst. Solids 147&148 (1992) 363.
[69] G.W. Scherer and G.E. Wheeler, in A. Moropoulou et al. (Eds), Proceedings of 4th International Symposium on the Conservation of Monuments, Rhodes, 1997, 355.

They concluded that the small radius of the pores in the network (around 3.5 nm) gives rise to the high capillary pressure values responsible for cracking.

Cracking is therefore generated by the high capillary pressures supported by the gel network during drying. In the case of stone consolidation products containing alkoxysilanes, this drying and cracking process occurs inside the stone, and a brittle xerogel is formed. Figure 3 illustrates the evolution of a commercial TEGOVAKON® V gel during drying under laboratory conditions.

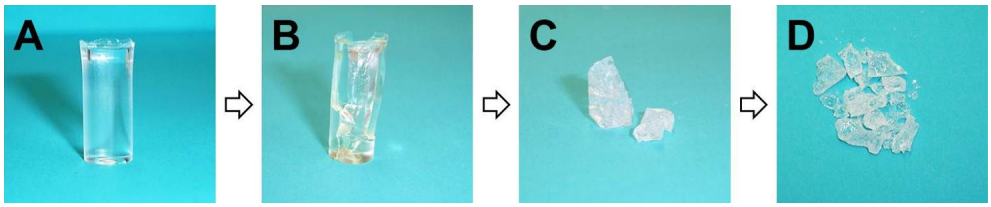

Figure 3 . Evolution of a commercial TEGOVAKON® V gel during drying under laboratory conditions. (A) Wet gel; (B) Contraction and slight cracking; (C) Cracked gel; and (D) Pulverized xerogel.

Our research group has investigated the fracture mechanism and texture of two popular stone consolidants WACKER® OH (Wacker) and TEGOVAKON® V (Evonik). The textural characterization of these materials showed that they were dense and microporous and that fracture was due to the high capillary pressure during drying.[70,71]

In order to reduce the capillary pressure during gel drying, Milianni et al.,[72] added colloidal nanoparticles to Conservare OH. An increase in gel pore size was achieved, cracking was avoided and subsequently, the mechanical properties of the composite obtained were improved. Similar results were obtained in our investigation, by adding 40 nm colloidal silica to the sols. The incorporation of colloidal nanoparticles generated an increase in the pore size of the gels and a decrease in capillary pressure.[73,74] However, all these

[70] M. J. Mosquera, J. Pozo, L. Esquivias, T. Rivas, B. Silva, J. Non-Cryst. Solids 311 (2002) 185.
[71] M. J. Mosquera, J. Pozo, L. Esquivias, J. Sol-gel Sci. Tech. 26 (2003) 1227.
[72] C. Miliani, M. L. Velo-Simpson, G. W. Scherer J. Cult. Herit. 8 (2007) 1.
[73] M. J. Mosquera, M. Bejarano, N. de la Rosa-Fox, L. Esquivias, Langmuir 19 (2003) 19.
[74] L. Esquivias, N. de la Rosa-Fox, M. Bejarano, M. J. Mosquera, Langmuir 20 (2004) 3416.

strategies caused an undesirable white-ish colour on darker-coloured stone surfaces.

Surfactant-synthesized nanomaterials for stone conservation

In the last decade, our group has designed a surfactant-synthesized route inspired by the synthesis of molecular sieves,[75,76] in order to prevent cracking. A typical synthesis of a molecular sieve involves mixing a silica polymeric precursor, water, alcohol, a catalyst and an ionic surfactant in a concentration above its critical micelle concentration. Pores are generated because micelles are formed in the sol, creating a liquid crystal, and are also present during the entire polymerization process. After the polymerization, the surfactant is usually removed by calcination or solvent extraction. Strong electrostatic interactions exist between the surfactant template and silica, which make impossible to remove the template without carrying out one of the previously cited removal processes.

Tanev and Pinnavaia designed a route using non-ionic surfactant templates including *n*-octylamine.[77] In polar solvents such as water (Figure 4), *n*-octylamine forms micelles in which the non-polar hydrophobic tails are oriented to the interior of the micelle, avoiding the contact with the water. The hydrophilic -NH_2 groups are oriented to the exterior of the micelle in order to interact with polar species such as water and silanol groups (obtained by the hydrolysis of the precursor alkoxy groups). The micelles act as a template because *n*-octylamine interacts with silanol groups through weaker hydrogen-bonding. Another advantage of this type of interaction is the possibility of removing the template by simple air drying/evaporation, as Prado et al. described.[78]

---

[75] C.T. Kresge, M.E. Leonowicz, W.J. Roth, J.C. Vartuli, Nature 359 (1992) 710.
[76] J. S. Beck, J. C. Vartuli, W. J. Roth, M. E. Leonowicz, C. T. Kresge, K.D.Schmitt, C. T. Chu, D. H. Olson, E. W. Sheppard, S. B. McCullen, J. B. Higgins, J. L. Schenker, Journal of American Chemical Society 114 (1992) 10834.
[77] P. Tanev, T. Pinnavaia, Science 267 (1995) 865.
[78] A. Prado, C. Airoldi, J. Mat. Chem. 12 (2002) 3823.

It is well known that, on porous building materials such as monumental stone, the polymerization must occur *in-situ*, so a feasible surfactant removal strategy must be provided.

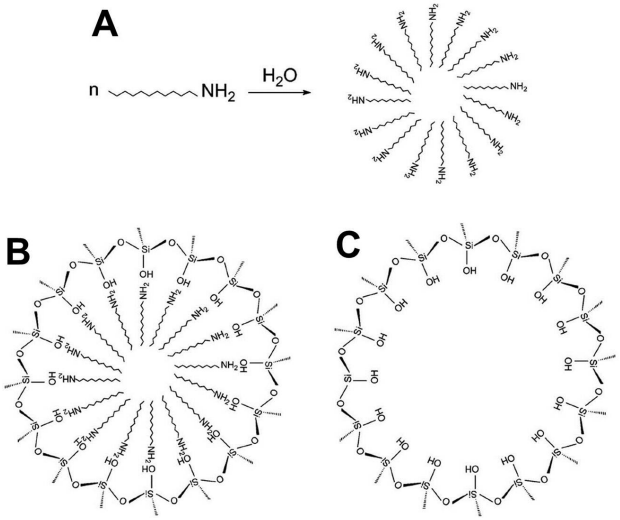

Figure 4. Illustration of the interactions ocurring during the synthesis of meso-structured molecular sieves obtained through a neutral surfactant template route. (A) Spherical micelle formation; (B) Interaction of silanol group with the surfactant-template in an aqueous medium; (C) After surfactant removal.[78]

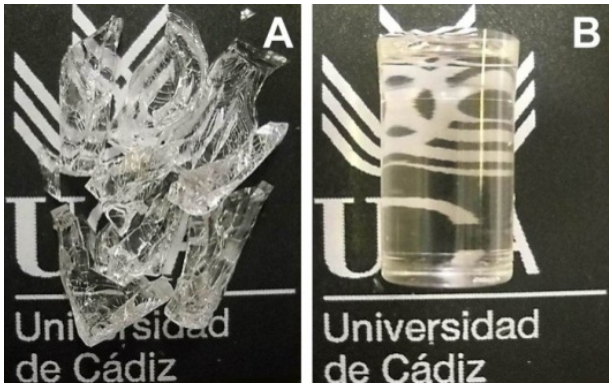

Figure 5. Photographs of the xerogels obtained in our laboratory. (A) from TEGOVAKON® V 100 commercial consolidant;(B) surfactant-synthesized nanomaterial developed in our laboratory.

Considering this, our group designed a synthesis in which *n*-octylamine was used with the object of obtaining a mesoporous material, and avoiding the need for undesirable calcinations/solvent extraction processes. The products obtained were crack-free monoliths (Figure 5). When applied on stone as sols, these materials showed improved strengthening properties when compared

with commercial stone consolidants.[79] In addition, this investigation generated a patent which is currently under exploitation.[80]

In an alternative route, and in order to provide hydrophobic properties to the nanomaterial, an organosiloxane PDMS (polydimethylsiloxane) with OH terminal groups, we added to a TEOS sol, in the presence of *n*-octylamine. An ORMOSIL[81] (organic-inorganic hybrid material) was obtained through the co-condensation of TEOS and PDMS. McKenzie et al.[82,83] have demonstrated that these hybrids present high elasticity. With this investigation, two main goals were achieved: 1) the desired elasticity was obtained and a crack-free material was generated; 2) a nanomaterial was designed with hydrophobic properties due to the effect generated by the methyl groups integrated in the surface of the material. In this way, two simultaneous effects on stone are achieved: consolidation and hydrophobicity. These nanomaterials present a controlled pore size due to *n*-octylamine pore templating and the improved mechanical properties of an ORMOSIL. These achievements were the subject of publications[84,85] and gave rise to a patent,[86] currently under exploitation.

Recently, we have developed a novel synthesis for producing nanomaterials that is VOC-free (free of volatile organic compounds),[87] by eliminating ethanol from the initial sol in our previous research.[84] The elimination of the solvent is essential to meet the criteria of the European Directive on the limitation of emissions of volatile organic compounds due to the use of organic solvents in certain activities and installations.[61] This innovation was also covered by a

[79] M. J. Mosquera, D. M. de los Santos, A. Montes, L. Valdez-Castro, Langmuir 24 (2008) 2772.
[80] M. J. Mosquera, A. Montes, D. M. de los Santos, Method of Strengthening Stone and Other Construction Materials, United States Patent and Trademark Office, 15-2-2007.
[81] H. Schmidt, J. Non-Cryst. Solids 73 (1985) 73, 681.
[82] J. D. Mackenzie, Y. Hu, J. Mater. Sci. 27 (1992) 4415.
[83] J.D. Mackenzie, Y.J. Chung, Y. Hu, J. Non-Cryst. Solids 147&148 (1992) 271.
[84] M. J. Mosquera, D. M. de los Santos, T. Rivas, Langmuir 26 (2010) 6737.
[85] M. J. Mosquera, D. M. de los Santos, T. Rivas, P. Sanmartin, B. Silva, Journal of Nano Research 8 (2009) 1.
[86] M.J. Mosquera, D. M de Los Santos, Procedimiento para hidrofugar y consolidar rocas y otros materiales de construcción, Oficina Española de Patentes y Marcas, 26-02-2010.
[87] J. F. Illescas; M.J. Mosquera, ACS Appl. Mat. Interfaces 4 (2012) 4259.

patent.[88] In these materials, PDMS acts to form bridges linking the silica particles. Figure 6 shows AFM images of the products obtained and the corresponding 3D structural models. The creation of a uniform network of silica particles by *n*-octylamine and the formation of bridges between silica nanoparticles by PDMS chains has been discussed.

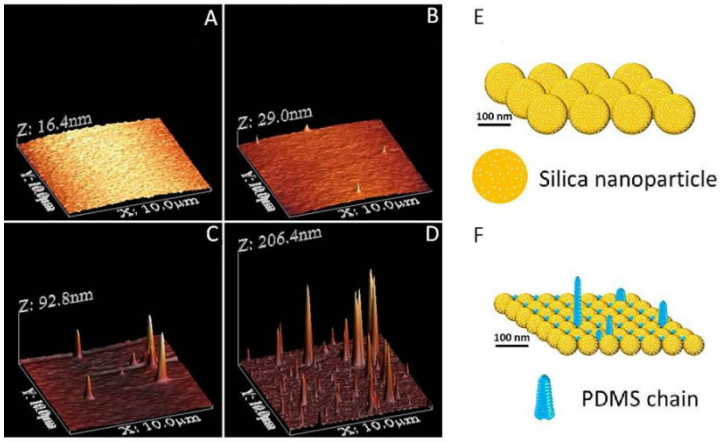

Figure 6 AFM 3D topography images of the silica nanomaterials' surface containing PDMS in the following % (v/v) proportion (A) 0% (B) 5% (C) 10% (D) 50%. (On right) 3D structural models for (E) silica nanomaterials and (F) silica-PDMS nanomaterials[101]

Further, the synthesis has been adapted to obtain hydrophobic products for application on pure carbonate stones. These have been shown to improve the robustness, hydrophobicity, water repellence, and stain resistance of the stone surface.[89] This development was also the subject of a patent, which included an additional improvement of hydrophobicity with respect to that reported in the article, achieved by adding SiO_2 nanoparticles to the silica sol.[90]

Application of TiO_2 photocatalyts on stone substrates

The use of photocatalysts together with building materials began in the early 1990's. The versatility of TiO_2, which can serve both as a photocatalytic material and a structural material, has facilitated its application in exterior construction materials and interior furnishing products, such as cement

[88] M.J. Mosquera, J. Illescas, Producto consolidante, hidrofugante y repelente de manchas para rocas carbonatadas y otros materiales de construcción, Oficina Española de Patentes y Marcas, 21-3-2011.
[89] J. F. Illescas, M. J. Mosquera, J. Phys Chem. C 115 (2011) 14624.
[90] M. J. Mosquera, J. Illescas, D. Facio, Producto para protección y restauración de rocas y otros materiales de construcción, Oficina Española de Patentes y Marcas. 16-02-2012.

mortar, exterior tiles, paving blocks, glass and PVC fabric.[33] The relevance of the subject justified holding a RILEM meeting (in English, the International Union of Laboratories and Experts in Construction Materials, Systems, and Structures) in 2007 with a view to discussing the applications of TiO_2 on building materials.[91]

In the case of building materials based on cement or lime (concretes and mortars), several attempts to mix the photocatalyst in their bulk, during their preparation processes, have been successfully carried out.[5,93-95] Results obtained[94] indicate that the addition of TiO_2 to cement gives photocatalytic properties to the material and can even improve its mechanical properties. However, few references are found in the literature about the application of TiO_2 photocatalysts in modern or ancient façades or on natural materials such as stone. In these cases, TiO_2 cannot obviously be included in the bulk of the material. Moreover, in the case of application on a building, the practical requirements are even stricter because it must be carried out *in-situ* at outdoor conditions, which can vary significantly. Moreover, no additional operations such as heating or solvent extraction can be carried out.

With reference to titanium dioxide application on stones, only a few studies are reported in the literature. Specifically, P25 particles dispersed in water have been applied on marble surfaces in order to prevent sulphation and bacterial activity;[95] these materials created a coating that cracked extensively on the marble surfaces under study. In other studies the biocidal action of TiO_2, has been considered, with no clear conclusions.[96] P25 slurry has also been applied on pumice stone for wastewater treatments; a significant decrease of photocatalytic efficiency was observed after 4 weeks, and this was attributed

[91] P. Baglioni, L. Cassar (Eds.), Proceedings of international RILEM symposium on photocatalysis, environment and construction materials ; Florence, 2007, 315.
[92] A. J. Fonseca, F. Pina, M. F. Macedo, N. Leal, A. Romanowska-Deskins, L. Laiz, A. Gómez-Bolea, C. Saiz-Jimenez, Int. Biodet. Biodegr. 64 (2010) 388.
[93] M. V. Diamanti, M. Ormellese, M. Pedeferri, Cement Concrete Res. 38 (2008) 1349.
[94] M. Lackhoff, X. Prieto, N. Nestle, F. Dehn, R. Niessner, Appl. Cat. B 43 (2003) 205.
[95] I. Poulios, P. Spathis, A. Grigoriadou, K. Delidou, P. Tsoumparis, J. Environ. Sci. Health A 34 (1999) 1455.
[96] D. Pinna, A.M. Lega, V. Mazzotti, Arkos 21 (2009) 18.

mainly to the elimination of TiO_2 from the stone surface.[97] More recently, TiO_2 nanoparticles dispersed in water[99-104] and in polymers[104,105] have been applied on stone surfaces as a self-cleaning treatment. Using such strategies, the long-term performance of the coating cannot be ensured due to the insufficient adhesion produced between the stone substrate and the TiO_2 particulate coating.[106]

[97] K. Rao, M. Subrahmanyam, P. Boule, Apply. Catal. B Environ. 49 (2004) 239.
[98] E. Quagliarini, F. Bondioli, G. Goffredo, A. Licciuli, P. Munafò, J. Cult. Herit. 13 (2012) 204.
[99] E. Quagliarini, F. Bondioli, G. Goffredo, A. Licciuli, P. Munafò, J. Cult. Herit. 2012, doi: 10.1016/j.culher.2012.02.006
[100] G. Potenza, A. Licciulli, D. Diso, S. Franza, A. Calia, M. Lettieri, G. Ciccarella, in P. Baglioni, L. Cassar (Eds.), Proceedings of international RILEM symposium on photocatalysis, environment and construction materials ; Florence, 2007, 315.
[101] L. Luvidi, G. Laguzzi, F. Gallese, A.M. Mecchi, G. Sidoti, in A. Ferrari (Ed.), Proceedings of 4th International Congress on Science and Technology for the Safeguard of Cultural Heritage in the Mediterrean Basin, Vol. II, Cairo, 2010, 495.
[102] A. Liciulli, A. Calia, M. Lettieri, D. Diso, M. Masieri, S. Franza, R. Amadelli, G. Casarano, J. Sol-gel. Sci. Technol 60 (2011) 437.
[103] E. Quagliarini, F. Bondioli, G. Goffredo, C. Cordoni, P. Munafò, Constr. Build. Mater. 37 (2012) 51.
[104] M. Noorjahan, M. P. Reddy, V. D. Kumari, B. Lavédrine, P. Boule, M. Subrahmanyam J. Photochem. Photobiol. A 156 (2003) 179.
[105] M. F. La Russa, S. A. Ruffolo, N. Rovella, C. M. Belfiore, A. M. Palermo, M. T. Guzzi; G. M. Crisci, Prog. Org. Coat. 74 (2012) 186.
[106] A. Rachel, M. M. Subrahmanyam, P. Boule, Apply. Catal. B Environ. 37 (2002) 301.

2. Justification

Atmospheric pollution has an adverse impact on structures and buildings in every city of the world. Particulate matter and other components like organic and elemental carbon, and nitrogen oxides, are deposited extensively on the surface and other large urban structures, contributing to the formation of an ugly brownish-gray to black crust. The deposition of these compounds on building façades has serious implications, not only aesthetic but also economical and ecological. Industry faces a major challenge in countering air pollution and specifically in devising ways of decomposing the organic species deposited on building surfaces, a task for which TiO_2 can be used as a photocatalyst in coatings applied to buildings and stone structures. The application of this photocatalyst on such surfaces should lower maintenance costs by reducing surface soiling; as a consequence, there would be less need for frequent and costly cleaning operations.

Considering the potential usefulness of TiO_2, we hypothesize that it will be possible to synthesize a material presenting photocatalytic activity, good adhesion and consolidation properties on stone by integrating preformed TiO_2 nanoparticles into a silica matrix in presence of a surfactant. There are several good reasons for choosing silica as a binder. It is known that it improves the mechanical, textural and thermal stability properties of TiO_2 used alone. In the case of a surfactant, this will be added to produce a mesostructured material with two objectives: 1) to prevent gel cracking during drying; 2) to improve the access to the photocatalytic sites.

The textural characterization (N_2 physisorption) and the microscopy studies (TEM, STEM and AFM) will allow us to understand better the particle morphology and, the access to the pores and will assist in the construction of nanostructural models. The characterization of the photocatalysts developed

will be also supported by other techniques including FTIR, UV-Vis, NMR spectroscopy, and X-ray diffraction.

In order to investigate the effectiveness of the products on stone, studies will be made of the mechanical properties of the stones after application of the photocatalysts; microscopy studies and other tests will be carried out. The photodegradation of methylene blue stains applied on stone will be used to evaluate the photocatalytic action of our products. Finally, a salt crystallization durability test will be also carried out.

For the optimization of the photocatalysts synthesized, we will also study the effect of TiO_2 loading and particle size. The potential benefits of these modifications should allow us to obtain a catalytic material with improved access to the Ti sites and higher activity.

It must also be acknowledged that the research performed for this Doctoral Thesis has been supported under the funding of several research projects:

- New materials for consolidation and protection of monumental stones", supported by Fundação para a Ciência e Tecnologia in its 2008 call (SFRH / BD / 43492 / 2008).
- Conservación de la piedra monumental. Nuevos Nanomateriales Consolidantes, Hidrofugantes y Autolimpiantes (MAT2010-16206, Ministerio de Ciencia y Tecnología 2011-2013)
- Regenera (Ministerio de Economía y Competitividad, Innpacto Call, 2011-2014)
- Nuevos nanomateriales para conservación del patrimonio historico-cultural andaluz (TEP-06386, Junta de Andalucía, 2011-2014)

The following companies have also demonstrated their interest under several research contracts:

- Tino Stone Group, S. A.
- Silicalia, S. L.

3. Objectives

Our research group has carried out extensive research in the synthesis of crack-free consolidant and hydrophobic materials for application on stone. The main objective of the work described in this Doctoral Thesis is to develop TiO_2 photocatalyst materials within a SiO_2 matrix for self-cleaning application on monumental stone. TiO_2 acts as the photocatalyst, and its performance in the photoxidation of methylene blue is evaluated. In addition, the hydrophobic properties of the product and the compatibility of its application as a stone consolidant are studied. In the work reported in this Doctoral Thesis the synthesis processes previously designed in our group have been modified with various specific objectives:

- A sol-gel strategy is to be designed by means of which a photocatalyst mesoporous material is obtained, using a surfactant as pore template.
- The influence of the pore template and TiO_2 nanoparticles in the properties of the final material will be studied.
- The influence of TiO_2 nanoparticles loading and size in the properties of the final material will be better understood.
- The properties of the photocatalyst material will be adjusted in order to improve the adsorption and photocatalytic degradation of methylene blue on monumental stone.
- A VOC-free synthesis route will be designed in order to increase the dry matter deposited on stone and avoid their harmful environmental effects.
- The sol-gel properties of the synthesized products will be characterized. The textural and structural studies of these nanomaterials will provide new information about their photocatalytic behaviour and, based on this information, the effect of the structure on their final properties and efficacy will be discussed.

- The self-cleaning, consolidant, adhesion and hydrophobic properties of our photocatalysts will be evaluated on typical stones.
- The properties of the photocatalysts synthesized in our laboratory will be compared with existing commercial materials.
- The colour change induced by the photocatalysts on stone will be evaluated.
- The improvements in durability of the stones treated with our photocatalysts when subjected to salt crystallization tests will be evaluated.

4. Results

4.1. Titania-silica nanocomposite photocatalysts with application in stone self-cleaning

Published in The Journal of Physical Chemistry C

THE JOURNAL OF PHYSICAL CHEMISTRY C

ARTICLE

pubs.acs.org/JPCC

Titania-Silica Nanocomposite Photocatalysts with Application in Stone Self-Cleaning

Luís Pinho and Maria J. Mosquera*

Departamento de Química-Física, Facultad de Ciencias, Campus Universitario Río San Pedro, Universidad de Cádiz, 11510 Puerto Real, Cádiz, Spain

Supporting Information

ABSTRACT: Mesoporous titania-silica composites that have photocatalytic activity have been synthesized by mixing ethoxysilane oligomers and titanium dioxide nanoparticles in the presence of a nonionic surfactant (*n*-octylamine). The resulting nanomaterials create effective adhesive and crack-free coatings for stone. These coatings give self-cleaning properties to stone and improve its mechanical resistance. In addition, the coating created has hydrophobic properties. For purposes of comparison, another two sets of photocatalytic materials have also been tested. The first of these has been obtained by an analogous synthesis in which *n*-octylamine is replaced by phosphoric acid; the second is a simple dispersion of titania nanoparticles in water. Both of these alternative materials produced coatings that crack and have poor adhesion on the stone tested; furthermore, they do not increase the mechanical resistance of the stone. These results confirm the valuable role played by *n*-octylamine in reducing the capillary pressure responsible for cracking, and in creating a mesoporous coating on the stone that enhances the self-cleaning properties, compared with the effect produced by the nanocomposite comprising similar particles embedded in a microporous silica matrix.

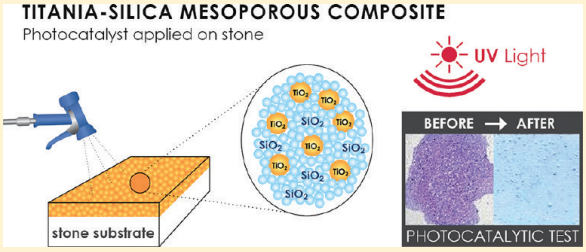

INTRODUCTION

Currently, titania is probably the most efficient common material with photocatalytic properties, very high stability, and very low cost.[1,2] Its unique combination of properties makes it very appropriate for many diverse applications in photochemical cells, self-cleaning materials, water purification, air cleaning, antitumor activity, and sterilization. Its development started with the description of an electrochemical photolysis phenomenon in 1972, by Honda and Fujishima.[3] Photons are absorbed by TiO_2, which generates electron−hole pairs, according to the equation:

$$TiO_2 + h\nu \leftrightarrow e^- + h^+ \quad (1)$$

In contact with water, free radicals are generated ($^{\bullet}O_2^-$ and $OH^{\bullet}$)

$$h^+ + H_2O_{ads} \leftrightarrow H^+_{ads} + OH^{\bullet}_{ads} \quad (2)$$

$$h^+ + OH^-_{ads} \leftrightarrow OH^{\bullet}_{ads} \quad (3)$$

These radicals are able to oxidize organic matter to water and carbon dioxide, leaving no other residue.[1]

In the case of self-cleaning applications, TiO_2 is deposited on the substrate as a thin film of thickness ranging from a few tens of nanometers to a few micrometers.[4] Titanium dioxide coatings can be prepared from titanium alkoxides through a simple sol−gel process, followed by a calcination treatment. This last operation at high temperature (>450 °C) promotes growth of rutile and anatase crystallites with photocatalytic activity and good adhesion to the substrate.[5,6] However, the most widely used photocatalysts are colloid TiO_2 nanoparticles, and more specifically Evonik Aeroxide TiO_2 P25.[7] Titania particles can also be subjected to calcination with particle sinterization and formation of covalent bonds between these nanoparticles with the object of producing materials that are considerably more robust and thermally stable than those prepared analogously from molecular precursors.[8]

The use of photocatalysts together with building materials began in the early 1990s. The versatility of TiO_2, which can serve both as a photocatalytic material and a structural material, has facilitated its application in exterior construction materials and interior furnishing materials, such as cement mortar, exterior tiles, paving blocks, glass, and PVC fabric.[9] With reference to titanium dioxide application on stones, only a few studies, with unsatisfactory results, are reported in the literature. Specifically, P25 particles dispersed in water have been applied on marble surfaces in order to prevent sulphation and bacterial activity;[10] these materials created a coating that cracked extensively on the marble surfaces under study. P25 slurry has also been applied on pumice stone for wastewater treatments; a significant decrease of photocatalytic efficiency was observed after 4 weeks, and this was mainly attributed to the elimination of TiO_2 from the stone surface.[11]

From these findings, our first objective has been to prepare a crack-free nanocomposite coating with good adherence to stone.

Received: August 4, 2011
Revised: September 14, 2011
Published: October 08, 2011

Such a coating should also give self-cleaning properties to the stone. The method for application of the coating must be simple, such as a spraying procedure, and the need for additional steps as calcination must be avoided because the coating will normally have to be applied in situ, on the external surface of a stone building. Moreover, high temperatures could damage the stone substrates. Our strategy is based on adding titanium dioxide colloidal particles to a silica oligomer in the presence of a surfactant. The target is to integrate TiO_2 particles into an effective silica matrix that is capable of adhering well to the stone. There are two reasons for adding surfactant: (1) to prevent cracking;[12−14] and (2) to enhance photocatalytic activity by creating a mesoporous nanocomposite.[4,15,16]

Synthesis strategies, in which mesoporous titanium dioxide films are obtained by using a surfactant as template have been widely reported in the literature.[17] Other strategies reported have employed surfactant-templated silica as a binding material for TiO_2 nanoparticles.[18,19] These particles are formed in situ within the porous matrix from a titanium precursor. The drawbacks associated with this synthesis are that the TiO_2 loading is quite low, and the capacity of the TiO_2 to crystallize into crystallites is severely limited by the low temperature of calcination permissible when using glass substrates.[20] Another approach is based on using preformed TiO_2 nanoparticles embedded inside surfactant-templated mesoporous films.[8,15,16,20−24] An ionic surfactant, such as Pluronic triblock copolymer or alkyl ammonium bromide, acts as a structure-directing agent to obtain mesoporous periodic structures. After the synthesis, the surfactant is removed by calcination or solid−liquid extraction.

In this work, we have synthesized a silica−titania nanocomposite starting from P25 titania particles mixed with a silica oligomer in the presence of *n*-octylamine. Our innovation with respect to the previously reported strategies is the employment of a nonionic surfactant to avoid the need for calcination or an extraction process. As we previously reported,[12−14] the surfactant can be removed very simply by drying under laboratory conditions. Silica interacts with the template by hydrogen-bonding; therefore, the removal of the surfactant in a neutral pathway must prove to be easier than the methods corresponding to the classic route involving electrostatic interactions between cationic surfactants and anionic inorganic. For the purposes of comparison, we also use another two different routes in this study. The three kinds of synthesis employed can be described as follows: (1) Aqueous dispersion of P25 particles; (2) Silica−titania nanocomposites are prepared from silica oligomer and titania nanoparticles in the presence of H_3PO_4; (3) Silica−titania nanocomposites are prepared from silica oligomer and P25 particles in the presence of *n*-octylamine.

For the three syntheses proposed, the proportion of titania to silica is varied from 0 to 2% w/v in each, in order to investigate its effect on the properties of the material. In the first part of the Results and Discussion section, we consider the characterization of the sol−gel properties of the materials synthesized. In the second part, we describe the application of these nanocomposites as a coating on a limestone surface, and evaluate their effectiveness for the following: (1) providing self-cleaning properties; (2) improving mechanical resistance of the coating; and (3) assuring its adherence to the substrate.

EXPERIMENTAL SECTION

Synthesis. The following reagents were used in the synthesis: (1) TES40 WN (Wacker Chemie AG, GmbH): according to the technical data sheet, this is an ethyl silicate providing approximately 41% of silica upon complete hydrolysis, and it contains many hydrolyzable ethoxy groups; (2) P25 (Evonik AEROXIDE TiO_2 P25): this material has an average primary particle size of 21 nm and a specific surface area (BET) of 50 ± 15 $m^2.g^{-1}$; (3) *n*-octylamine (Aldrich); 4. H_3PO_4 (Panreac). Three synthesis routes were followed:

(1) P25 particles were dispersed in distilled water under manual agitation.
(2) TES40 was mixed with P25 particles in the presence of H_3PO_4 under high-power ultrasonic agitation (125 $W \cdot cm^{-3}$); the proportion of H_3PO_4 to TES40 was 0.18% v/v. The total time of ultrasonic agitation was 10 min.
(3) TES40 was mixed with P25 particles in the presence of *n*-octylamine under the same agitation conditions. The proportion of *n*-octylamine to TES40 was 0.36% v/v.

For each of the three synthesis routes, P25 particles were added to the starting sol (or water) in each of the following ratios: 0, 0.5, 1 and 2% w/v. The three formulations tested have been designated as follows: P25; UCATiP (TES40/P25/H_3PO_4); and UCATiO (TES40/P25/*n*-octylamine) via the procedure devised at the University of Cadiz. The numbers indicate the % w/v of P25 included in the material. Scheme 1 shows a summary diagram of the starting sols.

Scheme 1. Summary Diagram of the Sols Tested

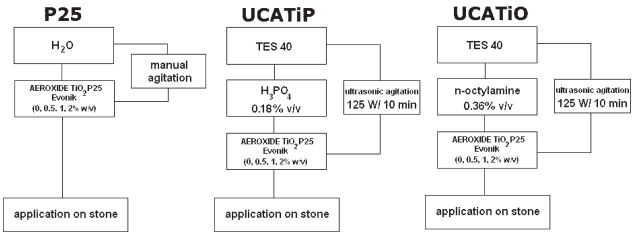

Immediately after the synthesis of the sols, their rheological properties were studied using a concentric cylinder viscosimeter (model DV-II+ with UL/Y adapter) from Brookfield. Experiments were performed at a constant temperature of 25 °C maintained by recirculated water from a thermostatic bath. A shear stress versus shear rate flow curve was generated. For comparison, the rheological properties of P25 aqueous dispersions were also evaluated.

Preparation and characterization of coatings. Coatings of the materials under study were obtained by deposition of 3 mL of sol on plastic Petri dishes with a diameter of 85 mm. Dishes were covered and maintained at laboratory conditions (relative humidity of 60% and temperature of 20 °C). Gel transition and spontaneous drying took place. The xerogels obtained were characterized after reaching constant weight.

Powdered coatings were used for X-ray diffraction (XRD), measured on a Bruker D8 advance diffractometer equipped with a secondary monochromator, Cu tube X-ray, using Cu kα radiation.

The pore volume, pore size distribution, and BET surface area of the coatings was characterized by Nitrogen Physisorption (Autosorb IQ from Quantachrome).

Transmission electron micrographs were obtained using high-angle annular dark field-scanning transmission electron microscopy (HAADF-STEM) by means of a JEOL 2010-FEG TEM/STEM electron microscope equipped with a JEOL HAADF detector.

The chemical bonds in the coatings under study were analyzed by Fourier Transformer Infrared Spectrophotometry (FTIR). The spectra were recorded in powder using a FTIR-8400S from Shimadzu (4 cm^{-1} resolution) in the region from 4000 to 600 cm^{-1}. Experiments were carried out in attenuated total reflection mode (ATR). In order to investigate surfactant removal as a function of time, FTIR spectra of the UCATiO gels were obtained, first immediately after the synthesis, and second after a period of 8 months had elapsed.

The materials were also visualized by Scanning Electron Microscopy (SEM) using a JEOL Quanta 200 Scanning Electron Microscope.

Application on Stone and Characterization. The stone selected for evaluating the effectiveness of the materials under study is a fossiliferous limestone with a homogeneous structure composed of a micritic matrix, containing recrystallized calcium carbonate grains, and skeletal fragments of mollusks, echinoderms, and foraminifera. Semiquantitative analysis by X-ray powder diffraction analysis enabled the mineralogical composition of stone to be identified; it is composed of calcite (98.5%) and α-quartz (1.5%). This stone was selected due to its whiteness, so the stains applied on its surface and self-cleaning effectiveness of the coatings under study could be checked more easily. For all of the experiments carried out, the stone samples were cut in the form of 5 × 5 × 2 cm slabs. For the water capillary absorption test, exceptionally, 5 cm-sided cubes were employed. The sols under study were applied by spraying onto the surfaces of the samples until saturation. The stone samples were then dried under laboratory conditions until reaching constant weight. Uptake of products and their corresponding dry matter were calculated. The samples corresponding to untreated stone and their treated counterparts were characterized by the procedures described below, after constant weight was reached.

A JEOL Quanta 200 scanning electron microscope (SEM) was used to visualize changes in the morphology of the stones after coating. Surface fragments of treated stone specimens and their untreated counterpart were visualized.

The adherence of the coating to the stone surface was evaluated by performing a peeling test using Scotch Magic tape (3M). The test was carried out according to previously reported methods.[25,26] The changes in stone surface morphology were visualized by SEM working in low-vacuum mode, and energy-dispersive X-ray spectroscopy (EDX) spectra were recorded in order to elucidate the variations in surface composition after the test.

The improvement in mechanical properties in treated stone was evaluated by using the drilling resistance measuring system (DRMS), by SINT Technology. Drill bits of 4.8 mm diameter were employed with a rotation speed of 200 rpm and penetration rate of 10 mm/min.

In order to investigate the hydrophobic behavior of the coatings under study, contact angles of the stone surfaces were measured using a commercial video-based, software-controlled contact angle analyzer, model OCA 15plus, from Dataphysics Instruments.

Changes in water absorption after treatments were evaluated by applying a test of water absorption by capillarity, as recommended in UNE-EN 1925.[27] Total water uptake values (TWU) obtained after 48 h were determined.

We also evaluated the possible disadvantage of these materials associated with changes in stone color induced by the treatments. This effect was determined using a solid reflection spectrophotometer, Colorflex model, from Hunterlab. The conditions used were as follows: illuminant D65 and observer 2°. CIELa*b* color space was used and variations in color were evaluated using the parameter: total color difference (ΔE^*).[28]

The effectiveness of the materials under study as self-cleaning coatings for stone surfaces was evaluated by using a test adapted from the literature.[29,30] First, 1 mL of a solution of 1 mM methylene blue (Panreac) in ethanol was deposited on treated stone specimens and their untreated counterparts. Next, stone samples were irradiated with UV light working at 365 nm in a Vilber Lourmat CN15.CL chamber with 2 tubes of 15 W. The distance between the samples and the tubes was approximately 20 cm. Color variations, recorded as a function of irradiation time, were determined by using the same procedure described above. The parameter total color difference (ΔE^*) was again evaluated.[28]

Table 1. Viscosity Values (Measured at 25° C), Textural Parameters Obtained from the Isotherms and the BJH Method for the Nanocomposites under Study

sample	viscosity (mPa·s)	S_{total} (m^2/g)	V_{pore} (cm^3/g)	pore size (nm)
P25-0.5	2.70	59	0.39	28
P25-1	2.73			
P25-2	2.75			
UCATiP-0	5.25	267	0.22	3.8
UCATiP-0.5	5.32	220	0.23	3.8
UCATiP-1	5.45	259	0.23	3.8
UCATiP-2	5.50	249	0.18	3.8
UCATIO-0	5.30	231	0.39	6.3
UCATiO-0.5	5.54	255	0.31	7.6
UCATiO-1	5.68	180	0.69	13.4
UCATiO-2	5.82	220	0.59	13.0

RESULTS AND DISCUSSION

Coatings Characterization. Prior to the preparation of the coatings, a rheological study of the sols was carried out. Although a shear-thinning behavior for aqueous titanium dioxide dispersions is commonly reported in the literature,[31] we observed a Newtonian behavior for the three concentrations of P25 aqueous dispersion studied, at the shear range evaluated. We explain this finding in terms of the low particle concentration in the dispersions under study. These viscosity data were obtained immediately after stirring the dispersions. After a few hours, the P25 particles tend to aggregate, and flocculation occurs for all of the concentrations studied. This demonstrates that the P25 aqueous dispersions prepared are not stable. UCATiP and UCATiO sols also showed Newtonian behavior at the shear range evaluated. The viscosity was calculated as the slope of the shear rate vs shear stress curve. In all of the cases, the linear regression coefficients were above 0.99. Viscosity values obtained are listed in Table 1. In the case of the P25 dispersions, the viscosity increased only slightly when the particle concentration was increased. In the case of the silica−titania sols under study, the addition of P25 promoted a more significant increase in viscosity, following a linear trend. In comparison with the commercial products, the values of the UCA sols synthesized in this study were only slightly higher than those corresponding to commercial sols. Specifically, we determined the viscosity for one of the most

popular commercial consolidants, Tegovakon V100 from Evonik; the viscosity of this solvent-free product was 4.48 mPa·s at 25 °C. Thus, we think these sols must penetrate into the stone in a similar way to that of the commercial sols. This is a key factor for achieving a consolidant effect on the stone.

Sol−gel transition of all the UCATiP and UCATiO sols deposited on plastic dishes occurred overnight, producing homogeneous nanocomposite gels. When P25 is mixed with TES40, we find that one of two different processes may occur: (1) flocculation of the P25 particles and subsequent creation of two different phases; or (2) the P25 particles are stable in the sol during the hydrolysis of TES40 and the condensation of silanols, and thus titania particles are integrated within the gel network. Obviously, the homogeneity of gels obtained indicates that stabilization of the particles is achieved by means of the two routes investigated in this work. We think the particles exhibit stability during the sol−gel transition because of an electrostatic repulsion phenomena, induced by pH-changes produced by H_3PO_4 or *n*-octylamine. As previously discussed,[32,33] the interaction between charged particles is well described by the DVLO theory, which is based on an algebraic sum of the attractive van der Waals and the repulsive double layer forces. Since the isoelectric point of the P25 particles is 6.5 for water, their isoelectric point in the sols prepared in our laboratory must be fairly close to this value. Therefore, adjusting the pH to higher or lower values by acid or basic addition to the sol must increase electrostatic repulsions and, subsequently, P25 dispersion stability must be enhanced. Electrostatic stabilization of P25 particles in polar organic solvents has previously been obtained by Kosmulski et al.[33] by adding an acid such as phosphoric acid and a base like triethylamine. Furthermore, it should be noted that H_3PO_4 works as an acid catalyst during sol−gel transition and *n*-octylamine acts as a basic catalyst in the same way. Thus, sol−gel transition took place in a maximum time of 24 h for the two series of sols tested.

We previously investigated other proportions of *n*-octylamine ranging from 0.016 to 1.8% v/v. We chose 0.36% v/v because it is the minimum concentration at which a stable titania particle dispersion can be obtained during the sol−gel transition time (24 h). Lower concentrations of surfactant resulted in phase separation. In addition, these sols with lower *n*-octylamine content do not gel spontaneously. This finding corroborates the role played by the surfactant as basic catalyst. Regarding the higher concentrations of the surfactant, they were not adopted because they gradually decreased the gel time. For the highest concentrations tested, the gel transition occurred immediately after synthesis. This short gel time is not sufficient for the sol to be applied to the substrate.

The X-ray patterns of the powdered form of the coatings under study are given in Figure 1. All of the materials show the typical amorphous silica pattern without any detectable ordered structure. We have previously obtained[34] similar patterns for silica gels synthesized from TEOS and *n*-octylamine. This confirms that our synthesis strategy does not promote an ordered pore structure, which is typical of most materials synthesized via a surfactant template. As previously reported,[23] the silica/titania films become an ordered mesostructure at higher drying temperatures. Thus, we assume that our drying at ambient temperature cannot produce an ordered silica structure.

We also observe that the X-ray patterns obtained show peaks previously reported as a pure anatase structure.[22,35] Specifically, the peaks assigned to anatase-type titania at around 25°, 38°, and

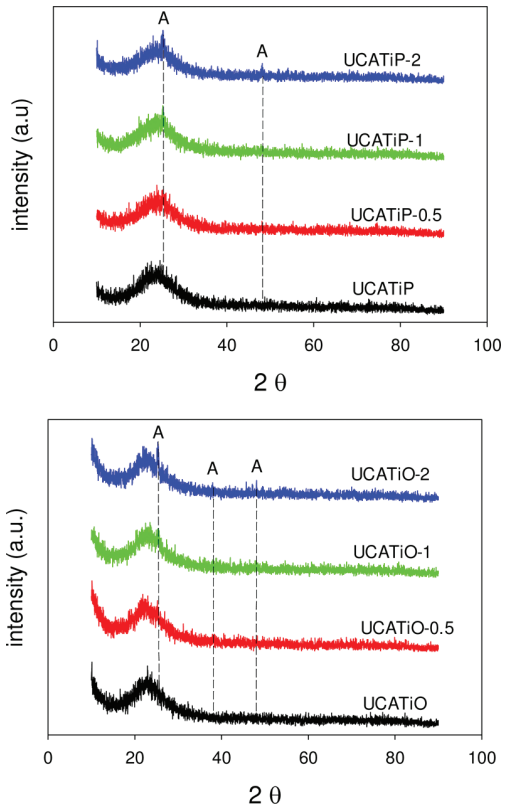

Figure 1. XRD patterns for the nanocomposite coatings under study.

48° were observed.[23] This demonstrates the loading of TiO_2 particles in the coatings under study. In addition, as reported in previous papers,[8,35] this verifies that the TiO_2 particles in the nanocomposites prepared in our laboratory exist as a separate domain embedded within the silica domains. As would be expected, these peaks in the patterns corresponding to the material with the lowest content of TiO_2 particles are difficult to appreciate, whereas their resolution and sharpness improve at higher TiO_2 contents.

Nitrogen adsorption−desorption isotherms corresponding to the coatings are shown in Figure 2, and the textural data obtained are given in Table 1. P25, which was also characterized for comparative purposes (see isotherm in Supporting Information), presents a type IV isotherm with an H1 hysteresis loop, as expected for an agglomerate of TiO_2 particles.[36] In the case of UCATiP materials, type I isotherms are observed, corresponding to microporous materials. These isotherms show a slight hysteresis typical of mesoporous materials. This profile is characteristic of materials consisting of a mesoporous network with a pore size close to microporous values.[36]

Regarding the materials designated UCATiO, the isotherms are type IV, showing an H1 hysteresis loop with parallel and nearly vertical branches. This loop is more clearly observed for materials with the highest TiO_2 content (1 and 2% w/v). As reported for P25,[36] this kind of hysteresis is attributed to materials consisting of agglomerated particles or compacted clusters of spherical particles arranged in a uniform way. These isotherm profiles therefore suggest that UCATiO gels are composed of a network of silica balls and the titania particles are integrated within this network. We have previously obtained[34] similar morphologies, consisting of a regular network

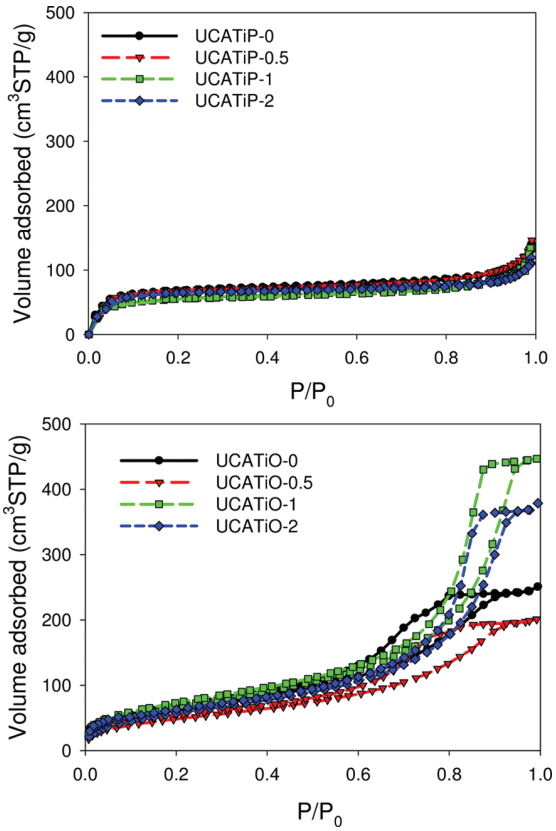

Figure 2. Nitrogen adsorption−desorption isotherms for the nanocomposite coatings under study.

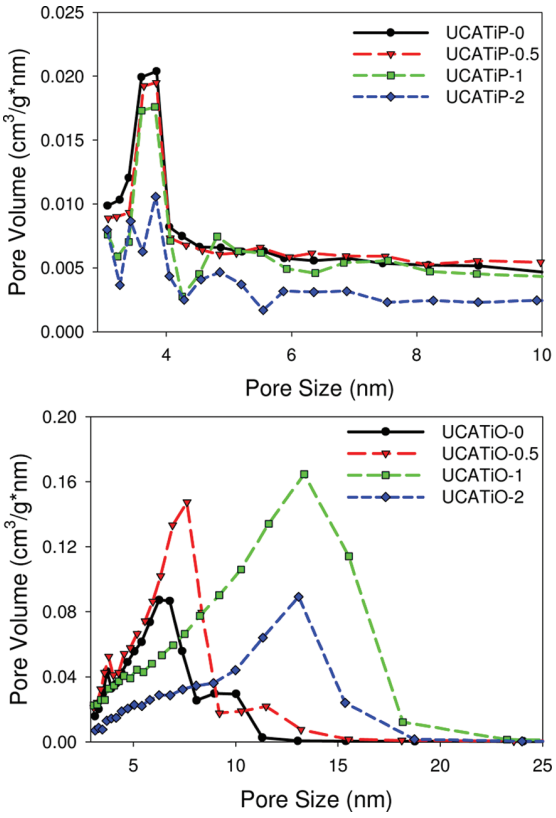

Figure 3. BJH pore size distribution for the nanocomposite coatings under study.

of uniform silica spheres for gels obtained from TEOS and *n*-octylamine.

The pore-size distribution (Figure 3) was determined using the Barret−Joyner−Halenda (BJH) method.[37] Pore volume (see Table 1) and pore size were significantly higher when the synthesis occurs in the presence of *n*-octylamine. Pore volume detected in the mesoporous range for UCATiP materials were 1 order of magnitude less than that obtained for the UCATiO coatings. As we demonstrated in our previous papers,[12−14,34] this feature indicates the role played by the surfactant: it coarsens the pores network and this subsequently reduces the capillary pressure responsible for cracking during the drying of the gel.

Concerning the effect of TiO_2 content on the pore structure of the coatings, we do not observe any significant differences for UCATiP materials. It is thought that the low pore volume detected at 3 nm can be attributed to the silica material in which the TiO_2 particles are embedded. In the case of the UCATiO materials, we observe a completely different behavior. The UCATiO gel without TiO_2 content and that with the lowest proportion of TiO_2 (0 and 0.5% w/v) presents pores of size around 6 nm, which are attributed to the silica network. As we have previously reported, the presence of surfactant promotes the coarsening of the gel network, increasing the size and uniformity of the pore network, as corroborated by nitrogen adsorption test data. The formation of this coarser network composed of polymeric balls is due to the *n*-octylamine. We assume that the pores detected correspond to the voids between the silica particles. For materials with the highest TiO_2 content, the pore size of the silica/titania composite is greater, at 13 nm. Since P25 particles present a mean pore size of 28 nm (see Table 1; pore size distribution is included as Supporting Information), a value taken to correspond to interparticulate space, we speculate that titania particles are intercalated in the interparticle spaces formed between the silica balls, created by the surfactant. Since pore size doubles when titania is integrated in the silica network, we believe that the silica particles are smaller than the P25 particles. Thus, P25 integration in the silica network produces greater heterogeneity in the pore size of the network. Regarding BET surface area (Table 1), although the pore volume is higher for the UCATiO materials, the two series show similar surface area values because the pore size of UCATiO composites is significantly higher than that corresponding to UCATiP materials.

These findings were supported by the transmission electron micrographs of the coatings. Figure 4 shows micrographs corresponding to UCATiP and UCATiO materials with the highest TiO_2 content. The HAADF-STEM micrograph of the UCATiP coating shows a material composed of individual TiO_2 particles (of around 20 nm size) and some aggregates (of 30−40 nm size) of titania particles embedded in a dense silica matrix, whereas the micrograph corresponding to UCATiO clearly shows a gel network composed of individual titania and silica particles. Uchiyama et al.[22] obtained a similar morphology for a coating prepared from titania particles with a smaller diameter (of around 7 nm) than those we employed— and a mesoporous structure; their coating was synthesized through the combination of a surfactant and a siliceous monomer. Yamauchi et al.[15,16] have also obtained a similar nanocomposite of P25 and silica particles.

dx.doi.org/10.1021/jp2074623 |J. Phys. Chem. C 2011, 115, 22851–22862

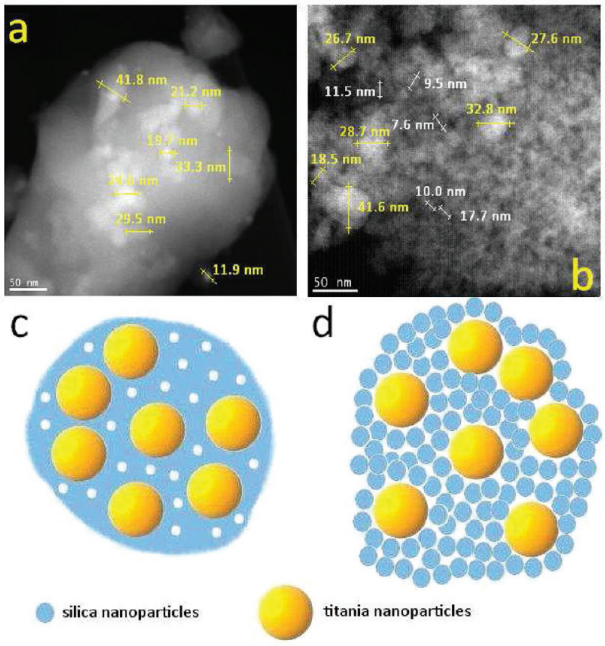

Figure 4. HAADF-STEM images of (a) UCATiP-2; and (b) UCATiO-2 coatings. Parts (c) and (d) are schematic models of these nanocomposites.

Our micrographs provide evidence of the presence of titania particles with similar size to those observed in the UCATiP nanocomposite. Concerning the silica network, an aggregation of mesoporous particles with a slightly lower diameter (7−15 nm) than the titania particles, can be observed. These findings confirm the greater pore size of the network for the coating materials with higher TiO_2 content, demonstrated by nitrogen physisorption. As is obvious, larger particles produce larger pores in the network. A schematic model of the structures of the composites is also included in Figure 4.

FTIR spectra of the coatings under study are shown in Figure 5. For comparative purposes, the spectrum of TES40 has been included as Supporting Information. All of the materials present the typical silica peaks.[12,38,39] Specifically, the bands located at 800 and 1080 cm^{-1} are attributed to Si−O−Si bending; the band at 960 cm^{-1} is attributed to Si−OH stretching; and the broad band in the 3400 cm^{-1} range is attributed to Si−OH groups with absorbed molecular water. This band may also contain the contribution of absorbed molecular water on Ti−OH from the surface of TiO_2 particles. In addition, another band associated with ethoxy groups of the silica precursor is also observed: the band located at 1300 cm^{-1} attributed to CH_2 twisting.[39] This last band confirms that all the ethoxy groups are hydrolyzed immediately after the synthesis. Comparison between the two sets of gel under study shows that UCATiO gels present sharper Si−O−Si peaks than UCATiP gels. This difference can be attributed to higher condensation of silanols in a ramified structure obtained through the effect of *n*-octylamine.

The possible presence of residual surfactant in the UCATiO material was investigated by carrying out FTIR assays at two time intervals (the first immediately after synthesis and another after 8 months). In the spectra obtained immediately after synthesis, we can observe a peak at 1400 cm^{-1}, which is attributed to amine C−N[12,13] stretching, from the surfactant. In addition, in the

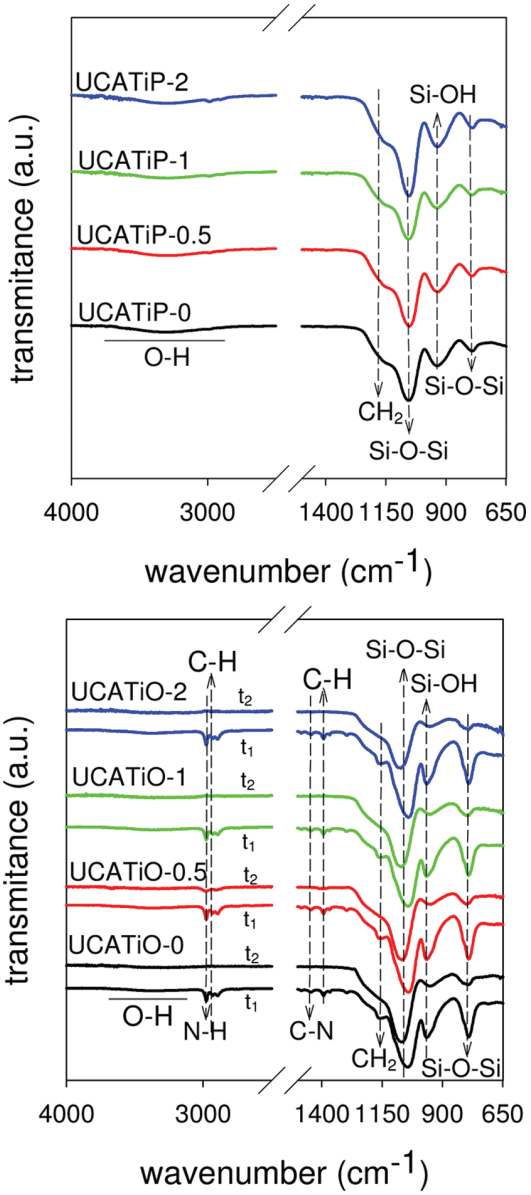

Figure 5. FTIR spectra for the coatings under study. UCATiO spectra were recorded at two time points: (t_1: immediately after the synthesis; t_2: after 8 months had elapsed).

spectra for this time, two bands at 2883 and 1430 cm^{-1} can be attributed to stretching and bending, respectively, of the C−H bond.

Finally, the peak at 2930 cm^{-1} corresponds to N−H stretching.[12,13] These peaks have almost disappeared after 8 months. From these results it can be concluded that n-octylamine is removed by simple exposure to laboratory conditions.

Moreover, the band at 1300 cm^{-1} attributed to ethoxy groups is significantly reduced after 8 months, confirming the hydrolysis and subsequent condensation of silica oligomers. However, the presence of a weak shoulder confirms that a small proportion of nonhydrolyzed ethoxy groups is present in the coatings under study.

Regarding the peaks associated with titania, it is often reported[40] that bands observed in the range 900−1000 cm^{-1} may be associated with Ti−OH and Si−O−Ti species. These bands could appear in our spectra due to co-condensation

between silica oligomer and titania particles. However, they are not visible because these bands are probably obscured by the peak attributed to Si−OH located at the same wavenumber.

Figure 6 shows the SEM micrographs of the coatings under study. We can observe significant differences in the morphology of the two sets of nanocomposites studied. The UCATiO materials form a homogeneous and continuous gel coating whereas the UCATiP materials create discontinuous films of aggregates. These features provide evidence supporting that from the FTIR spectra obtained. As previously reported, the UCATiO gels present sharper Si−O−Si peaks than the UCATiP gels due their higher degree of condensation in a cross-linked structure. The SEM micrographs also contribute to corroborating the structure model presented in Figure 4, since silica aggregates observed in UCATiP images show sizes of around 300−400 nm, which are similar to the size of the silica aggregates measured by HAADF-STEM for UCATiP2 (see also Figure 4).

Application on Stone and Characterization. The effectiveness of UCATiP and UCATiO nanocomposites was investigated on the surface of a limestone. For purposes of comparison, the effectiveness of aqueous dispersions of P25 at the same TiO_2 concentrations was also investigated. Uptake of the materials under study and dry matter are shown in Table 2.

The uptake of the P25 aqueous dispersion was slightly higher than that corresponding to the gel coatings because its viscosity is lower. However, dry matter values were significantly lower for P25 than for UCATiO and UCATiP, since the P25 dispersion only creates a deposit of particles on the surface of stone, whereas the two coating materials penetrate into the stone pore structure. Higher content of TiO_2 particles does not significantly modify the values for dry matter obtained. Comparing the two series of gels, the dry matter for the UCATiO nanocomposites was slightly higher.

Figure 7 shows SEM micrographs of stone specimens treated with the materials under study. The P25 and UCATiP materials create a dense and extensively cracked coating on the stone surface. In the case of the UCATiO materials, crack-free, homogeneous, and coarser coatings on the stone surface are observed.

This demonstrates that *n*-octylamine efficiently reduces the capillary pressure, which is the factor responsible for cracking, by coarsening the gel network pore size. Moreover, *n*-octylamine also reduces the surface tension of the starting sol, which also contributes to reducing the capillary pressure. Since one significant drawback of P25 applied on stone has been associated with a reduction in photocatalytic efficiency during long-term use, due to the elimination of TiO_2 from the stone surface,[11] we have investigated the degree of adhesion of these coatings synthesized in our laboratory on stone, by performing a peeling test adapted by the literature. Figure 8 shows the micrographs obtained by SEM and the EDX analyses carried out on tested and nontested areas. As expected, a gradual increase of titanium content is observed as P25 content is raised in the coatings analyzed. Cracks in the coatings are not observed due the different observation scale. In P25 coatings, an almost complete removal of the titania coating after the peeling test can be observed. This was confirmed by EDX analysis, since the high titanium peaks are completely removed for P25-0.5 and P25-1 and significantly reduced for P25-2, after the test.

The UCATiP coatings show similar adhesion performance than the P25 ones, as confirmed by the absent titanium peaks

Table 2. Properties of the Treated Stone Specimens and the Untreated Counterpart

sample	untreated	P25-0.5	P25-1	P25-2
uptake (%w/w)		2.09 ± 0.44	2.30 ± 0.59	2.55 ± 0.54
dry matter (%w/w)		0.04 ± 0.02	0.05 ± 0.03	0.05 ± 0.02
contact angle (deg)	61 ± 9	70 ± 12	65 ± 16	23 ± 4
TWU (%w/w)	2.72 ± 0.08			
ΔE^a		0.66 ± 0.21	1.57 ± 0.85	1.59 ± 0.83
sample	UCATiP-0	UCATiP-0.5	UCATiP-1	UCATiP-2
uptake (%w/w)	1.31 ± 0.29	1.43 ± 0.39	1.28 ± 0.24	1.15 ± 0.36
dry matter (%w/w)	0.89 ± 0.17	1.13 ± 0.31	1.07 ± 0.20	0.93 ± 0.30
contact angle (deg)	93 ± 2	92 ± 6	98 ± 2	96 ± 6
TWU (%w/w)	0.08 ± 0.01	0.08 ± 0.01	0.07 ± 0.01	0.09 ± 0.01
ΔE^a	3.66 ± 0.49	2.68 ± 0.31	2.27 ± 0.31	1.72 ± 0.25
sample	UCATiO-0	UCATiO-0.5	UCATiO-1	UCATiO-2
uptake (%w/w)	1.43 ± 0.09	2.48 ± 0.32	1.58 ± 0.19	1.70 ± 0.29
dry matter (%w/w)	1.05 ± 0.06	1.78 ± 0.23	1.15 ± 0.14	1.31 ± 0.23
contact angle (deg)	121 ± 1	118 ± 6	101 ± 6	88 ± 3
TWU (%w/w)	0.10 ± 0.00	0.09 ± 0.0	0.11 ± 0.00	0.10 ± 0.02
ΔE^a	5.92 ± 1.24	5.34 ± 0.32	4.40 ± 0.19	3.51 ± 0.40

[a] Data correspond to average values. Standard deviations are also included.

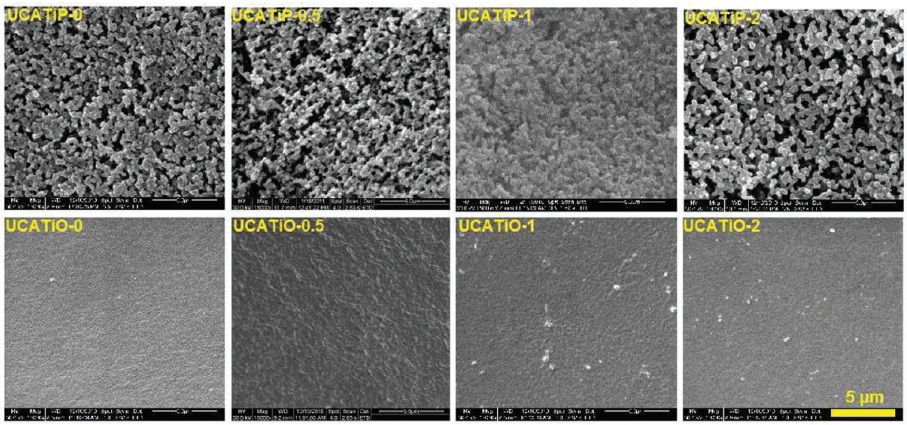

Figure 6. SEM micrographs of the nanocomposite coatings under study.

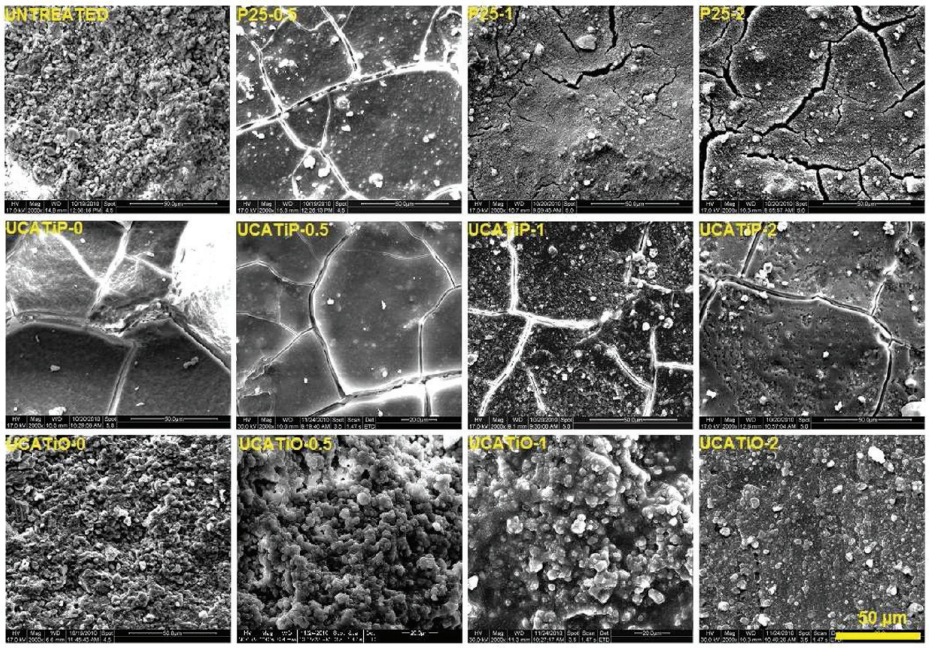

Figure 7. Scanning electron microscopy micrographs of the coatings on the limestone under study.

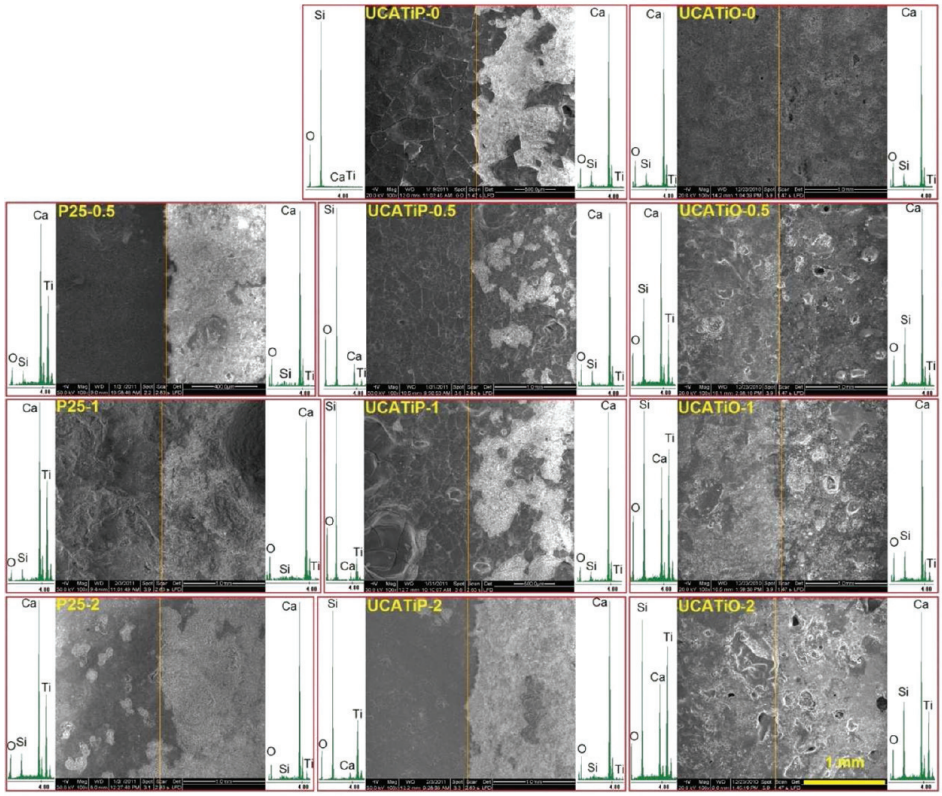

Figure 8. Scanning electron microscopy micrographs of the limestone under study after the peeling test. On the left side of each micrograph, nontested surface is presented, together with the corresponding EDX spectrum. On the right side, the corresponding tested surface and spectrum are presented.

shown by the coatings after the test. However, a significant reduction of TiO_2 content was observed for all the treatments tested. Concerning the calcium content (from limestone), we observe a significant increase in this peak after the peeling test, which confirms that the coating has been largely eliminated from the surface stone. For P25, an increased calcium peak is not

detected because the particles do not create a coating on the surface, and so components of the stone are also detected before the test.

In the case of the UCATiO coatings, differences in morphology between treated and nontreated zones are more difficult to observe. Regarding the EDX results, no significant changes were detected after the tests. These findings confirm that TiO_2 particles have been integrated into the silica matrix, which has been capable of adhering firmly to the stone. We can thus conclude that the inclusion of the photocatalyst in a silica coating is an interesting solution for keeping particles adhered well to the surface, providing long-term wear resistance.

We also investigated whether the mechanical resistance of a stone surface is improved after application of the coatings; this was done by measuring the drilling resistance of the untreated limestone and its treated counterparts. The results obtained are shown in Figure 9.

As expected, P25 deposited on stone does not produce any increased mechanical resistance. Nor do the UCATiP coatings increase the stone's resistance, either. However, in the case of the UCATiO materials, we observe a clear increase in drilling resistance to a depth of 4 mm. The ineffectiveness of the UCATiP coatings for consolidating stone is thought to be associated with the extensive cracking that occurs and with their poor adherence to the stone. In the case of the UCATiO materials, it is obvious that they create a homogeneous, crack-free coating that adheres well to the limestone. Moreover, the results confirm that octylamine is playing a valuable role in enhancing their effectiveness, since silicon-based products are known to be ineffective as consolidants on pure carbonate stones.[41] In a previous study, we found increased drilling resistance for the same limestone by using a silica/PDMS hybrid coating material obtained in presence of *n*-octylamine.[14]

Since the water is the main vehicle carrying the agents of decay, such as soluble salts, microorganisms, etc., that attack building stones, any hydrophilicity induced in the coatings by the P25 particles is undesirable. Therefore, we have also measured water droplet static contact angles (CA) on the surface of stone samples treated with the coatings under study and the untreated counterpart. Results obtained are given in Table 2. As expected, the untreated stone surface shows a hydrophilic behavior with a static CA of 60°. Stone surfaces treated with the P25 dispersions at lower concentrations show a similar droplet CA value as the untreated surface, whereas the P25 dispersion with the highest TiO_2 content induced a significant reduction in the CA value. This finding suggests that, in dispersions with lower concentrations, particles do not completely cover the stone surface and thus, the static CA of the surface is not modified. The low contact angle obtained for the P25-2 coating corroborates the hydrophilic character of P25. In the case of the UCATiP and UCATiO coatings, the hydrophobic behavior may be associated to the presence of some nonhydrolyzed ethoxy groups in the gel coatings under study. Contact angles obtained are slightly lower for the UCATiP coatings than those for UCATiO. We think that discontinuity observed for these coatings could be responsible for this slight reduction. In the case of the UCATiO materials, coatings show a clear hydrophobic behavior, with a linear decrease as the content of TiO_2 particles increases.

Regarding changes observed in contact angle values as TiO_2 content is increased, in the case of UCATiO materials, coatings show the expected linear decrease as the content of titania increases. However, UCATiP contact angles remain constant.

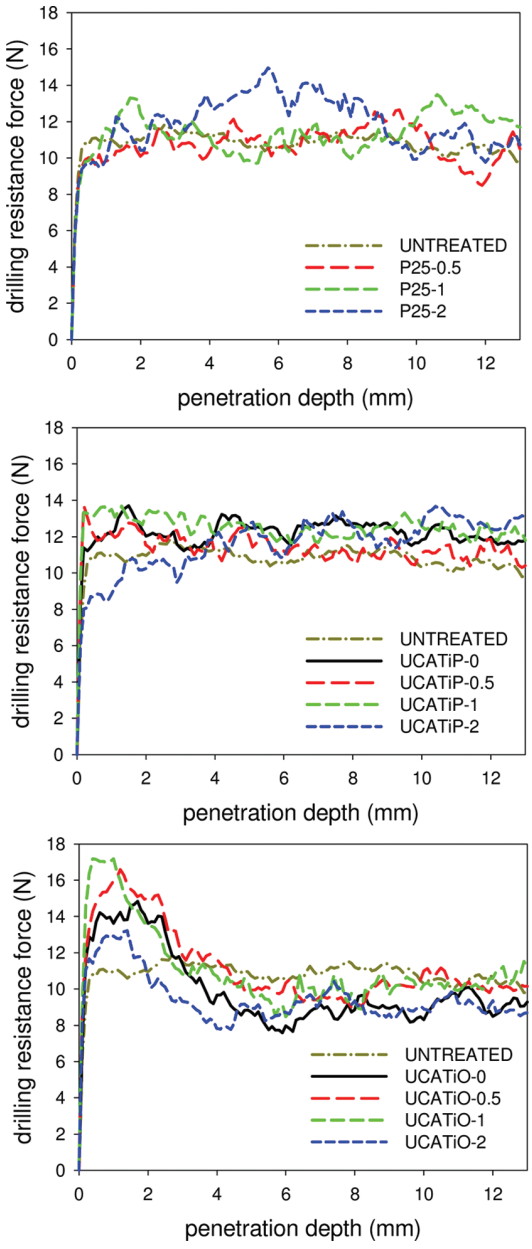

Figure 9. Drilling resistance measurements for the treated limestone under study.

As previously discussed, the UCATiP coatings are composed of titania particles integrated in a dense silica matrix with a low porosity. Thus, the titania particles are shielded by the silica matrix and, consequently, the accessibility of water to the titania is difficult. A similar discussion can be read in the paper by Horiuchi et al.[42] These authors stated that the enhancement of porosity in silica−titania thin films by the employement of structure-directing agents promotes the improvement of hydrophilic properties because of a capillary penetration effect.

We have tested the ability of the coatings to prevent water penetration into the stone, by applying a test of water absorption by capillarity. Total water uptake values (TWU) obtained after 48 h are shown in Table 2. The results confirm the hydrophobic behavior of the UCATiP and UCATiO coatings, since the uptake

values obtained are practically zero and significantly lower than that for the untreated counterpart. Moreover, no significant differences were found for coatings with differing TiO_2 content. These findings demonstrate that the inclusion of a small content of hydrophilic particles, i.e., P25, in a silica coating matrix does not induce capillary water absorption.

Total color difference values (ΔE^*) of the stone after the treatments are shown in Table 2. The P25 dispersions and UCATiP produced small values of ΔE^*, below the perception threshold ($\Delta E^*<3$).[28] The UCATiO coatings produced slightly greater changes in color, which were progressively reduced as TiO_2 content increases. We associate the color change with the effect due to *n*-octylamine, which imparts a slightly yellowish color to the white limestone tested. This disadvantage is progressively reduced as P25 content is raised, since the titania particles have a whitening effect.

Lastly and most importantly, we have investigated the self-cleaning properties of the coatings on the limestone tested by carrying out a photodegradation test of stains deposited previously on the stone surface. Methylene blue (MB) was used as the staining agent. The evolution of total color differences under UV light with the time was recorded and results are shown in Figure 10 for the three sets of coatings under study. Of all of the materials tested, the P25 dispersions present the most rapid bleaching of the MB stains. In the first 6 h, the stain is almost completely degraded (88% of the total change is observed after this period of time has elapsed). Comparing the performance of the various P25 dispersions, a modest increase in self-cleaning activity is found in line with higher TiO_2 content; the final ΔE^* values are 15, 9, and 7 for P25 content of 0.5, 1 and 2%, respectively.

In the case of the untreated stone, the final ΔE^* value reached is 30, after more than 800 h of exposure, corresponding to a "natural" reduction of 25%. MB bleaching under visible/UV light has been reported previously and this bleaching has been associated with a weak absorption of light undergone by the dye in the 350−520 nm range.[43,44] Thus, we think the degradation of MB on untreated limestone is induced by the light absorbed during its long exposure (around 800 h) to the UV lamp.

For the two series of nanocomposites materials, the MB degradation rate is slower than that presented by the P25 dispersions. This lower degradation rate can be explained by the low TiO_2 content in all the coatings prepared (a maximum of 2%). For all of the materials synthesized, two different rates of change can be clearly distinguished in the degradation profiles. Very rapid MB bleaching occurs in the first 7−12 h, accounting for around 80% of the total color variation recorded. Next, a slower rate of degradation is observed over the longer term. Again, small differences in ΔE^* values are found for the differing TiO_2 concentrations tested. These differences are appreciated mainly in the initial rate of degradation in which the coatings with the higher P25 content (1% and 2%) show larger falls in ΔE^* value. Considering the performance of the nanocomposites coatings prepared without TiO_2 particles, we also observe a bleaching effect under UV exposure. A degradation profile similar to that corresponding to the slower, second-stage rate for titania/silica composites is now observed.

The two findings reported above clearly confirm that the photocatalytic action of the titania particles produces most of the total degradation effect on the stain in the first few hours of exposure (the first part of the curve). We think that the second stage with a much slower rate of degradation may be caused by

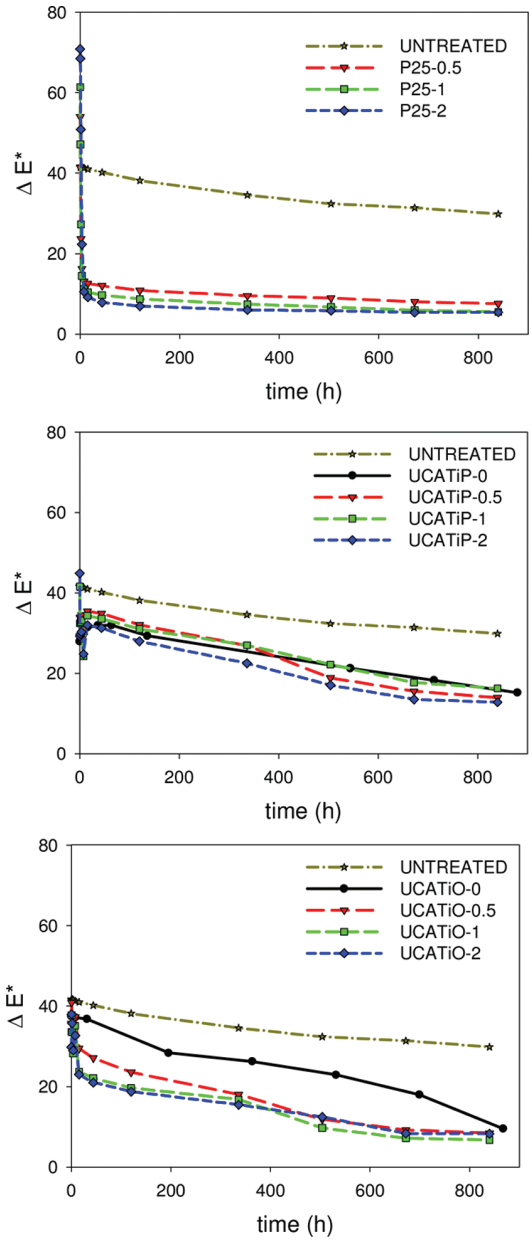

Figure 10. Evolution of total color difference (for methylene blue stains) on treated and untreated samples of limestone.

the silica/titania coating reducing the capacity of the MB to penetrate into the limestone pore structure. The greater the proportion of MB on the surface of the coated limestone, the greater the proportional degradation by the bleaching effect of the UV light absorbed. Variations found in the degradation kinetics between the UCATiP-0 and UCATiO-0 coatings corroborate our hypothesis, since the material with lower porosity (UCATiP-0), which was subsequently shown to be associated with lower penetration of MB into the pore structure of the limestone, induces a more rapid degradation than the UCATiO-0 coating.

Comparing the performance of the two series of gels, we found that the UCATiO gels show greater self-cleaning activity, since their rate of degradation in the rapid first stage is slightly higher and the final ΔE^* values produced in the longer term are lower.

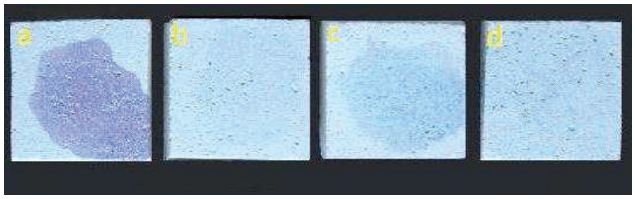

Figure 11. Photographs after the self-cleaning test of the surfaces of stone samples treated with the coatings under study, with 2% w/v TiO_2 content. (a) Untreated stone; (b) Stone treated with P25-2; (c) Stone treated with UCATiP-2; (d) Stone treated with UCATiO-2. The samples were previously stained with Methylene Blue and then irradiated with UV light (λ = 365 nm) for more than 800 h.

The UCATiP nanocomposites present final ΔE^* values of ~15, whereas the UCATiO materials show ΔE^* values of ~7. This last final value is similar to that obtained with the P25 dispersions

Figure 11 shows photographs of the stone surfaces under study after completion of the test. The samples illustrated are the stained limestone surfaces untreated and treated with the three different coatings with the highest TiO_2 content (2%). Photographs corresponding to the other coatings evaluated are shown as Supporting Information. It can be observed that the stone surface treated with the UCATiP-2 coating shows the lowest degradation of the MB stain. The degree of change in color induced by the P25-2 and UCATiO-2 nanocomposite coatings is similar.

The greater self-cleaning effect produced by the UCATiO coatings is explained by their higher porosity and the larger pore size of the gel network. As previous authors have reported,[15,16] the photocatalytic degradation of MB is clearly enhanced by the addition of TiO_2 particles to a silica mesoporous structure, in comparison with the effect observed when the particles are integrated in a dense microporous matrix. This enhancement effect was explained by these authors in terms of the increased BET surface area, which accelerates the diffusion of MB toward the reaction sites (i.e., toward the titania particles). The authors of this study have also reported previously that the presence of mesopores also assists rapid diffusion. As discussed earlier in this work, the UCATiO coatings create a pore structure in the gel network completely different from that corresponding to the UCATiP materials. According to the model proposed on the basis of the HAADF-STEM images (Figure 4), the UCATiO gels create a field of silica and titania particles with numerous voids between particles, making the sites with photocatalytic activity, the titania particles, much more accessible for the MB molecules. In the case of the UCATiP material, however, a dense and microporous silica gel with titania particles embedded is clearly observed; in this material, the photocatalytic sites will now be less accessible to the MB.

From these results, we conclude that the addition of titania particles to a silica mesoporous structure created using a surfactant as template creates a material with effective photocatalytic activity, and the MB bleaching obtained is similar to that obtained by the P25 aqueous dispersion. As a final note, it can be confirmed that this new nanocomposite coating developed in our laboratory will become available as a commercial product under an exploitation patent.[45]

CONCLUSIONS

An effective new synthesis method has been developed for producing titania-silica nanocomposite coatings for stone conservation with self-cleaning application. Composite coatings are prepared by dispersion of TiO_2 nanoparticles in a mesoporous silica matrix in the presence of a nonionic surfactant (*n*-octylamine). This surfactant acts in several distinctive ways in the synthesis: (1) it prevents the unwanted aggregation of titania particles in the starting sol; (2) it acts as a basic catalyst of the sol−gel transition; and (3) by serving as a template, it increases the pore size of the final material, thus preventing unwanted cracking. Moreover, the surfactant can be removed very simply by ambient air drying; therefore the user will be able to apply the starting sol, in situ, on the stone of the building or structure to be protected. Sol−gel transition occurs spontaneously, producing an effective nanocomposite coating on the building stone.

We have demonstrated that these new coating materials are capable of the following: (1) adhering firmly to the stone surface to ensure that the conservation and self-cleaning properties of the coating have a long-term effect; (2) increasing the mechanical resistance of the stone; (3) providing proven self-cleaning properties to the stone coating; and (4) providing hydrophobic properties to the coating. We have also shown that commercial titania particles applied as a water dispersion on stone do not create an effective coating that adheres to the substratum; therefore, such dispersions are of no practical use for protecting stonework.

Lastly, we have characterized the pore structure of the new material, and have proposed a model describing how titania particles are dispersed in a silica matrix composed of silica particles. We have also demonstrated that the mesoporous structure thus created enhances the self-cleaning properties of the material, compared with the effect produced by a material comprising similar particles embedded in a microporous silica matrix.

ASSOCIATED CONTENT

Supporting Information. Nitrogen adsorption isotherms and BJH pore size distribution for P25 particles under study; FTIR spectra for TES40 after an elapsed time of 8 months; Photographs of total color variation of the surfaces of stone samples treated with the coatings under study. The samples were previously stained with methylene blue and then irradiated with UV light (λ = 365 nm) for more than 800 h. This material is available free of charge via the Internet at http://pubs.acs.org.

AUTHOR INFORMATION

Corresponding Author

*Phone: (34)956016331; Fax: (34)956016471; E-mail: mariajesus.mosquera@uca.es.

ACKNOWLEDGMENT

We are grateful for financial support from the Spanish government/FEDER-EU (Project MAT2010-16206), and the government of Andalusia (project TEP-6386 and Group TEP-243). We also thank the company Tino Stone S.A. for financial support under a research contract. L.P. thanks the Fundação Ciência e Tecnologia for his predoctoral grant (SFRH/BD/43492/2008). We also thank Lidia Esther Chinchilla for assistance with the HAADF-STEM micrographs. Finally, we express our gratitude to Evonik for supplying P25 particles.

REFERENCES

(1) Fujishima, A.; Rao, T.; Tryk, D. *J. Photochem. Photobiol. C* **2000**, *1*, 1–21.
(2) Hashimoto, K.; Irie, H.; Fujishima, A. *AAPPS Bull.* **2007**, *17*, 12–28.
(3) Fujishima, A.; Honda, K. *Nature* **1972**, *238*, 37–38.
(4) Mills, A.; Hill, G.; Bhopal, S.; Parkin, I. P.; ÓNeill, S. A. *J. Photochem. Photobiol. A* **2003**, *160*, 185–194.
(5) Vicente, J. P.; Gacoin, T; Barboux, P.; Boilot, J. P.; Rondet, M.; Gueneau, L. *Int. J. Photoenergy* **2003**, *5*, 95–98.
(6) Puzenat, E.; Pichat, P. *J. Photochem. Photobiol. A* **2003**, *160*, 127–133.
(7) Aprile, C.; Corma, A.; García, H. *Phys. Chem. Chem. Phys.* **2008**, *10*, 769–783.
(8) Álvaro, M.; Aprile, C.; Benítez, M.; Carbonell, E.; García, H. *J. Phys. Chem. B* **2006**, *110*, 6661–6665.
(9) Chen, J.; Poon, C. S. *Build. Environ.* **2009**, *44*, 1899–1906.
(10) Poulios, I.; Spathis, P.; Grigoriadou, A.; Delidou, K.; Tsoumparis, P. *J. Environ. Sci. Health A* **1999**, *34*, 1455–1471.
(11) Rao, K.; Subrahmanyam, M.; Boule, P. *Appl. Catal. B: Environ.* **2004**, *49*, 239–249.
(12) Mosquera, M. J.; de los Santos, D. M.; Montes, A.; Valdez-Castro, L. *Langmuir* **2008**, *24*, 2772–2778.
(13) Mosquera, M. J.; De los Santos, D.; Rivas, T. *Langmuir* **2010**, *26*, 6737–6745.
(14) Illescas, J. F.; Mosquera, M. J. *J. Phys. Chem. C* **2011**, *115*, 14624−14634.
(15) Suzuki, N.; Jiang, X.; Radhakrishnan, L.; Takai, K.; Shimasaki, K.; Huang, Y. T.; Miyamoto, N.; Yamauchi, Y. *Bull. Chem. Soc. Jpn.* **2011**, *84*, 812–817.
(16) Yamauchi, Y.; Takeuchi, F.; Todoroki, S.; Sakka, Y.; Inoue, S. *Chem. Lett.* **2008**, *37*, 72–73.
(17) Crepaldi, E. L.; de Soler-Illia, G. J.; Grosso, D.; Cagnol, F.; Ribot, F.; Sanchez, C. *J. Am. Chem. Soc.* **2003**, *125*, 9770–9786.
(18) Reddy, E. P.; Sun, B.; Smirniotis, P. G. *J. Phys. Chem. B* **2004**, *108*, 17198–17205.
(19) López-Muñoz, M. J.; van Grieken, R.; Aguado, J.; Marugán, J. *Catal. Today* **2005**, *101*, 307–314.
(20) Allain, E; Besson, S.; Durand, C.; Moreau, M.; Gacoin, T.; Boilot, J. P. *Adv. Funct. Mater.* **2007**, *17*, 549–554.
(21) Inumaru, K.; Yasui, M.; Kasahara, T.; Yamaguchi, K.; Yasuda, A.; Yamanaka, S. *J. Mater. Chem.* **2011**, *21*, 12117−12125.
(22) Uchiyama, H.; Suzuki, K.; Oaki, Y.; Imai, H. *Mater. Sci. Eng., B* **2005**, *123*, 248–251.
(23) Shibata, H.; Ohkubo, T.; Kohno, H.; Rangsunvigit, P.; Sakai, H.; Abe, M. *J. Photochem. Photobiol. A* **2006**, *181*, 357–362.
(24) Inumaru, K.; Kasahara, T.; Yasui, M.; Yamanaka, S. *Chem. Commun.* **2005**, 2131–2133.
(25) Ling, L.; Phang, I.; Vancso, G.; Huskens, J.; Reinhoudt, D. *Langmuir* **2009**, *25*, 3260–3263.
(26) ISO 2409; Paints and varnishes. Cross-cut test. ISO, 2007.
(27) UNE-EN 1925; Natural Stone test methods. Determination of water absorption coefficient by capillarity. *AENOR*, 1999.
(28) Berns, R. S. *Billmeyer and Saltzman's Principles of Color Technology*; Wiley-Interscience: New York, 2000.
(29) Tatsuma, T.; Tachibana, S.; Tetsuya, M.; Tryk, D.; Fujishima, A. *J. Phys. Chem. B* **1999**, *103*, 8033–8035.
(30) ISO 10678; Fine ceramics (advanced ceramics, advanced technical ceramics); Determination of photocatalytic acitivity of surfaces in an aqueous medium by degradation of methylene blue. *ISO*, 2010.
(31) Mikulasek, P.; Wakeman, R. J.; Marchant, J. Q. *Chem. Eng. J.* **1997**, *67*, 97–102.
(32) Widegren, J.; Bergström, L. *J. Am. Ceram. Soc.* **2002**, *85*, 523–528.
(33) Kosmulski, M.; Prochniak, P.; Rosenholm, J. B. *J. Phys. Chem. C* **2009**, *113*, 12806–12810.
(34) Mosquera, M. J.; de los Santos, D. M.; Valdez-Castro, L.; Esquivias, L. *J. Non-Cryst. Solids* **2008**, *354*, 645–650.
(35) Li, Y.; Kim., S. J. *J. Phys. Chem. B* **2005**, *109*, 12309–12315.
(36) Kruk, M.; Jaroniec, M. *Chem. Mater.* **2001**, *13*, 3169–3183.
(37) Barret, E. P.; Joyner, L. G.; Halenda, P. P. *J. Am. Chem. Soc.* **1951**, *73*, 373–380.
(38) Tellez, L.; Rubio, J.; Rubio, F.; Morales, E.; Oteo, J. L. *J. Mater. Sci.* **2003**, *38*, 1773–1780.
(39) Fidalgo, A.; Ilharco, L. M. *J. Non-Cryst. Solids* **2004**, *348*, 128–137.
(40) Whang, C. M.; Yeo, S. C.; Kim, Y. H. *Bull. Korean Chem. Soc.* **2001**, *22*, 1366–1370.
(41) Ferreira, A. P.; Delgado, J. *J. Cultural Heritage* **2008**, *9*, 38–53.
(42) Horiuchi, Y.; Ura, H.; Kamegawa, T.; Mori, K.; Yamashita, H. *J. Phys. Chem. C* **2011**, *115*, 15410–15415.
(43) Mills, A.; Wang, J. *J. Photochem. Photobiol. A* **1999**, *127*, 123–134.
(44) Mrowetz, M.; Balcerski, W.; Colussi, A. J.; Hoffmann, M. R. *J. Phys. Chem B* **2004**, *108*, 17269–17273.
(45) Mosquera, M. J.; Pinho, L. Spanish Patent No. P201100741. Priority data: June 24, 2011.

Supporting Information

Titania-silica Nanocomposite Photocatalysts with Application in Stone Self-Cleaning

*Luís Pinho, María J. Mosquera**

Departamento de Química-Física, Facultad de Ciencias, Universidad de Cádiz, 11510 Puerto Real (Cádiz), Spain

*corresponding author: e-mail: mariajesus.mosquera@uca.es. Phone: (34)956016331. Fax: (34)956016471

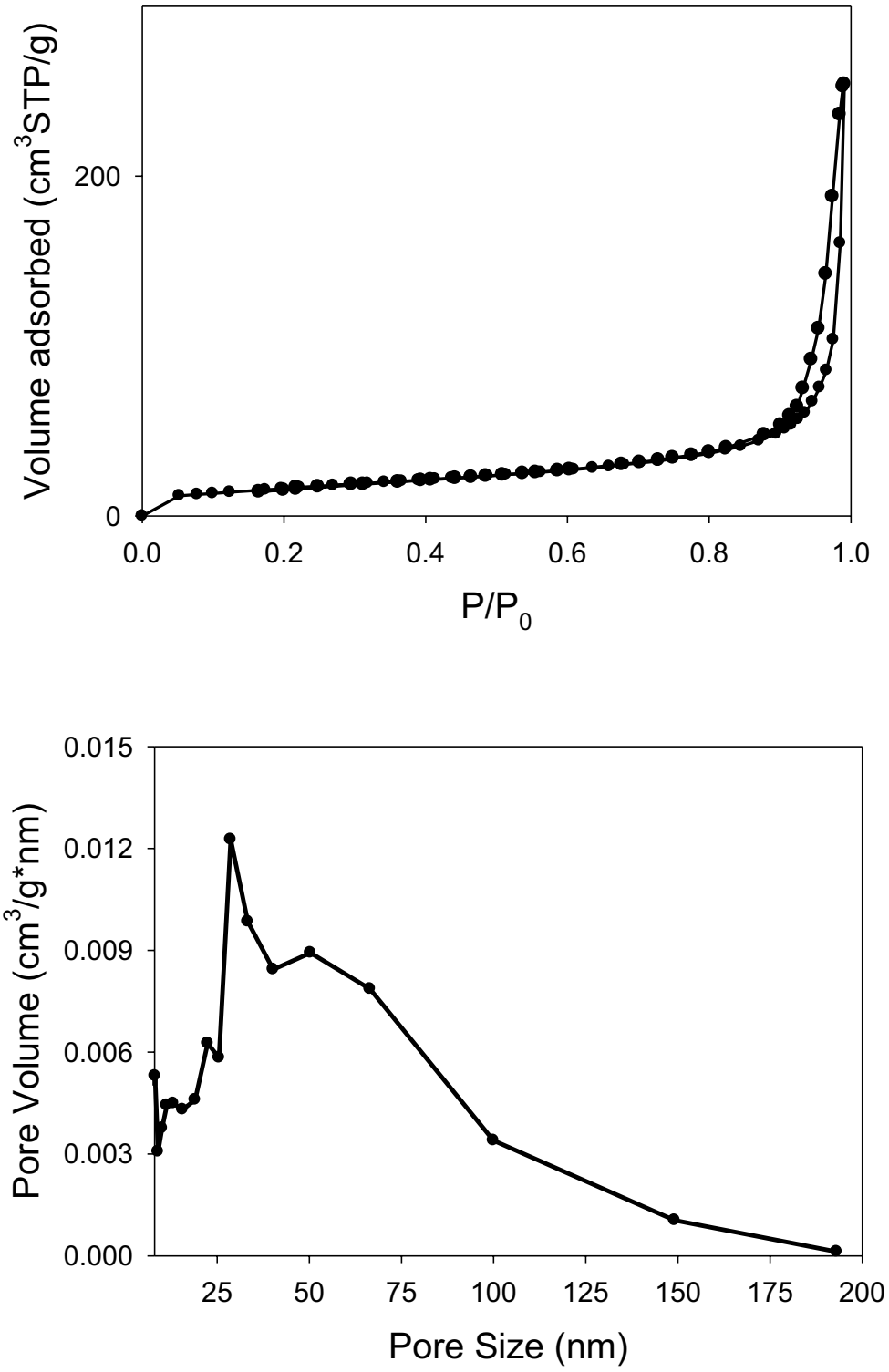

Figure 1. Nitrogen adsorption isotherms and BJH pore size distribution for P25 particles under study.

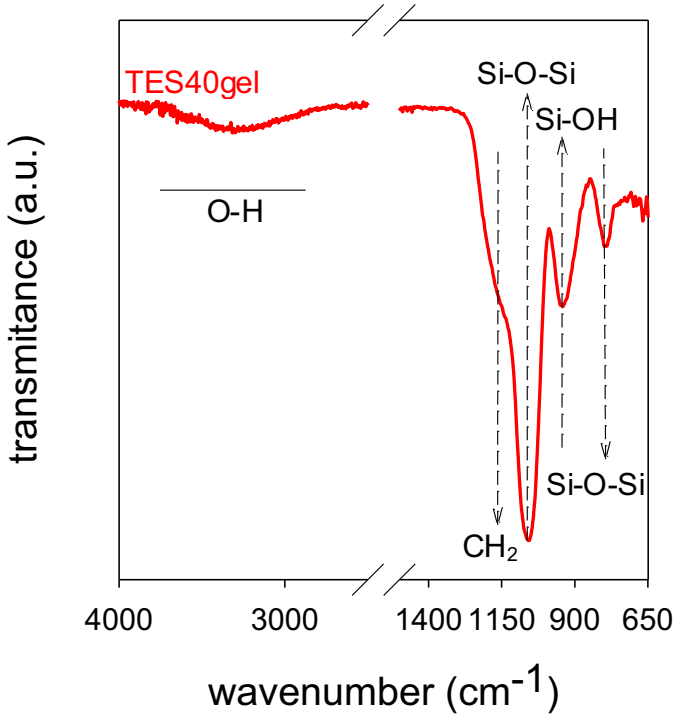

Figure 2. FTIR spectrum for TES40 after an elapsed time of 8 months.

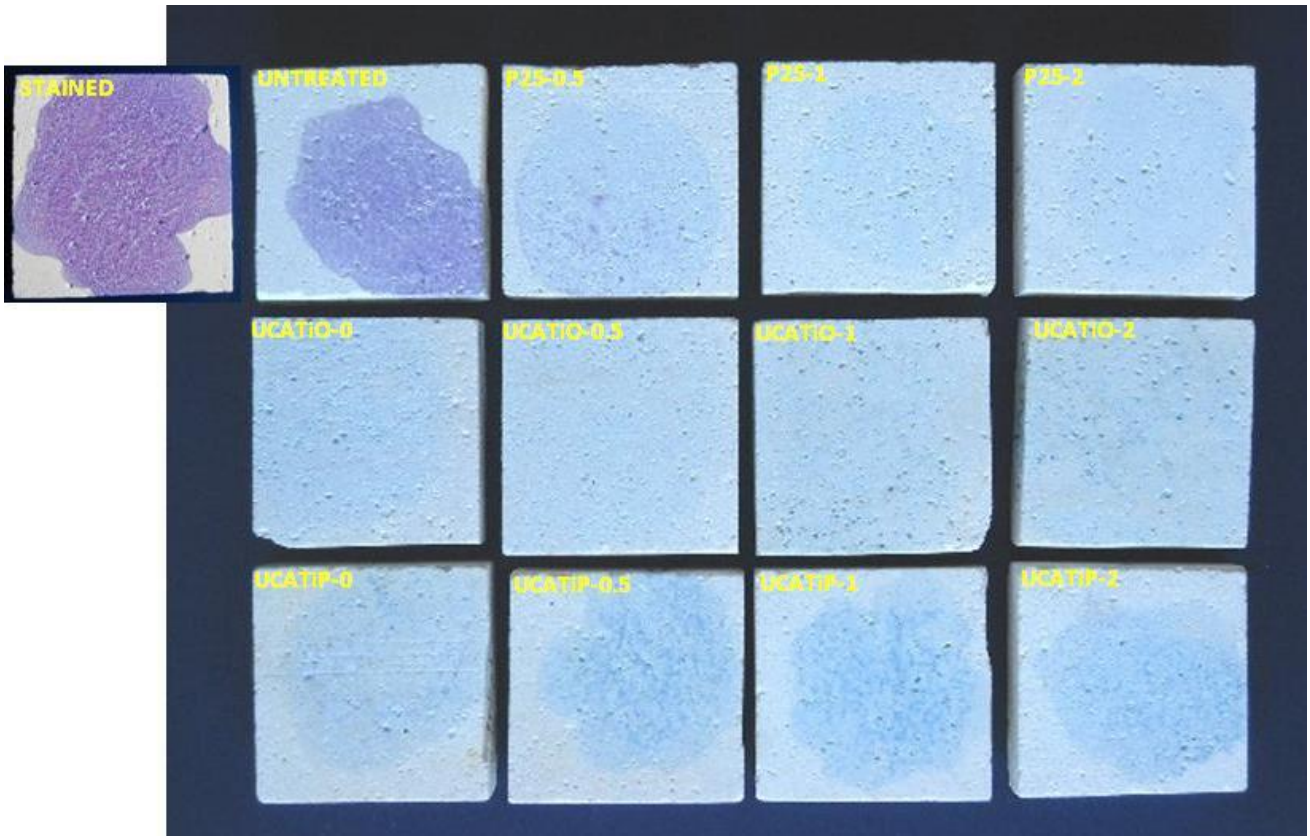

Figure 3. Images of the surfaces of stone samples treated with the coatings under study. The samples were previously stained with methylene blue and irradiated with UV light (λ=365 nm).

4.2. 2D and 3D characterization of a surfactant-synthesized TiO_2-SiO_2 mesoporous photocatalyst obtained at ambient temperature

Sent to Physical Chemistry Chemical Physics

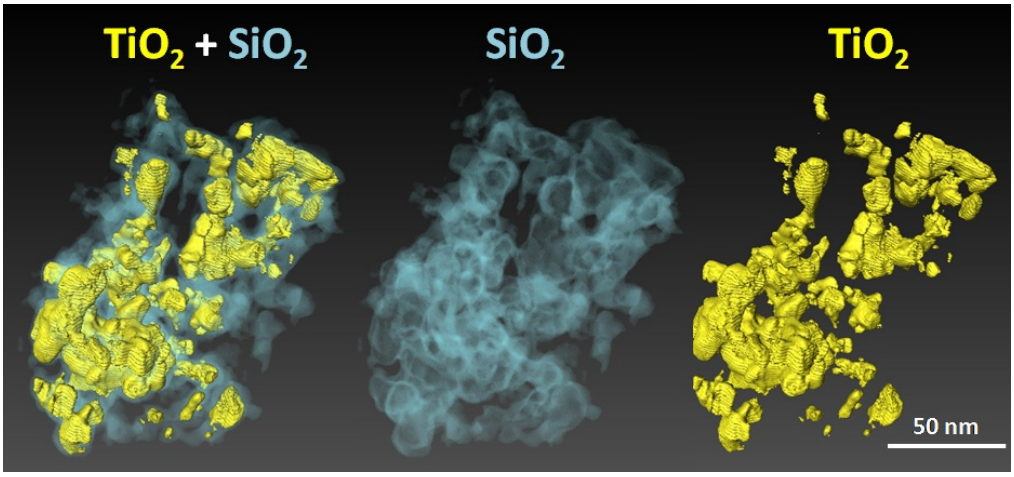

- We characterize the 2D and 3D structure of a novel surfactant-synthesized TiO_2-SiO_2 mesoporous photocatalyst.
- This provides insight into the material fine structure and spatial distribution of each component.

Cite this: DOI: 10.1039/c0xx00000x

www.rsc.org/xxxxxx

ARTICLE TYPE

2D and 3D characterization of a surfactant-synthesized TiO_2-SiO_2 mesoporous photocatalyst obtained at ambient temperature

Luís Pinho,[a] Juan-Carlos Hernández-Garrido[b], Juan J. Calvino[b] and Maria J. Mosquera*[a]

Received (in XXX, XXX) Xth XXXXXXXXX 20XX, Accepted Xth XXXXXXXXX 20XX

DOI: 10.1039/b000000x

A mesoporous TiO_2-SiO_2 nanocomposite photocatalyst has been prepared from TiO_2 nanoparticles and ethoxysilane oligomers in the presence of a non-ionic surfactant (*n*-octylamine). The 2D and 3D structure properties of the resulting nanomaterial are described. The use of 3D techniques, particularly HAADF-STEM electron tomography, together with 3D reconstructions and atomic force microscopy, provide insight into the fine structure of these materials. We find that n-octylamine creates a mesoporous silica structure in which titania nanoparticles are embedded, and that some of the titania is retained on the outer surface of the material. Rapid photodegradation of methylene blue dye is facilitated, due the synergistic effect of: (1) its adsorption into the composite mesoporous structure, and (2) its photodegradation by the superficial TiO_2.

Introduction

The remarkable performance of TiO_2-SiO_2 mesoporous composites in oxidation reactions has long attracted the attention of many researchers in the field of heterogeneous catalysis.[1] Their application as a photocatalyst has also ensured a lot of attention because, under UV light irradiation, these materials present photocatalytic and super-hydrophilic properties of TiO_2.[2] These composites offer numerous advantages since they combine TiO_2, which is an *n*-type semiconductor and active catalytic support, and SiO_2, which provides thermal stability and gives mechanical strength to the material.[3]

In the synthesis of these nanomaterials, nanocrystalline photoactive TiO_2 can be obtained by using molecular precursors or colloidal nanoparticles. However, some difficulties arise when TiO_2 nanoparticles are formed *in situ*, within the porous matrix of the material: the achievable TiO_2 loading is quite low, and the formation of TiO_2 photoactive crystals through a calcination process is severely limited by the low heating temperature imposed by some substrates. Improving the performance of TiO_2-SiO_2 nanocomposites represents an interesting potential alternative.[4]

Regarding the SiO_2 binder, it is important that it does not block the diffusion pathways between the organic species to be degraded and the radicals generated at the surface of the oxide.[4] In this context, these composites can assume several configurations such as zeolite,[5] HMS,[6] MCM,[7] SBA,[8] or MCF.[9]

The physical connection between titania and silica binder provides mechanical reinforcement of the substrate.[3] As Rolison et al. reported,[10] composite titania-silica materials can be obtained by mixing silica sols with solids such as titania nanoparticles, where silica acts as a "nanoglue" and facilitates molecular access to the titania photocatalyst inside the material.

Our research group has developed several one-step routes for producing mesoporous silica, organic-inorganic hybrid ormosils and even mesoporous silica-titania composites.[11-14] We produce crack-free mesoporous xerogels at ambient temperature by mixing n-octylamine and oligomeric ethoxysilane. *N*-octylamine acts as a sol-gel catalyst and as a structure-directing agent. Another advantage of this process is that there is no need for the addition of any volatile organic compounds (VOCs).[15]

In the case of the silica-titania nanocomposite,[14] we integrate pre-formed colloidal and crystalline titanium dioxide nanoparticles into an effective silica matrix that is capable of eliminating pollutants by photo-oxidation. The great advantage of this process is that heating is not required to remove the surfactant afterwards. Therefore, our sols are particularly suitable for applications where the substrate is thermally sensitive, and simple deposition methods (such as spraying) can be used, and are thus less costly than alternatives. The process is so simple that the sol-gel transition can even be produced *in situ* on a building stone or other material exposed outdoors. In these products, n-octylamine plays two additional roles: (1) it stabilizes the particle dispersion during sol-gel transition[16] (through pH increase and adsorption of the surfactant on the TiO_2 surface); and (2) it enhances the photocatalytic activity by creating a mesoporous nanocomposite.[14]

With respect to the second role referred to above, it is well-known that an important requirement for improvement of TiO_2-SiO_2 photocatalytic activity and sorption properties consists in finding the optimum combination of textural parameters such as surface area, pore size and volume, producing effective access to the titania photocatalyst.[4,9] However, the detailed surface

disposition and nanostructure of the TiO_2-SiO_2 system are not completely understood. Conventional electron microscopy images, obtained by means of the detection of secondary, back-scattered or transmitted electrons after interaction with the materials, provide only limited information about the structure of the nanomaterials.[10,14,17] The conventional electron micrographs can often be ambiguous because only 2D projections of the objects are recorded. Electron tomography, however, provides 3D projections, and this technique has proved to be a powerful tool enabling a more complete 3D characterization of mesostructured materials.[18] In particular, electron tomography has been used successfully to characterize nanomaterials including SiO_2[19,20] and TiO_2[21,22] as well as TiO_2-SiO_2 composites.[9]

Of all the possible imaging modes available for electron tomography, those based on high angle annular dark field (HAADF) imaging in the scanning transmission electron microscope (STEM) are the most suited to reveal the 3D structure of various kinds of nanomaterial because they reduce the contribution of diffraction contrast to image artifacts.[9,19,23-25] Another advantage associated with the use of a HAADF detector is that it captures electrons that undergo high-angle scattering, and the signal is approximately proportional to Z^2, where Z is the atomic number. It provides contrast sensitive to compositional changes, and allows the identification of components with different atomic numbers in nanocomposite materials.[26]

In this work, we synthesize a TiO_2-SiO_2nanocomposite using n-octylamine as catalyst and structure-directing agent. Since textural parameters and surface chemistry have a direct relationship with the photocatalytic effectiveness, we investigate the 3D-structure of this material using electron tomography from HAADF images obtained in a STEM. Use of the HAADF detector has also enabled us to locate very precisely the position of silica and titania nanoparticles in the nanocomposite, and to identify the interaction between the two oxides.

We have used a different technique, high-resolution transmission electron microscopy (HREM), with the object of obtaining images with a high diffraction contrast. These were then used to obtain better insights into the crystalline nature of the TiO_2.

In addition, since the surface morphology of the composites is important for their photocatalytic activity, we have obtained 2D and 3D images of the surface using amplitude-modulated atomic force microscopy (AM-AFM). The quality of these images is enhanced by the movement of the probe tip in the vertical Z axis. The analysis of the results provides detailed topographic information of the material's surface such as particle height profiles and distribution, and rugosity, at the nanometric scale.[27,28]

Finally, we characterize the degradation kinetics of methylene blue in aqueous phase, in the presence of this nanomaterial, under UV light and in dark conditions, in order to evaluate its photocatalytic activity.

Experimental Section

Synthesis

UCATiO was prepared from a starting sol containing an ethoxysilane oligomer TES40 WN (TES40, WackerChemie AG, GmbH), *n*-octylamine (Aldrich) and titania nanoparticles (AEROXIDE® TiO_2 P25, Evonik). According to the technical data sheet, TES40 is an ethyl silicate providing approximately 41% of silica when hydrolysis is complete; it also contains many hydrolysable ethoxy groups. According to the supplier, P25 has an average particle size of 21 nm and a specific surface area (BET) of 50 ± 15 $m^2.g^{-1}$. All of the reagents were used as received from the supplier.

In this synthesis, we mixed TES40 with P25 nanoparticles in the presence of *n*-octylamine, under ultrasonic agitation (125 $W{\cdot}cm^{-3}$, for 10 minutes). The proportions of *n*-octylamine and P25 to TES40 were 0.36% v/v and 4% w/v, respectively. The formulations have been designated as UCA via the procedure devised at the University of Cadiz, followed by Ti (for TiO_2) and O (for n-octylamine). To investigate the effect of TiO_2 nanoparticles on the topography of the material under study, we also prepared a control product following the same procedure but excluding TiO_2 nanoparticles. This product was denoted as UCAO.

The two sols synthesized were cast in plastic Petri dishes. Gelation and drying occurred by simple exposure of the cast sols to laboratory conditions (at relative humidity of 60% and temperature of 20ºC) until reaching a constant weight.

Nanomaterials characterization.

The materials were visualized by scanning electron microscopy (SEM) using a FEI Sirion with a field emission filament operating at 5kV. This instrument has a resolution of 1.5 nm, and is equipped with a 'through-the-lens' detector (TLD) working in ultra-high resolution (UHR) mode.

The surface of the photocatalyst was also investigated using atomic force microscopy (AFM, Nanotec Electrónica S.L.) operated in tapping mode. Roughness measurements were performed on 1x 1 μm^2 scans.

Textural characterization was performed by N_2 physisorption at 77 K, using a Quantchrome Autosorb IQ. The isotherms obtained were used to calculate pore volume and BET surface area of the powdered nanomaterials. The adsorption data were analyzed using a hybrid NLDFT approach[29] that allows quantification of both micro- and meso-pores. The hybrid NLDFT method also allows the calculation of the pore size distribution of materials containing pores of different geometry.

Transmission electron microscopy studies were performed in a JEOL 2010F TEM/STEM microscope, operating at 200 kV with 0.19 nm spatial resolution. This instrument is equipped with a JEOL high angle annular dark field (HAADF) detector and an Oxford X-Max Silicon Drift X-Ray Energy Dispersive Spectroscopy (XEDS) detector, enabling the acquisition of STEM images and compositional analysis either by spot mode or elemental mapping using a 0.5 nm electron probe. Samples were prepared by depositing a small amount of the powders directly onto Lacey-Carbon coated Cu grids. Both TEM and HAADF images were obtained.

3D characterization by electron tomography was performed by acquiring a tilt-series in HAADF-STEM mode, using an ultra-narrow gap Fischione 2030 holder in the tilt range of -64º to +62º, with images recorded every 2º. The following TEM parameters were controlled during the acquisition of the tilt series of

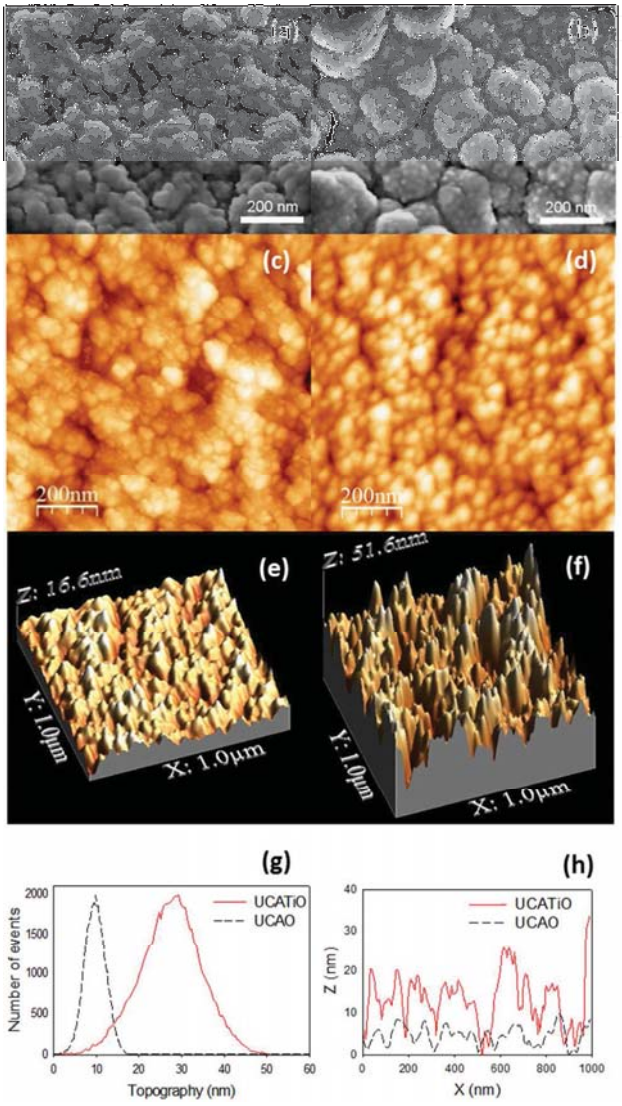

Fig. 1 Scanning electron microscopy images (a) & (b); 2D-AFM (c) & (d); 3D- AFM (e) & (f) of UCAO and UCATiO, respectively. Particle height distributions (Z-axis) (g) and typical roughness profiles (h) for UCAO and UCATiO are also presented.

projections: defocus, image shift, specimen tilt, and the condenser lens astigmatism. Once the acquisition of the tilt series was completed, images were spatially aligned by a cross-correlation algorithm using Inspect 3D software (FEI, The Netherlands), and 3D reconstructions were achieved using a simultaneous iterative reconstruction algorithm (SIRT) of consecutive 2D slices. To visualize a 3D model of the reconstruction, AMIRA 3.1 (Mercury Computer Systems) software was used to segment the data set manually, slice by slice, into discrete subvolumes corresponding to the silica support and TiO_2 agglomerates. The contrast in each slice was sufficient to identify each component of the reconstruction by eye, and to enable the support and agglomerates to be surface rendered; this allows easy and informative visualization and allows the surface area and volumes of the nanoparticles and support to be determined.

We have also investigated the photocatalytic activity of UCATiO by measuring the absorbance evolution with time of a methylene blue aqueous solution left in contact with this material under UV radiation. A quantity of 1 g of the photocatalyst was dispersed in 50 mL of a methylene blue 0.05 mM solution in a capped glass flask with a 5 mm diameter. The mixture was strongly stirred before starting an irradiation process of up to 30 min with a Velleman E27 UV-light bulb (15W), under constant magnetic stirring and without any optical filter. Volumes of 3 mL of the solution were sampled several times by opening the cap. The sampled solutions were centrifuged and the absorbance was measured with an ATI Unicam UV4 ultraviolet-visible spectrophotometer. After the measurement, the measured volume was returned to the glass flask. The photodegradation of the methylene blue solution without any material present was also carried out for comparison purposes. We also measured the absorbance evolution of MB left in contact with UCAO and UCATiO in dark conditions, in order to evaluate the MB adsorption obtained for these two materials.

Results and Discussion

Surface characterization

SEM micrographs of UCAO and its corresponding counterpart with TiO_2 nanoparticles (UCATiO) are shown in images 1a and 1b, respectively. The UCAO product consists of a configuration of silica nanoparticles of nearly uniform pore size. Previously, we have obtained a similar structure for synthesized silica materials obtained in presence of n-octylamine.[15,30] Silica nanomaterials with similar structures have been obtained by other authors in the presence of formamide,[31] ammonia[32] or octylamine.[33] Bogush and Zukoski[32] developed an aggregative growth model to explain the formation of these uniform silica nanoparticles in the presence of a basic medium, such as ammonia, in which the rate of condensation is faster than the hydrolysis. In our materials, we also speculate that formation of uniform silica nanoparticles occurs by an aggregation mechanism.[15] We think n-octylamine acts as a basic catalyst, promoting the condensation of silica oligomers present in the starting sol. The UCATiO product (Fig. 1b) also consisted of nanoparticles but of larger size.

In our previous papers,[14,15,30] the SEM images were obtained at lower magnifications. In this work the use of an ultra-high resolution detector allows us to confirm the previous observations and discriminate better the differences in the morphology of the two materials studied. UCAO forms a particulate material with a smaller and more homogeneous particle size (around 90 nm) than those corresponding to UCATiO (around 150 nm). In both cases, the aggregation of smaller nanoparticles can be observed, thus confirming the mechanism of growth proposed. We think that UCATiO aggregates (Fig. 1b) show higher average diameters due to the presence of TiO_2 nanoparticles mixed with the silica nanoparticles in the aggregates created. It is corroborated by the grains observed on the surface of the UCATiO aggregates, which may be generated by P25 nanoparticles. These grains are not visible in UCAO aggregates (Fig. 1a). Kontos et al.[28] also observed by SEM the agglomeration of titania nanoparticles in grains for hydrothermally treated pure TiO_2 films; these authors also attributed this finding to an aggregation phenomenon.

Table 1 RMS and average height values found for UCAO and UCATiO.

Topographic parameters (nm)	UCAO	UCATiO
RMS Roughness	2.453	7.229
Average height	9.79	27.72

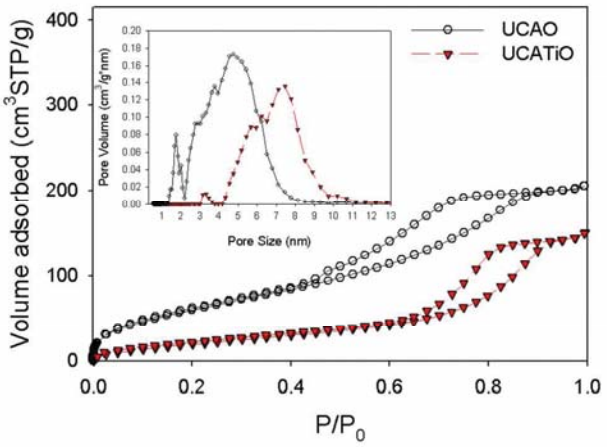

Fig. 2 Nitrogen Adsorption-desorption isotherms for UCAO and UCATiO. NLDFT pore size distributions are shown as an insert.

Table 2 Textural parameters obtained from the isotherms and the NLDFT method for UCATiO and UCAO.

	S_{total} (m^2/g)	V_{pore} (cm^3/g)	Pore size (nm)
UCATiO	90	0.21	7.5
UCAO	240	0.30	4.8

We investigated the surface topography of the two materials under study, using AFM. Fig. 1c and 1d show the 1 x 1 μm^2 2D top views, obtained for UCAO and UCATiO respectively. The corresponding 3D surface plots are shown in Fig. 1e and 1f. As observed, the materials consist of aggregates of spherical nanoparticles. Similarly, it is clear that their morphology presents important differences. UCAO comprises silica nanoparticle aggregates, as observed by SEM. In the case of UCATiO, thanks to the better 2D resolution provided by AFM, we observe larger aggregates because they include not only silica nanoparticle aggregates (of a size similar to those corresponding to UCAO) but also individual TiO_2 nanoparticles: some of these latter particles are presumably incorporated within the aggregates and others are exposed on their surface and hence visible.

3D surface images show that the addition of TiO_2 nanoparticles in UCATiO substantially modifies the surface morphology of the photocatalyst, since increased roughness is observed when TiO_2 nanoparticles are added to the starting sol. We associate this increase in the size of aggregates with the presence of TiO_2 nanoparticles. The reduced surface roughness of UCAO is associated with the aggregation of the silica nanoparticles alone. In a previous paper,[27] increasing the TiO_2 content was found to cause an increase in roughness for TiO_2-SiO_2 nanocomposites, confirming our hypothesis.

Fig. 1g shows the particle height (Z) distribution. In the case of UCAO, the narrow homogeneous Gaussian distribution reveals that silica aggregates show a uniform size distribution, as previously discussed. The UCATiO particle height (Z) distribution also shows a Gaussian distribution with a larger maximum (see Table 1), which confirms the presence of well-dispersed TiO_2 nanoparticles within the aggregates. As an example of the roughness profiles obtained, two of them are shown in Fig. 1h.

In order to confirm the structure data obtained by SEM and AFM, we also obtained nitrogen adsorption-desorption isotherms, which are shown in Figure 2. The corresponding textural data obtained are given in Table 2. The two isotherms are type IV, which is typical of mesoporous materials. The two products showed a type H2 hysteresis loop, characterized by a triangular shape and a steep desorption branch. These products can be classified as materials with relatively uniform channel-like pores[34,35] In addition, UCAO shows low adsorption at low pressure, which is indicative of microporosity in this material.

The inset included in Figure 2 shows the pore size distribution obtained using the NLDFT approach from the isotherm adsorption branches. We employed this procedure in order to obtain a pore size distribution integrating micro and mesopores present in the materials under study.[29] The product without TiO_2 (UCAO) showed micro and mesopores. Specifically, a small portion of pores was detected in the microporous region close to the mesopore range (from 1 to 2 nm), with most pores being in the size range of 2-8 nm. In the case of UCATiO, the pore size distribution showed significantly higher values, all of them in the mesopores region (ranging from 4 to 10 nm). These results confirm the data obtained by AFM and SEM. TiO_2 nanoparticles are integrated in the silica nanoparticles aggregates, increasing the size of the aggregates in the composite. This obviously increases the space between aggregates of the material, producing an increase in the pore size distribution. A similar trend was observed for previous silica-titania nanocomposites synthesized in our laboratory. The pore size of the material increased as titania nanoparticles content was raised.[14] Similarly, Zelenak et al.[8] associated this increase with the creation of interparticle space between the titania nanoparticles.

Regarding pore volume (see Table 2), this was slightly smaller when titania nanoparticles are included in the matrix; the reason could be that some of the titania nanoparticles fill the spaces between the aggregates.[8] In the case of surface area, as is obvious, it is higher for the material with lower pore size and higher pore volume (UCAO).

Figures 3a and 3e show representative HAADF-STEM and HREM images respectively of the UCATiO material. X-EDS mappings showing elemental distributions for Ti, Si and Si+Ti over the same area highlighted on the HAADF-STEM image are shown in Fig. 3b, 3c and 3d, respectively. The STEM micrograph (Z-contrast) shows a mesoporous material composed, mainly, of individual TiO_2 nanoparticles of around 20 nm, presenting a size similar to that stated by the manufacturer (21 nm). Some TiO_2 aggregates (of 30-40 nm size) are also observed. The SiO_2 nanoparticles show smaller sizes, of around 15 nm.

From the X-EDS maps obtained (Fig. 3b-3d) it can be confirmed that TiO_2 and SiO_2 are located in independent domains in the bulk of the material. In addition, the combination of the Si and Ti maps confirms that the network of SiO_2 nanoparticles surrounds the TiO_2 ones. Thus, SiO_2 could be acting as a matrix in a reinforced composite structure of the UCATiO photocatalyst.

In Figure 3e, an individual crystalline TiO_2 nanoparticle with an

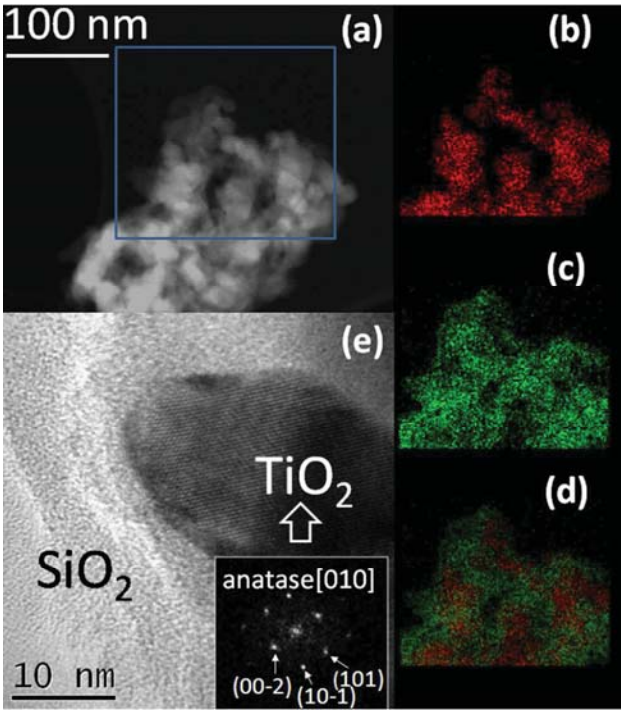

Fig. 3 Representative HAADF-STEM images: (a) of the UCATiO material and corresponding compositional maps for Ti (b); Si (c); Si and Ti together (d) obtained by X-EDS. The structural analysis from HREM imaging (e) confirms the presence of anatase in the TiO2 nanoparticles which are present in the UCATiO material.

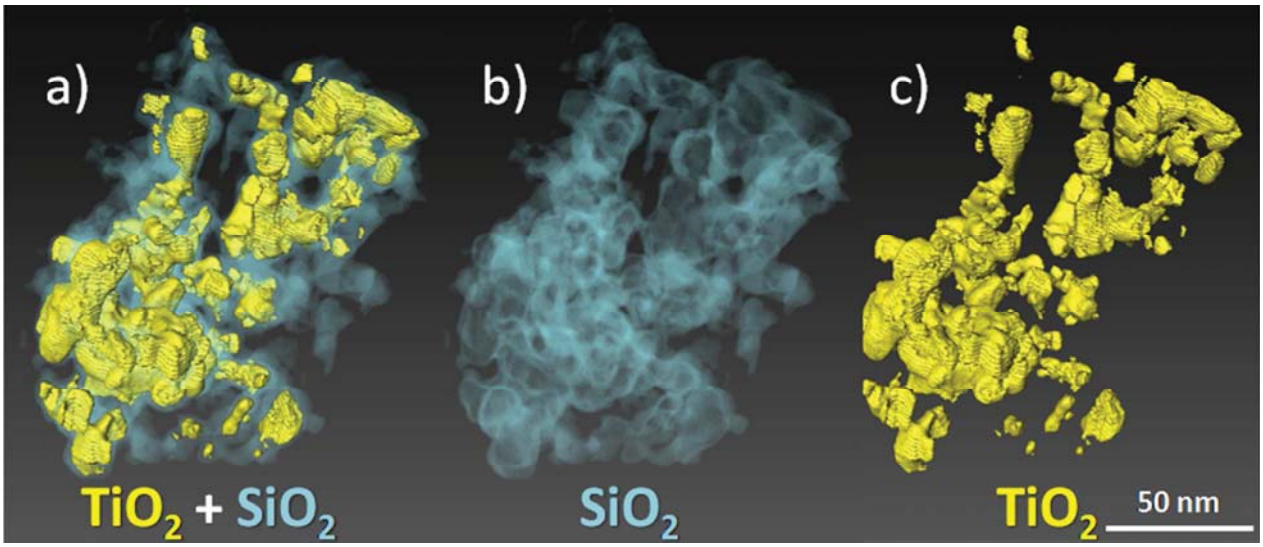

Fig. 4 3D reconstruction of the tomography series acquired for UCATiO. This allows an independent analysis of both the tridimensional structure and spatial distribution of TiO_2 and SiO_2.

estimated particle size of 20 nm can be observed supported in amorphous silica. At this scale, the HREM images illustrate two important features: firstly, analyzing their corresponding digital diffraction patterns (shown as an inset in Figure 3e), we can confirm the crystallographic nature of the various components: the application of a Fourier transformation to the visible lattice spacings present in the crystalline structure of our material reveals the presence of the (00-2), (10-1) and (101) crystallographic planes assigned to the anatase phase of titania. This confirms that anatase, the titania crystalline structure with photocatalytic activity, is present in the composite. Secondly, from the HREM images we can make a clear distinction between the two components of the nanomaterial synthesized in our laboratory, confirming the existing of two separate domains. In addition, we find a good agreement between the particle sizes obtained by STEM and HREM imaging.

In order to confirm the TiO_2/SiO_2 structure and relationships obtained by the STEM/HREM and X-EDS studies, a three dimensional characterization was performed by means of electron tomography. Figure 4 shows the reconstructed volume of the tomography series acquired for UCATiO, corresponding to (a) Si+Ti, (b) Si, and (c) Ti, in the sample analyzed. (A video showing the 3D reconstructed volume can be found in the Supplementary Information section). The 3D reconstruction allows the detailed analysis of the internal characteristics of the sample, which are not possible to observe in conventional 2D

images. This method of volume sectioning provides information related to the position of both components in the structural organization. In this context, we can observe (Figure 4a) a mesoporous composite structure with an independent spatial distribution of TiO_2 and SiO_2 nanoparticles. The volumes in yellow color correspond to TiO_2 nanoparticles. The regions in transparent blue correspond to the SiO_2 support. The observation of TiO_2+SiO_2 reconstructed volume allows us, firstly, to corroborate the presence of large voids between aggregates, which could correspond to pore space identified by physisorption. Again we observe two different domains for silica and titania.

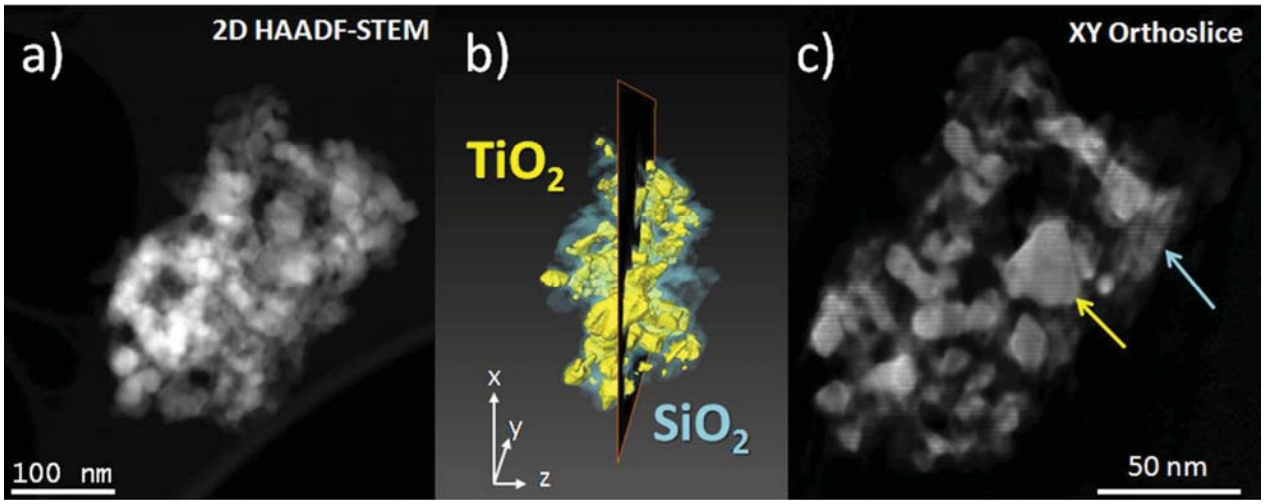

Fig. 5 2D HAADF-STEM image (a) of the analyzed sample during the tomography series acquisition. 3D reconstruction (b) of the analyzed sample. XY orthoslice (c) taken from the 3D reconstructed volume, taken perpendicular to the Z-direction. The yellow arrow indicates the location of TiO2 nanoparticles in areas that show higher brightness and well-defined boundaries. The blue arrow indicates the SiO2 particle binding support which corresponds to areas with lower brightness.

Figure 4b presents the individual configuration of the mesoporous silica matrix which surrounds the titania nanoparticles. Here we can clearly observe that the silica amorphous phase presents a shell-like structure which partially covers the supported individual crystalline titania particles. This information supports the conclusion that the interaction between TiO_2 and SiO_2 could be physical, through Van der Waals forces, as previously discussed by Gao et al.[3]

Figure 4c shows the individual TiO_2 nanoparticles present in the photocatalyst. These present a good dispersion, as a result of the ultrasound preparation process and the presence of *n*-octylamine as a dispersion stabilizer.[14,16] The dimensions and arrangement of the titania nanoparticles are also in good agreement with the information presented in Figure 3. It confirms again that individual nanoparticles are present in this composite. The horizontal streaking seen in the figure is a result of reconstruction artifacts resulting from the limited tilt range and number of images, together with differences in contrast between TiO_2 and SiO_2 nanoparticles

Figure 5a shows a 2D HAADF-STEM image from the tilt series. Fig. 5b presents a surface-rendered representation of the segmented 3D reconstructed volume of the sample analyzed; and an *XY* orthoslice taken from the 3D reconstructed volume is presented in Fig. 5c. The *XY* orthoslice taken from the 3D reconstructed volume, perpendicular to the *Z*-direction, is a good example of how this additional imaging tool helps us to understand better the relative locations of SiO_2 and TiO_2 nanoparticles. Images a and c in Fig. 5 are oriented such that a direct comparison between them can be made.

In the HAADF-STEM image (Fig. 5a), it is difficult to discriminate the configuration of the SiO_2 matrix around the TiO_2 nanoparticles. The advantages of using 3D characterization become evident when we compare this 2D image with the *XY* orthoslice (Fig. 5c). Both locations are indicated by arrows for guidance purposes. The yellow arrow indicates the location of TiO_2 nanoparticles in areas that show higher intensity and well-defined boundaries. The blue arrow indicates the SiO_2 nanoparticles binding support, which corresponds to areas with lower brightness. Firstly, this image confirms that the surface of the photocatalyst, observed by SEM and AFM (Fig. 1) shows a structure similar to its interior. We can also observe that there is significant pore volume within the bulk of the photocatalyst, providing good access to its interior for 'guest' molecules. Moreover, from a careful examination of the silica matrix we can corroborate the existence of voids inside the SiO_2 nanoparticles. We attribute the existence of these voids to the influence of the *n*-octylamine during the sol-gel process: this generates mesoporosity and should be valuable for enhancing the adsorption of 'guest' molecules.

Yamauchi et al.[36] reported the synthesis of a SiO_2/TiO_2 nanocomposite, and they used electron tomography as a tool for understanding better the location of TiO_2 nanoparticles. They concluded that the TiO_2 nanoparticles were totally embedded in the SiO_2 matrix, and that none of the TiO_2 nanoparticles was exposed on the outer surface, which was of great importance for the selective adsorption of guest molecules, according to these authors.

Similarly, Beyers et al,[9] also reported the advantages of the

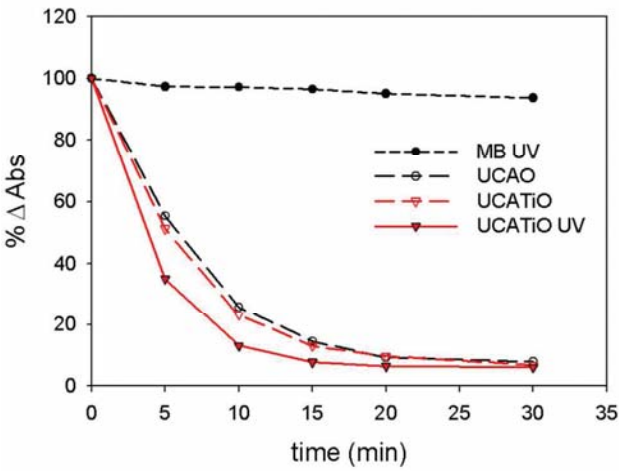

Fig. 6 Absorbance variation (in percentage) of a MB solution left in contact with UCATiO under UV light. Corresponding absorbance variations in dark conditions for UCATiO and UCAO are presented for comparison purposes. The absorbance variation of a MB solution in the absence of any material and irradiated with UV light is also shown.

deposition of TiO_2 nanoparticles inside a silica matrix in order to obtain an inert outer surface. However, these authors also reported the increase in photocatalytic activity when TiO_2 nanoparticles were located outside the matrix. In our case, our combined 2D-3D electron microscopy studies support the finding that TiO_2 nanoparticles in the photocatalyst exist both directly exposed on the surface and surrounded within the mesoporous matrix of SiO_2 nanoparticles. Considering this finding on the location of the TiO_2 nanoparticles, we believe the photocatalyst provides a good combination of potential adsorptive and photocatalytic properties.

We have also investigated the photocatalytic activity of UCATiO by measuring the absorbance evolution with time of a methylene blue aqueous solution left in contact with this material under UV radiation. The photodegradation of the methylene blue solution without any material present was also carried out for comparison purposes. We also measured the absorbance evolution of MB left in contact with UCAO and UCATiO in dark in order to evaluate the MB adsorption obtained for the two mesostructures under study. The results obtained are shown in Figure 6.

MB photodegradation under visible/UV light has been reported previously as being associated with the absorption of light undergone by the dye in the 350-520 nm range.[37] Thus, we think that the slight degradation observed of MB in aqueous solution is induced by the light absorbed during exposure to the UV radiation. In the case of UCATiO material, a significant reduction in absorbance is observed, suggesting that our nanocomposite is effective as a photocatalyst.

We also observed a reduction in MB absorbance when the test was carried out in dark. The reduction kinetic was very similar for the two materials evaluated. This suggests that it actually corresponds to the adsorption of MB in these meso-structured materials. As Suzuki et al. have reported,[38] the photocatalytic degradation of MB is clearly enhanced by the addition of TiO_2 nanoparticles to a silica mesoporous structure, in comparison with the effect observed when the titania nanoparticles are integrated in a dense microporous matrix. This enhancement of effect was explained by these authors in terms of the increased BET surface area, which accelerates the diffusion of MB towards the reaction sites (i.e. towards the TiO_2 nanoparticles). We also reported in a previous paper[14] that the presence of a mesoporous matrix assists rapid diffusion of this organic dye into the photoactive sites. By comparing the kinetics of the two materials, we do not find significant differences because they both are meso-structured, with only slight differences in pore size and in pore volume as reported in the physisorption results.

As final remarks, it is considered that UCATiO shows a fast reduction in absorbance in the first few minutes of exposure (up to 15 min) because the MB adsorption in the mesostructure matrix acts in a synergistic way with the photocatalytic action of TiO_2nanoparticles, in removing the dye from the aqueous medium. We think this effect is favored by the presence of TiO_2 both directly exposed on the surface (MB degradation) and surrounded by the matrix of mesoporous SiO_2 nanoparticles (MB adsorption), as observed in the combined 2D-3D electron microscopy studies. This new nanocomposite developed in our laboratory will become available as a commercial product under an exploitation patent.[39]

Conclusions

This study shows that the addition of pre-formed crystalline TiO_2 nanoparticles to surfactant-synthesized SiO_2 creates a material with effective photocatalytic activity. Our combined 2D-3D electron microscopy studies support the finding that a TiO_2-SiO_2 mesostructure has been obtained without performing thermal treatments or other additional methods for removal of the surfactant or for creating a crystalline photoactive phase. The material synthesized has a wide range of potential applications for thermally-sensitive substrates and substrates exposed to outdoor conditions. In addition, the complete characterization study carried out demonstrates that silica and titania are maintained as independent domains. This nanomaterial is composed of silica nanoparticles of nearly uniform size, created by an aggregation mechanism due the effect of n-octylamine. The pre-formed titania nanoparticles are integrated in the silica aggregates. We have also demonstrated that some of the titania remains outside the silica matrix, as individual nanoparticles, which permits a direct photodegradation. These features favor the fast removal of MB due the synergistic effect of its adsorption in the mesoporous silica structure and its photodegradation by titania nanoparticles.

Acknowledgments

We are grateful for financial support from the Spanish Government/FEDER-EU (Project MAT2010-16206 and Project Regenera, Innpacto subprogram), and the Government of Andalusia (project TEP-6386 and Group TEP-243). L.P. thanks the Fundação Ciência e Tecnologia for his predoctoral grant (SFRH/BD/43492/2008). We also thank to Prof. Jesús Ayuso for his support with the photocatalytic experiments.

Notes and references

[a]*Departamento de Química-Física, Facultad de Ciencias, Campus Universitario Río San Pedro, Universidad de Cádiz, 11510 Puerto Real, Cádiz, Spain. Fax: + 34 956 016471; Tel: + 34 956 016331; E-mail: mariajesus.mosquera@uca.es*

[b] *Departamento de Ciencia de los Materiales e Ingeniería Metalúrgica y Química Inorgánica, Facultad de Ciencias, Campus Rio San Pedro, Universidad de Cádiz, 11510 Puerto Real, Cádiz, Spain Fax: + 34 956 016288; Tel: +34 956012731; E-mail: jcarlos.hernandez@uca.es*

† Electronic Supplementary Information (ESI) available: [Movie showing the 3D reconstructed volume of the studied TiO_2/SiO_2 nanocomposite photocatalyst analyzed]. See DOI: 10.1039/b000000x/

1 W. Zhang, M. Fröba, J. Wang, P. Tanev, J. Wong, T. Pinnavaia, *J. Am. Chem. Soc.*1996, **118**, 9164-9171.
2 Fujishima, A.; Rao, T.; Tryk, D. *J. Photochem. Photobiol. C,* 2000, ***1***, 1-21.
3 X. Gao, I. E. Wachs, *Catal. Today* 1999, **51**, 233-254.
4 A. Pénard, T. Gacoin, J. Boilot, *Acc. Chem. Res*., 2007, **40**, 895-902.
5 M. Alvaro, E. Carbonell, V. Fornés, H. García, *Chem. Phys. Chem.*, 2006, **7**, 200-205.
6 Y. Zhang, C. Chen, H. Qing, R. Wu, H. Zou, *Chem. Commun.*, 2010, **12**, 2271-2273.
7 S. Wang, Y. Shi, X. Ma, J. Gong, *ACS Appl. Mater. Interfaces*, 2011, **3**, 2154-2160.
8 V. Zeleňak, V. Hornebecq, S. Mornet, O. Schäf, P. Llewellyn, *Chem. Mater.*, 2006, **18**, 3184-3191.
9 E. Beyers, E. Biermans, S. Ribbens, K. De Witte; M. Mertens; V. Meynen; S. Bals, G. Van Tendeloo, E. F. Vansant, P. Cool, *Appl. Catal. B*, 2009, **88**, 515-524.
10 C. A. Morris, M. L. Anderson, R. M. Stroud, C. I. Merzbacher, D. R. Rolison, *Science*, 1999, **284**, 622-624.
11 Mosquera, M.J.; de los Santos, D.M.; Montes, A.; Valdez-Castro, L. *Langmuir* 2008, **24**, 2772-2778.
12 Mosquera, M.J.; de los Santos, D.M; Rivas, T. *Langmuir* 2010, **26**, 6737-6745.
13 J. F. Illescas, M. J. Mosquera, *J. Phys Chem. C*, 2011, **115**, 14624-14634.
14 L. Pinho, M. J. Mosquera, *J. Phys Chem. C*, 2011, **115**, 22851-22862.
15 J.F. Illescas, M.J. Mosquera, *ACS Appl. Mat. & Int.*, 2012. DOI: 10.1021/am300964q
16 D. Siwinska, A. Kołodziejczak-Radzimska, A. Krysztafkiewicz, T. Jesionowski, *Appl. Surf. Sci*. 2009, **255**, 7337-7342.
17 K. Inumaru, M. Yasui, T. Kasahara, K. Yamaguchi, A. Yasuda, S. Yamanaka, *J. Mater. Chem.*, 2011, **21**, 12117-12125.
18 J.C. Hernández-Garrido, K. Yoshida, P.L. Gai, E.D. Boyes, C.H. Christensen, P.A. Midgley, *Catal. Today,* 2011, **160**, 165-169.
19 P. Linton, J. C. Hernandez-Garrido, P. A. Midgley, H. Wennerström, V. Alfredsson, *Phys. Chem. Chem. Phys*, 2009, **11**, 10973-10982.
20 Doren, E.; Temmerman, P.; Francisco, M.; Mast, J. J. Nanobiotechnol. 2011, 9, 17.
21 K. Yoshida, M. Makihara, N. Tanaka, S. Ayoagi, E. Nishibori, M. Sakata, E. Boyes, P. Gai, *Microsc. Microanal.*, 2011, **12**, 264-273.
22 S. Li, C. Chang, C. Lin, Y. Lin, C. Chang, J. Yang, M. Chu, C. Chen, *J. Am. Chem. Soc.*, 2011, **133**, 11614-11620.
23 M. Okuda, M. Takeguchi, Y. Zhu, A. Hashimoto, N. Ogawa, M. Tagaya, S. Chen, N. Hanagata, T. Ikoma, *Surf. Interface Anal*., 2010, **42**, 1548-1551.
24 S. Sueda, K. Yoshida, N. Tanaka, *Ultramicroscopy*, 2010, **110**, 1120-1127.
25 K. J. Batenburg, S. Bals; J. Sijbers, C. Kübel, P. A. Midgley, J. C. Hernández, U. Kaiser, E. R. Encina, E. A. Coronado, G. Van Tendeloo, *Ultramicroscopy*, 2009, **109**, 730-740.
26 J.M. Thomas, P.A. Midgley, T.J.V. Yates, J.S. Barnard, R. Raja, I. Arslan, M. Weyland, *Angew. Chem. Int. Ed.*, 2004, **43**, 6745-6747.
27 Y. V. Lim, H. Fan, Z. Shen, C. H. Kang, Y. Feng, S. Wang, *Appl. Phys. A*, 2009, **95**, 555-562.
28 A. I. Kontos, I. M. Arabatzis, D. S. Tsoukleris, A. G. Kontos, M. C. Bernard, D. E. Petrakis, P. Falaras, *Catal. Today*, 2005, **101**, 275-281.
29 M. Thommes, B. Smarsly, M. Groenewolt, P.I. Ravikovitch, A.V. Neimark, *Langmuir*, 2006, **22**, 756-764.
30 M.J. Mosquera, D.M. de los Santos, L. Valdez-Castro, L. Esquivias *J. Non-Cryst. Solids* 2008, **354**, 645-650.
31 G. Orcel, L.L. Hench, I. Artaki, J. Jonas, T.W. Zerda, *J. Non-Cryst. Solids* 1988, **105**, 223-231.
32 G.H. Bogush, C.F. Zukoski IV, *J. Colloid Interface Sci*., 1991, **142**, 19-34.
33 K. Kosuge, P.S. Singh, *Micro. & Mesoporous Mat.,* 2001, **44-45**, 139-145.
34 M. Kruk, M. Jaroniec, *Chem. Mater.*, 2001, **13**, 3169-3183.
35 M. Kruk, M. Jaroniec, A. Sayari, *Langmuir,* 1997, **13**, 6267-6273.
36 Y.Yamauchi, F. Takeuchi, S. Todoroki, Y. Sakka; S. Inoue *Chem. Lett.*, 2008, **37**, 72-73
37 A. Mills, J. Wang, *J. Photochem. Photobiol. A, Chem.*, 1999, **127**, 123-134.
38 N. Suzuki, X. Jiang, L. Radhakrishnan, K. Takai, K. Shimasaki, Y. Huang, N. Miyamoto, Y. Yamauchi, *Bull. Chem. Soc. Jpn.*, 2011, **84**, 812-817.
39 *Sp. Pat.* P201100741, 2011.

4.3. Photocatalytic activity of TiO_2–SiO_2 nanocomposites applied to buildings: influence of particle size and loading

Sent to Applied Catalysis B

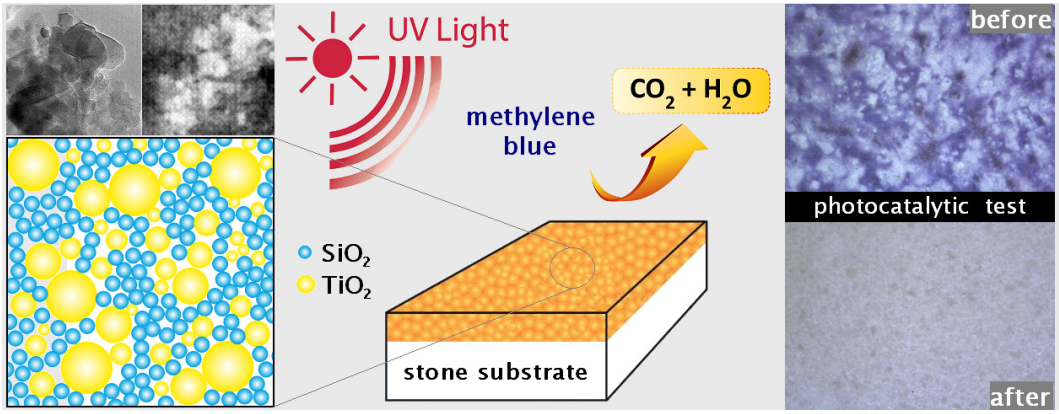

- Mesoporous TiO_2-SiO_2 photocatalyts have been successfully synthesized.
- A surfactant acts to coarsen the porous gel network, providing better access to photoactive sites
- The photocatalysts give self-cleaning properties to stone and improve its robustness
- Addition of larger and sharper TiO_2 particles with 4% w/v content improves effectiveness

Photocatalytic activity of TiO_2–SiO_2 nanocomposites applied to buildings: influence of particle size and loading

Luís Pinho, Maria J. Mosquera*

TEP-243 Nanomaterials Group. Departamento de Química-Física, Facultad de Ciencias, Campus Universitario Río San Pedro, Universidad de Cádiz, 11510 Puerto Real, Cádiz, Spain

*Corresponding author:e-mail: mariajesus.mosquera@uca.es.

Phone: (34)956016331. Fax: (34)956016471

Abstract

Atmospheric pollution has an evidently adverse impact on the aesthetics of urban buildings and structures. Thus, the synthesis of photocatalysts capable of removing pollutants deposited on the surface of stone and other building materials is a challenge to researchers. By a simple and low cost process we have synthesized mesoporous TiO_2-SiO_2 photocatalytic coatings that meet the requirements of outdoor application. These are new materials designed to give to the building material long-term self-cleaning and strengthening properties.

We have varied the loading and size of TiO_2 nanoparticles in order to investigate their effect on the photocatalytic activity. We find that the integration of larger and sharper titania particles in a silica network with a titania content of around 4% w/v significantly improves effectiveness, due to the enhanced availability of surface photoactive sites. For a higher TiO_2 content (10% w/v), photocatalytic action decreases because the porous volume is drastically reduced and consequently, access to photoactive sites is more difficult.

Key-words: TiO_2 photocatalyst; Mesoporous SiO_2 support; surfactant-synthesized material; self-cleaning properties; building materials; outdoor applications

1. Introduction

Atmospheric pollution has an adverse impact on structures and buildings in every city of the world. Particulate matter and other components like organic and elemental carbon, and nitrogen oxides, are deposited extensively on the surface of buildings, contributing to the formation of an ugly brownish-gray to black crust. The deposition of these compounds on building facades has serious implications, not only aesthetic but also economic and ecological. Scientists face a major challenge in countering air pollution and specifically in devising ways of decomposing the organic species deposited on building surfaces, a task for which TiO_2 can be used as a photocatalyst in coatings applied to buildings and stone structures. The application of this photocatalyst on such surfaces should lower maintenance costs by reducing surface soiling; as a consequence, there would be less need for frequent and costly cleaning operations [1].

Titania photocatalysis is produced according the following mechanism: photons are absorbed by TiO_2, which generates electron-hole pairs. In contact with water, free radicals ($^{\bullet}O_2^-$ and $OH^{\bullet}$) are generated, which are able to oxidize organic matter to water and carbon dioxide, leaving no other residue. It can thus work as a self-cleaning material on the surfaces of buildings and other materials exposed to atmospheric pollution [2].

In the case of building materials based on cement or lime (concretes, mortars, etc.), several successful attempts have been made to mix the photocatalyst in with the bulk material, during the processes by which these materials are prepared for use [1,3]. From the results obtained [3] it can be concluded that the addition of titania to cement, etc., gives photocatalytic properties to the material and can even improve its mechanical properties. However, few references are found in the literature about the application of TiO_2 photocatalysts in building materials previously formed, produced and erected, such as natural stone structures and existing buildings, ancient and modern. In these cases the conditions of application are very restrictive: because the TiO_2 cannot be incorporated when preparing the bulk material, it must necessarily be applied to the surface of the material as a coating of some kind. In the case of application to a major structure like a building, the requirements are even stricter because the

process must be carried out “in situ” under outdoor conditions, which can make the task significantly more complex and difficult. Moreover, any operation required additional to the actual application, such as heating or solvent extraction, can greatly increase the difficulties.

Regarding application on stone, in most of the references found in the literature TiO_2 particles are employed dispersed in water [4,5] or incorporated in commercial products consisting of an aqueous dispersion with TiO_2 and an acrylic polymer [6]. But the application of such strategies cannot ensure the long-term performance of the coating because TiO_2 particles deposited on the surface can easily be removed from external stonework and other facing materials [4,7].

One strategy for preventing the release of the TiO_2 from the surface to the environment [7,8] would be to immobilize the photocatalyst in, for example, a SiO_2 matrix [9-11]. In this context, there is a valuable information resource in the previous studies made of TiO_2-SiO_2 nanocomposites for various applications in heterogeneous catalysis [12-14], and in other studies about the fundamentals of titanium dioxide photocatalysis [15]; these provide us with information on the potential benefits of incorporating TiO_2 within a mesoporous SiO_2 matrix in order to obtain an improved catalytic material with better access to the titania sites and greater catalytic activity [12].

Photoactive nanocrystalline TiO_2 particles can be incorporated in a mesoporous silica matrix in several ways: 1. by mixing Ti alkoxide precursors with Si alkoxide [12-14]; 2. by grafting pre-synthesized silica with Ti alkoxide [16,17]; or 3. by mixing pre-formed titania colloidal nanoparticles in a Si alkoxide sol [9]. However, difficulties arise when Ti alkoxides are employed: 1. they hydrolyze much faster than Si alkoxides [14]; 2. the TiO_2 loading that can be achieved is quite low; and 3. the formation of photoactive TiO_2 crystals through a calcination process is severely limited by the low heating temperature imposed by some substrates [9]. In the case of grafting Ti alkoxide inside the silica matrix, this requires the gradual and time-consuming addition of the alkoxides to the silica in several deposition cycles [16]. Therefore, the synthesis of TiO_2-SiO_2 nanocomposites using preformed TiO_2 nanoparticles represents an interesting potential alternative in many fields [18-20]. In particular, it has good potential for application as in coating materials for buildings because the deposition method should involve a simple application,

with no need for any additional treatment, such as heating or solvent extraction, when applied to the exterior of the building.

We have recently designed several syntheses of products intended to protect building materials. We have prepared a consolidant product with hydrophobic properties [18-21], a stain-resistant product [22] and we have even prepared a self-cleaning product [11]. No thermal processing is required in the synthesis processes developed in our laboratory. Thus, our products find good application on thermally-sensitive substrates, are more cost-effective and, especially, meet the requirements necessary for application to exterior surfaces of buildings. Some of these products are now commercially available under the corresponding exploitation patents [24,25].

In the specific case of the self-cleaning product devised, a TiO_2-SiO_2 nanocomposite coating gives photocatalytic properties to stone surfaces. This product also penetrates into the pore structure of the stone, increasing its robustness. It consists of a colloidal dispersion of pre-formed titania nanoparticles dispersed in a sol of silica oligomers, in presence of a surfactant (*n*-octylamine), which is applied to stone and other building materials by means of an aerosol-assisted process. There are four fundamental reasons for adding a surfactant (such as *n*-octylamine) to our sols: 1. to prevent cracking by coarsening the pore structure of the gel network [26]; 2. to enhance photocatalytic activity by creating a mesoporous nanocomposite [11, 17-19]; 3. to improve the dispersion of TiO_2 nanoparticles by increasing pH [27]; and 4. to act as a basic catalyst of the sol-transition inside the pore structure of the stone [21,26].

Since the textural parameters of titania-silica nanomaterials, such as their pore architecture, surface area, pore volume, pore size and TiO_2/SiO_2 packing, play an important role in their performance as photocatalysts [17,18,20], the first objective of the work reported here is to investigate the role of the nanocomposites' structure on their effectiveness as a photocatalyst; this has been done by using in the synthesis process: 1. titania particles with a range of very different particle sizes, ranging from micrometer to nanometer scale; 2. different loadings of these titania particles. To achieve this objective,

we investigate the structure of these materials in depth using several techniques including SEM, TEM/STEM and nitrogen physisorption.

Our second objective is to understand the performance of these TiO_2-SiO_2 photocatalysts on stone. Thus, we apply the materials synthesized in our laboratory on a pure limestone employed in both modern and ancient buildings, and evaluate the performance of the products for: 1. photocatalytic properties; 2. adhesion on the stone surface; and 3. strengthening the stone substratum. In addition, we also evaluate the ability of these products to meet several other important requirements associated with protective coatings for stonework, such as hydrophobic properties and aesthetic characteristics (i.e. the product should not induce changes in the color or appearance of the stone).

2. Experimental Section

2.1. Synthesis. The following reagents were used in the synthesis process: 1. TES40 WN (Wacker Chemie AG, GmbH): according to the technical data sheet, this is an ethoxysilane (average polymerization grade of 5) providing approximately 41% of silica upon complete hydrolysis and many hydrolysable ethoxy groups; 2. *n*-octylamine (Aldrich); 3. commercial colloidal AP, P25, and P90 TiO_2 nanoparticles, with an average particle size of 20 μm, 21 nm and 14 nm, respectively. More information on crystallinity, particle size and textural parameters can be found in the Supplementary Information (Table 1). Syntheses were carried out as follows: TES40 was mixed with TiO_2 nanoparticles in the presence of *n*-octylamine under high-power ultrasonic agitation (125 $W \cdot cm^{-3}$). The proportion of n-octylamine to TES40 was 0.36% v/v. Next, TiO_2 nanoparticles were added to the starting sol in three different proportions: 1, 4 and 10% w/v. A set of formulations was prepared for each kind of particle tested. The formulations prepared were designated: S#AP, S#P25, S#P90 where # indicates the %w/v of TiO_2 particles included in the material (i.e. the loading). For comparative purposes, a silica material without TiO_2 nanoparticles was prepared according the same synthesis; this was designated S.

2.2. Sol-Gel Characterization. Immediately after the synthesis of the sols, their rheological properties were studied using a concentric cylinder viscosimeter (model DV-II+ with UL/Y adapter) from Brookfield. Experiments were performed at a constant temperature of 25ºC maintained by recirculated water from a thermostatic bath. A shear stress versus shear rate flow curve was generated. In addition, a shear stress vs. viscosity graph was also plotted. For comparison, the rheological properties of TES 40 were also evaluated.

Next, coatings of the materials under study were obtained by deposition of 3 ml of sol on plastic Petri dishes with a diameter of 85 mm. Dishes were covered and maintained at laboratory conditions (relative humidity of 60% and temperature of 20º C). Gel transition and spontaneous drying took place. The xerogels obtained were characterized after reaching constant weight.

Powdered coatings were used for X-ray diffraction (XRD), measured on a Bruker D8 advance diffractometer equipped with a secondary monochromator, Cu tube X-ray, using Cu K_α radiation. The photocatalyst coatings were visualized by Scanning Electron Microscopy (SEM) using a FEI Sirion instrument with a field emission filament operating at 5kV. This instrument has a resolution of 1.5 nm and it is equipped with a Through-Lens Detector (TLD) working in ultra-high resolution (UHR) mode. The pore volume, pore size distribution and BET surface area of the materials under study were characterized by Nitrogen Physisorption (Autosorb IQ, from Quantachrome).

Transmission electron microscopy studies were performed in a JEOL 2010F TEM/STEM microscope, operating at 200 kV with 0.19 nm spatial resolution. This instrument is equipped with a JEOL high angle annular dark field (HAADF) detector, enabling the acquisition of STEM images. Samples were prepared by depositing a small amount of the powders directly onto Lacey-Carbon coated Cu grids. Both TEM and HAADF images were obtained.

The chemical bonds in the coatings under study were analyzed by Fourier Transform Infrared Spectrophotometry (FTIR). The spectra were recorded in powder using a FTIR-8400S from Shimadzu (4 cm^{-1} resolution) in the region from 4000 to 650 cm^{-1}. Experiments were carried out in attenuated total reflection mode (ATR).

Diffusive reflectance UV-Vis spectra of the photocatalysts were recorded on a StellarNet Concave Grating spectrometer with an integrating sphere attachment using $BaSO_4$ powder as white reference. Single-pulse (SP) MAS-NMR experiments were carried out on a Bruker ADVANCE WB400 spectrometer equipped with a multinuclear probe. Samples of powdered materials were packed in 4 mm zirconia rotors and spun at 8 kHz. ^{29}Si MAS NMR spectra were acquired at a frequency of 79.49 MHz, using a pulse width of 1.8 μs (π/2 pulse length = 5.4 μs), a delay time of 60 s and scan number of 2000. The chemical shift values are reported in ppm from tetramethylsilane.

2.3. Application on stone and characterization. The stone selected for evaluating the effectiveness of the materials under study is a fossiliferous limestone with a homogeneous structure composed of a micritic matrix, containing recrystallized calcium carbonate grains, and skeletal fragments of mollusks, echinoderms and foraminifera. Semi-quantitative analysis by X-ray powder diffraction analysis enabled the mineralogical composition of stone to be identified; it is composed of calcite (98.5%) and α-quartz (1.5%). This stone was selected for its whiteness, so the stains applied on its surface and the self-cleaning effectiveness of the coatings under study could be checked more easily. For all the experiments carried out, the stone samples were cut in the form of 5x5x2 cm slabs. The sols under study were applied by spraying onto the surfaces of the samples until apparent refusal, this being understood to occur when the surfaces remained wet for 1 minute. After the application, the excess of sol was removed from the surface of the sample by air spraying, in order to form the thinnest possible surface film [27]. The stone samples were then dried under laboratory conditions until reaching constant weight. Uptake of products and their corresponding dry matter were calculated. The samples corresponding to untreated stone and their treated counterparts were characterized by the procedures described below, after constant weight was reached. All the results reported correspond to average values obtained from three stone samples.

Surface fragments of treated stone specimens and their untreated counterpart were visualized by Scanning Electron Microscopy (SEM) using the previously-cited FEI Sirion microscope, adopting the same conditions for observation. Cross-sections of the treated stones were observed in a JEOL 6460 LV

SEM equipped with an Oxford INCAx-sight 7573 X-ray Energy Dispersive Spectroscopy (X-EDS) detector. X-EDS elemental distribution mappings, BSE and SE images were recorded in order to elucidate the variations in surface composition and morphology for each treatment.

The adherence of the coating to the stone surface was evaluated by performing a peeling test using Scotch® Magic™ tape (3M). The test was carried out according to previously reported methods [28].

The improvement in mechanical properties in treated stone was evaluated using the drilling resistance measuring system (DRMS), by SINT Technology. Drill bits of 4.8 mm diameter were employed with a rotation speed of 200 rpm and penetration rate of 10 mm/min.

In order to investigate the hydrophobic behavior of the coatings under study, contact angles of the stone surfaces were measured using a commercial video-based, software-controlled contact angle analyzer, model OCA 15plus, from Dataphysics Instruments.

We also evaluated the possible disadvantage of these materials associated with changes in stone color induced by the treatments. This effect was determined using a solid reflection spectrophotometer, Colorflex model, from Hunterlab. The conditions used were: illuminant C and observer 2º. CIELa*b* color space was used and variations in color were evaluated using the parameter: total color difference (ΔE*) [29].

The effectiveness of the materials under study as self-cleaning coatings for stone surfaces was evaluated by using a test adapted from the literature [30]. First, 1 ml of a solution of 1 mM methylene blue (Panreac) in ethanol was deposited on treated stone specimens and their untreated counterparts. Next, stone samples were irradiated with UV light working at 365 nm in a Vilber Lourmat CN15.CL chamber with 2 tubes of 15 W. The distance between the samples and the tubes was approximately 20 cm. Color variations, recorded as a function of irradiation time, were determined using the same procedure described above. The parameter: total color difference (ΔE*) was again evaluated [29].

3. Results and Discussion

3.1. Sol-gel characterization. Our photocatalysts are prepared in a one-step synthesis and applied as aerosols at ambient temperature on porous substrates. Therefore, the rheological properties of the liquids applied on stone are a key factor for surface and in-depth distribution of the photocatalysts. Sols with lower viscosity should be able to penetrate deeper into the stone, which, *a priori*, could be desirable. Further, a low viscosity makes the use of an aerosol generator easier for applying the product in situ [31]. In order to test viscosity, a rheological study of the synthesized sols was carried out. These viscosity data were obtained immediately after ultrasonic stirring of the dispersions. Table 1 presents the viscosity values obtained for the sols under study. For comparison purposes, the viscosity of the silica precursor employed in the syntheses (TES 40) was also evaluated. Since the behavior shown by the prepared sols was always nearly Newtonian at the shear range evaluated, viscosity was calculated as the slope of the shear rate vs. shear stress curves. In the most of the cases, the linear regression coefficients were 0.99, with the linear fit being slightly more difficult for the highest TiO_2 loading. Figure 1 in the Supplementary Information presents the variation of the viscosity with shear stress for the sols evaluated. S10P90 has not been included in the representation because the values obtained were outside the measurement range.

The viscosity values obtained for the S sol and for the sols corresponding to the S#1 series (with the lowest TiO_2 proportion, 1% w/v) were very similar to those corresponding to commercial sols employed on stones and other building materials. Specifically, we determined the viscosity for one of the most popular commercial stone consolidants, Tegovakon V100 from Evonik; the viscosity of this solvent-free product was 5.25 mPa·s at 25ºC [32]. Thus, we conclude that the sols prepared in our laboratory must penetrate into the stone in a way similar to that of the commercial sols, assuring adequate penetration into the stone pore structure.

Comparing the viscosity values of TES40 and S sols, these values increased slightly when *n*-octylamine was added to TES40. This can easily be explained by the very rapid effect of *n*-octylamine as a sol-gel catalyst. In the case of the TiO_2-SiO_2 sols under study, the addition of TiO_2 nanoparticles promoted a

more significant increase in viscosity than that associated with *n*-octylamine. Two main trends can be observed:

Firstly, as expected, higher particle loading rates produce higher viscosity values, except at the lowest loading tested (1%). These loadings do not modify the rheological behavior of the S sol, as was previously reported [11,31] for TiO_2-SiO_2 sols with P25 TiO_2 nanoparticles at loadings of up to 2% w/v. In the case of higher loading rates, we explain the increase in viscosity values in terms of the increase in TiO_2 particle concentration in the dispersions under study, which produces more viscous dispersions. A similar behavior was previously reported by other authors [31,33]. In addition, we also observe a progressive evolution of our sols from Newtonian to a shear-thinning behavior with the increase of TiO_2 nanoparticles concentration (Figure S1). Similarly, Yang et al. [33] found that dispersions with increasing TiO_2 nanoparticles concentration assumed a progressively shear-thinning behavior from a Newtonian one. Mikulasek et al. [34] also observed a shear-thinning behavior for 30% w/v aqueous TiO_2 dispersions.

Secondly, for the same TiO_2 loading, we observe a clear trend in which the increase in particle size seems to produce lower viscosity. This is, *a priori*, a contradictory feature because AP particles with a size in the micrometric range should promote a significantly higher viscosity than those corresponding to particles with nanometer size scales (P25 and P90). In order to understand better their behavior, we observed AP, P25 and P90 nanoparticles by SEM, before and after ultrasonic stirring in water (particle concentration 1 %w/v), under the same stirring conditions employed in the syntheses (Fig 2. Supplementary information). As is clearly observed by microscopy, the average size of AP nanoparticles, after ultrasonic stirring in water, is significantly reduced from a micrometer to a nanometer scale, and is close to the size presented by P25 and P90 particles. We conclude that the average particle size of AP is reduced due to the strong cavitation power of ultrasonic stirring. Regarding the trend toward increased viscosity as TiO_2 particle size is reduced, this could be attributable to the agglomeration of TiO_2 nanoparticles. This agglomeration phenomenon has previously been reported for aqueous dispersions [33]. We speculate that the aggregation of TiO_2 nanoparticles is more

significant for the lowest average particle size tested (P90) as a consequence of their higher surface energy [35]. It is obvious that the aggregation takes place in order to reduce this high energy. This is a key question which will be discussed further later in this paper.

Sol-gel transition of all the sols deposited on plastic Petri dishes took place overnight, producing homogeneous composite gels. Our view is that the particles exhibit stability during the sol-gel transition because of an increase in pH values of the sol, produced by *n*-octylamine. In basic media, titania particles are negatively charged in the sol, because the pH is higher than the isoelectric point (IEP) of titania [36]. The IEP of P25 nanoparticles has been reported to be around 7 in water [37]. As previously discussed [34,37,38], the interaction between charged particles is based on an algebraic sum of the attractive van der Waals and the repulsive double layer forces. Near the IEP significant agglomeration takes place; large flocks with high hydrodynamic size are observed as the particle surface charge gets close to zero and attractive van der Waals forces dominate. When the pH is different from the IEP of TiO_2, surface charge is different from zero and the hydrodynamic size of the aggregates becomes smaller. We suppose that the IEP in the sols prepared in our laboratory, prior to *n*-octylamine addition, must be fairly close to this value. Therefore, adjusting the pH to a higher value by addition of a base (*n*-octylamine) to the sol must increase electrostatic repulsions and, subsequently, the stability of TiO_2 nanoparticles must be enhanced. In a similar way, electrostatic stabilization of P25 particles in polar organic solvents has previously been obtained by Kosmulsky et al. [38] by adding a base such as triethylamine. Other amines or amine-terminated surfactants are also reported to stabilize TiO_2 dispersions [36,39]. It should also be noted that *n*-octylamine plays an important role, acting as a basic catalyst during sol-gel transition. Thus, sol-gel transition took place overnight for the three series of sols tested. This catalytic effect is a key parameter for assuring a stable dispersion of sol containing TiO_2 particles.

The X-ray patterns of the coatings under study are given in Figure 1. AP, P90 and P25 TiO_2 nanoparticles, were also characterized for comparative purposes (see Fig 3 in Supporting information). Diffractograms of all three types of nanoparticle present typical anatase and rutile peaks. All the

materials prepared in our laboratory show a typical amorphous silica pattern at about 23º [40]. This confirms that our synthesis strategy does not promote an ordered pore structure, which is typical of most materials synthesized via a surfactant template. As previously reported [41], the TiO_2-SiO_2 films require a calcination process in order to produce an ordered mesostructure. Thus, we assume that our drying at ambient temperature cannot produce an ordered silica structure. In addition, we have previously obtained similar patterns for amorphous silica without any detectable order structure in gels synthesized from TEOS and *n*-octylamine [42]. We also observe that the X-ray patterns obtained show peaks previously reported to be related to pure anatase structure [40,43,44]. Specifically, the peaks assigned to anatase at around 25, 38 and 48º were observed [43], and these are evidently more intense as the TiO_2 loading is increased. This verifies that the TiO_2 nanoparticles in the coatings prepared in our laboratory exist as separate crystalline domains, embedded within the amorphous silica matrix [20,45].

Figure 2 shows SEM micrographs of the S material and the corresponding counterparts with TiO_2 nanoparticles, deposited on Petri dishes. All the materials form a homogeneous and continuous gel coating composed of aggregates visible at the magnification employed. Some differences can be observed with respect to the size of the aggregates comprising the gel network of the different nanocomposites under study. The S material consisted of a configuration of silica nanoparticles of nearly uniform pore size. We previously obtained a similar structure for synthesized silica materials obtained in the presence of *n*-octylamine [26] and for TiO_2-SiO_2 nanocomposites [11,32,45]. Silica nanomaterials with similar structures have been obtained by other authors in the presence of formamide [46], ammonia [47], and *n*-octylamine [48]. In this context, Bogush and Zukoski [47] developed an aggregative growth model to explain the formation of these uniform silica nanoparticles in a basic medium, such as ammonia, in which the rate of condensation is faster than the hydrolysis. In our materials, we also speculate that the formation of silica nanoparticles occurs by a similar aggregation mechanism [23,26]. We think that *n*-octylamine acts as a basic catalyst, promoting the condensation of silica oligomers present in the starting sol.

Comparatively, S forms a particulate material with a smaller and more homogeneous particle size

(around 90 nm) than those corresponding to any material including titania. When TiO_2 nanoparticles (Fig. 2) are added to the sols, aggregates composed of particles are also formed. In both cases, the aggregation of smaller silica nanoparticles can be observed, thus confirming the mechanism of growth proposed. Regarding the size of the aggregates, the composites present a larger average size due to the presence of TiO_2 nanoparticles mixed with those of SiO_2 , and show sizes ranging from 110 to 400 nm. In addition, in these composites, smaller particles (ranging from 20 to 50 nm) are observed on the surface of the aggregates, which we attribute to the presence of TiO_2 nanoparticles. These particles are not visible in S aggregates (Fig. 2a). Kontos et al. [48] also observed by SEM the formation of TiO_2 particles for hydrothermally treated pure TiO_2 films; these authors also attributed this finding to an aggregation phenomenon.

Regarding the effect of TiO_2 loading on the aggregate size, higher loadings cause a clear increase in the average particle size of the aggregates. This can be explained as a consequence of the larger size of the pre-formed TiO_2 nanoparticles employed in this study in comparison to the silica particles created during sol-gel transition, as postulated later when the TEM images are discussed. In addition, possible interactions produced between titania and n-octylamine, previously reported [36,50], may also play a role in the formation of aggregates. If some of the surfactant is adsorbed on the surface of the titania particles, less *n*-octylamine is available to catalyze the sol-gel transition when titania loading is raised. This could subsequently promote a suppressive effect of the silica condensation according to the proposed aggregation mechanism. This possibility is confirmed by the composites' appearance, which is more rigid for the materials without titania (S) and those with the lowest content (S1 series), which could be associated with a higher degree of silica condensation in these materials. Consequently, a gradual increase in titania loading results in the creation of smaller silica particles during the sol-gel transition. As previously indicated, these smaller particles are easily aggregated to the preformed titania particles due to their higher surface energy [35]. This produces a larger number of silica particles to be aggregated, thus creating larger aggregates. This assumption is particularly evident for S10P90 where very large aggregates are formed. This could be due to the greater adsorption of *n*-octylamine caused by

the large surface area of P90 TiO_2 nanoparticles.

Regarding the possible effect of the size of the titania particles, we do not observe a clear effect on the aggregate size. In the specific case of the highest titania loading, a larger aggregate size is clearly visible for S10P90 (see Fig.2). We again associated this increase with the higher degree of aggregation occurring between the titania particles with the lowest size (P90) and the large surface area of this particles previously commented. All of these results seem to suggest that there is a critical titania particle size for promoting aggregation, which could be estimated at between 21 nm (P25 average size) and 14 nm (P90 average size).

Further, these micrographs also confirm that the initial 20 μm size of AP nanoparticles is reduced from a micrometer to a nanometer scale, close to the size presented by P25 and P90 particles, due to the strong cavitation power of ultrasonic stirring, as previously discussed.

In order to investigate in more depth the porous structure of these materials and, especially, the distribution of silica and titania particles within the aggregates, nitrogen physisorption tests were carried out. Adsorption-desorption isotherms and BJH pore size distributions obtained from the isotherm desorption branches for the materials under study are also shown in Fig. 3.The textural data obtained are given in Table 2. AP, P90 and P25 TiO_2 nanoparticles, were also characterized for comparative purposes (see Fig. 4 and Table 2 as Supporting information). All of the commercial types of preformed titania particles present a type IV isotherm with a H1 hysteresis loop, as expected for an agglomerate of TiO_2 nanoparticles [51]. Textural information on AP and P25 nanoparticles is in good agreement with the differences in their particle size. AP nanoparticles present a lower surface area but higher pore volume and pore size, which should be due to its larger particle size. In the case of P90 nanoparticles, we expected them to show values similar to P25. However, for P90 the pore size is twice as large as that corresponding to P25. We assume that this difference is due to the phenomenon of aggregation among the smallest TiO_2 nanoparticles studied. This seems to confirm again that there is a critical size of titania nanoparticles, for their aggregation, of between 14 and 21 nm.

Considering the nanocomposites synthesized in our laboratory, all the materials, including S1 (without titania) show type IV isotherms as a consequence of the coarsening effect on the gel network exerted by n-octylamine [11]. Regarding hysteresis, most of the materials present a triangular hysteresis loop, classified as an H2 loop. In the case of the nanocomposites containing P25 particles, a type H1 hysteresis loop, characterized by parallel and nearly vertical branches, is observed. According to the literature [51], an H1 hysteresis loop is reported for materials that consist of spherical particles. In general, this loop is characteristic of materials with high uniformity of pore size and high connectivity between pores. Materials with H2 hysteresis present a similar structure but with lower connectivity. These isotherm profiles therefore suggest that all our materials are composed of a network of silica spheres, and the titania particles are integrated within this network. We have previously obtained similar morphologies [11], consisting of a dispersion of TiO_2 nanoparticles inside a regular matrix of uniform silica spheres. These results also confirm the aggregation mechanism previously proposed.

Some significant differences between these materials are observed in the titania loading effect on their texture. For titania loading rates of 1% and 4%, the SAP and SP90 materials show a pore size and pore volume similar to those obtained for the material without titania (S), while the values obtained for S1P25 are slightly higher. For the highest titania loading rate (10%), a significant reduction in pore volume is observed for SAP and S90. Other authors have found similar decreases in pore volume for increasing TiO_2 loadings [16,17]. This inverse relationship can be explained as a consequence of a higher proportion of non-porous TiO_2 nanoparticles being incorporated in the gel network.

In respect of pore size distribution, for all the titania loadings evaluated all the photocatalysts containing P25 present a more heterogeneous pore distribution at higher pore sizes. One possible explanation is that the P25 nanoparticles are more dispersed in the silica matrix. We think that AP and P90 particles, due to their larger size and greater aggregation, respectively, promote the creation of larger pore spaces inside the gel network. The size of these pores was measured by N_2 physisorption (see Table 2 in the Supplementary information), and for both of them it was around 40 nm. We speculate that these spaces are easily occupied by the silica particles created during the sol-gel transition. In the case of P25, pores

are smaller (around 20 nm, see Table 2 in the Supplementary information) and they thus cannot be occupied by the silica particles. Thus, a lower silica-titania packing that promotes a large pore size and a more heterogeneous distribution should be produced for materials containing P25. A similar trend was observed for TiO_2-SiO_2 nanocomposites previously synthesized in our laboratory from P25 titania particles and the same silica precursor employed in this study [11] for loadings ranging from 0% to 2%. Fattakhova-Rohlfing et al. [19] reported that the presence of TiO_2 nanoparticles could act to open the continuous siliceous framework. Similarly, Zelenak et al. [50] reported that interparticle space is created between the titania nanoparticles integrated within a silica matrix. Lastly, it is notable that the photocatalysts containing P90 and AP particles show significantly higher surface areas than those corresponding to P25 materials for loadings of 1% and 4%, because most of the porosity is constituted by pores of smaller size.

For a deeper investigation of the silica-titania distribution in these materials, we carried out a transmission electronic microscopy (TEM) study. Figure 4 shows representative images of S4AP, S4P25 and S4P90, acquired in TEM (4a,b,c) and HAADF-STEM (4d,e,f) modes. These photocatalysts were selected for this study to describe their structure in greater detail on the basis of their intermediate TiO_2-loading. In addition, they are of especial interest because, as will be discussed later, these three composites showed the most efficient photocatalytic behavior. In Figures 4a,b,c, individual TiO_2 nanoparticles can be observed perfectly clearly as inclusions in a SiO_2 mesoporous matrix.

These images illustrate three important features of our nanocomposites: 1. the existence of two clearly distinct and separate domains corresponding to TiO_2 and SiO_2; 2. TiO_2 presents a crystalline configuration due to the visible lattice spacing present in the structure of the material, whereas SiO_2 presents an amorphous configuration in the absence of this lattice spacing; and 3. variations in the size of TiO_2 nanoparticles and in their distribution, in the three photocatalysts, are clearly visible in the images. Figures 4d,e,f (STEM images with Z-contrast) show individual TiO_2 nanoparticles of different sizes (visibly brighter) inside the SiO_2 mesostructure. These images are particularly valuable for providing better insight into the SiO_2 porous network (which appears less bright in the image), and

allowing us to confirm the TiO_2 and SiO_2 particle sizes obtained in TEM images. From these images, the following features can be established: P25 and P90 TiO_2 nanoparticles integrated in the SiO_2 matrices present an average particle size similar to that stated by the manufacturer for the individual particles (21 nm and 14 nm, respectively). It is significant that numerous aggregates of 30-80 nm size are clearly observed in the image of S4P90 whereas the S4P25 composite is composed basically of individual particles. In the case of AP particles, their disaggregation produced by ultrasound stirring resulted in the presence, in the S4AP material, of TiO_2 nanoparticles with an elongated particle shape and with a particle size of around 40-50 nm. This particle size is larger than those corresponding to S4P25 and S4P90. In addition, some smaller particles are also present.

Considering next the SiO_2 nanoparticles formed, we observe that their size is around 15-20 nm, very similar to the size of individual P25 particles. This could result in a lower degree of packing among silica and P25 titania particles than that obtained for the other preformed titania particles included in this study. In the case of AP and P90 titania particles, these produce a larger pore space (around 40 nm) into which the silica particles are more easily packed. In order to illustrate our hypothesis, a schematic model of the structures of the composites is also included in Figures 4g,h,i.

FTIR spectra of the nanomaterials under study are presented in Figure 5. All the materials, present two peaks typical of siloxanes, located at 795 and 1045 cm^{-1}, corresponding to bending and stretching vibrations, respectively [26,44]. Each spectrum also shows a peak adjacent to the stretching vibration, located at 1161 cm^{-1}. This double band (1045−1161 cm^{-1}) is associated with chains of high-molecular weight siloxanes [23,52]. This demonstrates that the sol-gel transition was effective and consequently, a high-molecular weight silica polymer has been created.

For increasing TiO_2 nanoparticles content in the photocatalysts, we observe a decrease in transmittance of between 750-650 cm^{-1}. Zelenak et al [50] attributed differences of around 620 cm^{-1} to vibrations in the TiO_2 bulk phase. After thermal treatment at 650, 850 and 1000 ºC, these authors also observed a transmittance decrease in the previously-cited range and attributed it to the growth of TiO_2

nanoparticles. Thus, we think that this reduction is caused by increasing the loading of TiO_2 nanoparticles integrated in the silica matrix.

The peak at 970 cm^{-1} shown in the spectra of the photocatalysts calls for particular attention. It can be attributed, *a priori*, to Si−OH stretching vibration [26]. However, the typical broad band shown for silica gels at 3750-3250 cm^{-1} associated with hydrogen-bonded silanol groups with absorbed molecular water, which should be detected together with any –OH bond, shows a weak signal in these spectra [26]. Consequently, we think that the 970 cm^{-1} peak could also be attributed to Si−N stretching vibration [53], due to hydrogen-bonded interactions that occur between the silica and the n-octylamine. Similarly, we [23] recently reported the presence of this Si-N interaction in the materials prepared from TES40, water and *n*-octylamine. We confirm the presence of *n*-octylamine in the photocatalysts tested in several other peaks observed in the spectra. Specifically, the bands at 1392 and 1444 cm^{-1} are attributed to *n*-octylamine C−N stretching [26,54] and C−H bending [21,54], respectively. In addition, we observe a peak at 1485 cm^{-1} which, according to the literature [55], results from amino groups strongly hydrogen-bonded to free silanols. This confirms that the *n*-octylamine interactions with the silica precursor are produced by hydrogen bonds. The presence of n-octylamine in these spectra confirms that it was not completely removed during drying. In a recent paper [23], we also observe that n-octylamine was partially retained in silica gels dried under the same conditions.

Another contribution to the intensity of the 970 cm^{-1} peak could be that of Ti-O-Si vibrations. In previous studies, a band attributed to these vibrations is usually observed in the 950-960 cm^{-1} zone [44]. Other authors have reported that the absorption in this zone results from both Ti-O-Si and $Si-O^-$ contributions [14]. However, the TEM images (Fig.4) confirm that TiO_2 and SiO_2 are maintained in separate domains in our composites and consequently, an incorporation of Ti in the silica lattice has not taken place. Therefore, the interaction produced between TiO_2 and SiO_2 corresponds to van der Waals physical bonds instead of chemically-bonded Ti-O-Si linkages [56].

We also observed three bands, at 2890 cm^{-1}, 2930 cm^{-1} and 2975 cm^{-1}, which we relate respectively to $-CH_3$ symmetric stretching, $–CH_2$ asymmetric stretching and $-CH_3$ asymmetric stretching [52]; these

three bands are more evident in the case of S10 photocatalysts. These bands may be associated with ethoxy groups from non-hydrolyzed oligomers present in the material. Another band is observed at 1296 cm^{-1}, corresponding to CH_2 twist vibration, which could also be attributed to ethoxy groups [57]. A higher intensity of all these peaks is observed in the materials with higher titania content, confirming that TiO_2 particles exert a suppressive effect on silica hydrolysis and condensation, and consequently more non-hydrolyzed oligomers are present, as we have discussed in preceding paragraphs. In addition, the spectrum of S showed a much lower intensity for these peaks than any other of the materials.

The diffuse reflectance UV-Vis spectra obtained for all the photocatalysts are shown in Figure 6, with the object of evaluating the absorption range of the titania integrated in the silica matrix. All the photocatalysts show absorption in the UV range (up to 400 nm), and no absorption in the visible range. This means that the inclusion of TiO_2 nanoparticles in a silica matrix does not produce absorption in the visible range, as might be expected, for instance, in doping processes. Moreover, by comparing all our spectra with others previously obtained for TiO_2 P25 nanoparticles [58], we can corroborate that there is no significant change of absorption after the inclusion of TiO_2 in a silica matrix. Similarly, Alvaro et al. [20] reported that the absorption bands were intrinsically inherent to the presence of TiO_2 nanoparticles and were not altered by the presence of silica domains in the solid, because Ti-O-Si bonds corresponding to a truly mixed oxide were not present in the material. This finding confirms that silica and titania are present in separate domains in the nanocomposites studied, as we previously observed by TEM (Fig. 4). Considering the location of the titania within the silica matrix, Zelenak et al. [50] reported that titania absorption in the 350-400 nm range is related to the presence of a TiO_2 phase in the silica pore system or pore walls. We observed absorption in a similar range (320-400 nm), which again confirms that titania and silica are present in separate domains.

The ^{29}Si NMR spectra for all the xerogels obtained are shown in Figure 7. All of the materials under study show two peaks at chemical shifts of −100 ppm and −110 ppm corresponding, respectively, to Q3 and Q4 structural units. In all these materials, except those with the highest titania loading (S10 serie), the Q4 peak, attributable to tetrafunctional buildings, is higher than that corresponding to Q3, indicating

a more cross-linked framework due the effect of *n*-octylamine. This higher degree of reticulation is typical of silica species condensed as particles [59]. It was also observed in silica particle mesostructures obtained using amine surfactants as a template [60]; and this was recently confirmed by us in silica materials prepared with *n*-octylamine [23]. This finding confirms that *n*-octylamine produces nanomaterials composed of a network of silica particles, as was visualized by SEM and TEM (see Figures 2 and 4). The lower intensity observed in Q4 for S10 materials indicates, *a priori*, that less reticulation is produced.

Another significant difference according to the TiO_2 content was also observed. The three spectra from the photocatalysts containing the highest proportion of TiO_2 (S10) presented Q1 (−89 ppm) and Q2 (−91 ppm) units in conjunction with Q3 and Q4 species. Davis et al. [14] also observed an increase in signals corresponding to a reduced silica reticulation as TiO_2 content was raised. In our case, we speculate that this difference is due to an incomplete condensation of silica and consequently, some ethoxy groups are present in the material. This information is in good agreement with the increase of -CH_2- and -CH3 detected through FTIR, and with the increased aggregate size detected by SEM. Here, we can confirm that these larger aggregates are also less condensed silica structures. In the case of photocatalysts with the lowest TiO_2 content, the signals from Q1 and Q2 are either absent or observed as a very weak signal. This finding confirms the role played by the *n*-octylamine as catalyst during the sol−gel transition, and the inhibition of its catalytic action by the presence of TiO_2, previously discussed in this manuscript.

3.2. Application on stone, and characterization. The photocatalysts synthesized in this study were sprayed as sols, under laboratory conditions, onto a building limestone in order to investigate its photocatalytic behavior, its penetration depth, adhesion to the stone, and strengthening properties. For comparison purposes, the effectiveness of S, which is only composed of titania, was also evaluated. Uptake and dry matter of the sols under study are shown in Table 3. Although some variations were found between samples due the heterogeneity of the limestone samples, we observe certain trends, as follows: the S sol produces the lowest uptake and dry matter among the sols applied. Uptake and dry

matter percentages also seem to show a tendency to increase as TiO_2 nanoparticles content is raised. These trends are explained because the higher TiO_2 nanoparticles content means that the liquid content in the sol is lower, and thus less sol could evaporate during the sol application. Moreover, sol could also evaporate partially because carbonate stones slow down the sol-gel transition, as reported by Wheeler et al. [61].

Figure 8 shows SEM images of stone specimens treated with the photocatalysts under study and their counterpart without titania. All of the materials under study form a crack-free, homogeneous and coarse coating on the stone surface. This confirms the contribution of n-octylamine to reducing the capillary pressure responsible for cracking. As we have previously stated [11,21,28,32], the surfactant reduces capillary pressure in two different ways: 1. by coarsening the gel network pore size; and 2. by reducing the surface tension of the starting sol. It should also be noted that the coarsening produced by n-octylamine must also improve the access to photoactive sites, thus increasing the photocatalytic activity. We also observe some changes in the morphology of the coatings when TiO_2 nanoparticles are integrated in the silica network. Specifically, the higher titania loading produces larger aggregates, in good agreement with the behavior observed from the coatings produced on Petri dishes previously discussed in this paper (Fig. 2). This allows us to corroborate that the stone substrate has little influence in the final surface morphology of these photocatalysts.

We investigated the penetration depth of the sols by using SEM to visualize a cross section of the limestone samples treated. X-EDS elemental mappings for Ti and Si were also obtained. All the sols show a similar behavior when they are applied on the stone. As an example, the X-EDS mappings obtained for cross-sections of limestone treated with S#AP photocatalysts are shown in Fig. 9. Mappings corresponding to limestone samples treated with S are also included for comparison purposes. These mappings allow us to confirm that S presents a deep penetration of Si across all the depth range evaluated. S1AP shows that both Ti and Si penetrate to a very similar depth. In the case of the materials with higher titania loading (S4AP and S10AP), we also observe a significant accumulation of Ti and Si

on the stone surface. This finding could be associated with the higher viscosity of these coatings with the highest contents in titania particles.

In order to confirm this conjecture, Fig 10a presents a BSE image of the cross-section of the limestone sample treated with S4AP. Images with higher magnification were obtained on the surface (indicated in blue, Figs. 10b and c) and in the interior (indicated in yellow, Figs. 10d and e) of the stone in SE and BSE modes, respectively. From this more detailed analysis of the cross section of S4AP we can observe that a thin photoactive surface film is formed (Fig. 10b) which also penetrates between the stone grains. The presence of the photocatalyst between the grains is clearly visible in Fig. 10c because of the higher atomic number of Ca with respect to Si. We thereby corroborate that our photocatalyst is able to adhere to the limestone, a characteristic essential for its potential long-term performance [7]. We do not obtain the same result for the deeper zones of the limestone (Fig. 10d, SE mode and Fig. 10e, BSE mode), probably because the deeper zone has a lower content of S4AP, as confirmed by the results previously obtained by SEM.

Since one significant drawback of commercial products applied on stone has been the reduced photocatalytic efficiency found during long-term use, due to the elimination of TiO_2 from the stone surface [7,11], we have also investigated the degree of adhesion of the coatings applied on stone, by performing a peeling test adapted from the literature [28]. Table 3 shows the weight lost by the untreated stone and its treated counterparts after testing.

The greatest loss of mass after the peeling test is observed for the untreated stone (see Table 3). This happens because the untreated stone surface presents a considerable amount of loose matter which can easily be detached through our adhesion testing method. Stone samples treated with S and S1 photocatalysts show almost negligible loss of mass (see Table 1). These findings confirm that TiO_2 has been integrated into the silica matrix, which has, in turn, adhered firmly to the stone. In this respect, the inclusion of the photocatalyst in a mesoporous silica coating is an interesting solution for keeping particles well adhered to the surface, to provide long-term wear resistance.

For higher TiO_2 nanoparticles content the test removed a slightly larger amount of material from the stone surface, reaching a maximum for the coatings with the highest TiO_2 content (S10). We associate this result with the formation of a less condensed and more detachable composite on the limestone surface for coatings with the highest titania loadings, as was previously confirmed through ^{29}Si NMR. We also investigated whether any enhanced strengthening of the stone was produced by the products applied; this was done by measuring and comparing the drilling resistance of the untreated limestone and its treated counterparts. The device used has been designed specifically to evaluate mechanical resistance of stone, and provides a very high discriminating power [62]. Figure 11 shows the profiles obtained in this study.

Some significant differences were observed in line with variation in the titania loading. The material without titania (S) produces the greatest increase in mechanical resistance; and the samples treated with the lowest titania loading composites show resistance values similar to those obtained for the stone treated with the material without TiO_2. This demonstrates that a 1% loading is not enough to modify the robustness produced by the composite formed into the stone pore structure. The materials with higher titania loading showed reduced drilling resistance. This result could be explained as a consequence of the very low degree of reticulation and condensation of the gel networks, as we have previously discussed.

Comparing the two materials with the higher titania loadings, we observe that the 4% loading produced the least reduction in stone resistance, nearly to the value obtained for the untreated stone. We attribute this behavior to titania particles being more robust than the silica gel network. We also consider that these test results confirm that *n*-octylamine is playing a valuable role in enhancing the robustness of the treated stone, since silicon-based products are known to be ineffective as consolidants on pure carbonate stones [27,63]. In a previous study, we found increased drilling resistance for the same limestone using a SiO_2/TiO_2 hybrid coating material obtained in the presence of *n*-octylamine [11].

Since water is the main vehicle carrying the agents of decay, such as soluble salts, microorganisms, etc., that attack building materials, any hydrophilicity in a coating would be undesirable. Therefore, we have

also measured water droplet static contact angles on the surface of stone samples treated with the photocatalysts under study. Results obtained are given in Table 3. The untreated limestones samples show a low contact angle (61º) due to the hydrophilic character of the stone. We observe that static contact angles are higher for the stones treated with composites with the lower TiO_2 nanoparticles contents. Specifically, the S1 and S4 photocatalysts show a hydrophobic behavior, with a static contact angle value higher than 90º or close to this value. When more TiO_2 nanoparticles are loaded in the photocatalysts, there is a decreasing tendency in the static contact angles due the hydrophilic character of TiO_2 nanoparticles, as we have reported before [11]. These results demonstrate that the nanocomposites with 1% and 4% titania loading do not produce water absorption and thus can be employed as protective coatings in stones and other building materials.

Another very practical limitation on the prospective employment of these products would be encountered if they produced changes in the color of the stone treated. Therefore, total color difference values (ΔE^*) of the stone induced by the photocatalysts were measured and these results are given in Table 3. All the photocatalysts produced color changes close to the generally accepted threshold value $\Delta E^* \leq 5$, even for the most restrictive applications such as ancient building restoration [64]. This parameter is particularly critical for materials containing TiO_2, which is widely used as a white pigment for its considerable hiding power. By dispersing particles of sizes reduced to the nanoscale, these coatings also reduce the hiding power of TiO_2 and minimize the possibilities of significant color change. In addition, we propose removing the excess of sol on the stone surface directly after its application. We confirmed that, by using this application method, it was possible to reduce the color change to suitable values for application on stone surfaces and buildings.

Finally, and most importantly, we have investigated the self-cleaning properties of the photocatalyists synthesized in our laboratory and applied to the limestone tested, by carrying out a photo-degradation test of stains deposited previously on the stone surface. Methylene blue (MB) was used as the staining agent, dissolved in ethanol in order to ensure rapid evaporation of all the liquid. The evolution of total color differences (ΔE^*) under UV light, with the time was recorded, and results are shown in Figure 12,

for the photocatalysts under study. Limestones treated with S and also untreated samples were included in this test for comparison purposes. In order to confirm the changes in color undergone by the specimens under study, Figure 13 shows images, observed by optical microscopy, of the surface of the stone samples, obtained at the end of the photocatalytic test.

The conditions of this test make the following comments relevant: 1. It was performed in the absence of liquid water and with low relative humidity (around 30%); therefore, degradation times are necessarily slower than in experiments carried out in high moisture, because the generation of $OH^{\bullet}$ free radicals is reduced; in our view, if these products are applied on buildings outdoors, the moisture present in the environment would probably accelerate the photodegradation process; 2. Our test has been carried out in the presence of atmospheric oxygen and at neutral pH conditions, thus ensuring that all the color variations are due to the elimination of MB, and not to the undesirable formation of the leuco form of MB (LMB) [65]; 3. We have evaluated photodegradation by measuring the total color variation parameter because this is usually considered for portable color measurement; this makes it very useful for testing the degradation, in situ, in construction, restoration or rehabilitation of buildings.

Regarding the results obtained (see Fig. 12), the final ΔE^* value reached for the untreated stone is 38.3, after more than 1000 hours of exposure, corresponding to a "natural" reduction of 17%. Bleaching of methylene blue (MB) under visible/UV light has been reported previously, and this bleaching has been associated with the absorption of light undergone by the dye in the 350-520 nm range [65].

In the case of the limestone samples treated with the photocatalysts synthesized in this study, from the profiles two different rates of degradation at different times can be clearly distinguished. Very rapid MB bleaching occurs in the first 72 h. Next, a slower rate of degradation is observed over the longer term. As we reported previously [11,32], we think the photocatalytic action of the TiO_2 particles produces most of the total degradation effect on the stain in the first few hours of exposure (the first part of the curve). We speculate that the second stage, with a much slower rate of degradation, may be caused by an effect of the SiO_2/TiO_2 coating initially reducing the capacity of the MB to penetrate into the limestone pore structure. Thus, MB is retained on the stone surface where it can be degraded more

easily than that located deeper in the pore structure of untreated stone. This hypothesis is corroborated by the behavior observed for the stone samples treated with the material without TiO_2 (S). Obviously, the first stage of curve associated with the photocatalytic action of the TiO_2 is not observed in these samples. However, a degradation profile similar to that corresponding to the second stage shown in the samples coated with the nanocomposites is clearly observed. We again attribute this degradation profile to the effect of silica coating reducing MB penetration into the limestone pore structure.

Considering now the effect of the TiO_2 loading on the photocatalytic performance of the nanocomposites under study, we observe that increasing the TiO_2 content from 1% to 4 % enhances the photocatalytic activity, as was expected. This is confirmed by the significantly shorter first stage of the curve (due to photocatalytic activity) in materials containing 1% titania loading. However, increasing the titania loading to 10% is clearly counterproductive. The final color observed on the stone surface of the samples confirms this conclusion (see Fig. 13). We explain this significantly reduced photocatalytic activity in terms of the structure of these nanocomposites. The substantial reduction in pore volume and BET surface area for the materials containing the highest titania content (see Table 2 and Fig.3) could be responsible for the reduced photocatalytic effectiveness observed. We [11] and other authors [18] have previously reported that the photocatalytic degradation of MB is clearly enhanced by the addition of TiO_2 particles to a SiO_2 mesoporous structure, in contrast with the weaker effect observed when the particles are integrated in a dense microporous matrix.

From the results discussed above, we can conclude that mesostructure of the photocatalyst, created by the n-octylamine, plays an important role in the photocatalytic activity of the materials under study. Thus, the nanocomposites with the highest titania loading, remarkably, show the weakest photocatalytic activity due to their very small pore size and specific surface; in fact, they hardly present any pores in the mesopore range. In contrast, the effectiveness of the other photocatalysts is enhanced because they are mesoporous materials with a larger surface area and pore volume. Other authors have obtained similar results [16,17,19,50]. This enhancement effect in photocatalytic activity was explained by Suzuki et al. in terms of the increased BET surface area, which accelerates the diffusion of MB towards

the reaction sites (i.e. towards the TiO_2 nanoparticles). In addition, we [11] have reported that the presence of mesopores also assists rapid MB diffusion. Moreover, we think a synergistic effect occurs with the SiO_2 matrix, which acts as an absorber and provides access to the TiO_2 photocatalytic sites. This hypothesis is clearly confirmed by the degradation profiles observed in the photocatalysts with highest titania loading, in which degradation profile is significantly lower because access to photoactive sites was significantly reduced.

A comparison of the three nanocomposites loaded to 4% with TiO_2 of different particle size also reveals certain differences. Specifically, S4AP, S4P90 and S4P25 present final ΔE^* values of 7.4, 11.8 and 16.6, respectively. The lower pore volume and pore size of S4P25 may be the explanation why it performs worse than the other two S4 photocatalysts (see Table 2), supporting the above hypothesis. The size of the TiO_2 particles used has a clear effect on photocatalytic performance of these materials. We find that the S#AP photocatalysts always show a better performance than the S#P90 and S#P25 counterparts. It seems that the higher average size and the sharper shape of the TiO_2 nanoparticles present in S#AP, as observed by TEM/STEM, favors their photocatalytic effectiveness. The effect of particle size on TiO_2 photocatalysts has been reported previously by several authors [65-67], who found that larger titania particles have greater effective surface area for greater photon absorption and electron-hole generation and, thus, produce a better photocatalytic performance. Regarding to the effect of particle shape, Li and Liu [69] suggested previously that sharper titania particles could be inherently more reactive in photo-oxidation. In our case, the AP particles used are sharper than the other types because the high-power ultrasonic agitation applied in the synthesis changes the particles from a regular spherical form (see Fig. 2 in the Supplementary information) to an irregular and sharper shape (see Fig. 4).

Another complementary characteristic that may enhance the photocathalytic activity in the S4AP materials is their higher BET surface area. We observe that the increasing surface area for S4 materials promotes increased photocatalytic effect (AP>P90>P25). This trend was confirmed by Yoshida et al. [70]. This effect is not observed with the other loadings tested either because titania content is too low

(S1) or because a non-porous network is created (S10). The final color observed on the stone surface confirms that the S#P25 and S#P90 photocatalysts have a weaker photocatalytic performance in comparison with the S#AP nanocomposites (Fig. 13).

4. Conclusions

We have designed an innovative synthesis route for producing TiO_2-SiO_2 photocatalysts with application on stones and other building materials. A surfactant constituent acts: 1. to disperse the titania particles; 2. to catalyze the sol-gel transition; and 3. to coarsen the porous gel network, thus providing better access to photoactive sites. We demonstrate that these photocatalysts present self-cleaning properties on the limestone evaluated, are able to adhere firmly to the stone, and improve stone robustness.

From our in-depth investigation of the texture of these photocatalysts, we conclude that this is a key parameter for the efficacy of the photocatalytic activity. Specifically, the incorporation of larger and sharper titania particles within a silica network significantly improves the effectiveness of the photocatalyst on the stone, and subsequently enhances its self-cleaning effect. We attribute this improvement to the high availability of photoactive surface sites in these materials.

We also demonstrate that increasing the titania loading (up to an optimal content of 4%) produces an improvement in photocatalytic activity. For a higher content (10%), this activity decreases, because the pore volume of the nanocomposite is drastically reduced and consequently, access to photoactive sites is more difficult. Moreover, a 10% loading has the following disadvantages, due to the n-octylamine reducing the catalytic effect during sol-gel transition: 1. weaker adherence to the stone; and 2. less strengthening imparted to the stone.

Finally, we believe that the photocatalysts synthesized have clear practical applications, because the products obtained by this route meet the user requirements for a photocatalytic coating that can be applied externally, outdoors, in a simple and low-cost process, and which preserves the aesthetic qualities of the stone.

Acknowledgments

We are grateful for financial support from the Spanish Government/FEDER-EU (Project MAT2010-16206 and Project Regenera, Innpacto subprogram), and the Government of Andalusia (project TEP-6386 and Group TEP-243). L.P. thanks the Fundação Ciência e Tecnologia for his predoctoral grant (SFRH/BD/43492/2008). We also thank Dr. Javier Navas, Eng. Francesco Scavello, Dr. Mónica Alvarez de Buergo and IGM-CSIC-UCM for their help with UV spectra, viscosity data interpretation and drilling resistance measurements, respectively.

References

1. I. Karastasios, M. S. Katsiotis, V. Likodimos, A. Kontos, G. Papavassiliou, P. Falaras, V. Kilikoglou, Appl. Catal. B 95 (2010) 78.
2. A. Fujishima, T. Rao, D. Tryk, J. Photochem. Photobiol. C 1 (2000) 1.
3. M. Lackhoff, X. Prieto, N. Nestle, F. Dehn, R. Niessner, Appl. Cat. B (2003) 205.
4. I. Poulios, P. Spathis, A. Grigoriadou, K. Delidou, P. Tsoumparis, J. Environ. Sci. Health A 34 (1999) 1455.
5. E. Quagliarini, F. Bondioli, G. Goffredo, C. Cordoni, P. Munafò, Const. Build. Mat. 37 (2012) 51.
6. M. F. La Russa, S. A. Ruffolo, N. Rovella, C. M. Belfiore, A. M. Palermo, M. T. Guzzi; G. M. Crisci, Prog. Org. Coat. 74 (2012) 186.
7. K. Rao, M. Subrahmanyam, P. Boule, Apply. Catal. B Environ. 49 (2004) 239.
8. L.Windler, C. Lorenz, N. von Goetz, K. Hungerbühler, M. Amberg, M. Heuberger, B. Nowack, Environ. Sci. Technol. 46 (2012) 8181.
9. A. Pénard, T. Gacoin, J. Boilot, Acc. Chem. Res. 40 (2007) 895.

10. H. Kibombo, R. Peng, S. Rasalingam, R. Koodali, Catal. Sci. Technol. 2 (2012) 1737.
11. L. Pinho, M. J. Mosquera, J. Phys Chem. C 115 (2011) 22851.
12. W. Zhang, M. Fröba, J. Wang, P. Tanev, J. Wong, T. Pinnavaia, J. Am. Chem. Soc. 118 (1996) 9164.
13. M. Kruk, M. Jaroniec, A. Sayari, Microporous Mater. 9 (1997) 173.
14. R. Davis, Z. Liu, Chem. Mater. 9 (1997) 2311.
15. A. Fujishima, K. Honda, Nature 238 (1972) 1.
16. K. De Witte, V. Meynen, M. Mertens, O. I. Lebedev, G. Van Tendeloo, A. Sepúlveda-Escribano, F. Rodríguez-Reinoso, E. F. Vansant, P. Cool, Appl. Cat. B, 84 (2008) 125.
17. E. Beyers, E. Biermans, S. Ribbens, K. De Witte; M. Mertens; V. Meynen; S. Bals, G. Van Tendeloo, E. F. Vansant, P. Cool, Appl. Catal. B 88 (2009) 515.
18. N. Suzuki, X. Jiang, L. Radhakrishnan, K. Takai, K. Shimasaki, Y. Huang, N. Miyamoto, Y. Yamauchi, Bull. Chem. Soc. Jpn. 84 (2011) 812.
19. D. Fattakhova-Rohlfing, J. Szeifert, Q. Yu,; V. Kalousek, R. Rathouský, T. Bein, Chem. Mater. 21 (2009) 2410.
20. M. Alvaro, E. Carbonell, V. Fornés, H. García, Chem. Phys. Chem. 7 (2006) 200.
21. M. J. Mosquera, D. M. de los Santos, T. Rivas, Langmuir 26 (2010) 6737.
22. J. F. Illescas, M. J. Mosquera, J. Phys Chem. C 115 (2011) 14624.
23. J. F. Illescas; M.J. Mosquera, Appl. Mat. Interfaces 4 (2012) 4259.
24. M.J. Mosquera, A. Montes, D. M. de Los Santos, US Patent: US 11/997,356.
25. M. J. Mosquera, L. Pinho, Spanish Patent No. P201100741. Priority date: June 24, 2011.
26. M. J. Mosquera, D. M. de los Santos, A. Montes, L. Valdez-Castro, Langmuir 24 (2008) 2772.
27. A. P. Ferreira Pinto, J. Delgado Rodrigues, J. Cultural Heritage 9 (2008) 38.
28. M. Drdácký, J. Lesák, S. Rescic, Z. Slížková; P. Tiano, J. Valach, Materials and Structures 45 (2012) 505.

29. R.S. Berns, Billmeyer and Saltzman's principles of color technology; Wiley-Interscience: New York, 2000.
30. ISO 10678; Fine ceramics (advanced ceramics, advanced technical ceramics); Determination of photocatalytic activity of surfaces in an aqueous medium by degradation of methylene blue. ISO, 2010.
31. P. O. Vasiliev, B. Faure, J. B. S. Ng, L. Bergström, J. Colloid. Interf. Sci. 319 (2008) 144.
32. L. Pinho, M. J. Mosquera, Prog. Org. Coat. (2012) submitted
33. H. Yang, C. Li, H. Gu, T. Fang, J. Colloid Interf. Sci. 236 (2001) 69-103.
34. P. Mikulasek; R. J. Wakeman, J.Q. Marchant, Chem. Eng. J. 67 (1997) 97.
35. X. Zhang, B. Xia, H. Ye, Y. Zhang, B. Xiao, L. Yan, H. Lv, B. Jiang, J. Mater. Chem. 22 (2012) 13132.
36. E. Beyers, P. Cool, E. Vansant, J. Phys Chem B. 109 (2005) 10081.
37. K. Suttiponparnit, J. Jiang, M. Sahu, S. Suvachittanont, T. Charinpanitkul, P. Biswas, Nanoscale Res. Lett. 6 (2011) 1.
38. M. Kosmulski, P. Prochniak, J.B. Rosenholm, J. Phys. Chem. C 113 (2009) 12806.
39. B. Erdem, E. D. Sudol, V. L. Dimonie, M. S. El-Aasser, J. Polym. Sci. Pol. Chem. 38 (2000) 4419.
40. C. Yu, H. Chu, Y. Wan, D. Zhao, J. Mater. Chem. 20 (2010) 4705.
41. H. Shibata, T. Ohkubo, H. Kohno, P. Rangsunvigit, H. Sakai, M. Abe, J. Photochem. Photobiol. A 181 (2006) 357.
42. M. J. Mosquera, D. M. de los Santos, L. Valdez-Castro, L. Esquivias, J. Non-Cryst. Solids 354 (2008) 645.
43. G. Zhang, J. Yi, J. Shim, J. Lee, W. Choi, Appl. Cat. B 102 (2011) 139.
44. A. Mirabedini, S.M. Mirabedini, A. A. Babalou, S. Pazokifard, Prog. Org. Coat. 72 (2011) 453.
45. L. Pinho, M. J. Mosquera, J. C. Hernández-Garrido, J. Calvino, Phys. Chem. Chem. Phys. (2012) submitted

46. G. Orcel, L. L. Hench, I. Artaki, J. Jonas, T. W. Zerda, J. Non-Cryst. Solids 105 (1988) 223.

47. G. H. Bogush, C. F. Zukoski, J. Colloid Interf. Sci. 142 (1991) 19.

48. K. Kosuge, P. S. Singh, Micro. &Mesoporous Mat. 44-45 (2001) 139.

49. A. I. Kontos, I. M. Arabatzis, D. S. Tsoukleris, A. G. Kontos, M. C. Bernard, D. E. Petrakis, P. Falaras, Catal. Today 101 (2005) 275.

50. V. Zeleňak, V. Hornebecq, S. Mornet, O. Schäf, P. Llewellyn, Chem. Mater. 18 (2006) 3184.

51. M. Kruk, M. Jaroniec, Chem. Mater. 13 (2001) 13 3169.

52. Z. Demjén, B. Pukánsky, E. Foldes, J. Nagy, J. Colloid. Interface Sci. 190 (1997) 427.

53. M. Sekine, S. Katayama, M. Mitomo, J. Non-Cryst. Solids 134 (1991) 199.

54. A. Prado, C. Airoldi, J. Mater. Chem. 12 (2002) 3823.

55. C.H. Weigel, Kellner, R., Fresenius Z. Anal. Chem. 335 (1989) 663.

56. X. Gao, I. E. Wachs, Catal. Today 51 (1999) 233.

57. P. Innocenzi, J. Non-Cryst. Solids 316 (2003) 309.

58. S. W. Verbruggen, K. Masschaele, E. Moortgat, T. E. Korany, B. Hauchecorne, J. A. Martens, S. Lenaerts Catal. Sci. Technol. (2012) doi: 10.1039/C2CY20123B

59. F. Babonneau, Polyhedron 13 (1994) 1123.

60. P.T. Tanev, T. Pinnavaia, J. Chem. Mater. 8 (1996) 2068.

61. G. Wheeler, Alkoxysilanes and the consolidation of stone, The Getty Conservation Institute: Los Angeles CA, 2005.

62. J. Delgado Rodrigues, A. Ferreira Pinto, D. Costa, J. Cult. Herit. 3 (2002) 117.

63. E. Zendri, G. Biscontin, I. Nardini, S. Riato, Const. Build. Mat. 21 (2007) 1098.

64. C. Miliani, M. L. Velo-Simpson, G. W. Scherer J. Cult. Herit. 8 (2007) 1.

65. A. Mills, J. Wang, J. Photochem. Photobiol. A, Chem. 127 (1999) 123.

66. T. P. Chou, Q. Zhang, B. Russo, G. E. Fryxell, G. Cao, J. Phys. Chem. C 111 (2007) 6296.

67. Z. Zhang, C. Wang, R. Zakaria, J. Ying, J. Phys. Chem. B 102 (1998) 10871.

68. J. T. Carneiro, A. R. Almeida, J. A. Moulijn, G. Mul, Phys. Chem. Chem. Phys. 12 (2010) 2744.

69. Y. Li, Z. Liu, J. Am. Chem. Soc. 133 (2011) 15743.

70. K. Yoshida, M. Makihara, N. Tanaka, S. Ayoagi, E. Nishibori, M. Sakata, E. Boyes, P. Gai, Microsc. Microanal. 12 (2011) 264.

Table(s)

Table 1. Viscosity for the sols under study

products	viscosity (mPa.s)		
	AP	**P25**	**P90**
TES40		4.82	
S		5.09	
S1	5.99	6.23	6.41
S4	11.1	11.65	10.49
S10	28.08	44.56	-

Table 2. Textural parameters obtained from the isotherms and by the BJH method for the TiO_2-SiO_2 photocatalysts under study. The data presented in simple form, square brackets and in parenthesis, correspond to AP, P25 and P90 photocatalysts, respectively

product series	S_{total} (m^2/g)	V_{pore} (cm^3/g)	pore size (nm)
S	231	0.39	6.3
S1	124 [180] (130)	0.22 [0.69] (0.29)	6.9 [13.4] (8.8)
S4	396 [90] (301)	0.49 [0.29] (0.45)	4.9 [11.7] (6.0)
S10	8.2 [90] (35.3)	0.07 [0.31] 0.07	- [13.8] (-)

Table 3. Properties of the treated stone specimens and the untreated counterparts

	% (w/v) TiO_2	uptake (% w/w)	dry matter (% w/w)	material removed by peeling (mg)	contact angle	ΔE *
U	-	-	-	2.3 ± 0.1	-	-
S	0	1.40 ± 0.05	0.82 ± 0.01	0.3 ± 0.1	91 ± 4	3.35 ± 0.10
AP	1	1.96 ± 0.17	1.31 ± 0.23	0.2 ± 0.0	99 ± 13	3.31 ± 0.18
	4	2.68 ± 0.00	1.44 ± 0.40	0.4 ± 0.2	90 ± 2	2.20 ± 0.19
	10	2.26 ± 0.36	1.57 ± 0.45	1.0 ± 0.0	85 ± 4	4.51 ± 1.89
P25	1	1.77 ± 0.60	1.64 ± 0.21	0.1 ± 0.1	106 ± 6	2.41 ± 0.30
	4	2.97 ± 0.03	1.44 ± 0.41	0.6 ± 0.2	79 ± 3	4.60 ± 0.13
	10	1.97 ± 0.01	1.26 ± 0.04	2.0 ± 0.9	85 ± 4	2.95 ± 0.05
P90	1	2.00 ± 0.05	0.95 ± 0.03	0.3 ± 0.1	102 ± 6	3.66 ± 0.03
	4	1.89 ± 0.03	1.23 ± 0.01	0.8 ± 0.4	90 ± 2	3.19 ± 0.20
	10	2.16 ± 0.49	1.61 ± 0.39	0.7 ± 0.4	87 ± 3	3.01 ± 0.08

*Data correspond to average values. Standard deviations are also included.

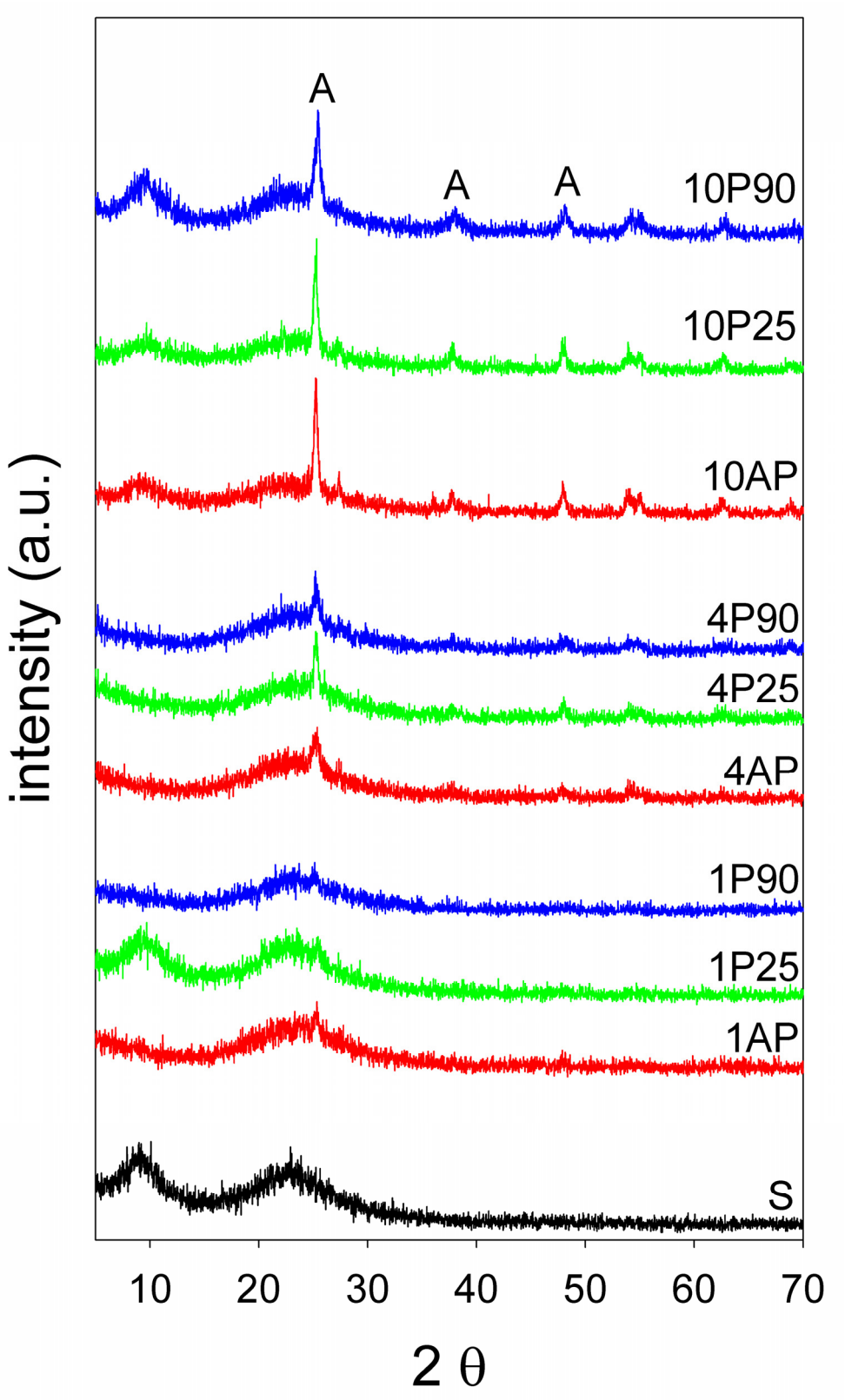
A
A
A
10P90
10P25
10AP
4P90
4P25
4AP
1P90
1P25
1AP
S
intensity (a.u.)
10
20
30
40
50
60
70
2 θ

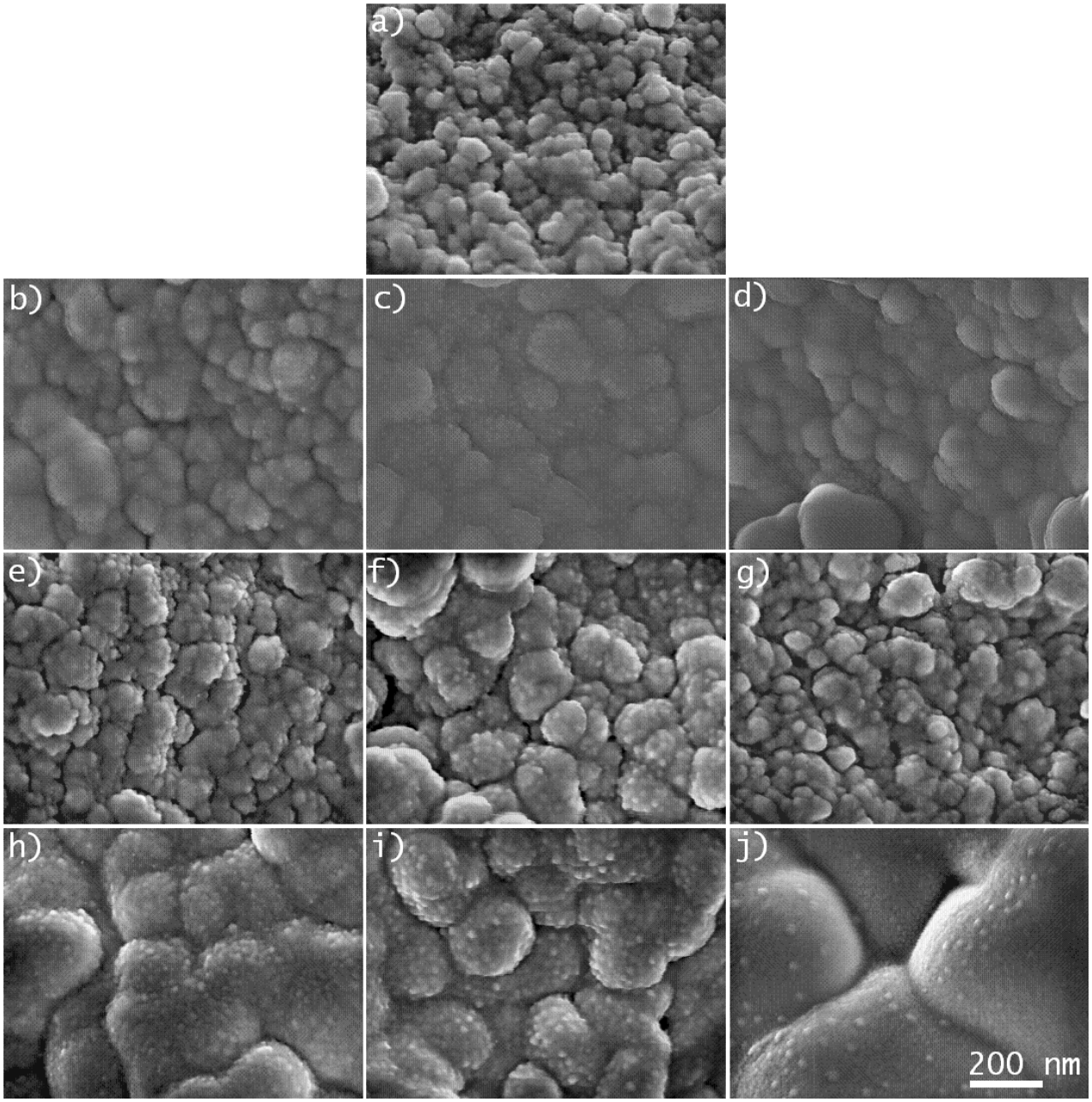
a)
b)
c)
d)
e)
f)
g)
h)
i)
j)
200 nm

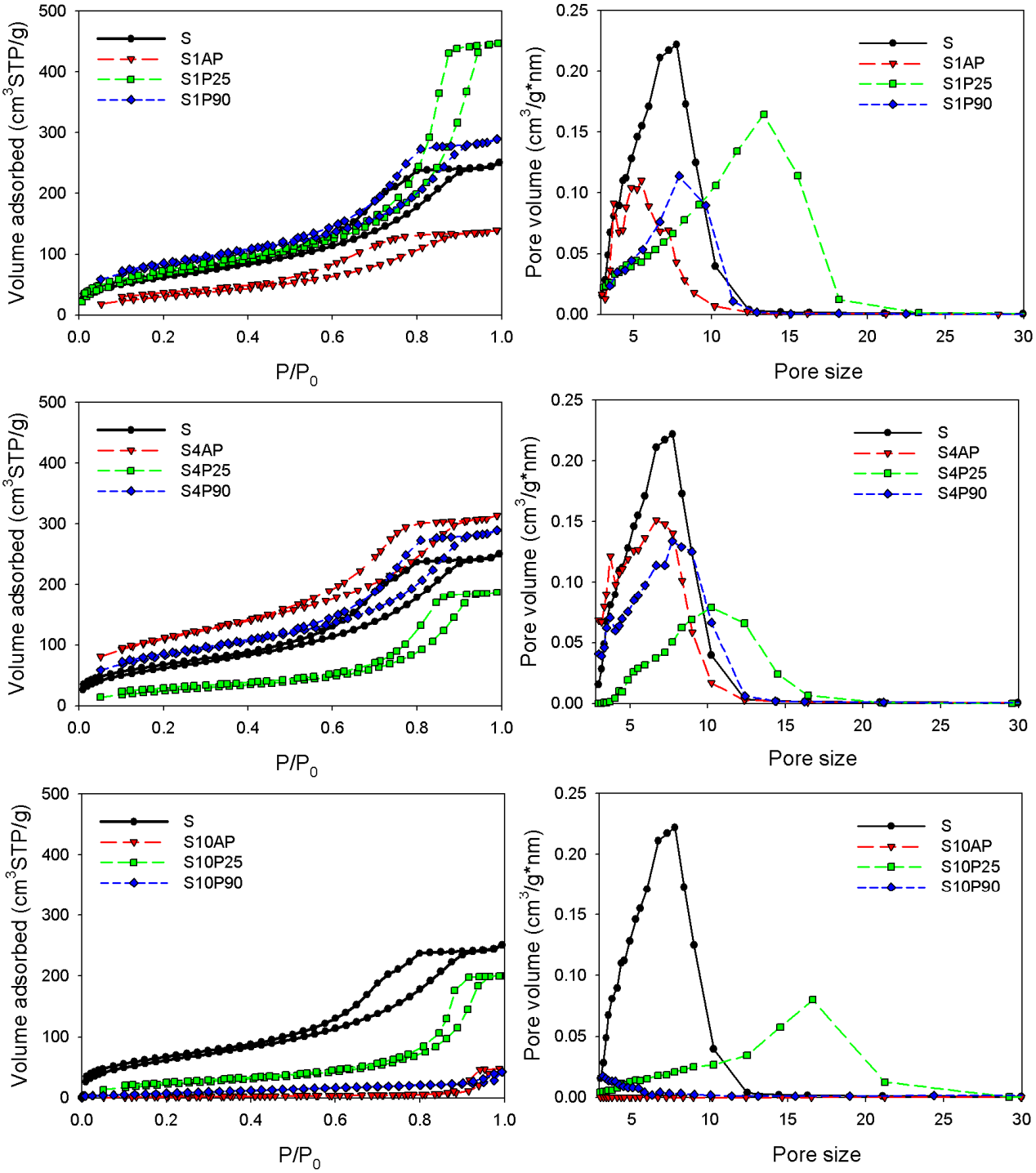
Volume adsorbed (cm3STP/g)
P/P0
S
S1AP
S1P25
S1P90
Pore volume (cm3/g*nm)
Pore size
S
S4AP
S4P25
S4P90
S10AP
S10P25
S10P90

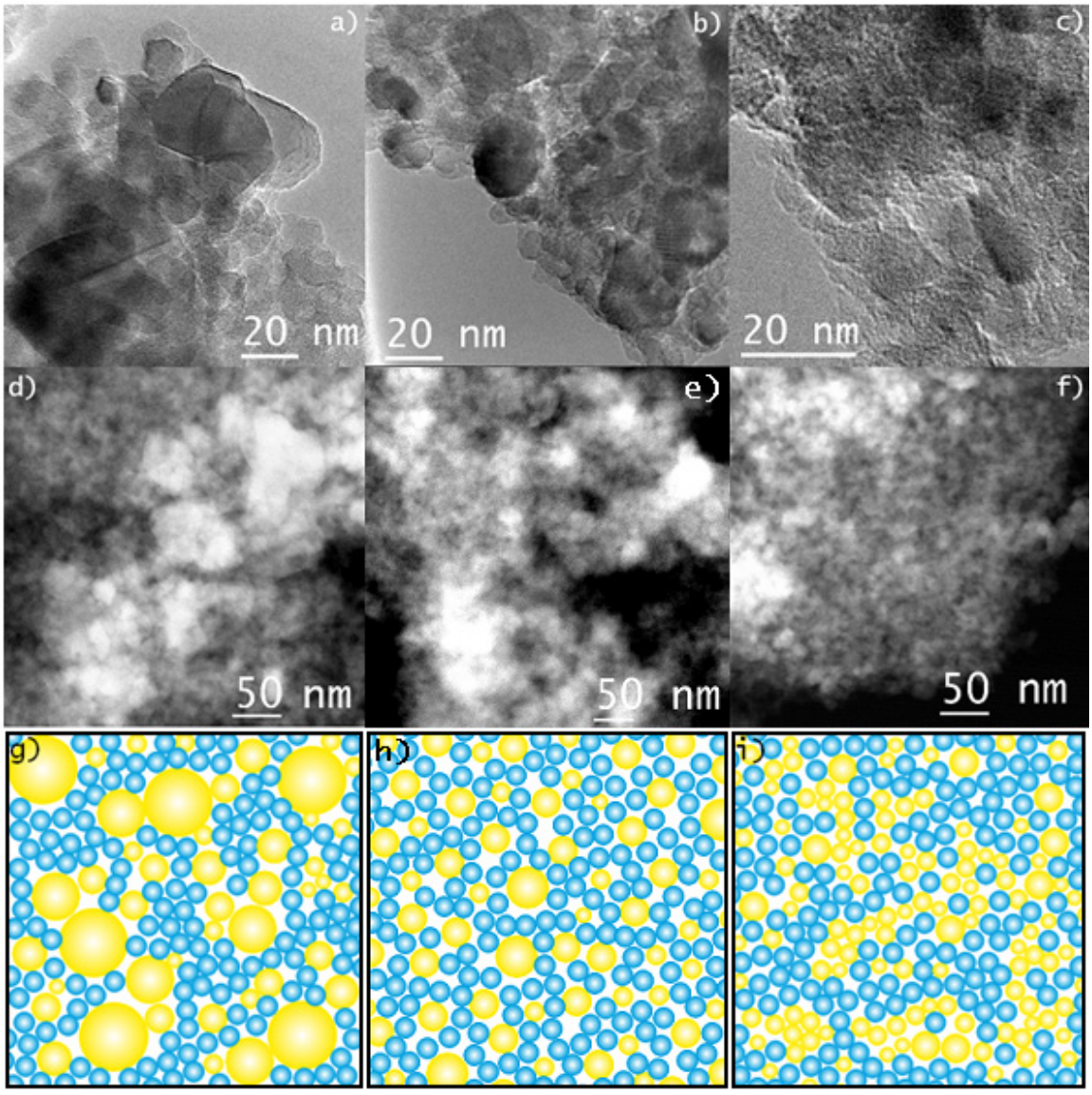
a)
20 nm
b)
20 nm
c)
20 nm
d)
50 nm
e)
50 nm
f)
50 nm
g)
h)
i)

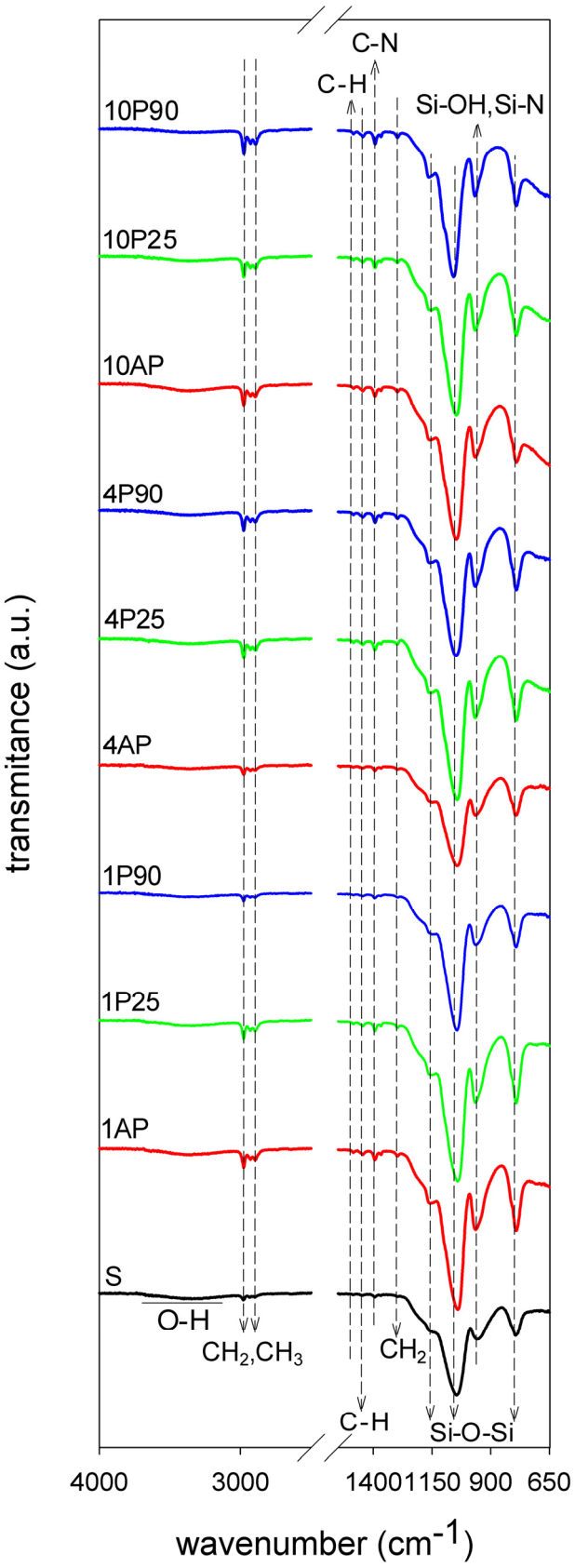
C-N
C-H
Si-OH,Si-N
10P90
10P25
10AP
4P90
4P25
4AP
1P90
1P25
1AP
S
O-H
CH2,CH3
CH2
C-H
Si-O-Si
transmitance (a.u.)
4000
3000
1400
1150
900
650
wavenumber (cm-1)

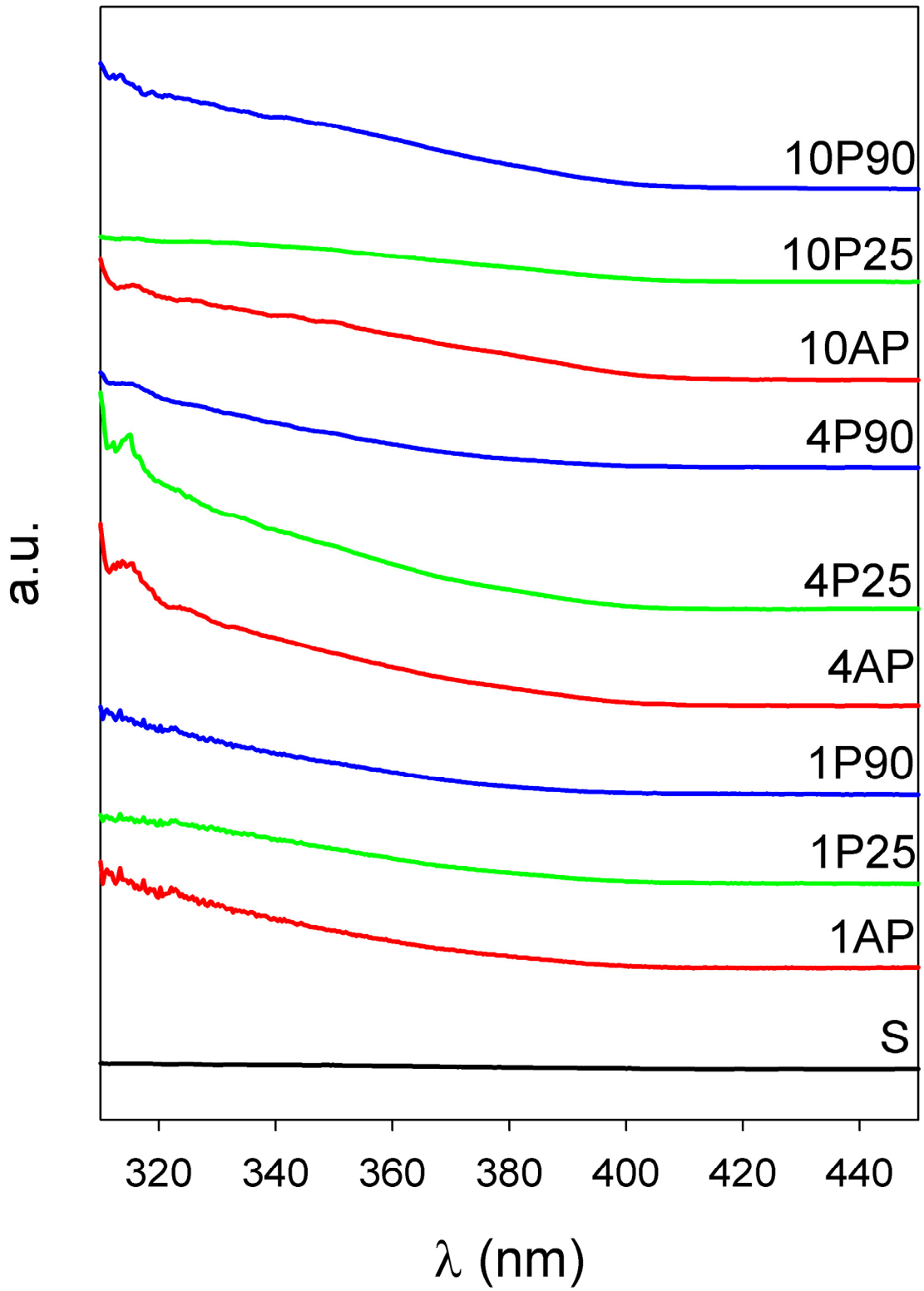
10P90
10P25
10AP
4P90
4P25
4AP
1P90
1P25
1AP
S
a.u.
320
340
360
380
400
420
440
λ (nm)

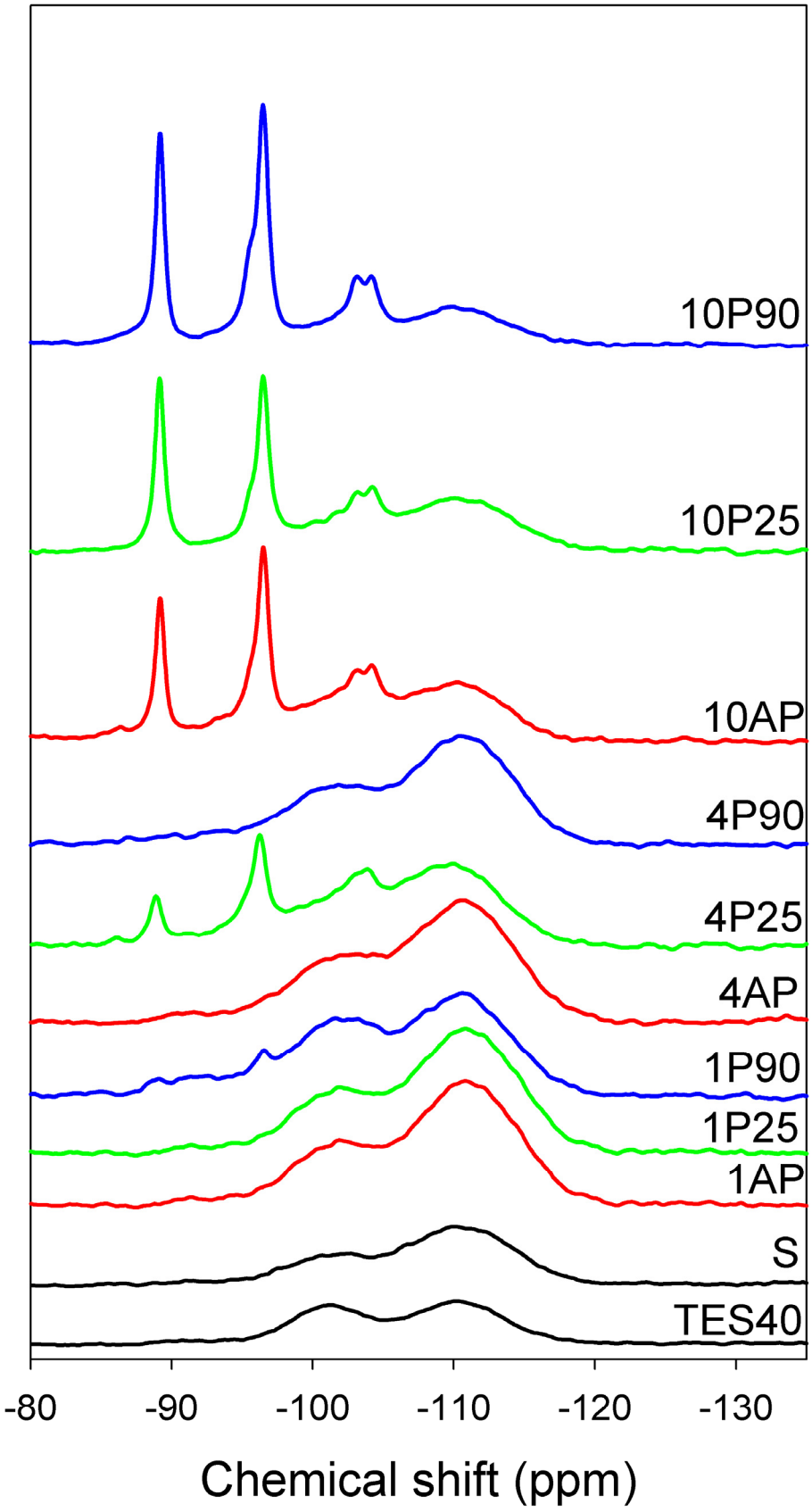
10P90
10P25
10AP
4P90
4P25
4AP
1P90
1P25
1AP
S
TES40
-80
-90
-100
-110
-120
-130
Chemical shift (ppm)

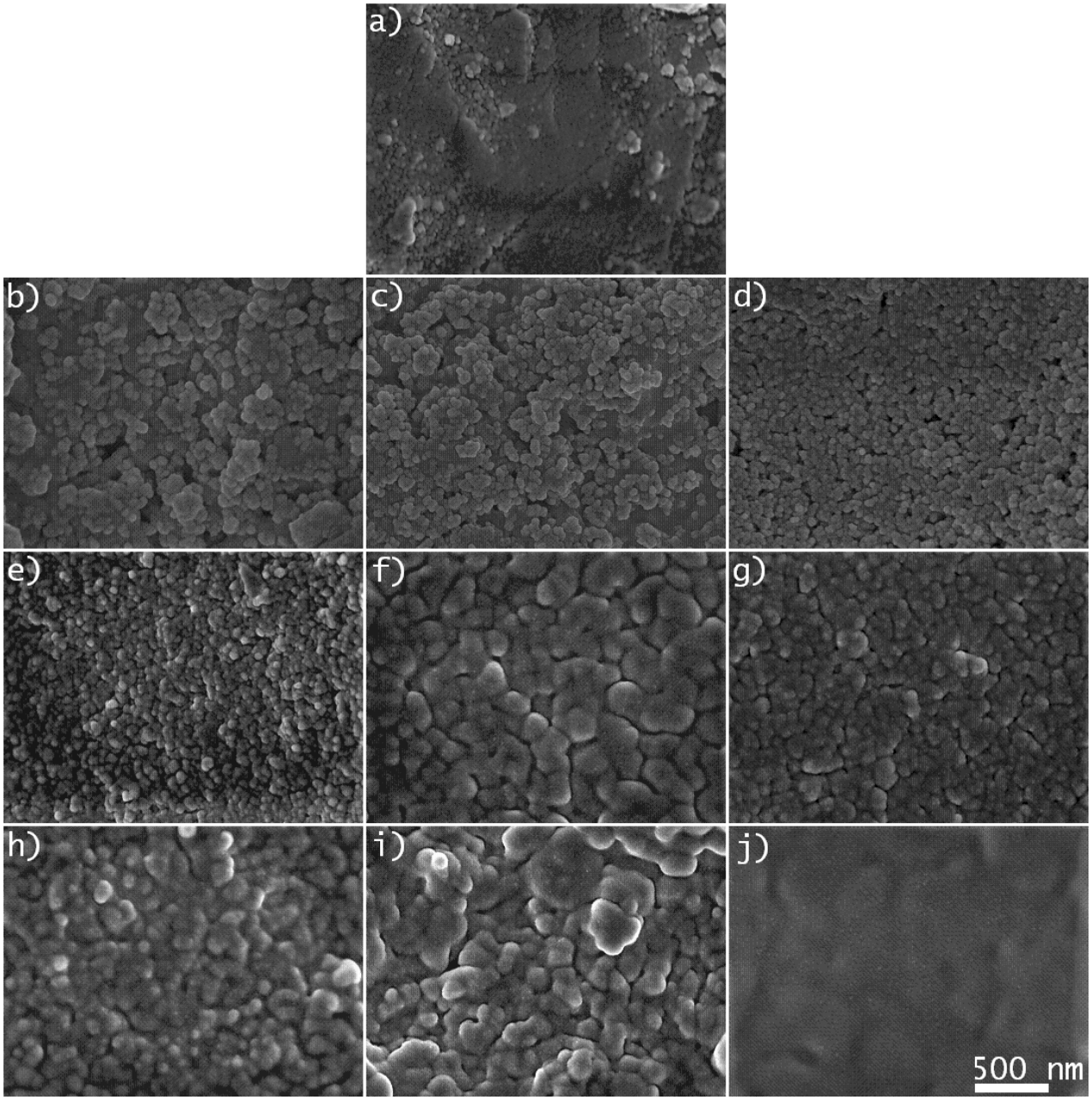
a)
b)
c)
d)
e)
f)
g)
h)
i)
j)
500 nm

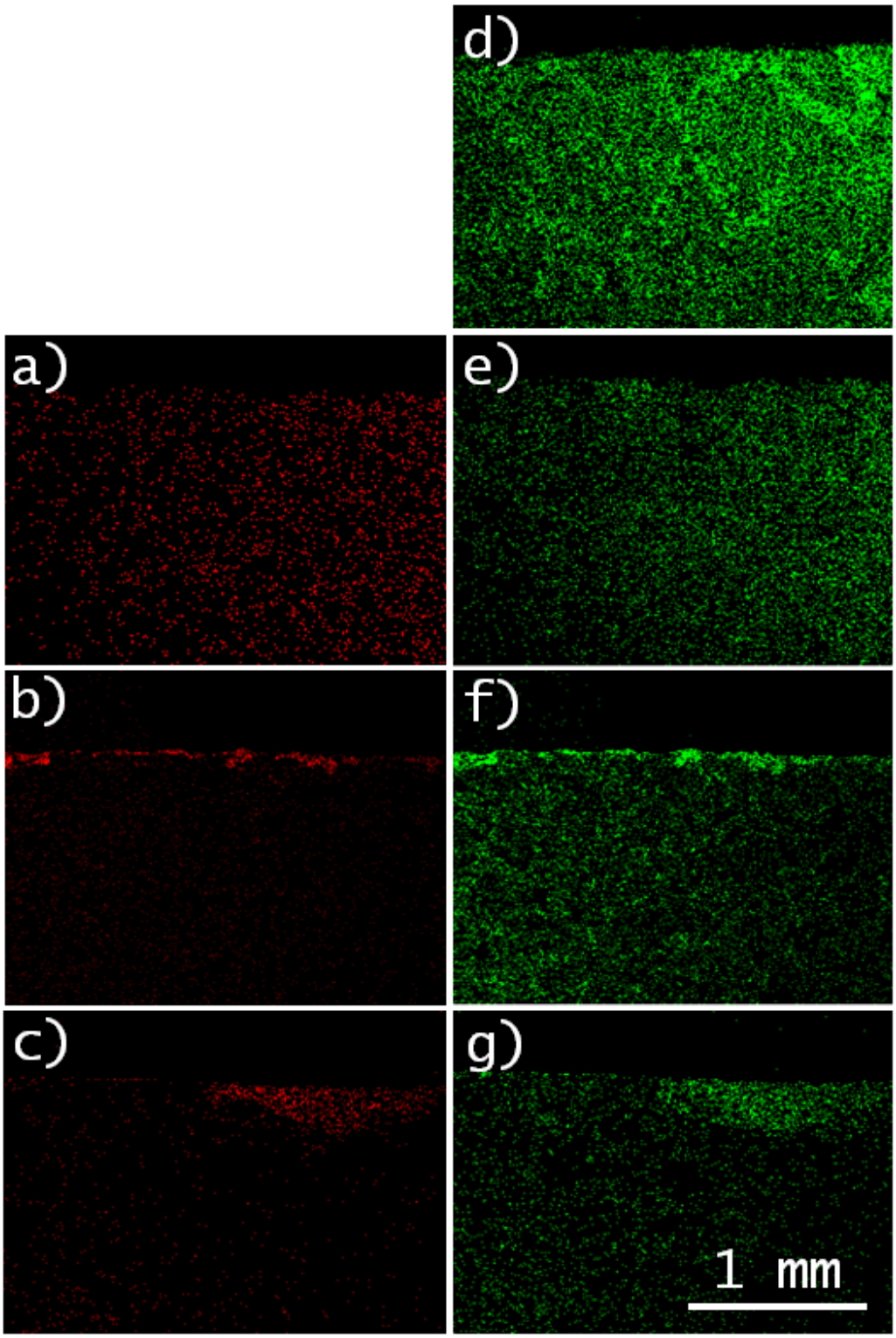
d)
a)
e)
b)
f)
c)
g)
1 mm

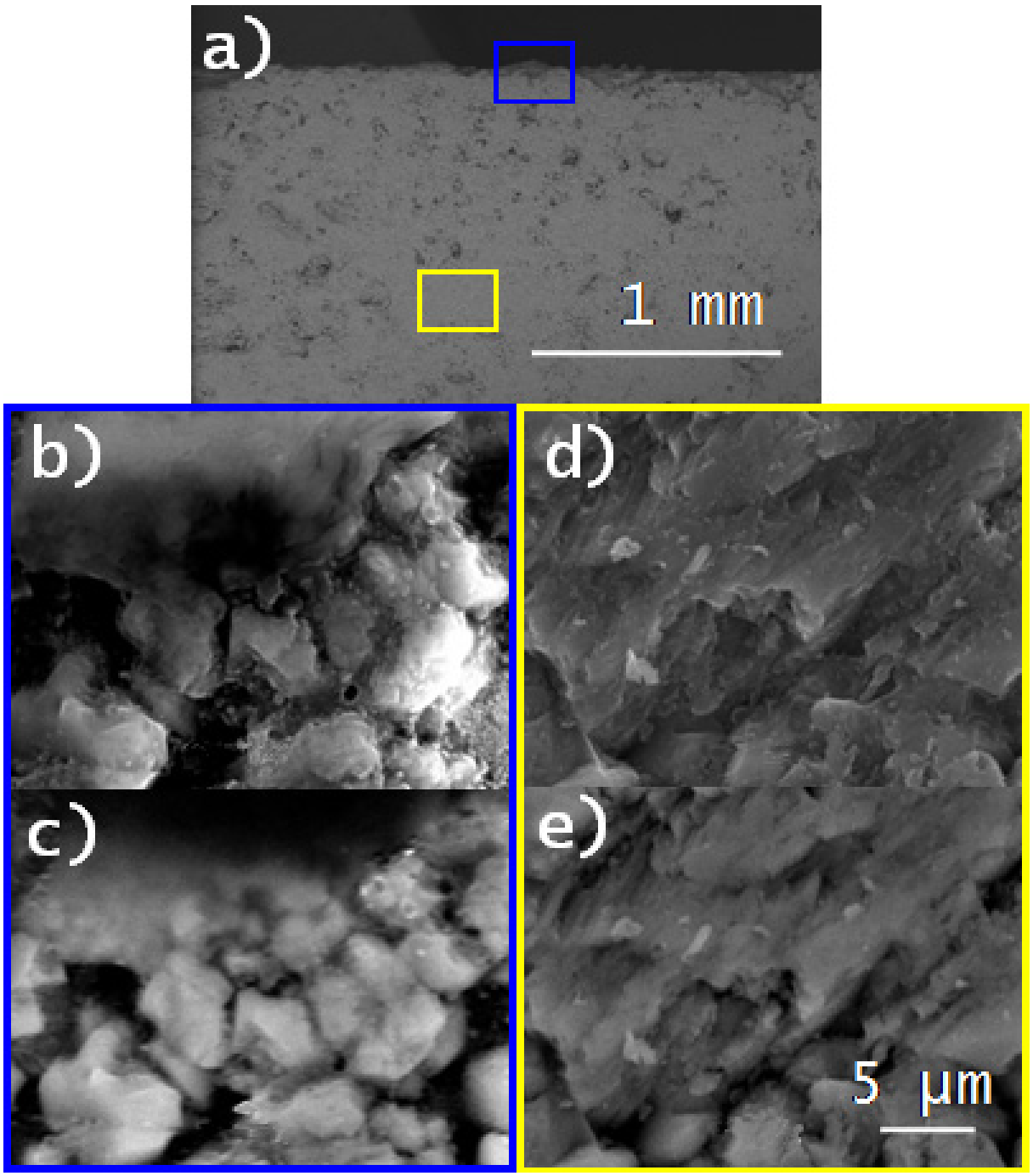
a)
1 mm
b)
c)
d)
e)
5 µm

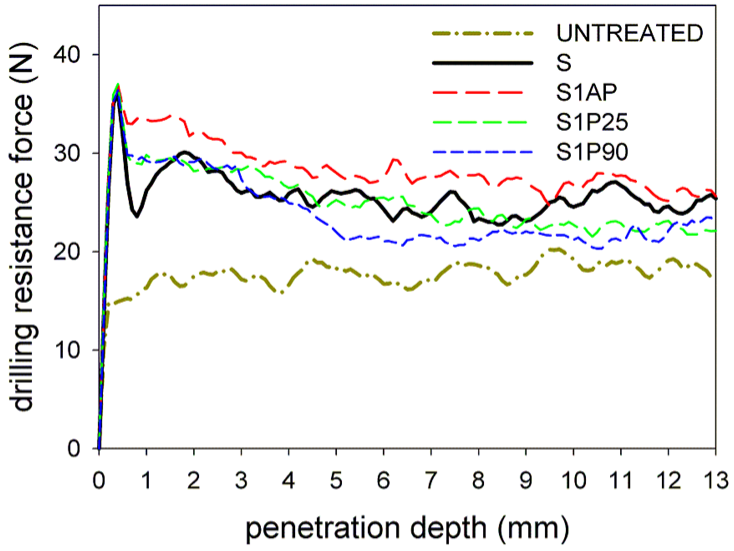
drilling resistance force (N)
penetration depth (mm)
UNTREATED
S
S1AP
S1P25
S1P90

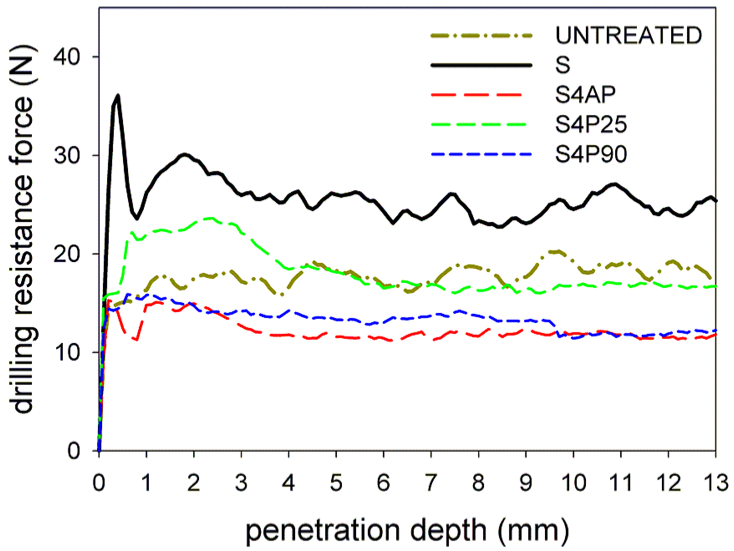
drilling resistance force (N)
penetration depth (mm)
UNTREATED
S
S4AP
S4P25
S4P90

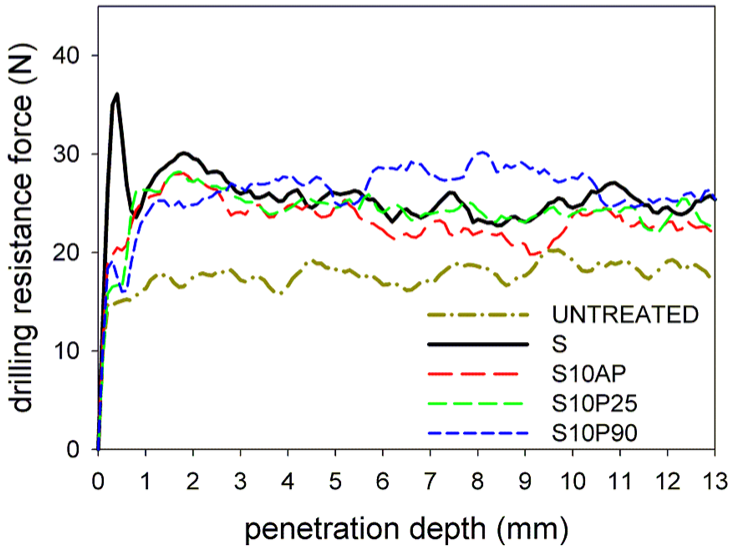
drilling resistance force (N)
penetration depth (mm)
UNTREATED
S
S10AP
S10P25
S10P90

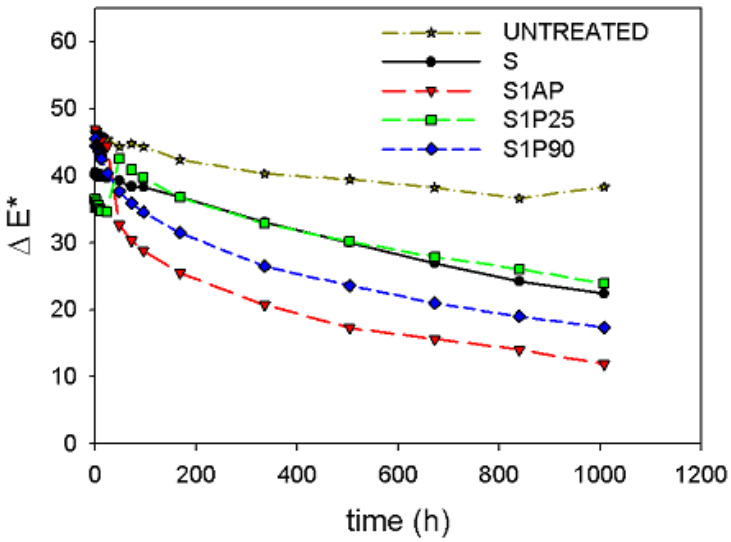
UNTREATED
S
S1AP
S1P25
S1P90
Δ E*
time (h)
0
10
20
30
40
50
60
0
200
400
600
800
1000
1200

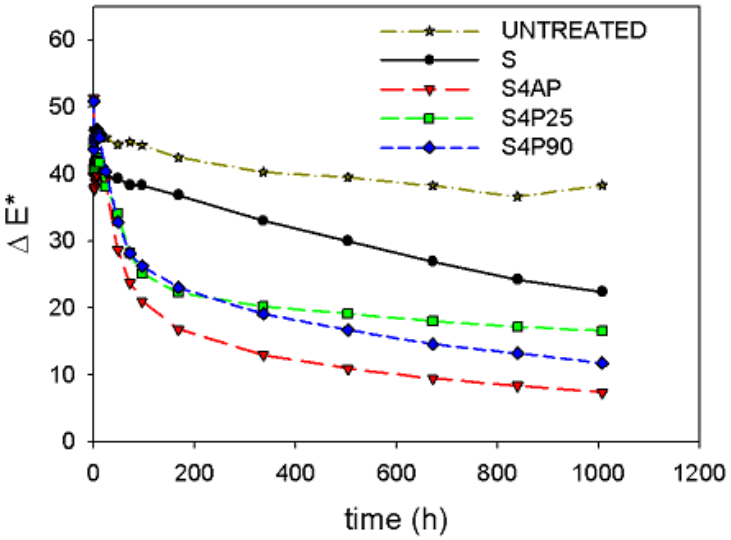
UNTREATED
S
S4AP
S4P25
S4P90
Δ E*
time (h)
0
10
20
30
40
50
60
0
200
400
600
800
1000
1200

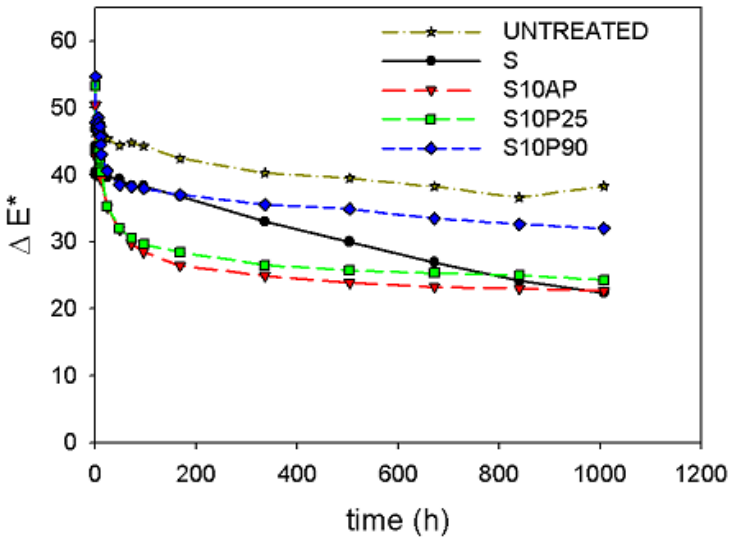
UNTREATED
S
S10AP
S10P25
S10P90
Δ E*
time (h)
0
10
20
30
40
50
60
0
200
400
600
800
1000
1200

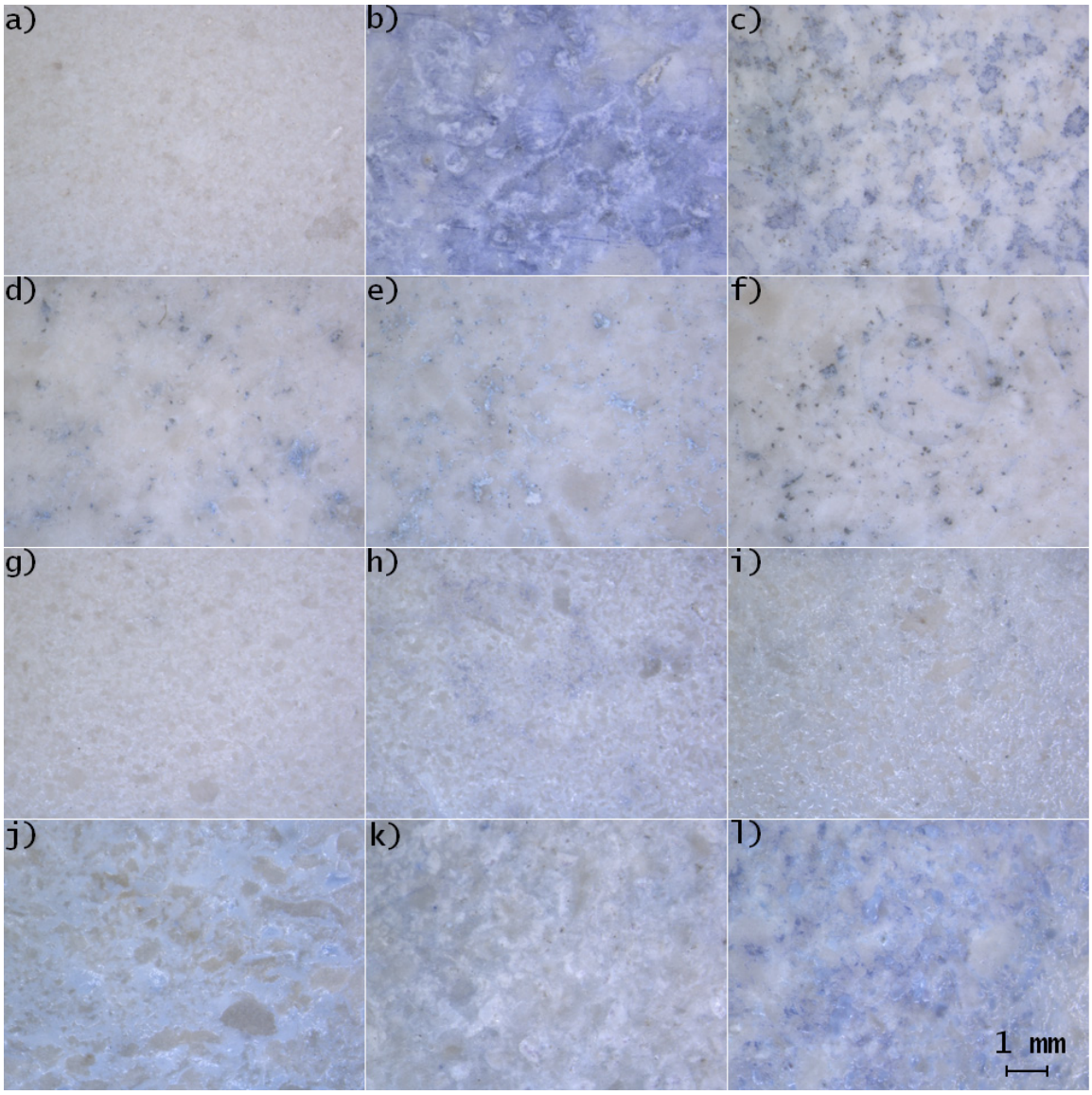
a)
b)
c)
d)
e)
f)
g)
h)
i)
j)
k)
l)
1 mm

Figure Captions

Figure 1. X-ray patterns for the photocatalysts under study

Fig. 2 SEM images of the photocatalysts under study. (a) S, (b) S1AP, (c) S1P25, (d) S1P90, (e) S4AP, (f) S4P25, (g) S4P90, (h) S10AP, (i) S10P25, (j) S10P90.

Figure 3. Isotherms and BJH pore size distributions for the photocatalysts under study.

Figure 4. Representative images of: (a) (d) S4AP, (b) (e) S4P25 and (c) (f) S4P90 obtained in TEM and HAADF-STEM modes, respectively. Schematic cross-sectional representations of (g) S4AP, (h) SP25 and (i) SP90 are also included. Ti and Si are indicated in yellow and blue, respectively.

Figure 5. FTIR spectra of the photocatalysts under study.

Figure 6. UV-Vis diffuse reflectance spectra of the photocatalysts under study.

Figure 7. ^{29}Si NMR spectra of the photocatalysts under study.

Figure 8. SEM images of the photocatalysts under study applied on stone. (a) S, (b) S1AP, (c) S1P25, (d) S1P90, (e) S4AP, (f) S4P25, (g) S4P90, (h) S10AP, (i) S10P25, (j) S10P90.

Fig 9. X-EDS elemental mappings for Ti (red) and Si (green) present in the cross section of limestone samples treated with (d) S , (a) (e) S1AP, (b) (f) S4AP, and (c) (g) S10AP.

Fig 10. Surface (b) (c) and in-depth (d) (e) images of the cross section of the limestone sample treated with S4AP. (b) d) were obtained in SE and (a) (c) (e) in BSE imaging mode. The area analyzed in (a) corresponds to the X-EDS elemental mappings present in Fig. 9 (a) (e).

Figure 11. Drilling resistance profiles for the limestone under study after the application of our photocatalysts.

Figure 12. Evolution of total color difference (for methylene blue stains) on treated and untreated samples of limestone. The samples were previously stained with Methylene Blue and then irradiated with UV light (λ_{min}=365 nm) for more than 1000 hours.

Figure 13. Representative optical microscopy images of the final color of the stone surface obtained after the self-cleaning test consisting of more than 1000 hours of UV light (λ_{min}=365 nm) irradiation. Image (a) corresponds to the untreated stone sample before staining and is included for comparison purposes. The untreated stone sample tested corresponds to (b). The samples subjected to treatment and tested are (c) S, (d) S1AP, (e) S1P25, (f) S1P90, (g) S4AP , (h) S4P25, (i) S4P90, (j) S10AP, (k) S10P25, (l) S10P90.

Supplementary Information

Table 1. Technical data provided by the supplier for TiO_2 nanoparticles

	Average primary particle size (nm)	Specific surface area ($m^2.g^{-1}$)	pH (in 4% dispersion)
AP	20 x 10^3	50 ± 15	3.0 - 4.5
P25	21	50 ± 15	3.5 – 4.5
P90	14	90 ± 20	3.2 – 4.2

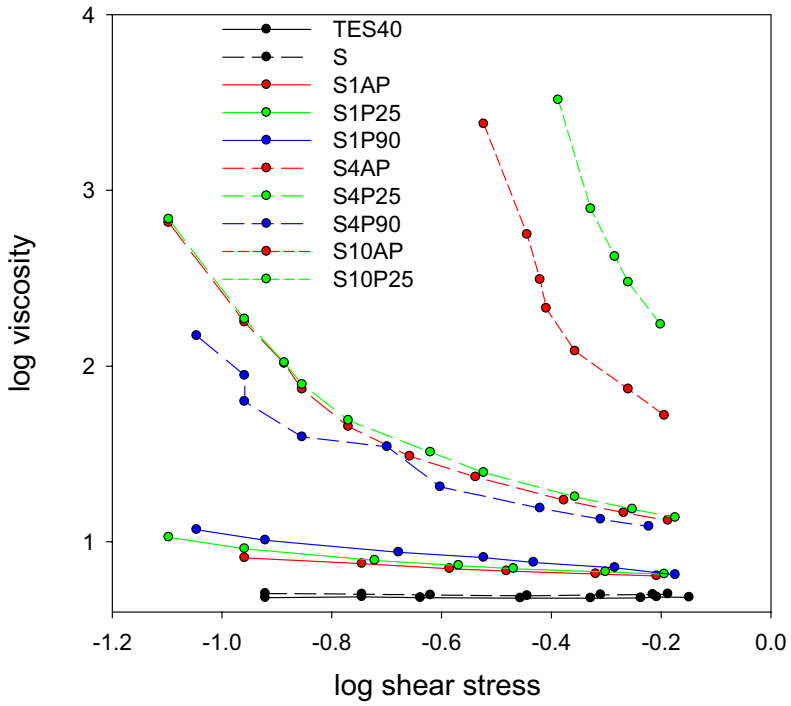

Fig.1. Variation of the viscosity with shear stress for the sols evaluated

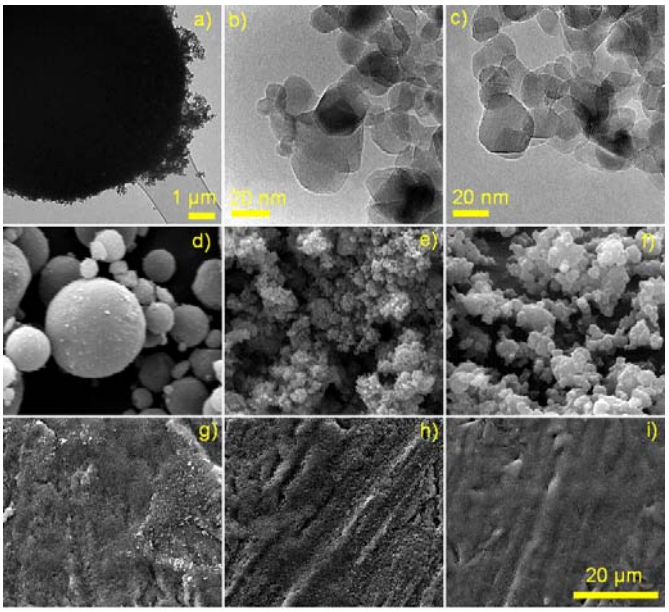

Fig. 2 Transmission electron microscopy a) b) c), SEM images of as-supplied d) e) f) and SEM images after ultrasonic stirring in water (g) h) i) images of the TiO_2 nanoparticles used in this study. The images in each row are presented from left to right in the following order: AP, P25 and P90.

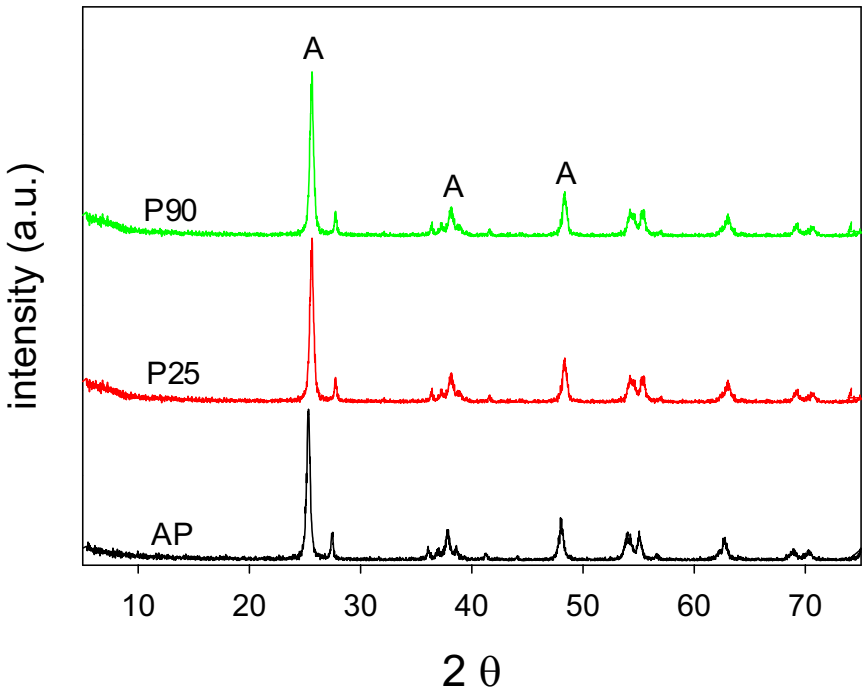

Fig 3. Diffractograms of the TiO_2 nanoparticles used in our syntheses.

Table 2. Textural parameters and crystal size obtained the TiO_2 particles under study.

	S_{total} (m^2/g)	V_{pore} (cm^3/g)	pore size (nm)	crystal size (nm)
AP	57	0.62	43.7	22.0
P25	57	0.30	21.2	22.6
P90	118	1.24	40.2	15.07

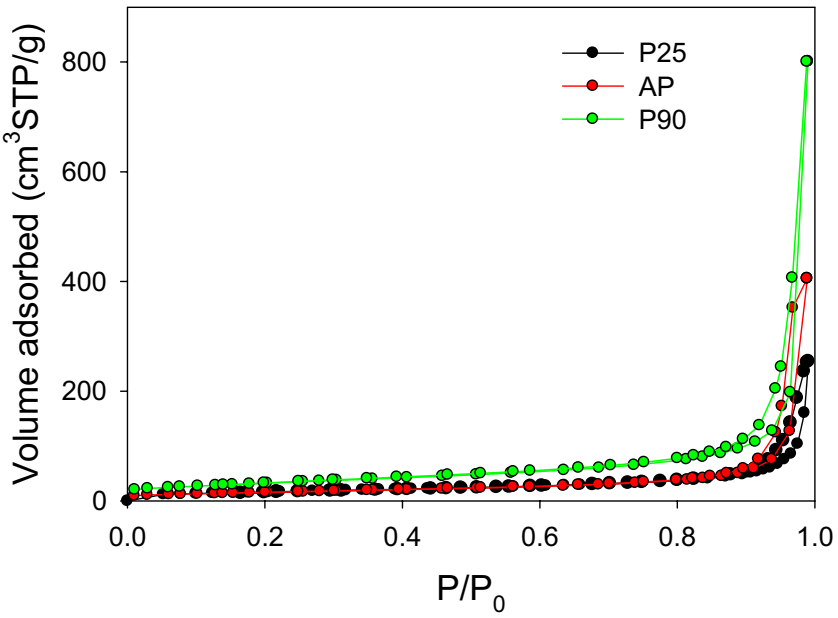

Fig. 4 N_2 adsorption-desorption isotherms corresponding to the TiO_2 nanoparticles used in our synthesis.

4.4. A novel TiO_2–SiO_2 nanocomposite converts a very friable stone into a self-cleaning building material

Sent to Applied Surface Science

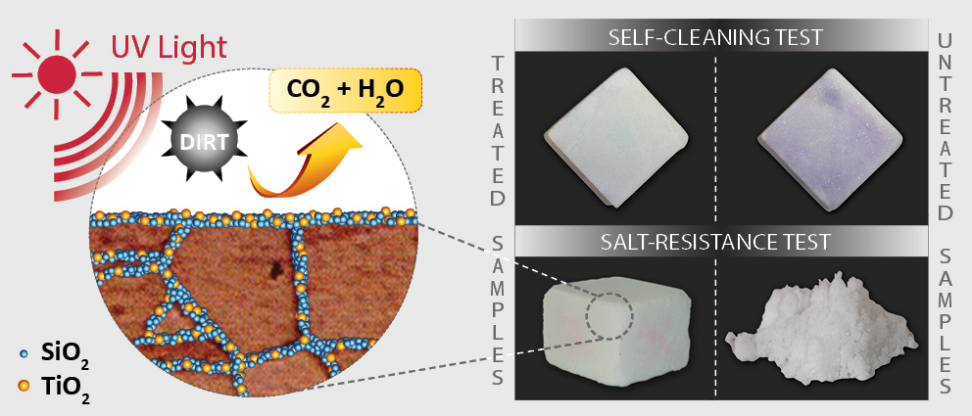

- An extremely friable stone is transformed into a building material
- A TiO_2-SiO_2 nanocomposite is formed inside the pore structure of the stone
- It creates a crack-free coating, which adheres firmly to the stone surface
- This nanomaterial increases mechanical resistance and durability of the stone
- It also provides self-cleaning properties to the stone

A novel TiO_2–SiO_2 nanocomposite converts a very friable stone into a self-cleaning building material

*Luís Pinho, Farid Elhaddad, Darío S. Facio, Maria J. Mosquera**

Departamento de Química-Física, Facultad de Ciencias, Campus Universitario Río San Pedro, Universidad de Cádiz, 11510 Puerto Real, Cádiz, Spain,

*Corresponding author: e-mail: mariajesus.mosquera@uca.es.

Phone: (34)956016331. Fax: (34)956016471

Abstract

A TiO_2-SiO_2 nanocomposite material was formed inside the pore structure of a very friable carbonate stone by simple spraying of a sol containing silica oligomers, titania particles and a non-ionic surfactant (n-octylamine). The resulting nanomaterial provides an effective adhesive and crack-free surface layer to the stone, and gives it self-cleaning properties. In addition, it efficiently penetrates into the pores of the stone, significantly improving its mechanical resistance, and is thus capable of converting an extremely friable stone into a building material with self-cleaning properties. Another important advantage of the nanocomposite is that it substantially improves protection against salt crystallization degradation mechanisms. In the trial described, the untreated stone is reduced to a completely powdered material after 3 cycles of $NaSO_4$ crystallization degradation, whereas stone treated with this novel product remains practically unaltered after 30 cycles. For comparison purposes, two commercial products (with consolidant and photocatalytic properties) were also tested, and both alternative materials produced coatings that crack and provide less mechanical resistance to the stone than this product. These results also confirm the valuable role played by *n*-octylamine in reducing the capillary pressure responsible for consolidant cracking, and in promoting silica polymerization inside the pores of the non-reactive pure carbonate stone.

Key-words: stone; non-ionic surfactant; TiO_2-SiO_2 nanocomposite; self-cleaning agent; consolidant, salt-resistant product

1. Introduction

Natural stone of diverse types is employed as construction material around the world, for reasons of esthetic appeal and elegance but mainly for its durability. Demand for natural stone is, therefore, usually limited to the more durable varieties, such as granites, marbles and some sandstones. Another type of stone, pure carbonates, presents an exceptionally bright white color, which is much appreciated by consumers as a building material for floors, walls and external facades. However, this natural rock has low mechanical resistance and is easily stained, thus inhibiting it commercial application. Therefore, the development of a treatment product specifically intended to enhance the robustness and durability of carbonate stone, and with self-cleaning properties, should be of considerable interest for architecture and construction.

Since the early discovery of the self-cleaning properties of titanium dioxide [1], it has been considered to be the most efficient, stable and cheap photocatalytic material available [2,3]. In recent years, the application TiO_2 to very widely different substrates, such as textiles [4,7], plastics [8-12] and glasses [13-16], has been widely reported. However, its application to various types of stone has been much more limited [17-21]. It is commonly employed as an aqueous dispersion of titania particles [17,19,20]. The results obtained for these products on stone are not wholly satisfactory, for two reasons: (1) a cracked coating is formed on stone [17], and (2) the titania is easily removed from the stone surface [18].

Nowadays, most commercial products applied for the protection of stonework and other building materials contain alkoxysilane monomers or oligomers [22]. These species polymerize, *in situ*, inside the pore structure of the stone, by a classical sol-gel process; this improves properties of the product such as its mechanical resistance or its hydrophobic behavior. Two main reactions take place during sol-gel transition: (1) hydrolysis of alkoxy groups to create silanols; (2) polymerization by condensation of silanol groups from the products. In addition, condensation also occurs between silanol groups from the products and those present in the siliceous mineral surface of the stone. The advantages of these products, widely reported in the literature, are: (1) the low viscosity of the monomer or oligomer

facilities penetration deeper into the pore structure of the stone; (2) environmental moisture is sufficient to produce the hydrolysis process; and (3) stable siloxane polymers are created, of a composition similar to the siliceous minerals of the stone.

However, a well-known drawback of these products, which is characteristic of all the sol-gel materials, is their tendency to crack during their drying process [23]. It is obvious that a cracked substance cannot protect the treated stone very effectively. In earlier work, our research group has developed surfactant-synthesized nanomaterials specifically designed for protecting and restoring various types of stone and other building materials [24-29]. The inclusion of the surfactant provides an efficient means of preventing cracking of the gel by reducing the capillary pressure; this effect is the result of two factors: (1) a coarsening of the gel network; and (2) decreased solvent surface tension. Adopting to this strategy, we have prepared consolidants [24-28], hydrophobic products [25-28] and stain-resistant materials [28]. In a recent paper [29], we describe the addition of titanium dioxide particles to a silica oligomer, in the presence of the surfactant, in order to produce a self-cleaning product for stonework and other building materials.

In this paper, we report the application of a sol containing titania particles and silica oligomer, to an extremely low-compaction and friable dolostone with an exceptionally bright white color. This dolostone is very prone to severe disaggregation, and can easily break into several pieces on routine manipulation. Consequently, this esthetically-attractive stone is totally unusable as a building material. The aim of the work described is to convert the dolostone into a self-cleaning building material with adequate mechanical resistance. If achieved, this would make the dolostone a significant new product in the market for building stone. Specifically, the present study is focused on evaluating the effectiveness on the dolostone under study for: (1) providing self-cleaning properties; (2) improving mechanical resistance; and (3) adherence to the substrate. We also investigate the durability of the stones treated, by applying a standard crystallization test. The effectiveness shown by this nanocomposite product as a consolidant and self-cleaning product has also been compared, in additional tests, with a commercial photocatalytic product and a commercial consolidant which were also evaluated on the same dolostone.

Another well-known and serious drawback of existing commercial siloxane products [22-30] is their very limited effectiveness as a consolidant of pure carbonate stones not containing siliceous minerals; there are two reasons for this deficiency: (1) carbonates slows the sol-gel transition [31]; and (2) carbonate salts do not have active –OH groups on their surface which could react with alkoxysilanes included in the products [32]. Hence chemical bonds between the stone and the consolidant product are not created. However, the significant increase in mechanical resistance observed in the dolostone under study after application of the nanocomposite synthesized in our laboratory demonstrates the useful contribution made by n-octylamine in the interaction between a non-siliceous stone and this siloxane product, which is also discussed in the present paper.

2. Experimental

The titalia-silica nanocomposite was prepared from a starting sol containing TES40 WN (Wacker Chemie AG, GmbH), P25 particles (Evonik AEROXIDE® TiO_2 P25) and *n*-octylamine (Aldrich). According to the technical data sheet, TES 40 WN (hereafter TES40) is a mixture of monomeric and oligomeric ethoxysilanes. The average chain length is approximately 5 Si-O units. P25 has an average primary particle size of 21 nm and a specific surface area (BET) of $50\pm15 m^2 \cdot g^{-1}$. The Sol was prepared by mixing TES40 with P25 particles in the presence of *n*-octylamine under ultrasonic agitation (125 $W \cdot cm^{-3}$) for 10 minutes. The proportion of *n*-octylamine and P25 to TES40 was 0.36% v/v and 2% w/v, respectively. The formulation has been designated as UCATiO-2 via the procedure devised at the University of Cadiz (the number indicates the % w/v of P25 included in the material).

After synthesis, the product was applied to the dolostone samples under study. For comparison, a popular commercial consolidant, Tegovakon V100 (hereafter TV100), supplied by Evonik, has also been applied. TV100 is a solvent-free one-component consolidant consisting of partially pre-polymerized TEOS and dioctyltin dilaurate (DOTL) catalyst. A commercial photocatalytic coating, E503 supplied by Nanocer, was also applied. According to the material data sheet, E503 is a TiO_2-

containing water-based sol with 7500-10000 ppm of the oxide. Prior to their application to the stone, the rheological properties of the products were studied, using a concentric cylinder viscosimeter (model DV-II+ with UL/Y adapter) from Brookfield. Experiments were performed at a constant temperature of 25ºC maintained by recirculated water from a thermostatic bath. A shear stress versus shear rate flow curve was generated.

The stone selected is a very friable dolostone composed of magnesium carbonate (99%). It presents evident disaggregation problems due to its geological formation and/or natural aging processes. This stone was selected particularly because of its high degree of whiteness, which makes it a suitable candidate for self-cleaning treatment application. For all the experiments carried out, the stone samples were cut in the form of 5x5x2 cm slabs. The sols under study were applied by spraying onto the upper surface of the samples, in 5 periods of 5 seconds, during a total time of 25 seconds. The stone samples were then dried under laboratory conditions until reaching constant weight. Uptake of products and their corresponding dry matter by the stone samples was calculated. The samples corresponding to untreated stone and their treated counterparts were characterized by the procedures described below, after constant weight was reached. All the results reported correspond to average values obtained from three stone samples.

A JEOL Quanta 200 scanning electron microscope (SEM) was used to visualize changes in the morphology of the stones after coating. Surface fragments of treated stone specimens and their untreated counterpart were visualized.

The chemical bonds in the treated samples under study were analyzed by Fourier Transformer Infrared Spectrophotometry (FTIR). The spectra were recorded in powder using a FTIR-8400S from Shimadzu (4 cm^{-1} resolution) in the region from 4000 to 650 cm^{-1}. Experiments were carried out in attenuated total reflection mode (ATR). FTIR spectra of powdered fragments of untreated and treated samples were obtained.

The adherence of the coating to the stone surface was evaluated by performing a peeling test using Scotch® Magic™ tape (3M). The test was carried out according to previously reported methods

[29,33,34]. The changes in stone surface morphology were visualized by SEM working in low-vacuum mode, and energy-dispersive X-ray spectroscopy (EDX) spectra were recorded in order to elucidate the variations in surface composition after the test.

The improvement in mechanical properties in treated stone was evaluated means of the Standard procedure Vickers hardness test, using a Universal Centaur RB-2/200 hardness tester. The loading was 30 Kg during 30 seconds, with a preload time of 15 seconds. 10 measurements were made for each stone specimen. Vickers hardness (VH) was calculated according the following equation:

$$VH = \frac{1.8544 \cdot W}{d^2} \quad (1)$$

where W is the load over the surface area of the indentation; d is the indentation diagonal.

The improvement in mechanical properties was also measured using the drilling resistance measuring system (DRMS), by SINT Technology. Drill bits of 4.8 mm diameter were employed with a rotation speed of 600 rpm and penetration rate of 5 mm/min. For each specimen, 10 holes were carried out.

We also evaluated the possible disadvantage of this material associated with changes in stone color induced by the treatment. This effect was determined using a solid reflection spectrophotometer, Colorflex model, from Hunterlab. For each specimen, color changes were tested on five points on the surface. The conditions used were: illuminant C and observer 10º. CIELa*b* color space was used and variations in color were evaluated using the parameter: total color difference (ΔE^*) [35].

The effectiveness of the materials under study as self-cleaning coatings for stone surfaces was evaluated by using a test adapted from the literature [29,36,37]. First, 1 ml of a solution of 1 mM methylene blue (Panreac) in ethanol was deposited on treated stone specimens and their untreated counterparts. Next, stone samples were irradiated with UV light working at 365 nm in a Vilber Lourmat CN15.CL chamber with 2 tubes of 15 W. The distance between the samples and the tubes was approximately 20 cm. Color variations, recorded as a function of irradiation time, were determined

using the same procedure described above. The parameter: total color difference (ΔE^*) was again evaluated.

In order to evaluate the durability of the products, an aging test by sodium sulphate crystallization was carried out. In this case, the sols were applied to all the 6 faces of the specimen. This test was performed according to the standard UNE-EN 12370 [38]. Immersion of specimens in the salt solution was substituted by capillary rise in order to make the test more aggressive. Each cycle consisted of three steps: (1) partial immersion in salt solution during 2 hours; (2) drying at 100ºC during 10 hours; and (3) cooling of the samples under laboratory conditions. After 30 cycles, the samples were immersed in distilled water during 24 h to remove the salts deposited inside the pores and next they were washed with normal water. Samples were then dried at 100ºC during another 24 hours, and the weight lost was determined.

3. Results and Discussion

A rheological study of the sols was carried out, and viscosity data were obtained immediately after stirring the dispersions. E503, TV100 and UCATiO-2 sols showed Newtonian behavior at the shear range evaluated. The viscosity was calculated as the slope of the shear rate vs. shear stress curve. In all the cases, the linear regression coefficients were above 0.99. The value obtained for the UCATiO-2 sol was only slightly higher (5.82 mPa·s) than that corresponding to the commercial TV100 sol (5.25 mPa·s). This result suggests that UCA product should penetrate into a stone substrate to a depth similar to that corresponding to the commercial consolidant. Penetration is a key factor for achieving a suitable consolidant effect on the stone. E503 shows a much lower value (0.282 mPa·s) because it is mainly constituted by water.

The product uptake and dry matter values obtained after application of the products to the dolostone samples are shown in Table 1. For TV100 and UCA products these values are similar; however, E503 shows a significantly lower dry matter value because its solvent content is very high.

Figure 1 shows SEM micrographs of stone specimens treated with the products under study. TV100 creates a dense and vitreous coating on the stone surface. The microporous nature of this product, characterized using nitrogen physisorption in our previous papers [24-27], is responsible for the formation of this coating.

Table 1. Properties of the treated stone specimens and their untreated counterpart

Product	Untreated	TV100	E503	UCATiO-2
uptake (%w/w)	----	0.53±0.01	0.40 ± 0.06	0.44 ± 0.20
dry matter (%w/w)	----	0.30±0.04	0.12 ± 0.11	0.30 ± 0.15
material removed by peeling (mg)	34.5±14.9	1.9±1.1	15.9 ± 1.4	2.3 ± 0.1
Vickers hardness (kP/mm^2)	49.33±15.21	54.17±3.37	-----	62.72 ± 5.32
ΔE*	----	16.00 ± 3.39	1.05 ± 0.79	6.96 ± 0.69

*Data correspond to average values. Standard deviations are also included.

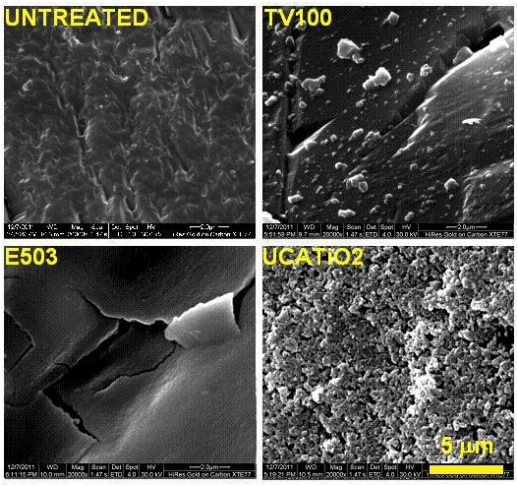

Figure 1. Scanning electron microscopy micrographs of the coatings on the dolostone under study.

E503, in turn, seems to create a thin and easy detachable surface layer. Both commercial coatings present fractures. In the case of the UCATiO-2 material, a crack-free, homogeneous and coarse coating on the stone surface is observed. The formation of this crack-free coating has previously been explained as a consequence of the role played by the surfactant n-octylamine, which reduces the capillary pressure while the gel is drying, as explained in the Introduction section [24-29].

FTIR spectra of the treated stone samples and their untreated counterpart are shown in Figure 2. All the samples present the carbonate peaks, which are characteristic of all carbonate stones including the dolostone used in this work. Specifically, the peaks at 1420, 880 and 730 cm^{-1} correspond to asymmetric, out-of-plane and in-plane bending vibration modes of the anion CO_3^{2-}, respectively [39]. The spectra corresponding to the untreated dolostone and the stone sample treated with E503 do not present any additional peak. We relate the similarity between treated and untreated dolostone spectra with the low dry matter value obtained for E503.

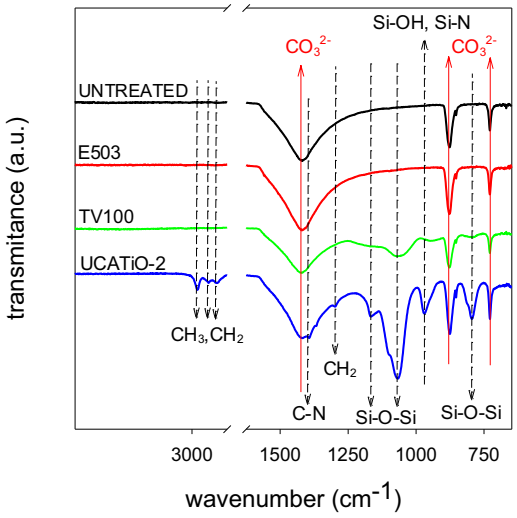

Figure 2. FTIR spectra for the samples under study.

In the case of the dolostone samples treated with TV100 and UCATiO-2, we observe some additional peaks in the spectra. In particular, there are two peaks corresponding to typical siloxane vibrations, located at 800 and 1070 cm^{-1}, corresponding to bending and stretching vibrations, respectively [40]. This confirms the presence of silica gels in the surface of the two treated stones. However, the intensity of these two peaks is different, being significantly lower in the stone treated with the commercial product. This confirms the poor effect of commercial siloxane products on pure carbonate stones reported in the literature [22]. The higher intensity of Si-O-Si bonds observed in the stone treated with our product can be attributed to the role played by n-octylamine, which may accelerate the condensation process in the carbonate stone [28,29]. This hypothesis is also confirmed by other additional Si-O-Si

peak presented by the stone treated with the UCA product. Specifically, this sample showed a peak adjacent to the stretching vibration, located at 1161 cm^{-1}. Demjén et al. [32] associated this double band (1070-1161 cm^{-1}) to the formation of high-molecular weight siloxane chains with a ladder-type structure. We also found this double band in silica xerogels prepared in presence of n-octylamine [41]. In the case of the TV100 product, this additional band was not observed and subsequently, a cyclic, low-molecular weight polymeric siloxane structure could have been formed, according to these authors. These authors found this double band in $CaCO_3$ treated with amino functional silanes. They concluded that the primary amine group promotes the formation of high- molecular weight siloxane polymers due to its catalytic effect on polycondensation.

The peak at 970 cm^{-1} shown in the spectra of the UCA product deserves particular attention. It can be attributed, *a priori*, to Si-OH stretching [42]. However, the absence of a broad band at 3750-3250 cm^{-1}, associated with hydrogen-bonded silanol groups with absorbed molecular water, suggests that silanol groups are not present in this coating. Consequently, we think that the 970 cm^{-1} peak could be attributed to Si-N stretching vibration, which is located in the same region [41,43]. In addition, Han et al. [44] confirmed that Si-N interaction occurred between methylamine and zeolite. According to these authors, the strong hydrogen bonding interaction results in the H atom of the amine group attacking the Si-O framework to form Si-O···H···N bond, which leads to the formation of Si-N bonds in the zeolites. Similarly, we think hydrogen bonding created between n-octylamine and the silica oligomer could also generate silica nitration.

In the stone treated with the UCA product, we also observed a band related to the asymmetric vibration of the CH_2 group at 2974 cm^{-1} and to the symmetric vibration of the CH_3 and CH_2 groups at 2928 and 2852 cm^{-1}, respectively. All of these are associated with alkyl chains, according the literature.[32] These peaks could be associated with the surfactant residues or even with ethoxy groups from non-hydrolyzed oligomers. In the spectrum of this stone sample, we also observe a band at 1300 cm^{-1}, corresponding to CH_2 twist vibration, which could be also attributed to ethoxy groups [45]. The

spectrum of the stone treated with TV100 did not show these bands. Finally, the slight peak at 1365 could be attributed to amine C-N stretching [24].

A noticeable feature is the absence of a peak associated with titania in the spectrum of the UCA coating. It is often reported that the bands observed in the range 900-1000 cm^{-1} may be associated with Ti-OH and Si-O-Ti species [46]. Thus, these peaks could appear in our spectrum due to co-condensation between silica oligomer and titania particles. However, they are not visible because these bands are probably obscured by the peak attributed to Si-OH and Si-N located at the same wavenumber [29,43].

Since one significant drawback of commercial products applied on stone has been associated with a reduction in photocatalytic efficiency during long-term use, due to the elimination of TiO_2 from the stone surface [18,29], we have investigated the degree of adhesion of the coatings applied on stone, by performing a peeling test, adapted from the literature. Figure 3 shows the micrographs obtained by SEM and the EDX analyses carried out on tested and non-tested areas. Table 1 shows the weight lost by the untreated stone and its treated counterparts after testing.

On comparing titanium content present in the surface of the stones, as expected, the greatest content is observed for the stone sample treated with UCATiO-2 (Fig. 3). E503 is a water-based product with extremely low titanium dioxide content (0.75-1%). This may explain why the titanium peak is very low for the stone treated with this commercial product. After complete drying TV100 is a silicon dioxide gel and therefore, presents no EDX peaks for titanium, and only silicon peaks are present in its spectrum.

Regarding to the SEM micrographs obtained, we observe clear differences between samples due to the products applied. The stone treated with TV100 shows a dense coating, typical of a microporous material. The removal of a very small amount of material from the sample surface is observed after peeling, with some stone mineral being observed in the micrograph. This is confirmed by observing a slight decrease of Si in the EDX analysis after the peeling test. Concerning the mass of the amount removed for TV100, only a slight loss of mass is observed (see Table 1). The micrograph for E503 shows a severely-cracked, friable and easily-detachable surface. In this case, a significant amount of material is removed from the stone surface (see Table 1). Since this product is largely eliminated from

the stone surface, we consider that it has little potential use for stone with low cohesion, such as the dolostone under study. Concerning the changes in titanium content after peeling, no significant differences can be observed, probably because its content is too low to observe these changes.

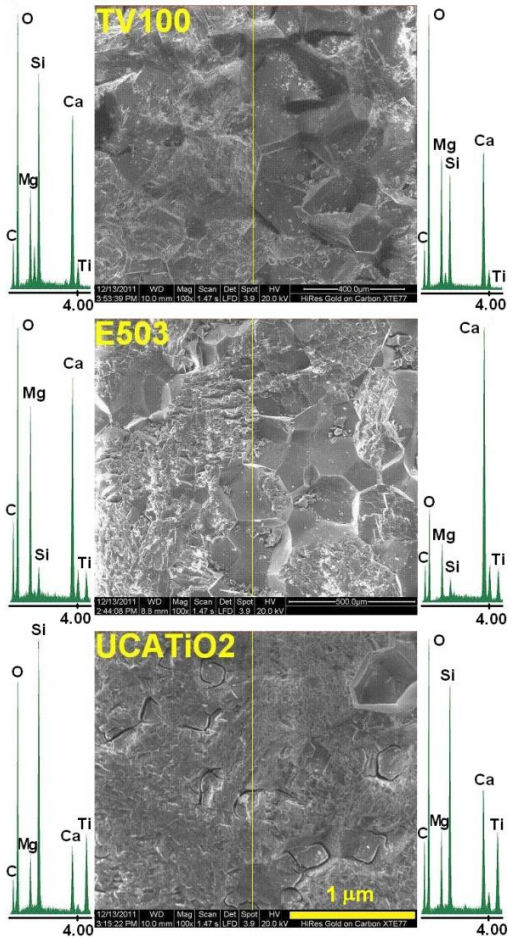

Figure 3. Scanning electron microscopy micrographs of the dolostone under study after the peeling test. On the left side of each micrograph, the non-tested surface is presented, together with the corresponding EDX spectrum. On the right side, the corresponding tested surface and spectrum are presented.

In the case of UCATiO-2, the micrograph obtained does not show any changes in the stone surface. Moreover, the EDX results confirm that no significant surface mass removal occurred after the tests. In respect of the amount of mass removed, the data obtained show only a slight loss of mass (see Table 1), similar to the result obtained for TV100. These findings confirm that TiO_2 has been integrated into the silica matrix, which has been capable of adhering firmly to the stone. Thus, we can conclude that the

inclusion of the photocatalyst in a mesoporous silica coating is an interesting solution for keeping particles tightly adhered to the treated surface, providing long-term wear resistance.

An important objective of this work is to improve the robustness of the stone under study, so that it can be utilized as a viable building material. Therefore, we have evaluated changes in two of the mechanical properties of the stone, i.e. hardness and drilling resistance, after application of each product. E503 was not considered in this evaluation because it is not a consolidant product. Changes in Vickers hardness of the stone surface after treatment are given in Table 1. We observed increases in the surface hardness after application of the two products under study, with this increase being significantly greater in the samples treated with UCATiO-2.

Drilling resistance results are shown in Figure 4. TV100 increases the stone's resistance in the surface zone (to a depth of 5 mm). However, after application of the UCA product, the drilling resistance is increased by a factor of 6 in the full depth evaluated of 30 mm.

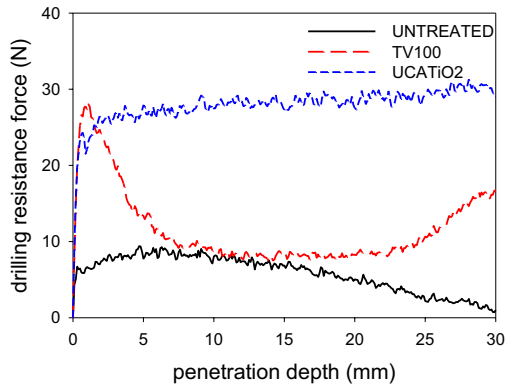

Figure 4. Drilling resistance force measurements for the treated dolostone under study

These results demonstrate that *n*-octylamine is playing a significant role in enhancing the consolidant effectiveness of siloxane, since silicon-based products are known to be ineffective as consolidants in pure carbonate stones [22,30]. This confirms the role played by the n-octylamine favoring the interaction between the siloxane and the apolar carbonate stone, as we previously observed for a pure limestone [29]. Earlier, Demjen and col. [32] had reported that amino-functional silanes adhere strongly

to the surface of $CaCO_3$. They discussed this effect in the following terms: the primary amine group promotes adhesion due to its catalytic effect on siloxane polycondensation. We think the primary amine group of the n-octylamine could play a similar role. It is confirmed by the FTIR spectrum previously discussed, in which the siloxane peaks observed the for UCA product are of significantly higher intensity than the peaks corresponding to TV100 (without octylamine). It is also corroborated by the presence of a double Si-O-Si peak, which is assigned to the formation of high molecular weight polysiloxanes [32].

We also evaluated changes in color following the treatments applied to the dolostone studied. Total color difference values (ΔE*) are shown in Table 1. Due to the low dry matter deposited on the stone surface, E503 produced low values of ΔE*, below the perception threshold (ΔE*<3) [35]. UCATiO-2 produced color changes near the generally accepted threshold value (ΔE*≤5), even for the most restrictive applications (ancient building restoration) [47]. In the case of the TV100 product, this produced an unacceptable color change (ΔE*=16) on the dolostone under study. We think the UCA product significantly inhibits color change in this extremely white carbonate stone because the titania particles have a notable whitening effect [29].

We have investigated the self-cleaning properties of the products on the dolostone tested by carrying out a photo-degradation test of stains previously deposited on the stone surface. Methylene blue (MB) was used as the staining agent. The evolution of total color differences under UV light over time was recorded and results are shown in Figure 5 for the two coatings with self-cleaning properties under study. TV100 was not included in this test because it has no self-cleaning properties.

The untreated stone showed a gradual reduction in the stain; after more than 800 hours of exposure its final ΔE* value was 19.07 (a reduction of 34%). The MB bleaching under visible/UV light has previously been reported, and is associated with the progressive absorption of light by the dye in the 350-520 nm range [48,49].

In the case of the stones treated with the two products with self-cleaning properties under study, we observe a similar behavior in MB degradation. Specifically, two different rates of degradation at different times can be distinguished clearly in the profiles. Very rapid MB bleaching occurs in the first 72 h, accounting for around 70% of the total color variation recorded. Next, a slower rate of degradation is observed over the longer term. The final ΔE* value obtained was 4.23 for the stone treated with the UCA product, whereas stone treated with E503 showed a slightly higher final ΔE* value (6.67). This variation between products may be associated with higher TiO_2 content (2%) of the UCATiO-2 product compared with that of E503 (0.75-1%).

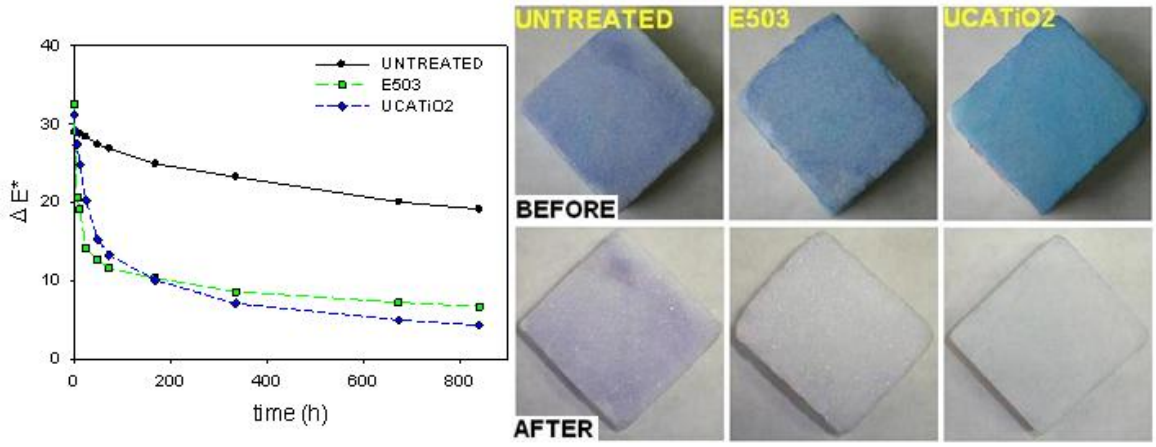

Figure 5. On the left side, the evolution of total color difference (for methylene blue stains) on treated and untreated samples of dolostone is presented. On the right side, we present photographs after the self-cleaning test of the surfaces of stone samples treated with the coatings under study. The samples were previously stained with Methylene Blue and then irradiated with UV light (λ=365 nm) for more than 800 hours.

The two findings reported above clearly confirm that the photocatalytic action of the titania particles produces most of the total degradation effect on the stain in the first few hours of exposure (the first part of the curve). In the case of the UCATiO-2 product, we think that the second stage with a much slower rate of degradation may be caused by the silica/titania coating reducing the capacity of the MB to penetrate into the limestone pore structure. This hypothesis is supported by the degradation profiles of

pure P25 particles on a limestone, which we previously published [29]. That study revealed that it is possible to obtain faster MB degradation with pure TiO_2 particles. P25 particles induced a single rate of degradation, with the stain being almost totally degraded in the first 6 hours.

Figure 5 also shows photographs of the stone surfaces under study before and after completion of the test. Before the start of the test, it can be observed that the untreated stone surface shows an MB stain significantly similar to that of the surface treated with E503. This is probably due to the insufficient cohesion of E503, which allows the staining MB solution to penetrate deep in the stone, as it does in the untreated sample. In the case of UCATiO-2, a more intense initial blue color is observed in the surface stone because UCATiO-2 creates a crack-free, homogeneous coating preventing the MB penetration into the stone pore structure.

We also consider that the self-cleaning effect produced by the UCATiO-2 coating is partly induced by the coarse texture of its gel network. As Yamauchi et al. have reported [50], the photocatalytic degradation of MB is clearly enhanced by the addition of TiO_2 particles to a silica mesoporous structure, in contrast to the effect observed when the particles are integrated in a dense microporous matrix. The explanation of this enhancement effect given by these authors is that mesopores accelerate the diffusion of MB towards the reaction sites (i.e. towards the titania particles). As discussed earlier in this paper, the UCATiO-2 coatings also create a mesoporous coating on the stone.

Finally, we subjected the stone samples to a salt crystallization test in order to evaluate the durability of the treatment. Figure 6 shows the weight loss of the treated dolostone samples and its untreated counterparts during the test. On the right side, photographs are also shown of the dolostone treated with the products under study and their untreated counterpart. The 'before and after' of these photographs illustrate the condition before subjecting the samples to the salt crystallization test and to their condition when the test was finished for each sample (corresponding to the last point in the graphic presented in Figure 6).

As observed in the pictures, the untreated stone sample has completely disintegrated after the 4^{th} cycle. Coincidently, TV100 has lost almost 50% of its mass by the 4^{th} cycle. The samples treated with

UCATiO-2 remain almost unaltered until the 20th cycle, and even after the 30th cycle show a fairly good behavior. In the case of the untreated stone, the results obtained confirm that it is a very friable stone, totally unsuitable for use as a building material. Regarding the samples treated with TV100, we think that the poor mechanical properties achieved for the stones treated (see Fig. 4) are responsible for its limited durability. As previously discussed, the low mechanical resistance could be due to the combined effect of the following factors: (1) extensive cracking that occurs for TV100 coatings (Fig. 1); (2) poor interaction between a siloxane-based product and carbonate stones; this was confirmed in the present paper by the FTIR spectra obtained; and (3) the presence of micropores in a stone generates high sodium sulfate crystallization pressures, which give rise to significant damage to the porous substrate [51]. Therefore, the microporosity of TV100 could also increase its susceptibility to sodium sulfate crystallization damage.

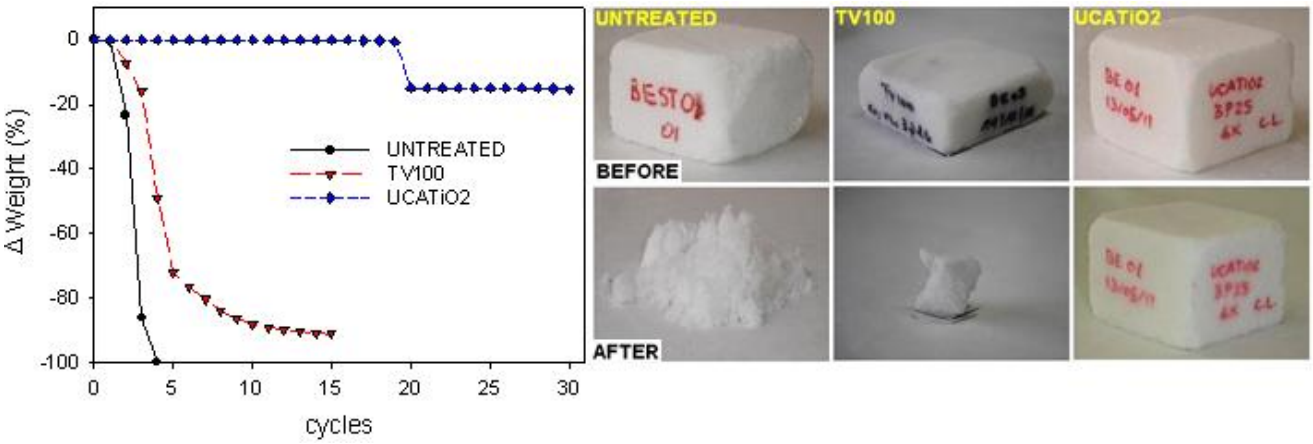

Figure 6. On the left side, the weight loss of the dolostone samples treated with TV100, UCATiO-2 and their untreated counterpart during the salt crystallization test is represented. On the right side, the photographs show the treated stone samples and their untreated counterpart after completion of the salt crystallization test (Untreated, 4 cycles; TV100, 15 cycles; UCATiO-2, 30 cycles).

In the case of UCATiO-2, a homogeneous, crack-free coating that adheres well to the dolostone is created with greater in-depth mechanical resistance. This explains why UCATiO-2 gives very good durability on the dolostone substrate. Again, we think *n*-octylamine is making a significant contribution

to enhancing the durability, since it not only prevents cracking but also facilitates the interaction with the carbonate stone, as discussed extensively in previous paragraphs.

The TiO_2 particles could also increase the durability of the treatment when subjected to crystallization salts, as Miliani et al. reported for silica consolidants modified with TiO_2 particles applied on a sandstone [47]. As a final remark, it may be of interest that the dolostone under study, protected with the products synthesized in our laboratory, is going to be commercialized under an exploitation patent [52].

4. Conclusions

We have transformed an extremely weakly-compacted and friable dolostone, currently unsuitable for application in building, into a suitable building material by means of a simple and low-cost procedure. This consists specifically of spraying onto the stone surface a newly-developed sol. This sol contains silica oligomers, titania particles and n-octylamine, and by this treatment, a TiO_2-SiO_2 nanocomposite consolidant material is formed inside the pore structure of the stone. We have demonstrated that this nanomaterial is capable of: (1) creating a crack-free coating, which adheres firmly to the stone surface and ensures that the conservation and self-cleaning properties of the coating have a long-term effect; (2) significantly increasing the mechanical resistance of the stone; (3) providing proven self-cleaning properties to the stone; and (4) making the stone suitably durable to degradation by salt crystallization.

Moreover, we have demonstrated that two commercial products tested (a consolidant and a self-cleaning agent) produce coatings that crack and generate less mechanical resistance for the stone than our product.

These results obtained in this paper confirm the valuable role played by *n*-octylamine in: (1) creating a mesoporous structure which reduces the capillary pressure which is responsible for cracking and increases the self-cleaning properties of the coating; and (2) promoting silica polymerization in the pores of the non-reactive pure carbonate stone.

Acknowledgments

We are grateful for financial support from the Spanish Government/FEDER-EU (Project MAT2010-16206 and Project Regenera (Innpacto subprogram), and the Government of Andalusia (project TEP-6386 and Group TEP-243). We also thank the company Tino Stone S.A. for financial support under a research contract. L.P. thanks the Fundação Ciência e Tecnologia for his pre-doctoral grant (SFRH/BD/43492/2008).

References

(1) A. Fujishima, K. Honda, Nature 238 (1972) 37-38.

(2) A. Fujishima, T. Rao, D. Tryk, J. Photochem. Photobiol. C 1 (2000) 1-21.

(3) K. Hashimoto, H. Irie, A. Fujishima, AAPPS Bull. 17 (2007) 12-28.

(4) A. Bozzi, T. Yuranova, J. Kiwi, J. Photochem. Photobiol. A 172 (2005) 27-34.

(5) K. Qi, W. Daoud, J. Xin, C. Mak, W. Tang, W. Cheung, J. Mater. Chem. 16 (2006) 4567-4574.

(6) M. Uddin, F. Cesano, D. Scarano, F. Bonino, G. Agostini, G. Spoto, S. Bordiga, A. Zecchina, J. Photochem. Photobiol. A 199 (2008) 64-72.

(7) D. Wu, M. Long, ACS Appl. Mater. Interfaces 3 (2011) 4770-4774.

(8) K. Tennakone, C. Tilakaratne, I. Kottegoda, J. Photochem. Photobiol. A 87 (1995) 177-179.

(9) S. Lam, A. Soetanto, R. Amal, J. Nanopart. Res. 11 (2009) 1971-1979.

(10) R. Fatteh, A. Ismail, R. Dillert, D. Bahnemann, J. Phys. Chem. C 115 (2011) 10405-10411.

(11) K. Nakata, M. Sakai, O. Tsuyoshi, T. Murakami, K. Takagi, A. Fujishima, Langmuir 27 (2011) 3275-3278.

(12) H. Chen, C. Liang, H. Huang, J. Chen, R. Vittal, C. Lin, K. Wu, K. Ho, Chem. Commun. 47 (2011) 8346-8348.

(13) Y. Paz, Z. Luo, L. Rabenberg, A. Heller, J. Mat. Res. 11 (1995) 2842-2848.

(14) T. Watanabe, Thin Solid Films 351 (1999) 260-263.

(15) J. Chen, C. S. Poon, Build. Environ. 44 (2009) 1899-1906.

(16) B. Xi, L.K. Verma, J. Li, C.S. Bathia, A.J. Danner, H. Yang, H.C. Zeng, ACS Appl. Mater. Interfaces 4 (2012) 1093-1102.

(17) I. Poulios, P. Spathis, A. Grigoriadou, K. Delidou, P. Tsoumparis, J. Environ. Sci. Health A 34 (1999) 1455-1471.

(18) K. Rao, M. Subrahmanyam, P. Boule, Appl. Catal. B: Environ. 49 (2004) 239-249.

(19) E. Quagliarini, F. Bondioli, G. Goffredo, A. Licciuli, P. Munafò, J. Cult. Herit. 13 (2012) 204-209.

(20) E. Quagliarini, F. Bondioli, G. Goffredo, C. Cordoni, P. Munafò, Constr. Build. Mater. 37 (2012) 51-57.

(21) M.F. La Russa, S.A. Ruffolo, N. Rovella, C.M. Belfiore, A.M. Palermo, M.T. Guzzi, G.M. Crisci, Progress Org. Coat. 74 (2012) 186-191.

(22) G. Wheeler, Alkoxysilanes and the Consolidation of Stone, The Getty Conservation Institute, Los Angeles, 2005.

(23) G.W. Scherer, J. Am. Ceram. Soc. 73 (1990) 3-14.

(24) M.J. Mosquera, D.M. de los Santos, A. Montes, L. Valdez-Castro, Langmuir 24 (2008) 2772-2778.

(25) M.J. Mosquera, D.M. de los Santos, L. Valdez-Castro, L. Esquivias, J. Non-Cryst. Solids 354 (2008) 645-650.

(26) M.J. Mosquera, D.M. de los Santos, T. Rivas, P. Sanmartín, B. Silva, J. Nano Res. 8 (2009) 1-12.

(27) M.J. Mosquera, D.M. de los Santos, T. Rivas, Langmuir 26 (2010) 6737-6745.

(28) J.F. Illescas, M.J. Mosquera, J. Phys. Chem. C 115 (2011) 14624-14634.

(29) L. Pinho, M.J. Mosquera, J. Phys. Chem. C 115 (2011) 22851-22862.

(30) A.P. Ferreira Pinto, J. Delgado Rodrigues, J. Cultural Heritage 9 (2008) 38-53.

(31) C. Danehey, G. Wheeler, S.H. Su, The influence of quartz and calcite on polymerization of methyltrimethoxysilane, in: Proceedings of the 17th International Congress on Deterioration and Conservation of Stone, Lisbon, 1992, 1043-1052.

(32) Z. Demjén, B. Purkánszky, E. Földes, J. Nagy, J. Colloid & Inter. Sci. 190 (1997) 427-436.

(33) L. Ling, I. Phang, G. Vancso, J. Huskens, D. Reinhoudt, Langmuir 25 (2009) 3260-3263.

(34) M. Drdácký, J. Lesák, S. Rescic, Z. Slízková, P. Tiano, J. Valach, Mater. & Struct. 45 (2012) 505-520.

(35) R.S. Berns, Billmeyer and Saltzman's principles of color technology, Wiley-Interscience, New York, 2000.

(36) T. Tatsuma, S. Tachibana, M. Tetsuya, D. Tryk, A. Fujishima, J. Phys. Chem. B 103 (1999) 8033-8035.

(37) ISO 10678 Fine ceramics (advanced ceramics, advanced technical ceramics) Determination of photocatalytic acitivity of surfaces in an aqueous medium by degradation of methylene blue. ISO, 2010.

(38) UNE-EN 12370. (1999) Natural stone test methods. Determination of resistance to salt crystallization. AENOR, Madrid, Spain.

(39) A. Sdiri, T. Higashi, T. Hatta, F. Jamoussi, N. Tase, Environ. Earth Sci. 61 (2010) 1275-1287.

(40) L. Tellez, J. Rubio, F. Rubio, E. Morales, J.L. Oteo, J. Mater. Sci. 38 (2003) 1773-1780.

(41) J.F. Illescas, M.J. Mosquera, ACS Appl. Mat. Interfaces 4 (2012) 4259-4269.

(42) G. Orcel, J. Phalippou, L.L. Hench, J. Non-Cryst. Solids 88 (1986) 114-130.

(43) M. Sekine, S. Katayama, M. Mitomo, J. Non-Cryst. Solids 134 (1991) 199-207.

(44) A.J. Han, J. Guo, H. Yu, Y. Zeng, Y.F. Huang, H.Y. He, Y.C. Long, ChemPhysChem 7 (2006) 607-613.

(45) P. Innocenzi, J. Non-Cryst. Solids 316 (2003) 309-319.

(46) C.M. Whang, S.C. Yeo, Y.H. Kim, Bull. Korean. Chem. Soc. 22 (2001) 1366-1370.

(47) C. Miliani, M.L. Velo-Simpson, G.W. Scherer, J. Cult. Her. 8 (2007) 1-6.

(48) A. Mills, J. Wang, J. Photochem. Photobiol. A 127 (1999) 123-134.

(49) M. Mrowetz, W. Balcerski, A.J. Colussi, M.R. Hoffmann, J. Phys. Chem B 108 (2004) 17269-17273.

(50) N. Suzuki, X. Jiang, L. Radhakrishnan, K. Takai, K. Shimasaki, Y. Huang, Y. Yamauchi, Bull. Chem. Soc. Jpn. 84 (2011) 812-817.

(51) C. Rodríguez-Navarro, E. Doehne, E. Sebastián, Cement Concrete Res 30 (2000), 1527-1534.

(52) M.J. Mosquera, L. Pinho, Spanish Patent No. P201100741. Priority data: June 24, 2011.

Figure 1

Click here to download high resolution image

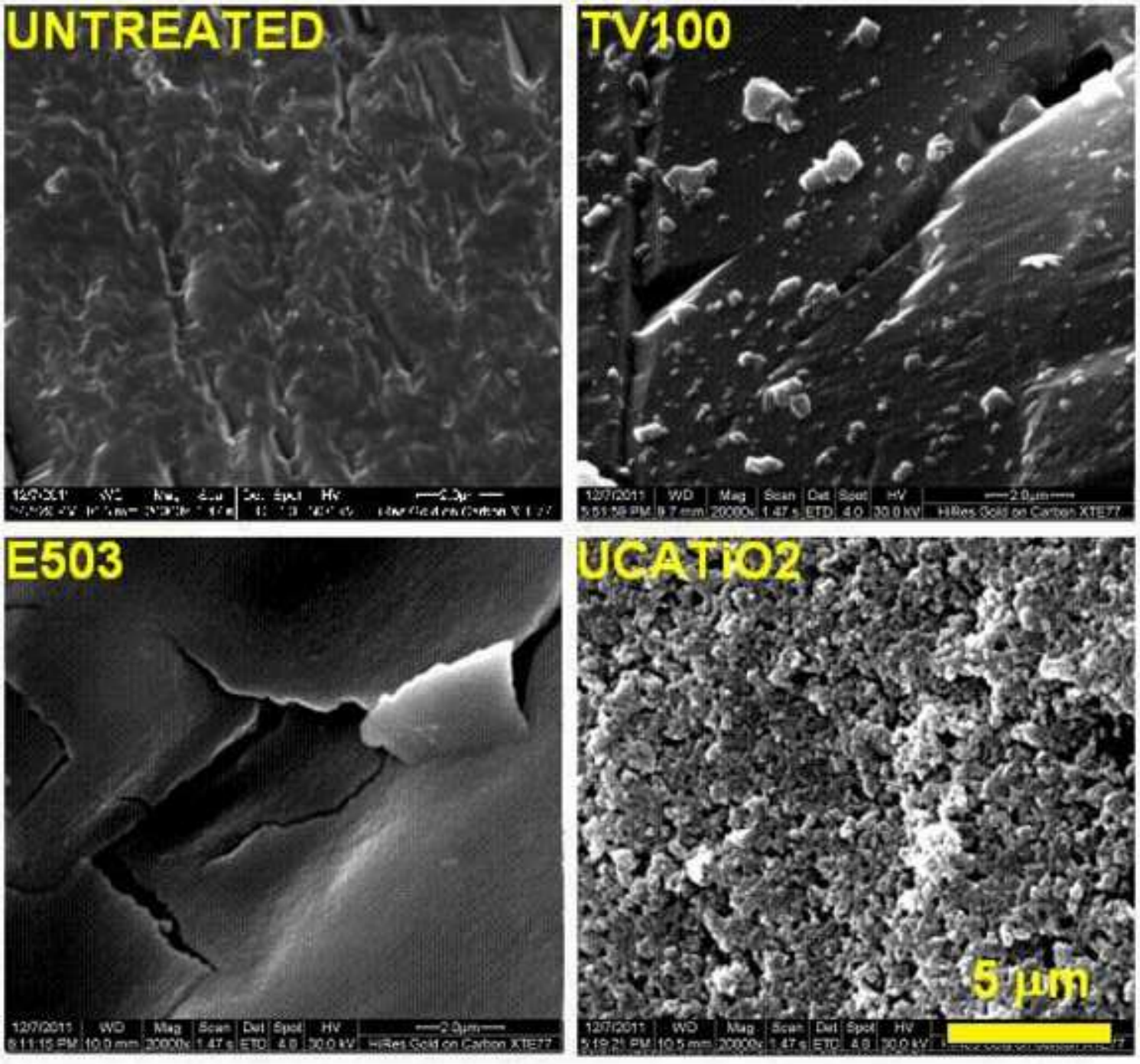

Figure 2

Click here to download high resolution image

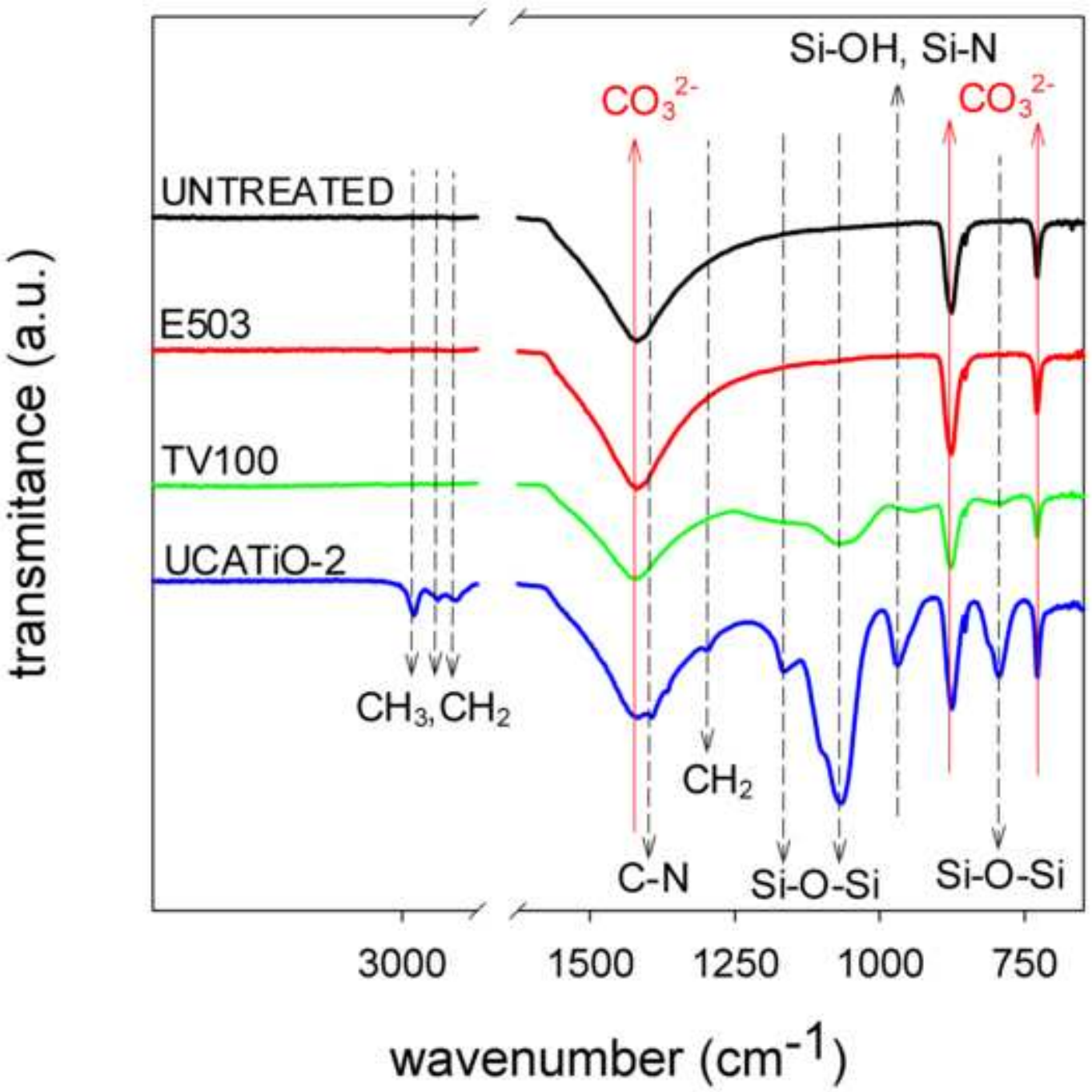

Figure 3

Click here to download high resolution image

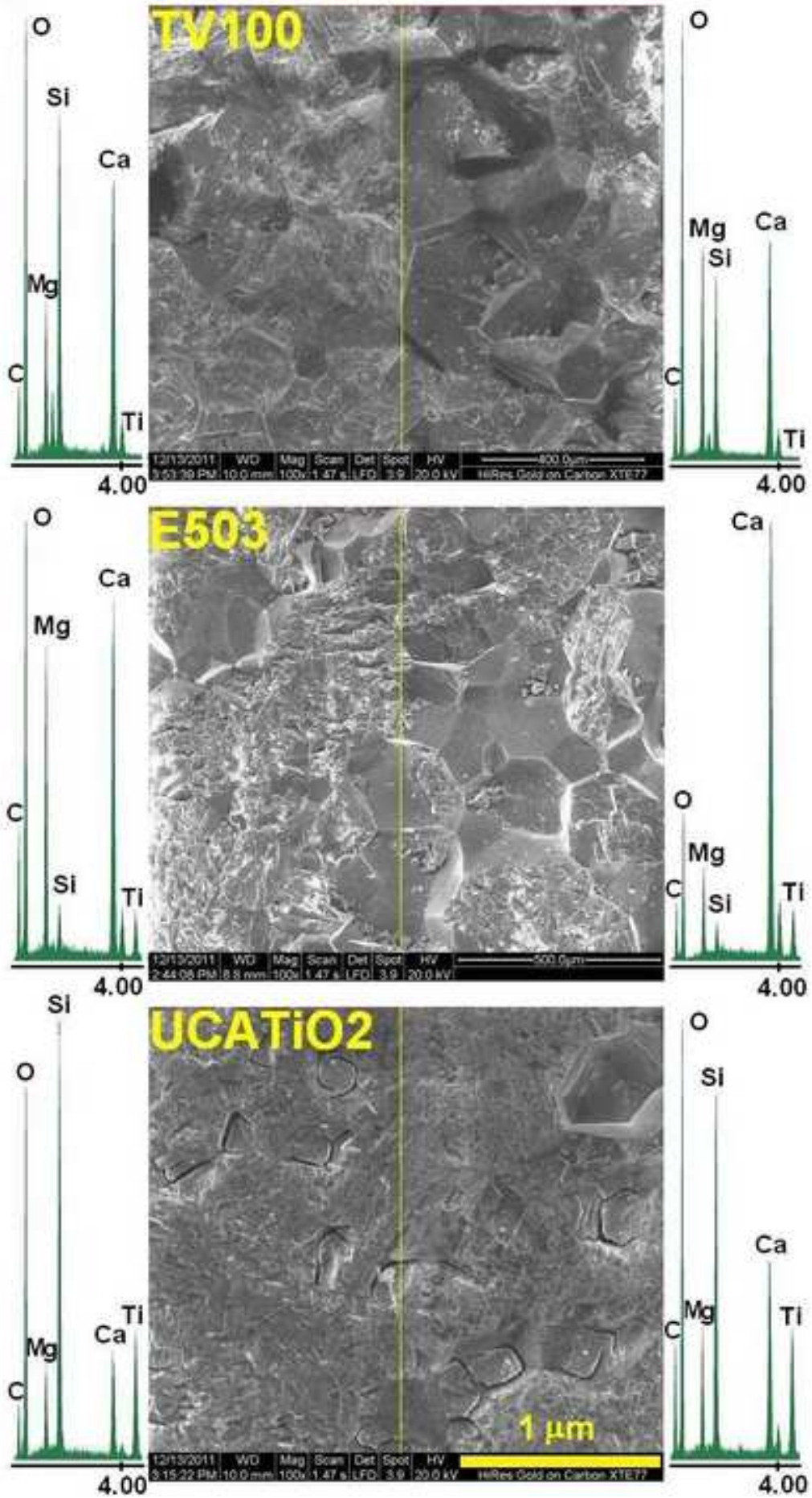

Figure 4

Click here to download high resolution image

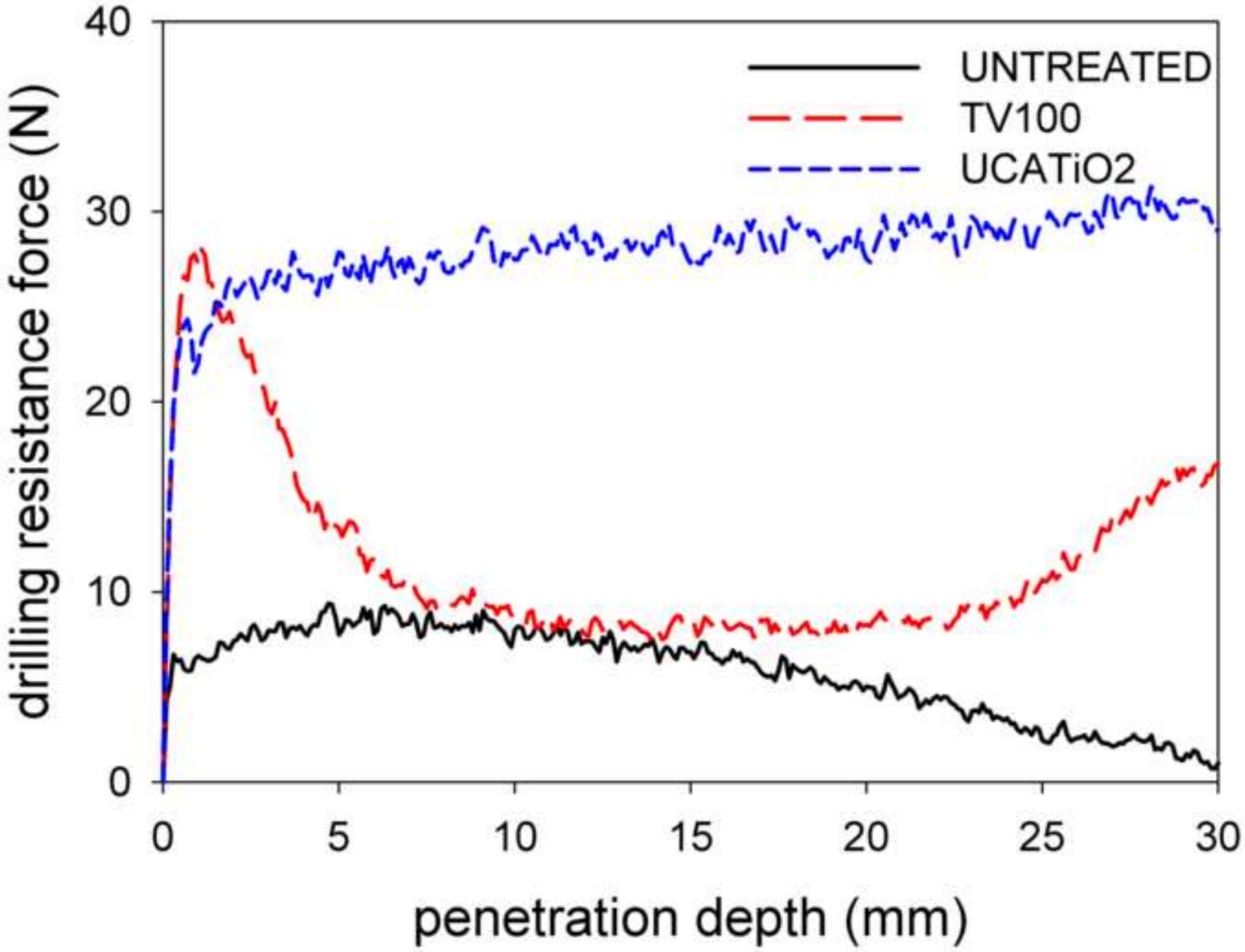

Figure 5

Click here to download high resolution image

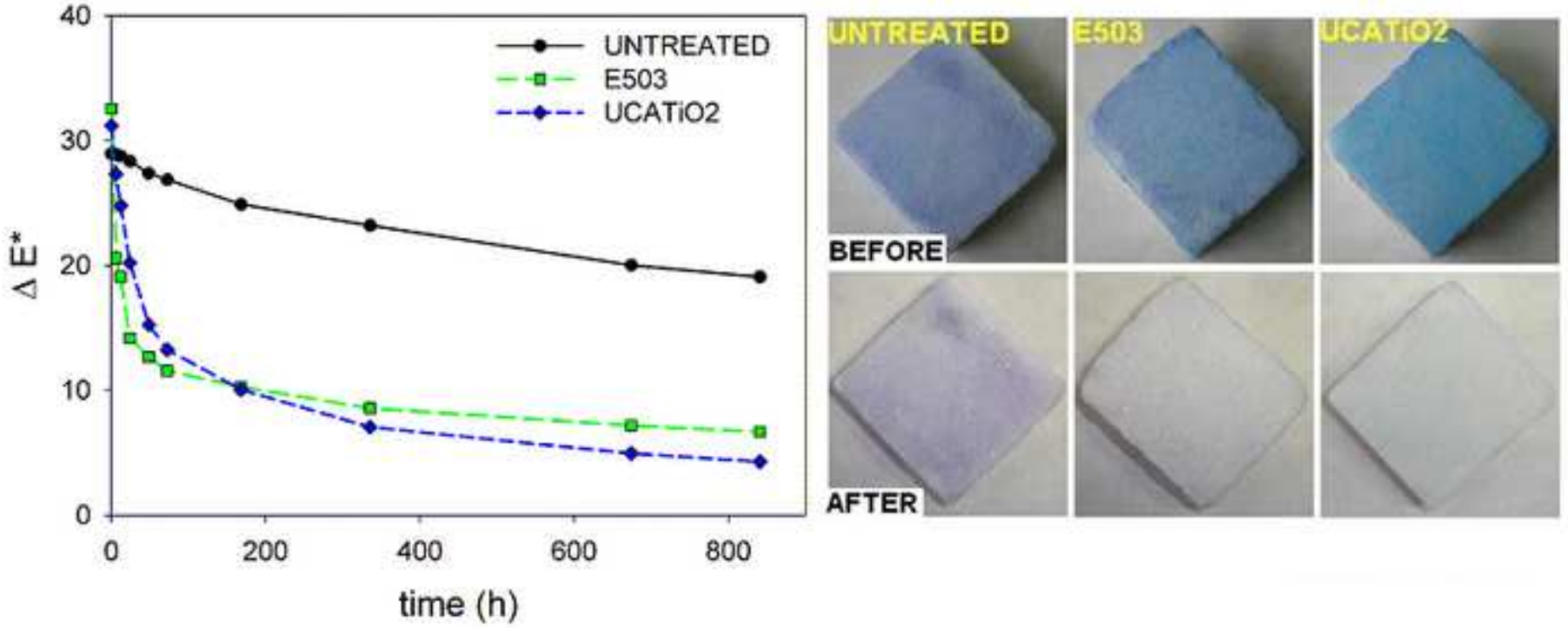

Figure 6

Click here to download high resolution image

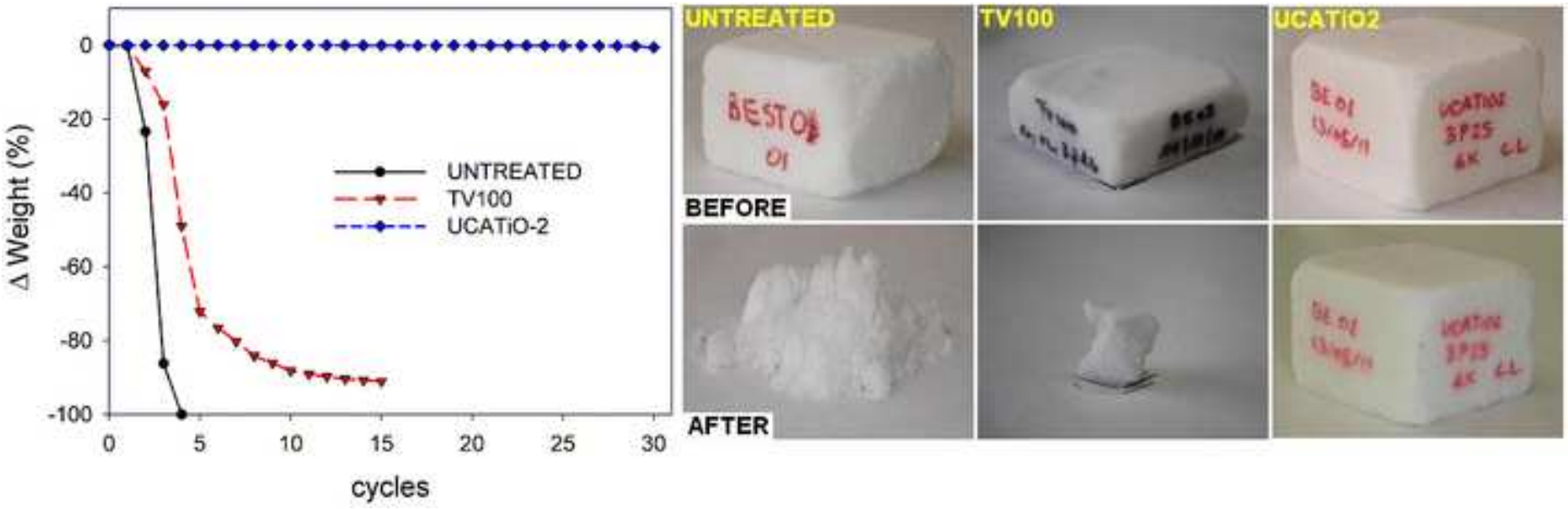

5. General discussion

In the work carried out for this Doctoral Thesis, we developed new TiO_2-SiO_2 nanocomposites and we investigated their photocatalytic and mechanical properties for self-cleaning applications on monumental stones. Firstly, we have studied the photocatalytic properties of TiO_2 nanoparticles and the consequences of embedding them inside a surfactant-synthesized matrix for application on stone. Secondly, particle size and loading were modified in order to optimize the texture and photocatalytic activity of the mesoporous TiO_2-SiO_2 nanocomposites obtained. In order to organize the following discussion, we divided it into several different sections, according to the experimental information obtained.

Firstly, we characterized the sol-gel properties of the nanocomposites under study. Concretely, we evaluated the rheology of the sols synthesized and we described the most important features of the sol-gel process. Further, we performed a thorough textural, structural and chemical characterization of the photocatalysts. Secondly, we applied the sols synthesized on two different carbonate stones. The photocatalytic activity was measured on coatings created on stone. Mechanical properties, such as adhesion and drilling resistance were also evaluated. In order to investigate the possible negative effects induced by the treatments on the surface of the stones, we measured changes in colour and hydric properties. Finally, we have tested the durability against sodium sulphate crystallization of the synthesized photocatalysts on a rock with severe disgregation problems.

5.1. Sol-gel characterization

Rheology and sol-gel transition

Our photocatalysts are prepared in a one-step synthesis and applied as aerosols at ambient temperature on stone. A low viscosity makes the use of an aerosol generator easier for applying the product *in-situ*. Further, sols with lower viscosity should be able to penetrate deeper in the stone. In order to test viscosity, a rheological study of the synthesized sols was carried out.

Since the behavior shown by the prepared sols was always nearly Newtonian at the shear range evaluated, viscosity was calculated as the slope of the shear rate vs. shear stress curves. In the most of the cases, the linear regression coefficients were 0.99, becoming the linear fit slightly more difficult for the highest TiO_2 loading prepared (10 % w/v, in Chapter 4.3).

Comparing the viscosity values of TES 40 and S sols (Chapter 4.3, Table 1), these values increased slightly when *n*-octylamine was added to TES 40. This can easily be explained by the very rapid effect of *n*-octylamine as a sol-gel catalyst.

Regarding the effect of the addition of TiO_2 nanoparticles in the viscosity of the sols, we observed that they produce a more significant increase in viscosity than that associated with *n*-octylamine. We also verified that TiO_2 contents up to 2% w/v do not change the Newtonian behavior of the Si sol (Chapter 4.1, Table 1). The addition of higher TiO_2 loadings promoted a significant increase in viscosity (Chapter 4.3, Table 1). Similarly, higher viscosities have been measured by Yang et al. for aqueous dispersions of TiO_2 nanoparticles with increasing particle concentration.[107] Vasiliev et al.[108] also obtained higher

[107] H. Yang, C. Li, H. Gu, T. Fang, J. Colloid Interf. Sci. 236 (2001) 69.
[108] P. O. Vasiliev, B. Faure, J. B. S. Ng, L. Bergström, J. Colloid. Interf. Sci. 319 (2008) 144.

viscosity values for increasing TiO_2 loading in both ethanol and water-based TEOS + C_{16}TAB + TiO_2 dispersions.

In addition, we also observe a progressive evolution of our sols from a Newtonian behavior to a shear-thinning one with the increase of TiO_2 nanoparticles concentration (Chapter 4.3 Figure 1, in Supplementary Information). Yang et al.[107] found that dispersions with increasing TiO_2 nanoparticles concentration assumed a progressively shear-thinning behavior from a Newtonian one. Similarly, Mikulasek et al.,[109] also observed a shear-thinning behavior for 30% w/v aqueous TiO_2 dispersions.

We also varied the features of the TiO_2 nanoparticles included in the sols by employing commercial preformed TiO_2 particles with several different average sizes. Specifically, we used AP, P25 and P90 nanoparticles (from Evonik) with an average particle size of 20 μm, 21 nm and 14 nm, respectively. The variation of the viscosity with shear stress for the sols evaluated is presented in Chapter 4.3, Figure 1 in Supplementary Information. The values obtained for the sol containing P90 TiO2 nanoparticles with 10% w/v loading were out of the measurement range and have not been included in the representation. In order to understand better their behavior, we observed AP, P25 and P90 nanoparticles by SEM, before and after ultrasonic stirring in water (Chapter 4.3, Figure 2 in Supplementary Information). In this experiment, particle concentration was 1 % w/v and stirring was performed in the same conditions employed in the syntheses. As is clearly observed by microscopy, the average particle size of AP nanoparticles, after ultrasonic stirring in water, is significantly reduced from a micrometer to a nanometer scale, and is close to the one presented by P25 and P90 particles. We conclude that the average particle size of AP nanoparticles is reduced due to the strong cavitation power of ultrasonic stirring.

We observe a clear trend in which the increase in particle size seems to produce lower viscosity. This could be attributable to the agglomeration of TiO_2

[109] P. Mikulasek, R. J. Wakeman, J. Q. Marchant, Chem. Eng. J. 67 (1997) 97.

nanoparticles. This agglomeration phenomenon was earlier reported for aqueous dispersions.[107] We speculate that the aggregation of TiO_2 nanoparticles is more significant for the lowest average particle size tested (P90) as a consequence of their higher surface energy.[110]

Finally, we would like to remark that the viscosity values of the sols synthesized in our studies were only slightly higher than those corresponding to commercial sols. Commercial stone consolidants, such as TEGOVAKON® V100 from Evonik, present viscosity values of 4.48-5.25 mPa·s at 25ºC. Thus, we think that our sols must penetrate into the stone in a similar way to commercial ones. The self-cleaning commercial product E503 (employed in Chapter 4.4) contains TiO_2 nanoparticles dispersed in water (0.75-1% w/v). This product shows a much lower value (0.282 mPa·s) than our products because it is mainly constituted by water.

Sol-gel transition of all the sols prepared in the work undertaken for this Doctoral Thesis took place overnight (a maximum time of 24 hours) in plastic Petri dishes, producing homogeneous nanocomposites. When TiO_2 nanoparticles are mixed with SiO_2 precursors, such as TES40, we find that one of the two following processes may occur: 1) flocculation of the TiO_2 nanoparticles and subsequent creation of two different phases; or 2) the TiO_2 nanoparticles are stable in the sol during the sol-gel transition and are effectively integrated within the gel network. Obviously, the homogeneity of gels obtained indicates that stabilization of the particles is achieved by means of the route investigated. In the following paragraph, we explain this stabilization in further detail.

In order to enhance particles stability during the sol-gel transition, we first induced pH-changes either by adding an acid (H_3PO_4) or a base (*n*-octylamine) to create an electrostatic repulsion phenomenon in the sol (Chapter 4.1). As

[110] X. Zhang, B. Xia, H. Ye, Y. Zhang, B. Xiao, L. Yan, H. Lv, B. Jiang, J. Mater. Chem. 22 (2012) 13132.
[111] J. Widegren, L. Bergström, J. Am. Ceram. Soc. 85 (2002) 523.
[112] M. Kosmulski, P. Prochniak, J. B. Rosenholm, J. Phys. Chem C. 113 (2009) 12806.

previously discussed,[112-114] and according to the DVLO theory, the interaction between charged particles is a result of the algebraic sum of the attractive van der Waals and the repulsive double layer forces. Near the isoelectric point (IEP) significant agglomeration takes place; large flocks with high hydrodynamic size are observed as the particle surface charge gets close to zero and attractive van der Waals forces dominate. When the pH is different from the IEP of TiO_2, the surface charge is different from zero and the hydrodynamic size of the aggregates becomes smaller. The IEP of P25 nanoparticles has been reported to be around 7 in water.[113,114] We suppose that the IEP in the sols prepared in our laboratory, prior to *n*-octylamine addition, must be fairly close to this value. Therefore, adjusting the pH to higher value by the addition of a base, or lower values by the addition of an acid to the sol must increase electrostatic repulsions and, subsequently, the stability of the TiO_2 nanoparticles dispersions must be enhanced. In a similar way, electrostatic stabilization of TiO_2 nanoparticles in polar organic solvents has previously been obtained by Kosmulski et al.[112] by adding an acid such as H_3PO_4 or a base like triethylamine.

Further, concentrations of *n*-octylamine ranging from 0.016 to 1.8% v/v were investigated in order to optimize the dispersion of TiO_2 nanoparticles. We chose 0.36% v/v because it is the minimum concentration at which a stable TiO_2 nanoparticle dispersion can be obtained during the sol-gel transition time (tipically around 24 hours). Lower concentrations of surfactant resulted in phase separation. In addition, these sols with lower *n*-octylamine content do not gel spontaneously. This finding corroborates the role played by the surfactant as basic catalyst (Chapter 4.1). Regarding the higher concentrations of the surfactant, they were not adopted because they gradually decreased the gel time. For the highest concentrations tested, the gel transition occurred immediately after synthesis. For our application, the gel time must be long enough to penetrate inside the stone substrate.

---

[113] K. Suttiponparnit, J. Jiang, M. Sahu, S. Suvachittanont, T. Charinpanitkul, P. Biswas, Nanoscale Res. Lett. 6 (2011) 1.
[114] N. T. Boncagni, J. M. Otaegui, E. Warner, T. Curran, J. Ren, M. M. F. Cortalezzi, Environ. Sci. Tecnhol. 43 (2009) 7699.

In summary, we think that TiO_2 nanoparticles exhibit stability during the sol-gel transition because of several electrostatic repulsion phenomena. Firstly, as we previously referred, this repulsion is induced by the increase in pH values produced by *n*-octylamine. Thus, *n*-octylamine prevents TiO_2 particles aggregation into the sol by increasing the pH value. Secondly, when we increase TiO_2 loading, the repulsion between TiO_2 nanoparticles particles themselves is also increased[113]. Finally, amines or amine-terminated surfactants are also reported to adsorb on the surface of TiO_2 nanoparticles, enhance repulsion between them, and therefore, stabilize TiO_2 dispersions.[116-118]

Crystalline structure

The X-ray patterns of the powdered form of the coatings under study are given in Chapter 4.1, Figure 1 and in Chapter 4.3, Figure 1. The materials synthesized in our laboratory show the typical amorphous silica pattern without any detectable ordered structure at about 23º.[118] We have previously obtained similar patterns for silica gels synthesized from TEOS and *n*-octylamine.[119] This confirms that our synthesis strategy does not promote an ordered pore structure, which is typical of most materials synthesized via a surfactant template. As previously reported,[120] the TiO_2-SiO_2 films require a calcination process in order to produce an ordered mesostructure.

We also observe that the X-ray patterns obtained show peaks previously reported as a pure anatase structure.[118,121] Specifically, we observe the peaks assigned to anatase-type titania at around 25, 38 and 48º[120] being obviously

[115] E. Beyers, P. Cool, E. Vansant, J. Phys Chem. B 109 (2005) 10081.
[116] D. Siwinska, A. Kołodziejczak-Radzimska, A. Krysztafkiewicz, T. Jesionowski, Appl. Surf. Sci. 255 (2009) 7337.
[117] B. Erdem, E. D. Sudol, V. L. Dimonie, M. S. El-Aasser, J. Polym. Sci. Polym. Chem. 38 (2000) 4419.
[118] C. Yu, H. Chu, Y. Wan, D. Zhao, J. Mater. Chem. 20 (2010) 4705.
[119] M. J. Mosquera, D. M. de los Santos, L. Valdez-Castro, L. Esquivias, J. Non-Cryst. Solids 354 (2008) 645.
[120] H. Shibata, T. Ohkubo, H. Kohno, P. Rangsunvigit, H. Sakai, M. Abe, J. Photochem. Photobiol. A 181 (2006) 357.
[121] A. Mirabedini, S. M. Mirabedini, A. A. Babalou, S. Pazokifard, Prog. Org. Coat. 72 (2011) 453.

more intense as the TiO_2 loading is increased. This verifies that the TiO_2 nanoparticles in the coatings prepared in our laboratory exist as separate crystalline domains, embedded within the silica amorphous matrix.[41]

Textural characterization

Nitrogen adsorption-desorption isotherms corresponding to the photocatalysts synthesized are shown in the Chapter 4.1, Figure 2; Chapter 4.2, Figure 2 and Chapter 4.3, Figure 3 and the textural data obtained are given in Chapter 4.1, Table 1; Chapter 4.2, Table 2 and Chapter 4.3, Table 2. Textural properties of AP, P90 and P25 TiO_2 nanoparticles, were also characterized for comparative purposes (Chapter 4.1, Figure 1; Chapter 4.3, Figure 4 and Table 2, both as Supporting Information). All of the commercial types of TiO_2 particles present a type IV isotherm with a H1 hysteresis loop, as expected for an agglomerate of TiO_2 nanoparticles (Chapter 4.3, Figure 4 and Table 2 both as Supporting Information).[122] Textural information on AP and P25 nanoparticles is in good agreement with the differences in their particle size. AP nanoparticles present a lower surface area but higher pore volume and pore size, which should be due to its larger particle size. In the case of P90 nanoparticles, we expected them to show values similar to P25. However, for P90 the pore size is twice as large as that corresponding to P25. We assume that this difference is due to the phenomenon of aggregation among the smallest TiO_2 nanoparticles studied. This seems to confirm again that there is a critical size of titania nanoparticles, for their aggregation, of between 14 and 21 nm.

We also investigated the texture of TiO_2-SiO_2 nanocomposites obtained by mixing TES40 and P25 TiO_2 nanoparticles in presence of H_3PO_4, which acts as a sol-gel catalyst (UCATiP, Chapter 4.1, Figure 2). These materials showed type I isotherms, corresponding to microporous materials with a slight hysteresis typical of mesoporous materials. This profile is characteristic of materials consisting of a mesoporous network with a pore size close to microporous values.[122]

[122] M .Kruk, M. Jaroniec, Chem. Mater. 13 (2001) 3169.

The textural information for TiO_2-SiO_2 nanocomposites synthesized in presence of *n*-octylamine is presented in Chapter 4.1, Figure 2; Chapter 4.2, Figure 2; Chapter 4.3, Figure 3 and the textural data obtained are given in Chapter 4.1, Table 1; Chapter 4.2, Table 2 and Chapter 4.3, Table 2.

All the materials, including the ones without TiO_2, show type IV isotherms as a consequence of the coarsening effect on the gel network exerted by *n*-octylamine. Regarding hysteresis, most of the materials present a triangular hysteresis loop and a steep desorption branch, classified as an H2 loop. In the case of the nanocomposites containing P25 particles, a type H1 hysteresis loop, characterized by parallel and nearly vertical branches, is observed. According to the literature,[122] an H1 hysteresis loop is reported for materials that consist of spherical particles. In general, this loop is characteristic of materials with high uniformity of pore size and high connectivity between pores. Materials with H2 hysteresis present a similar structure but with lower connectivity. These isotherm profiles therefore suggest that all our materials are composed of a network of silica spheres and the titania particles are integrated within this network.

The pore-size distribution (Chapter 4.3, Figure 3) was determined using the Barret-Joyner-Halenda[123] (BJH) and the NLDFT[124] methods. We employed NLDFT in order to obtain a pore size distribution integrating micro and mesopores present in the materials under study. In the Chapter 4.1, Table 1, we observe that pore volume and pore size were significantly higher when the synthesis occurs in the presence of *n*-octylamine.

In Chapter 4.2, Figure 2 the inset shows the pore size distribution obtained using the NLDFT approach from the isotherm adsorption branches. The product without TiO_2 showed micro and mesopores. In the case of the TiO_2-SiO_2 nanocomposite, the pore size distribution showed significantly higher values, all of them in the mesopores region (ranging from 4 to 10 nm). TiO_2

[123] E. P. Barret, L. G. Joyner, P. P. Halenda, J. Am. Chem. Soc. 73 (1951) 373.
[124] M. Thommes, B. Smarsly, M. Groenewolt, P.I. Ravikovitch, A.V. Neimark, Langmuir 22 (2006) 756.

nanoparticles are integrated in the silica nanoparticles aggregates, increasing the size of the aggregates in the composite. This obviously increases the space between aggregates of the material, producing an increase in the pore size distribution. Zelenak et al.[46] associated this increase with the creation of interparticle space between the titania nanoparticles. Pore volume was slightly smaller when titania nanoparticles are included in the matrix (Chapter 4.2, Table 2) the reason could be that some of the TiO_2 nanoparticles fill the spaces between the aggregates.[46] In the case of surface area, as is obvious, it is higher for the material with lower pore size and higher pore volume.

Regarding the TiO_2 loading effect on the texture of our photocatalysts (Chapter 4.3, Figure 3), some significant differences are observed. For TiO_2 loading rates of 1% and 4%, the materials containing AP and P90 particles show a pore size and pore volume similar to those obtained from the material without TiO_2. Moreover, for the highest TiO_2 loading rate (10% w/v), a significant reduction in pore volume is observed for the materials containing AP and P90 particles. Other authors have found similar decreases in pore volume for increasing TiO_2 loadings.[19,20] This inverse relationship can be explained as a consequence of a higher proportion of non-porous TiO_2 nanoparticles being incorporated in the gel network.

Regarding the effect of TiO_2 particle size (Chapter 4.3, Figure 3), a more heterogeneous pore distribution is clearly observed for materials with P25 particles. One possible explanation is that the P25 nanoparticles are more dispersed in the silica matrix. We think that AP and P90 particles, due to their larger size and greater aggregation, respectively, promote the creation of larger pore spaces inside the gel network. The size of these pores was measured by N_2 physisorption (Chapter 4.3, Table 2 in Supplementary Information), and for both of them it was around 40 nm. We speculate that these spaces are easily occupied by the silica particles created during the sol-gel transition. In the case of P25, pores are smaller (around 20 nm, see Chapter 4.3, Table 2 in Supplementary Information) and they thus cannot be occupied by the silica particles. Thus, a lower silica-titania packing that promotes a large pore size

and a more heterogeneous distribution should be produced for materials containing P25. Fattakhova-Rohlfing et al.[40] reported that the presence of TiO_2 nanoparticles could act to open the continuous siliceous framework. Similarly, Zelenak et al.[46] reported that interparticle space is created between the TiO_2 nanoparticles integrated within a SiO_2 matrix. Lastly, it is notable that the photocatalysts containing P90 and AP particles show significantly higher surface areas than those corresponding to P25 materials for loadings of 1 and 4%, because most of the porosity is constituted by pores of smaller size.

Microscopy studies

Scanning electron microscopy (SEM)

In Chapter 4.1, Figure 6 shows the SEM micrographs corresponding to the materials prepared in presence of H_3PO_4 and in presence of *n*-octylamine. The surfactant-synthesized TiO_2-SiO_2 nanocomposites form a homogeneous and continuous gel coating whereas the H_3PO_4-catalyzed materials create discontinuous films of aggregates.

In Chapter 4.3, Figure 2, in Chapter 4.2, Figure 1 and in Chapter 4.3 Figure 2 show SEM micrographs of pure silica materials and their corresponding counterparts with TiO_2 nanoparticles (AP, P25 and P90). Some differences can be observed with relation to size of the aggregates comprising the gel network of the different nanocomposites under study. The pure silica materials consisted of a configuration of silica nanoparticles of smaller and more homogeneous particle size (around 90 nm) than those corresponding to TiO_2-SiO_2 composites. When TiO_2 particles are added to the sols, the resulting aggregates show sizes ranging from 110 to 400 nm. Smaller TiO_2 nanoparticles (ranging 20-50 nm) are observed on the surface of these aggregates. These particles are not visible in pure silica materials. Kontos et al.[59] also observed by SEM the agglomeration of titania nanoparticles for hydrothermally treated pure TiO_2 films; these authors also attributed this finding to an aggregation phenomenon.

Regarding the effect of TiO_2 loading on the aggregate size, higher loadings cause a clear increase in the average particle size of the aggregates. This can be explained as a consequence of the larger size of the preformed TiO_2 nanoparticles employed in this study in comparison to the silica nanoparticles created during sol-gel transition, as postulated later when the TEM images are discussed. In addition, possible interactions produced between TiO_2 and surfactants, previously reported[46,115] may also play a role in the formation of aggregates. If some of the surfactant is adsorbed in the TiO_2 particles, less *n*-octylamine is available to catalyze the sol-gel transition when TiO_2 loading is raised. This could subsequently promote a suppressive effect of the silica condensation according to the proposed aggregation mechanism. This possibility is confirmed by the composite's appearance, which is more rigid for the materials without TiO_2 and those with 1% w/v TiO_2 content which could be associated with a higher degree of silica condensation in these materials. Consequently, a gradual increase in TiO_2 loading results in the creation of smaller silica particles during the sol-gel transition. As previously indicated, these smaller particles are easily aggregated to the preformed TiO_2 particles due to their higher surface energy.[110] This produces a larger number of SiO_2 particles to be aggregated, thus creating larger aggregates. This assumption is particularly evident for materials containing P90 nanoparticles and the highest TiO_2 loading (10% w/v) where very large aggregates are formed. This could be due to the greater adsorption of *n*-octylamine caused by the high surface area of P90 TiO_2 nanoparticles.

Regarding the possible effect of the size of TiO_2 particles, we do not observe a clear effect on the aggregate size. In the specific case of the highest TiO_2 loading, a larger aggregate size is clearly visible for the materials containing 10% w/v P90 TiO_2 nanoparticles (see Chapter 4.3, Figure 2). We again associated this increase with the higher degree of aggregation occurring between the TiO_2 nanoparticles with the lowest size (P90) and the large surface area of these particles previously commented. All of these results seem to suggest that there is a critical TiO_2 particle size for promoting aggregation,

which could be estimated at between 21 nm (P25 average size) and 14 nm (P90 average size).

Further, these micrographs also confirm that the initial 20 μm size of AP nanoparticles is reduced from a micrometer to a nanometer scale, close to the size presented by P25 and P90 nanoparticles, due to the strong cavitation power of ultrasonic stirring, as previously discussed.

Atomic force microscopy (AFM)

We investigated the surface topography of a TiO_2-SiO_2 nanocomposite and its counterpart without TiO_2, using AFM. In Chapter 4.2, Figures 1c,d show respectively, the 1 x 1 μm^2 2D top views, obtained for the SiO_2 material and its TiO_2-SiO_2 counterpart. The corresponding 3D surface plots are shown in Figure 1e and 1f. As observed, the material without TiO_2 comprises silica nanoparticle aggregates, as observed by SEM. In the case of the TiO_2-SiO_2 nanocomposite, thanks to the better resolution provided by AFM, we observe larger aggregates because they include not only silica nanoparticle aggregates (of a size similar to those corresponding to the SiO_2 material) but also individual TiO_2 nanoparticles: some of these latter particles are presumably incorporated within the aggregates and others are exposed on their surface and hence visible.

3D surface images show that the addition of TiO_2 nanoparticles to SiO_2 substantially influences the surface morphology of the photocatalyst, since increased roughness is observed when TiO_2 nanoparticles are added to the starting sol. We associate this increase in the size of aggregates with the presence of TiO_2 nanoparticles. The reduced surface roughness of the SiO_2 material is associated with the aggregation of the silica nanoparticles alone. In a previous paper,[125] increasing the TiO_2 content was found to cause an increase in roughness for TiO_2-SiO_2 nanocomposites, confirming our hypothesis.

[125] Y. V. Lim, H. Fan, Z. Shen, C. H. Kang, Y. Feng, S. Wang, Appl. Phys. A, 2009, 95, 555.

Transmission electron microscopy (TEM/STEM)

In Chapter 4.1, Figure 4 shows images corresponding to the TiO_2-SiO_2 nanocomposite obtained by an acid catalysis process (H_3PO_4) and to the material obtained by a basic catalysis process (*n*-octylamine). The HAADF-STEM image of the H_3PO_4-synthesized nanocomposite shows a material composed of individual TiO_2 particles (of around 20 nm size) and some aggregates (of 30-40 nm size) of TiO_2 particles embedded in a dense silica matrix. The image corresponding to the *n*-octylamine-synthesized nanocomposite clearly shows a gel network composed of individual TiO_2 and SiO_2 nanoparticles. Yamauchi et al.[38] have also obtained a similar nanocomposite constisting of TiO_2 and SiO_2 particles.

Further investigation provided us a better structural insight into our materials. In Chapter 4.2, Figures 3a and 3e show representative HAADF-STEM and HREM images respectively of a *n*-octylamine-synthesized TiO_2-SiO_2 nanocomposite with 4% w/v P25 loading. X-EDS mappings showing elemental distributions for Ti, Si and Si+Ti over the same area highlighted on the HAADF-STEM image are shown respectively, in Chapter 4.2, Figure 3b,c,d. The STEM micrograph (Z-contrast) shows a mesoporous material composed, mainly, of individual TiO_2 nanoparticles of around 20 nm, presenting a size similar to that stated by the manufacturer (21 nm). Some TiO_2 aggregates (of 30-40 nm size) are also observed. The SiO_2 nanoparticles show smaller sizes, of around 15 nm. From the X-EDS maps obtained (Chapter 4.2, Figure 3b-3d) it can be confirmed that TiO_2 and SiO_2 are located in independent domains in the bulk of the material. In addition, the combination of the Si and Ti maps confirms that the network of SiO_2 nanoparticles surrounds the TiO_2 ones. Thus, SiO_2 could be acting as a matrix producing a reinforced composite structure in this photocatalyst.

In Chapter 4.2, Figure 3e, an individual crystalline TiO_2 nanoparticle with an estimated particle size of 20 nm can be observed supported in amorphous silica. At this scale, the HREM images illustrate two important features: firstly, analyzing their corresponding digital diffraction patterns, we can confirm the

crystallographic nature of TiO_2. Further, the application of a Fourier transformation to the visible lattice spacings present in the crystalline structure of our material reveals the presence of the (00-2), (10-1) and (101) crystallographic planes assigned to the anatase phase of titania. This confirms that anatase, the titania crystalline structure with photocatalytic activity, is present in the composite. Secondly, from the HREM images we can make a clear distinction between the two components of the nanomaterial synthesized in our laboratory, confirming the existing of two separate domains. In addition, we find a good agreement between the particle sizes obtained by STEM and HREM imaging.

We also investigated the structure of our surfactant-synthesized TiO_2-SiO_2 photocatalysts when TiO_2 nanoparticles size was modified. In Chapter 4.3, Figure 4 shows representative images obtained of the nanocomposites containing 4% w/v TiO_2 particles loading with three different sizes (AP, P25 and P90), acquired in TEM and HAADF-STEM mode. All these photocatalysts were selected for this study to describe their structure in greater detail on the basis of their intermediate TiO_2-loading (4% w/v). In addition, they are of especial interest because, as will be discussed later, these three composites showed the most efficient photocatalytic behavior. In Chapter, 4.3 Figures 4a,b,c, individual TiO_2 nanoparticles can be observed perfectly clearly as inclusions in a SiO_2 mesoporous matrix. These images illustrate three important features of our nanocomposites: 1) the existence of two clearly distinct and separate domains corresponding to TiO_2 and SiO_2; 2) TiO_2 presents a crystalline configuration due to the visible lattice spacing present in the structure of the material, whereas SiO_2 presents an amorphous configuration in the absence of this lattice spacing; and 3) variations in the size of TiO_2 nanoparticles and in their distribution, in the three photocatalysts, are clearly visible in the images. In Chapter 4.3, Figures 4d,e,f (STEM images with Z-contrast) show individual TiO_2 nanoparticles of different sizes (visibly brighter) inside the SiO_2 mesostructure. These images are particularly valuable for providing a better insight into the SiO_2 porous network (which appears less brightness in the image), and allowing us to confirm the TiO_2 and SiO_2 particle

sizes obtained in TEM images. From these micrographs, the following features can be established: P25 and P90 TiO_2 nanoparticles integrated in the SiO_2 matrices present an average particle size similar to that stated by the manufacturer for the individual particles (21 nm, 14 nm, respectively). It is also significant that numerous aggregates of 30-80 nm size are clearly observed in the image of S4P90 whereas the S4P25 composite is composed basically of individual particles. In the case of AP particles, their disaggregation produced by ultrasound stirring resulted in the presence, of TiO_2 nanoparticles with an elongated particle shape and with a particle size of around 40-50 nm. This particle size is larger than those corresponding to the materials containing P25 and P90 particles. In addition, some smaller particles are also present.

Regarding the SiO_2 nanoparticles formed, we observe that their size, around 15-20 nm, is very similar to the size of individual P25 nanoparticles. This could result in a lower degree of packing among SiO_2 and TiO_2 P25 particles than that obtained for the other preformed TiO_2 particles included in this study. In the case of AP and P90 TiO_2 particles, these produce a larger pore space (around 40 nm) into which the SiO_2 nanoparticles are more easily packed. We think that this happens due to a larger particle size, in the case of AP, and due to a higher aggregation, in the case of P90 particles. In order to illustrate our hypothesis, a schematic model of the structures of the composites is also included in Chapter 4.3, Figure 4g,h,i.

Electron tomography studies

In order to confirm the TiO_2-SiO_2 structure and relationships obtained by the STEM/HREM and X-EDS studies, a three dimensional characterization was performed by means of electron tomography. In Chapter 4.2, Figure 4 shows the reconstructed volume of the tomography series acquired for the TiO_2-SiO_2 nanocomposite containing a 4% loading of P25 TiO_2. The images obtained correspond to (a) Si+Ti, (b) Si, and (c) Ti, in the sample analyzed. (A video showing the 3D reconstructed volume can be found in a CD together with this Doctoral Thesis). The 3D reconstruction allows the detailed analysis of the

internal characteristics of the sample, which are not possible to observe in conventional 2D images.

This method of volume sectioning provides information related to the position of both components in the structural organization. In this context, we can observe (Chapter 4.2, Figure 4a) a mesoporous composite structure with an independent spatial distribution of TiO_2 and SiO_2 nanoparticles. The volumes in yellow color correspond to TiO_2 nanoparticles. The regions in transparent blue correspond to the SiO_2 support. The observation of TiO_2+SiO_2 reconstructed volume allows us, firstly, to corroborate the presence of large voids between aggregates, which could correspond to pore space identified by physisorption. Again we observe two different domains for SiO_2 and TiO_2.

In Chapter 4.2, Figure 4b presents the individual configuration of the mesoporous silica matrix which surrounds the TiO_2 nanoparticles. Here we can clearly observe that the silica amorphous phase presents a shell-like structure which partially covers the supported individual crystalline titania particles. This information supports the conclusion that the interaction between TiO_2 and SiO_2 could be physical, through Van der Waals forces, as previously discussed by Gao et al.[43]

In Chapter 4.2, Figure 4c shows the individual TiO_2 nanoparticles present in the photocatalyst. The dimensions and arrangement of the titania nanoparticles are also in good agreement with the information presented in Chapter 4.2, Figure 3. It confirms again that individual nanoparticles are present in this composite.

In Chapter 4.2, Figure 5a shows a 2D HAADF-STEM image from the tilt series. Figure 5b presents a surface-rendered representation of the segmented 3D reconstructed volume of the sample analyzed and an XY orthoslice taken from the 3D reconstructed volume, perpendicular to the Z-direction is presented in Figure 5c. The XY orthoslice is a good example of how this additional imaging tool helps us to understand better the relative locations of

SiO_2 and TiO_2 nanoparticles. Figures 5a,c are oriented such that a direct comparison between them can be made.

In the HAADF-STEM image (Chapter 4.2, Figure 5a), it is difficult to discriminate the configuration of the SiO_2 matrix around the TiO_2 nanoparticles. The advantages of using 3D characterization become evident when we compare this 2D image with the *XY* orthoslice (4.2 Figure 5c). Both locations are indicated by arrows for guidance purposes. The yellow arrow indicates the location of TiO_2 nanoparticles in areas that show higher intensity and well-defined boundaries. The blue arrow indicates the SiO_2 nanoparticles binding support, which corresponds to areas with lower brightness. Firstly, this image confirms that the surface of the photocatalyst, observed by SEM and AFM (Chapter 4.2, Figure 1) shows a structure similar to its interior. We can also observe that there is significant pore volume within the bulk of the photocatalyst, providing good access to its interior for 'guest' molecules. Moreover, from a careful examination of the silica matrix we can corroborate the existence of voids inside the SiO_2 nanoparticles. We attribute the existence of these voids to the influence of the *n*-octylamine during the sol-gel process: this generates mesoporosity and should be valuable for enhancing the adsorption of 'guest' molecules.

Yamauchi et al.[126] reported the synthesis of a TiO_2-SiO_2 nanocomposite, and they used electron tomography as a tool for understanding better the location of TiO_2 nanoparticles. They concluded that the TiO_2 nanoparticles were totally embedded in the SiO_2 matrix, and that none of the TiO_2 nanoparticles was exposed on the outer surface, which was of great importance for the selective adsorption of guest molecules, according to these authors.

Similarly, Beyers et al.,[20] also reported the advantages of the deposition of TiO_2 nanoparticles inside a silica matrix in order to obtain an inert outer surface. However, these authors also reported the increase in photocatalytic activity when TiO_2 nanoparticles were located outside the matrix. In our case,

[126] Y. Yamauchi, F. Takeuchi, S. Todoroki, Y. Sakka, S. Inoue, Chem. Lett. 37 (2008) 72.

our combined 2D-3D electron microscopy studies support the finding that TiO_2 nanoparticles in the photocatalyst exist both directly exposed on the surface and surrounded within the mesoporous matrix of SiO_2 nanoparticles. Considering this finding on the location of the TiO_2 nanoparticles, we believe the photocatalyst provides a good combination of potential adsorptive and photocatalytic properties.

Spectroscopy studies

FTIR Spectroscopy

All the materials synthesized in the work undertaken for this Doctoral Thesis present typical silica peaks (Chapter 4.1 Figure 5, 4.3 Figure 5). These are located at 795 and 1045 cm^{-1}, corresponding to bending and stretching vibrations, respectively.[79] Each spectrum also shows a peak adjacent to the stretching vibration, located at 1161 cm^{-1}. This double band (1045−1161 cm^{-1}) is associated with chains of high-molecular weight siloxanes.[87,127] This demonstrates that the sol-gel transition was effective and consequently, a high-molecular weight silica polymer has been created. The broad band in the 3400 cm^{-1} range, when present, is attributed to Si-OH groups with absorbed molecular water. This band may also contain the contribution of absorbed molecular water on Ti-OH from the surface of TiO_2 particles.

For increasing TiO_2 nanoparticles content in the photocatalysts (Chapter 4.3, Figure 5), we observe a decrease in transmitance between 750 and 650 cm^{-1}. Zelenak et al.[46] attributed differences in transmitance around 620 cm^{-1} to vibrations in the TiO_2 bulk phase. After thermal treatment at 650, 850 and 1000 ºC these authors also observed a transmittance decrease in the previously-cited range and attributed it to the growth of TiO_2 nanoparticles. Thus, we think that this reduction is caused by increasing the loading of TiO_2 nanoparticles integrated in the silica matrix.

[127] Z. Demjén, B. Pubánsky, E. Foldes, J. Nagy, J. Colloid. Interface Sci. 190 (1997) 427.

The peak at 970 cm^{-1} shown in the spectra of the photocatalysts (Chapter 4.3, Figure 5) calls for particular attention. It can be attributed, *a priori*, to Si-OH stretching vibration.[79] However, the typical broad band shown for silica gels at 3750-3250 cm^{-1} associated with hydrogen-bonded silanol groups with absorbed molecular water, which should be detected together with any -OH bond, shows a weak signal in these spectra. Consequently, we think that the 970 cm^{-1} peak could also be attributed to Si-N stretching vibration,[128] due to hydrogen-bonded interactions that occur between silica and the *n*-octylamine. Similarly, we recently reported the presence of this Si-N interaction in the materials prepared from TES40, water and *n*-octylamine.[87] We confirm the presence of *n*-octylamine in the photocatalysts tested in several other peaks observed in the spectra. Specifically, the bands at 1392 and 1444 cm^{-1}, are attributed to *n*-octylamine C-N stretching and C-H bending,[78] respectively. In addition, we observe a peak at 1485 cm^{-1} which, according to the literature,[129] results from amino groups strongly hydrogen-bonded to free silanols. This confirms that the *n*-octylamine interactions with the silica precursor are produced by hydrogen bonds. The presence of *n*-octylamine in these spectra confirms that it was not completely removed during drying. In a recent paper, we also observe that *n*-octylamine was partially retained in silica gels dried under the same conditions.[87]

Another contribution to the intensity of the 970 cm^{-1} peak could be that of Ti-O-Si vibrations. In previous studies, a band attributed to these vibrations is usually observed in the 950-960 cm^{-1} zone.[121] Other authors have reported that the absorption in this zone results from both Ti-O-Si and $Si-O^-$ contributions.[13] However, the TEM images (Chapter 4.3, Figure 4) confirm that TiO_2 and SiO_2 are maintained in separate domains in our composites and consequently, an incorporation of Ti in the silica lattice has not taken place. Therefore, we think that the interaction produced between TiO_2 and SiO_2 corresponds to van der Waals physical bonds instead of chemically-bonded Ti-O-Si linkages.[43]

---

[128] M. Sekine, S. Katayama, M. Mitomo, J. Non-Cryst. Solids 124 (1991) 199.
[129] C. H. Weigel, R. Kellner, Fresen Z. Anal. Chem. 335 (1989) 663.

We also observed three bands at 2890 cm^{-1}, 2930 cm^{-1} and 2975 cm^{-1} which we relate respectively to -CH_3 symetric stretching, -CH_2 assymetric stretching and -CH_3 assymetric stretching.[127] These bands may be associated to ethoxy groups from non-hydrolyzed oligomers present in the material. Another band is observed at 1296 cm^{-1}, corresponding to CH_2 twisting vibration, which could be also attributed to ethoxy groups.[130]A higher intensity of all these peaks is observed in the materials with higher TiO_2 content, confirming that TiO_2 particles exert a suppressive effect on silica hydrolysis and condensation, and consequently more non-hydrolized groups are present, as we have discussed in preceding paragraphs. The spectrum corresponding to the material synthesized in the absence of TiO_2 nanoparticles showed a much lower intensity for these peaks than any other of the materials, confirming this hypothesis.

UV-Vis spectroscopy

The diffuse reflectance UV-Vis spectra obtained for all the photocatalysts are shown in Chapter 4.3, Figure 6. All the photocatalysts show absorption in the UV range (up to 400 nm) and no absorption in the visible range. This means that the inclusion of TiO_2 nanoparticles in a silica matrix does not produce absorption in the visible range, as might be expected, for instance, in doping processes. Moreover, by comparing all our spectra with others previously obtained for TiO_2 P25 nanoparticles,[131] we can corroborate that there is no significant change of absorption after the inclusion of TiO_2 in a silica matrix. Similarly, Alvaro et al.[41] reported that the absorption bands in analogous TiO_2-SiO_2 composites were intrinsically inherent to the presence of TiO_2 nanoparticles. The same bands were not altered by the presence of silica domains in the solid because Ti-O-Si bonds corresponding to a truly mixed oxide were not present in the material. This finding confirms that SiO_2 and TiO_2 are present in separate domains in the nanocomposites studied, as we previously observed by TEM (Chapter 4.2, Figure 4). Regarding the location of TiO_2 within the SiO_2 matrix, Zelenak et al.[46] reported that TiO_2 absorption in

[130] P. Innocenzi, J. Non-Cryst. Solids 316 (2003) 309.
[131] S. W. Verbruggen, K. Masschaele, E. Moortgat, T. E. Korany, B. Hauchecorne, J. A. Martens, S. Lenaerts, Catal. Sci. Technol. 2 (2012) 2311.

350-400 nm range is related to the presence of a TiO_2 phase in the silica pore system or pore walls. We observed absorption in a similar range (320-400 nm), which again confirms that TiO_2 and SiO_2 are present in separate domains.

NMR spectroscopy

^{29}Si NMR spectra for some materials synthesized are shown in Chapter 4.3, Figure 7. All the materials showed two peaks at chemical shifts of −100 ppm and −110 ppm corresponding, respectively, to Q3 and Q4 structural units. In all these materials, the Q4 peak, attributable to tetrafunctional buildings, is higher than that corresponding to Q3, indicating a more cross-linked framework due to the effect of *n*-octylamine. This higher degree of reticulation is typical of silica species condensed as particles.[132] It was also observed in silica particle mesostructures obtained by using amine surfactants as a template.[87,133] This finding confirms that *n*-octylamine produces nanomaterials composed of a network of silica particles, as was visualized by SEM and TEM (see 4.3 Figures 2 and 4). The lower intensity observed in Q4 for the materials containing 10% w/v TiO_2 (the highest of the tested loadings) indicates, *a priori*, that less reticulation is produced.

Another significant difference according to the TiO_2 content was also observed. The three spectra from the photocatalysts containing the highest proportion of TiO_2 presented Q1 (−89 ppm) and Q2 (−91 ppm) units in conjunction with Q3 and Q4 species. Davis et al.[13] also observed an increase in signals corresponding to a reduced silica reticulation as TiO_2 content was raised. In our case, we speculate that this difference is due to an incomplete condensation of silica and consequently, some ethoxy groups are present in the material. This information is in good agreement with the increase of $-CH_2-$ and $-CH_3$ detected through FTIR, and the increased aggregate size detected by SEM. Here, we can confirm that these larger aggregates are also less condensed silica structures. In the case of photocatalysts with the lowest TiO_2 content, the

[132] F. Babonneau, Polyhedron 13 (1994) 1123.
[133] P.T. Tanev, T. Pinnavaia, J. Chem. Mater. 8 (1996) 2068.

signals from Q1 and Q2 are either absent or observed as a very weak signal. This finding confirms the role played by the *n*-octylamine as catalyst during the sol-gel transition and the inhibition of its catalytic action by the presence of TiO_2.

5.2. Application on stone

Uptake and dry matter

The TiO_2-SiO_2 photocatalysts prepared in the work carried out for this Doctoral Thesis were sprayed as sols onto a limestone, (Chapters 4.1 and 4.3) under laboratory conditions, in order to investigate its photocatalytic behavior, its penetration depth, adhesion and strengthening properties. In the Chapter 4.4, the photocatalyst synthesized in our laboratory was applied on a very friable dolostone. The sols were applied by spraying onto the surfaces of the samples until apparent refusal, this being understood to occur when the surfaces remained wet for 1 minute. After the application, the excess of sol was removed from the surface of the sample by air spraying, in order to form the thinnest possible surface film.[134] For comparison purposes, the effectiveness of TiO_2 nanoparticles aqueous dispersions, H_3PO_4-catalyzed TiO_2-SiO_2 composites and pure silica materials was also evaluated. Uptake of the materials under study and dry matter on the limestone samples are shown in Chapter 4.1, Table 2 and Chapter 4.3, Table 3, In the case of the dolostone, the results are shown in Chapter 4.4, Table 1.

In the case of the limestone, uptake and dry matter percentages seem to show tendency to increase as TiO_2 nanoparticles content is raised. These trends are explained because the higher TiO_2 nanoparticles content means that the liquid content in the sol is lower, and thus less sol could evaporate during the sol

[134] A. P. Ferreira Pinto, J. Delgado Rodrigues, J. Cultural Heritage 9 (2008) 38.

application. Moreover, sol could also evaporate partially because carbonate stones slow down the sol-gel transition, as reported by Wheeler et al.[135]

In the case of the dolostone, the uptake of the TiO_2 aqueous dispersions corresponding to the commercial product E503 (Chapter 4.4, Table 1) was slightly higher than the uptake of the TiO_2-SiO_2 nanocomposites. This might be due to the lower viscosity of the TiO_2 aqueous dispersion. On the contrary, dry matter values were significantly lower for TiO_2 aqueous dispersion than for the TiO_2-SiO_2 nanocomposites. We hypothesize that the aqueous dispersions creates a deposit of particles on the surface of stone whereas the nanocomposites penetrate into the stone pore structure.

Scanning electron microscopy studies

Figure 7 (Chapter 4.1) and Figure 8 (Chapter 4.3) show SEM micrographs of the limestone specimens treated with the materials under study. In Chapter 4.4, Figure 1 shows images corresponding to the dolostone treated.

As observed in the images, TiO_2 aqueous dispersions and H_3PO_4-catalyzed SiO_2 materials create a dense and extensively cracked coating on the limestone surface. E503 product creates a thin and easily detachable surface layer on the dolostone treated. TEGOVAKON® V 100 (Chapter 4.4, Figure 1) creates a dense, carcking and vitreous coating on the dolostone surface. The microporous nature of this product, characterized using nitrogen physisorption in our previous papers,[79] is responsible for the formation of a cracked coating.

SEM images of stone specimens treated with the surfactant-synthesized photocatalysts and its counterpart without TiO_2 show that a crack-free, homogeneous and coarse coating is created on the two stone surfaces. This confirms the contribution of *n*-octylamine to reducing the capillary pressure responsible for cracking. As we have previously stated,[79,84] the surfactant reduces capillary pressure in two different ways: 1) by coarsening the gel

[135] G. Wheeler, Alkoxysilanes and the consolidation of stone, The Getty Conservation Institute: Los Angeles CA, 2005.

network pore size; and 2) by reducing the surface tension of the starting sol. It should also be noted that the coarsening produced by *n*-octylamine must also improve the access to photoactive sites, thus increasing the photocatalytic activity.

We also observe some changes in the morphology of the coatings when TiO_2 nanoparticles are integrated in the SiO_2 network. Specifically, the higher TiO_2 loading produces larger aggregates, in good agreement with the behavior observed from the materials produced on Petri dishes (Chapter 4.3, Figure 2). This allows us to corroborate that the stone substrate has little influence in the final surface morphology of these photocatalysts.

We investigated the penetration depth of the sols by using SEM to visualize a cross section of the limestone samples treated. X-EDS elemental mappings for Ti and Si were also obtained. All the sols show a similar behavior when they are applied on the stone. As an example, the X-EDS mappings obtained for cross-sections of limestone treated with the TiO_2-SiO_2 photocatalysts containing AP particles are shown in Chapter 4.3, Figure 9. Mappings corresponding to limestone samples treated with the material without TiO_2 particles are also included for comparison purposes. These mappings allow us to confirm that the material without TiO_2 presents a deep penetration of Si across all the depth range evaluated. The material with the lowest TiO_2 loading shows that both Ti and Si penetrate to a very similar depth. In the case of the materials with higher TiO_2 loading (4% and 10%), we observe a significant accumulation of Ti and Si on the stone surface. This finding could be associated with the higher viscosity of these coatings with the highest contents in titania particles.

In order to confirm this conjecture, in Chapter 4.3, Fig 10a presents a BSE image of the cross-section of the limestone sample treated with 4% w/v AP particles. Images with higher magnification were obtained on the surface (indicated in blue, in Chapter 4.3, Figure 10b,c) and in the interior (indicated in yellow, in Chapter 4.3, Figure 10d,e) of the stone in SE and BSE modes, respectively. From this more detailed analysis of the cross section of stone

treated with this material, we can observe that a thin photoactive surface film is formed (Chapter 4.3, Figure 10b) which also penetrates between the stone grains. The presence of the photocatalyst between the grains is clearly visible in Figure 10c because of the higher atomic number of Ca with respect to Si. We thereby corroborate that out photocatalyst is able to adhere to the limestone, ensuring its potential long-term performance. We do not obtain the same result for deeper zones of the stone cross section (Figure 10d, SE mode and Figure 10e, BSE mode), probably because the deeper zone has a lower content of the photocatalyst, as confirmed by the results previously obtained by SEM.

FTIR spectroscopy on stone substrates

FTIR spectra of the treated dolostone samples and their untreated counterpart are shown in Chapter 4.4, Figure 2. All the samples present the carbonate peaks, which are characteristic of all carbonate stones including the dolostone used in this work. Specifically, the peaks at 1420, 880 and 730 cm^{-1} correspond to asymmetric, out-of-plane and in-plane bending vibration modes of the anion CO_3^{2-}, respectively.[136] The spectra corresponding to the untreated dolostone and the stone sample treated with the commercial product E503 do not present any additional peak. We relate the similarity between treated and untreated dolostone spectra with the low dry matter value obtained for E503.

In the case of the dolostone samples treated with TEGOVAKON® V 100 and our coating, we observe some additional peaks in the spectra. In particular, there are two peaks corresponding to typical siloxane vibrations, located at 800 and 1070 cm^{-1}, corresponding to bending and stretching vibrations, respectively.[79] This confirms the presence of silica gels in the surface of the two treated stones. However, the intensity of these two peaks is different, being significantly lower in the stone treated with the commercial product. This confirms the poor effect of commercial siloxane products on pure carbonate stones reported in the literature.[135] The higher intensity of Si-O-Si bonds observed in the stone treated with our product can be attributed to the role

[136] A. Sdiri, T. Higashi, T. Hatta, F. Jamoussi, N. Tase, Environ. Earth Sci. 61 (2010) 1275.

played by *n*-octylamine, which may accelerate the condensation process in the carbonate stone.[89] This hypothesis is also confirmed by other additional Si-O-Si peak presented by the stone treated with the UCA product. Specifically, this sample showed a peak adjacent to the stretching vibration, located at 1161 cm^{-1}. Demjén et al.[127] associated this double band (1070-1161 cm^{-1}) to the formation of high-molecular weight siloxane chains with a ladder-type structure. We also found this double band in silica xerogels prepared in presence of *n*-octylamine.[87] In the case of the TEGOVAKON® V 100 product, this additional band was not observed and subsequently, a cyclic, low-molecular weight polymeric siloxane structure could have been formed, according to these authors. Specifically, they found this double band in $CaCO_3$ treated with amino functional silanes. They concluded that the primary amine group promotes the formation of high- molecular weight siloxane polymers due to its catalytic effect on polycondensation.

Mechanical properties

Adhesion tests

One significant drawback of TiO_2 particles applied as an aqueous dispersion on stone has been the reduced photocatalytic efficiency found during long-term use, due to the elimination of TiO_2 from the stone surface.[97] Thus, we have also investigated the degree of adhesion of our materials applied on stone by performing a peeling test adapted from the literature.[137]

In Chapter 4.1, Figure 8 shows the images obtained by SEM and the EDX analyses carried out on tested and non-tested areas after application of an aqueous dispersion of TiO_2 P25. On the left side, images corresponding to untested sample areas and spectra are presented. On the right side of the same image, we present the data corresponding to tested areas. In P25 coatings, an almost complete removal of the TiO_2 coating after the peeling test can be observed. The TiO_2 peaks are significantly reduced after the test, confirming

[137] M. Drdácký, J. Lesák, S. Rescic, Z. Slížková; P. Tiano, J. Valach, Mater. Struct. 45 (2012) 505.

the poor adhesion of the particles to the limestone surface. A similar situation is observed in the dolostone (Chapter 4.4, Figure 3). It shows a severely-cracked, friable and easily-detachable surface, corresponding to the commercial E503 (aqueous dispersion of TiO_2). Similarly to the aqueous dispersions of P25 applied on limestone, a significant amount of material is removed from the stone surface (Chapter 4.4, Table 1). Since this product is largely eliminated from the stone surface, we consider that it has little potential use for stone with low cohesion. Concerning the changes in titanium content after peeling, no significant differences can be observed, probably because its content is too low to observe these changes.

On the contrary, stone samples treated with surfactant-synthesized pure silica material and with TiO_2-SiO_2 nanocomposite photocatalysts (1% w/v TiO_2 loading) show almost negligible loss of mass (Chapter 4.3, Table 1). These findings confirm that TiO_2 has been integrated into the silica matrix, which has, in turn, adhered firmly to the stone. In this respect, the inclusion of the photocatalyst in a mesoporous silica coating is an interesting solution for keeping particles well adhered to the surface, to provide long-term wear resistance.

For higher TiO_2 nanoparticles content, the test removed a slightly larger amount of material from the stone surface, reaching a maximum for the coatings with the highest TiO_2 content (10% w/v). We associate this result with the formation of a less condensed and more detachable composite on the limestone surface for coatings with the highest titania loadings, as was previously confirmed through ^{29}Si NMR.

Drilling resistance

We also investigated whether any enhanced strengthening of the stone was produced by the products applied; this was done by measuring and comparing the drilling resistance of the untreated limestone and its treated counterparts. The results obtained are shown in Chapter 4.1, Figure 9 and in Chapter 4.3,

Figure 11. In the case of the dolostone, the results corresponding to DRMS measurements are shown in Chapter 4.4, Figure 4.

As expected, the aqueous dispersion of P25 deposited on stone (Chapter 4.1, Figure 9) does not produce any increase in mechanical resistance whereas our products increase significantly the resistance of the stone. Some significant differences were observed (Chapter 4.1, Figure 9, 4.3 Figure 11) in line with variations in the TiO_2 loading. As a general trend, we observe that the samples treated with 1% w/v TiO_2 loading composites and the samples treated with materials without TiO_2 show similar increases in drilling resistance. This demonstrates that 1% loading is not enough to modify the robustness produced by the composite formed into the stone pore structure. The materials with higher TiO_2 loading showed reduced drilling resistance. This result could be explained as a consequence of the very low degree of reticulation and condensation of the gel networks as previously we have previously discussed.

In the case of the dolostone tested, TEGOVAKON® V 100 (Chapter 4.4, Figure 4) increases the stone's resistance to a depth of 5 mm. On the same stone, the application of the TiO_2-SiO_2 nanocomposite with 2% w/v TiO_2 nanoparticles loading increased the drilling by a factor of 6 in the full depth evaluated of 30 mm.

Finally, we would like to remark that also consider that all the results confirm that *n*-octylamine is playing a valuable role in enhancing the robustness of the treated stone, since silicon-based products are known to be ineffective as consolidants on pure carbonate stones.[134,138]

Static water contact angles

Since water is the main vehicle carrying the agents of decay, such as soluble salts and microorganisms that attack building materials, any hydrophilicity in a coating would be undesirable. Therefore, we have also measured water droplet static contact angles (CA) on the surface of stone samples treated with

[138] E. Zendri, G. Biscontin, I. Nardini, S. Riato, Const. Build. Mat. 21 (2007) 1098.

the photocatalysts under study. Results obtained for the limestone evaluated are given in Chapter 4.1, Table 1. In the case of the dolostone, the results are shown in Chapter 4.4, Table 3.

As expected, the untreated limestone surface shows a hydrophilic behavior with a static CA of 61º. Stone surfaces treated with the P25 dispersions at lower concentrations present a similar droplet CA value as the untreated surface, whereas the P25 dispersion with the highest TiO_2 content induced a significant reduction in the CA value. This finding suggests that, in dispersions with lower concentrations, particles do not completely cover the stone surface and thus, the static CA of the surface is not modified. The low contact angle obtained for the aqueous dispersion with the highest TiO_2 concentration (2% w/v) corroborates the hydrophilic character of P25.

In the case of the TiO_2-SiO_2 nanocomposites under study, an inverse relationship between TiO_2 loading and static CA value in obtained. These results obtained confirm that the nanocomposites with 1% and 4% w/v TiO_2 loading do not produce water absorption and thus can be employed as protective coatings in stones and other building materials.

Color change evaluation

Total color difference values (ΔE^*) of the limestone after the application of the nanocomposites are shown in Chapter 4.1, Table 2. The P25 dispersions produced small values of ΔE^*, below the generally accepted perception threshold ($\Delta E^* \leq 5$), even for the most restrictive applications (ancient building restoration)[72]. In TiO_2-SiO_2 nanocomposites (Chapter 4.3, Table 3), all the photocatalysts produced color changes close to the threshold considered previously. We think that color changes are not significative because we dispersed particles of sizes reduced to the nanoscale, these coatings also reduce the hiding power of TiO_2 and minimize the possibilities of significant color change. In addition, we removed the excess of sol on the stone surface just after application. We confirmed that, by using this application method, it was

possible to reduce the color change to suitable values for application on stone surfaces and buildings.

In the case of the dolostone treated, the TiO_2-SiO_2 nanocomposite applied also produced a ΔE^* below the perception threshold (Chapter 4.4, Table 1). TEGOVAKON® V 100 produced an unacceptable color change (ΔE^*=16).

Evaluation of photoactivity

Finally, and most importantly, we have investigated the self-cleaning properties of the photocatalysts synthesized in our laboratory on the two stones tested by carrying out a photo-degradation test of stains deposited previously on the stone surfaces. Methylene blue (MB) was used as the staining agent dissolved in ethanol in order to ensure rapid evaporation of the liquid. The evolution of total color differences (ΔE^*) under UV light, with the time was recorded. Stones treated with pure silica materials, stones treated with commercial materials and also untreated samples were included in these tests for comparison purposes. In order to confirm the changes in colour experimented by the specimens under study, we also obtained images of the surface stone samples, by conventional photography (Chapter 2.1, Chapter 2.4) or by optical microscopy, at the end of the photocatalytic test (Chapter 2.3).

The conditions of this test make the following comments relevant: 1) it was performed in the absence of liquid water and with low relative humidity (around 30%); therefore, degradation times are necessarily slower than in experiments carried out on high moisture because the generation of $OH^{\bullet}$ free radicals is reduced; in our view, if these products are applied on building outdoors, the moisture present in the environment could probably accelerate the photodegradation process; 2) our test has been carried out in presence of atmospheric oxygen and at neutral pH conditions, ensuring that all the colour variations are due to the elimination of MB and not to the undesirable formation of the leuco form of MB (LMB);[139] 3) we have evaluated photodegradation by measuring the total color variation parameter because

[139] A. Mills, J. Wang, J. Photochem. Photobiol. A, Chem. 127 (1999) 123.

this is usually considered for portable color measurement; this makes it very useful for testing the degradation of methylene blue *in-situ*, in construction, restoration or rehabilitation buildings.

The evolution of ΔE^* under UV light with the time was recorded and results corresponding to the limestone tested are shown in Chapter 4.1, Figure 10 and Chapter 4.3, Figure 12. The Chapter 4.4, Figure 5 presents results corresponding to the dolostone evaluated. Images of the samples of the stone surfaces under study after completion of the test are also presented in Chapter 4.1, Figure 11; Chapter 4.3, Figure 13 and Chapter 4.4, Figure 5.

In the case of the untreated stone samples, the final ΔE^* value reached is around 25% for the limestone and 34% for the dolostone. This MB bleaching under visible/UV light has been reported previously and has been associated with the absorption of light undergone by the dye in the 350-520 nm range.[139]

Of all of the materials tested, the TiO_2 P25 dispersions (Chapter 4.1, Figure 10) present the most rapid bleaching of the MB stains. In the first 6 h, the stain is almost completely degraded (88% of the total change is observed after this period of time has elapsed). Comparing the performance of the various P25 dispersions, a modest increase in self-cleaning activity is found in line with higher TiO_2 content; the final ΔE^* values are 15, 9, and 7 for P25 content of 0.5, 1 and 2%, respectively.

In general, the MB degradation rate for the two series of TiO_2-SiO_2 nanocomposites tested is slower than that presented by pure TiO_2 nanoparticles P25 dispersions (Chapter 4.1, Figure 10). This lower degradation rate can be explained by the low TiO_2 content in all the coatings prepared (a maximum of 2%). In addition, all the materials synthesized show two clearly different rates of MB bleaching in the degradation profiles. Very rapid MB bleaching occurs in the first 7-12 h, accounting for around 80% of the total color variation recorded. Next, a slower rate of degradation is observed over the longer term. Again, small differences in ΔE^* values are found for the differing TiO_2 concentrations tested. These differences are appreciated mainly

in the initial rate of degradation in which the coatings with the higher P25 content (1% and 2%) show larger falls in ΔE^* value.

Considering the performance of the nanocomposites coatings prepared without TiO_2 particles, we also observe a bleaching effect under UV exposure (Chapter 4.1, Figure 10; Chapter 4.3, Figure 12). A degradation profile similar to that corresponding to the slower, second-stage rate for TiO_2-SiO_2 composites is now observed. Next, a slower rate of degradation is observed over the longer term. We associated the second stage with a much slower rate of degradation may be caused by an effect of the TiO_2-SiO_2 coating reducing initially the capacity of the MB to penetrate into the limestone pore structure. Thus, MB is retained on the stone surface, where it can be more easily degraded than that located inside the untreated stone pore structure. The variations found in the degradation kinetics between the coatings obtained in absence of surfactant (containing H_3PO_4 as sol-gel catalyst) and in presence of a surfactant (*n*-octylamine) confirm our hypothesis (Chapter 4.1, Figure 10). The material with lower porosity (obtained in absence of the surfactant), which was subsequently shown to be associated with lower penetration of MB into the pore structure of the limestone, induces a more rapid degradation than the coating with greater porosity (surfactant-synthesized).

The two findings reported above clearly confirm that the photocatalytic action of the TiO_2 particles produces most of the total degradation effect on the stain in the first few hours of exposure (the first part of the curve) for TiO_2-SiO_2 photocatalysts.

We think that the second stage with a much slower rate of degradation may be caused by the TiO_2-SiO_2 coating reducing the capacity of the MB to penetrate into the limestone pore structure. The greater the proportion of MB on the surface of the coated limestone, the greater the proportional degradation by the bleaching effect of the UV light absorbed.

Further, if we compare the performance of the two series of photocatalysts, we find that the surfactant-synthesized materials show greater self-cleaning

activity, since their rate of degradation in the rapid first stage is slightly higher and the final ΔE^* values produced in the longer term are lower.

In Chapter 4.1, Figure 11 shows photographs of the stone surfaces under study after completion of the test. The samples illustrated are the stained limestone surfaces untreated and treated with the three different coatings with the highest TiO_2 content (2%). Photographs corresponding to the other coatings evaluated are shown in Chapter 4.1, Figure 3, as Supporting Information. It can be observed that the stone surface treated with the H_3PO_4-catalyzed material shows the lowest degradation of the MB stain. The degree of change in color induced by the TiO_2 nanoparticles and the surfactant-synthesized TiO_2-SiO_2 photocatalyst is similar.

The greater self-cleaning effect produced by the surfactant-synthesized TiO_2-SiO_2 photocatalysts is explained by their higher porosity and the larger pore size of the gel network. As previous authors have reported,[38,126] the photocatalytic degradation of MB is clearly enhanced by the addition of TiO_2 particles to a SiO_2 mesoporous structure, in comparison with the effect observed when the particles are integrated in a dense microporous matrix. This enhancement effect was explained by these authors in terms of the increased BET surface area, which accelerates the diffusion of MB toward the reaction sites (i.e., toward the TiO_2 particles). The authors of this study have also reported previously that the presence of mesopores also assists rapid diffusion. Surfactant-synthesized TiO_2-SiO_2 photocatalysts create a field of SiO_2 and TiO_2 nanoparticles, which presents a pore structure with numerous voids between particles, making the sites with photocatalytic activity, the titania particles, much more accessible for the MB molecules. This hypothesis is illustrated in the model proposed on the basis of the HAADF-STEM images (Chapter 4.1, Figure 4) obtained for these materials.

In the case of the photocatalyst obtained in the absence of a surfactant, a dense and microporous SiO_2 gel with TiO_2 nanoparticles embedded is clearly observed; in this material, the photocatalytic sites will be less accessible to the MB.

From these results, we conclude that the addition of TiO_2 nanoparticles to a silica mesoporous structure created using a surfactant as template creates a material with effective photocatalytic activity, and the MB bleaching obtained is similar to that obtained by the P25 TiO_2 nanoparticles.

Considering now the effect of the TiO_2 loading on the photocatalytic performance of the nanocomposites under study (Chapter 4.3, Figure 12) we observe that increasing the TiO_2 amount from 1 to 4 % enhances the photocatalytic activity, as was expected. This is confirmed by the significantly shorter first stage of the curve (due to photocatalytic activity of TiO_2 nanoparticles) in materials containing 1% TiO_2 loading. However, increasing the TiO_2 loading to 10% is clearly counterproductive. The final color observed on the stone surface of the samples confirms this conclusion (Chapter 4.3, Figure 13). We explain this significant reduced photoactivity in terms of the structure of these nanocomposites. The substantial reduction in pore volume and BET surface area for the materials containing the highest TiO_2 content (Chapter 4.3, Table 2 and Figure 3) could be responsible for their reduced photoactivity.

From the results discussed above, we can conclude that mesostructure of the photocatalyst, created by the *n*-octylamine, plays an important role in the photocatalytic activity of the materials under study. Thus, the nanocomposites with the highest TiO_2 loading, remarkably, show the weakest photoactivity due to their smaller pore size and specific surface; in fact, they hardly present any pores in the mesopore range. In contrast, the effectiveness of the other photocatalysts is enhanced because they are mesoporous materials with a larger surface area and pore volume. This enhancement effect in photocatalytic activity was explained by Suzuki et al.[38] in terms of the increased BET surface area, which accelerates the diffusion of MB towards the reaction sites (i.e. towards the TiO_2 nanoparticles). In addition, we think that a synergistic effect occurs with the SiO_2 matrix, which acts as an absorber and provides access to TiO_2 photocatalytic sites. This hypothesis is clearly confirmed by the degradation profiles observed in the photocatalysts with

highest TiO_2 loading, in which degradation profile is significantly lower because the access to photoactive sites was significantly reduced.

A comparison of the three photocatalysts loaded to 4% with TiO_2 of different particle size also reveals certain differences. Specifically, the photocatalyts containing AP, P90 and P25 particles present final ΔE^* values of 7.4, 11.8 and 16.6, respectively (Chapter 4.3, Figure 12). The lower pore volume of the photocatalyst containing P25 nanoparticles may be the explanation why it performs worse than the other two 4 % w/v photocatalysts (Chapter 4.3, Table 2), supporting the above hypothesis.

As describe in the previous paragraph, the size of the TiO_2 particles used has a clear effect on photocatalytic performance of these materials. We find that the AP photocatalysts always show a better performance than the P90 or P25 counterparts for all the loadings tested. It seems that the higher average size and the sharper shape of TiO_2 nanoparticles present in AP, as observed by TEM/STEM, favors their photoactivity. The effect of particle size on TiO_2 photocatalysts was previously reported by several authors,[140-142] who found that larger TiO_2 particles have greater effective surface area for greater photon absorption and electron-hole generation and thus, produce a better photocatalytic performance. Regarding to the effect of particle shape, Li and Liu[143] suggested previously that sharper TiO_2 particles could be inherently more reactive in photo-oxidation. In our case, the AP particles are sharper than the other types because the high-power ultrasonic agitation applied in the synthesis changes the particles from a regular spherical form (Chapter 4.3, Figure 2 in Supplementary Information) to an irregular sharper one (Chapter 4.3, Figure 4).

Another complementary characteristic that may enhance photoactivity in S4AP materials is their higher BET surface area. We observe that the

[140] T. P. Chou, Q. Zhang, B. Russo, G. E. Fryxell, G. Cao, J. Phys. Chem. C.
[141] Z. Zhang, C. Wang, R. Zakaria, J. Ying, J. Phys. Chem. B 102 (1998) 10871.
[142] J. T. Carneiro, A. R. Almeida, J. A. Moulijn, G. Mul, Phys. Chem. Chem. Phys. 12 (2010) 2744.
[143] Y. Li, Z. Liu, J. Am. Chem. Soc. 133 (2011) 15743.

increasing surface area for materials with TiO_2 4% w/v loading promotes an increase in the photocatalytic effect (AP>P90>P25). This trend was confirmed by Yoshida et al.[51] This effect is not observed with the other loadings tested either because TiO_2 content is too low (1% w/v) or because a non-porous network is created (10% w/v). The final color observed on the stone surface confirms that P25 and P90 TiO_2-SiO_2 photocatalysts present inferior photocatalytic performance when compared with AP ones (Chapter 4.3, Figure 13).

We also carried out a comparison between the performance of commercial self-cleaning products and our products when applied on a dolostone. We have observed a similar behavior in MB degradation for dolostone samples treated with commercial E503 and surfactant-synthesized TiO_2-SiO_2 nanocomposite (2% w/v TiO_2 P25 loading) (Chapter 4.4, Figure 5). The final ΔE^* value obtained was 4.23 for the stone treated with our product, whereas stone treated with E503 showed a slightly higher final ΔE^* value (6.67). This variation between products may be associated with higher TiO_2 content (2% w/v) of our product compared with that of E503 (0.75-1% w/v). If we compare the effect on the limestone previously tested with the effect produced on the dolostone, we conclude that they are similar.

Durability against salt crystallization

Finally, we subjected the very friable dolostone samples to a salt crystallization test in order to evaluate the durability induced by the treatment. In Chapter 4.4, Figure 6 shows the weight loss of the treated dolostone samples and its untreated counterparts during the test. On the right side, photographs are also shown of the dolostone treated with the products under study and their untreated counterpart. The 'before and after' of these photographs illustrate the condition before subjecting the samples to the salt crystallization test and to their condition when the test was finished for each sample (corresponding to the last point in the graphic presented in Chapter 4.4, Figure 6).

As observed in the pictures, the untreated stone sample has completely disintegrated after the 4th cycle. Coincidently, commercial TEGOVAKON® V 100 has lost almost 50% of its mass by the 4th cycle. The samples treated with our surfactant-synthesized TiO_2-SiO_2 nanocomposite (2% w/v TiO_2 P25 loading) remain almost unaltered until the 20th cycle, and even after the 30th cycle show a fairly good behavior. In the case of the untreated stone, the results obtained confirm that it is a very friable stone, totally unsuitable for use as a building material. Regarding the samples treated with TEGOVAKON® V 100, we think that the poor mechanical properties achieved for the stones treated (in Chapter 4.4, Figure 4) are responsible for its limited durability. As previously discussed, the low mechanical resistance could be due to the combined effect of the following factors: 1) extensive cracking that occurs for TEGOVAKON® V 100 coatings (Chapter 4.4, Figure 1); 2) poor interaction between a siloxane-based product and carbonate stones; 3) the presence of micropores in a stone generates high sodium sulfate crystallization pressures, which give rise to significant damage to the porous substrate.[144] Therefore, the microporosity of TEGOVAKON® V 100 could also increase its susceptibility to sodium sulfate crystallization damage.

In the case of our product a homogeneous, crack-free coating that adheres well to the dolostone is created with greater in-depth mechanical resistance. This explains why our TiO_2-SiO_2 composite gives very good durability on the dolostone substrate. Again, we think *n*-octylamine is making a significant contribution to enhancing the durability, since it not only prevents cracking but also facilitates the interaction with the carbonate stone, as discussed extensively in previous paragraphs. The TiO_2 particles could also increase the durability of the treatment when subjected to crystallization salts, as Miliani et al. reported for silica consolidants modified with TiO_2 particles applied on a sandstone.[72]

[144] C.Rodríguez-Navarro, E. Doehne, E. Sebastián, Cement Concrete Res. 30 (2000) 1527.

6. Conclusions

From the results obtained in the work undertaken for the Doctoral thesis presented it can be concluded that mesoporous silica-supported TiO_2 photocatalysts with the requirements suitable for self-cleaning application on monumental building stones have been successfully synthesized. The products synthesized have a clear practical application since they can be employed outdoors by means of a simple and low cost process.

In addition, the following specific conclusions are drawn regarding the synthesis and characterization of the photocatalysts:

- A solvent-free synthesis process for TiO_2-SiO_2 photocatalysts has been developed, in which preformed TiO_2 nanoparticles and an oligomeric ethoxysilane are mixed in the presence of *n*-octylamine.
- The sols can be applied on the surface of stonework, as aerosols, by means of a simple process. *N*-octylamine prevents the aggregation of TiO_2 particles within the sol by increasing the pH value.
- The sol-gel transition occurs spontaneously inside the stone pore structure due to the catalytic effect of *n*-octylamine.
- *N*-octylamine also prevents gel cracking during drying inside the stone by increasing the pore size and by reducing the surface tension of the liquid sol.
- The coarsening effect created by the *n*-octylamine also enhances the photocatalytic activity of the material, by increasing the access of contaminants to photoactive sites.
- The SiO_2 gel network is composed of particles of nearly uniform size, created by an aggregation mechanism produced by the *n*-octylamine.
- The TiO_2 particles are integrated inside a mesoporous silica matrix, with TiO_2 and SiO_2 being maintained as separate domains, with no observable chemical interaction.

Regarding the effectiveness of our photocatalysts on building stone, we can conclude:

- The photocatalysts synthesized have demonstrated their self-cleaning efficacy on building stones.
- The photocatalysts also adhere firmly to stone surfaces. This should ensure that the conservation and self-cleaning properties of the coating created have a long-term effect.
- Photocatalytic activity is improved when larger and sharper titania particles are integrated into the silica mesoporous gel network.
- Photocatalytic activity is optimal for a TiO_2 content of around 4% w/v. At higher contents, the activity is reduced because the pore volume of the nanocomposite is drastically reduced.
- The nanocomposites produced also increase the mechanical resistance of stones. They were even able to convert a very friable stone, currently not usable for application in building, into a suitable building material.
- Two existing commercial products tested (a consolidant and a self-cleaning agent) produce coatings that crack and generate less mechanical resistance for the stone than our products.
- The products developed do not produce negative effects on building stones, such as colour change or hydrophilic properties.
- Our materials also make the stone suitably durable against degradation by salt crystallization.

7. References

1) A. Fujishima, K. Honda, Nature 238 (1972) 37.

2) R. Portela Rodríguez, Eliminación fotocatalítica de H_2S en aire mediante TiO_2 soportado sobre sustratos transparentes en el UV-A, Universidad de Santiago de Compostela: Santiago de Compostela (2008).

3) A. Fujishima, T. Rao, D. Tryk, J. Photochem. Photobiol. C 1 (2000) 1.

4) http://www.toto.co.jp/docs/hyd_patent_en/hydro_img/ill01.gif (25/11/2009)

5) I. Karatasios, M. S. Katsiotis, V. Likodimos, A. Kontos, G. Papavassiliou, P. Falaras, V. Kilikoglou, Appl. Catal. B 95 (2010) 78.

6) C. Aprile, A. Corma, H. García, Phys. Chem. Chem. Phys. 10 (2008) 769.

7) M. Bideau, B. Claudel, C. Dubien, L. Faure, H. Kazouan, J. Photochem. Photobiol. A 91 (1995) 137.

8) L.Windler, C. Lorenz, N. von Goetz, K. Hungerbühler, M. Amberg, M. Heuberger, B. Nowack, Environ. Sci. Technol. 46 (2012) 8181.

9) N. T. Boncagni, J. M. Otaegui, E. Warner, T. Curran, J. Ren, M. M. F. Cortalezzi, Environ. Sci. Technol. 43 (2009) 7699.

10) L. Rejinders, Polym. Degrad. Stabil. 94 (2009) 873.

11) C. A. Morris, M. L. Anderson, R. M. Stroud, C. I. Merzbacher, D. R. Rolison, Science 284 (1999) 622.

12) H. Kibombo, R. Peng, S. Rasalingam, R. Koodali, Catal. Sci. Technol. 2 (2012) 1737.

13) R. J. Davis, Z. Liu, Chem. Mater. 9 (1997) 2311.

14) J. J. Calvino, M. A. Cauqui, G. Cifredo, L. Esquivias, J. A. Pérez, M. Ramírez del Solar, J. M. Rodríguez-Izquierdo, J. Mater. Sci. 28 (1993) 2191.

15) S. Gontier, A. Teruel, Zeolites 15 (1995) 601.

16) W. Zhang, M. Fröba, J. Wang, P. Tanev, J. Wong, T. Pinnavaia, J. Am. Chem. Soc. 118 (1996) 9164.

17) M. Kruk, M. Jaroniec, A. Sayari, Microporous Mater. 9 (1997) 173.

18) M. A. Cauqui, J. M. Rodríguez-Izquierdo, J. Non-Cryst. Sol. 147 (1992) 724.

19) K. de Witte, V. Meynen, M. Mertens, O. I. Lebedev, G. Van Tendeloo, A. Sepúlveda-Escribano, F. Rodríguez-Reinoso, E. F. Vansant, P. Cool, Appl. Cat. B, 84 (2008) 125.
20) E. Beyers, E. Biermans, S. Ribbens, K. de Witte, M. Mertens, V. Meynen, S. Bals, G. van Tendeloo, E. F. Vansant, P. Cool, Appl. Catal. B 88 (2009) 515.
21) M. M. Haridas, S. Datta, J. R. Bellare, Ceramics International 25 (1999) 601.
22) A. Bozzi, T. Yuranova, J. Kiwi, J. Photochem. Photobiol. A 172 (2005) 27.
23) K. Qi, W. Daoud, J. Xin, C. Mak, W. Tang, W. Cheung, J. Mater. Chem. 16 (2006) 4567.
24) M. Uddin, F. Cesano, D. Scarano, F. Bonino, G. Agostini, G. Spoto, S. Bordiga, A. Zecchina, J. Photochem. Photobiol. A 199 (2008) 64.
25) D. Wu, M. Long, ACS Appl. Mater. Interfaces 3 (2011) 4770.
26) K. Tennakone, C. Tilakaratne, I. Kottegoda, J. Photochem. Photobiol. A 87 (1995) 177.
27) H. Chen, C. Liang, H. Huang, J. Chen, R. Vittal, C. Lin, K. Wu, K. Ho, Chem. Commun. 47 (2011) 346.
28) S. Lam, A. Soetanto, R. Amal, J. Nanopart. Res. 11 (2009) 1971.
29) R. Fatteh, A. Ismail, R. Dillert, D. Bahnemann, J. Phys. Chem. C 115 (2011) 10405.
30) K. Nakata, M. Sakai M, O. Tsuyoshi, T. Murakami, K. Takagi, A. Fujishima, Langmuir 27 (2011) 3275.
31) Y. Paz, Z. Luo, L. Rabenberg, A. Heller, J. Mat. Res. 11 (1995) 2842.
32) T. Watanabe, A. Nakajima, R. Wang R, M. Minabe, S. Koizumi, A. Fujishima, K. Hashimoto, Thin Solid Films 351 (1999) 260.
33) J. Chen, C. S. Poon, Build. Environ. 44 (2009) 1899.
34) B. Xi, L.K. Verma, J. Li, C.S. Bathia, A.J. Danner, H. Yang, H.C. Zeng, ACS Appl. Mater. Interfaces 4 (2012) 1093.
35) A. Pénard, T. Gacoin, J. Boilot, Acc. Chem. Res. 40 (2007) 895.
36) C. P. Scherer, C. G. Pantano, J. Non-Cryst. Solids 354 (2008) 645.
37) M. Machida, K. Norimoto, T. Watanabe, K. Hashimoto, A. Fujishima, J. Mater. Sci. 34 (1999) 2569.

38) N. Suzuki, X. Jiang, L. Radhakrishnan, K. Takai, K. Shimasaki, Y. Huang, N. Miyamoto, Y. Yamauchi, Bull. Chem. Soc. Jpn. 84 (2011) 812.

39) K. Inumaru, M. Yasui, T. Kasahara, K. Yamaguchi, A. Yasuda, S. Yamanaka, J. Mater. Chem. 21 (2011) 12117.

40) D. Fattakhova-Rohlfing, J. Szeifert, Q. Yu,; V. Kalousek, R. Rathouský, T. Bein, Chem. Mater. 21 (2009) 2410.

41) M. Alvaro, E. Carbonell, V. Fornés, H. García, Chem. Phys. Chem. 7 (2006) 200.

42) E. Allain, S. Besson, C. Durand, M. Moreau, T. Gacoin, J. P. Boilot, Adv. Funct. Mater. 17 (2007) 549.

43) X. Gao, I. E. Wachs, Catal. Today 51 (1999) 233.

44) Y. Zhang, C. Chen, H. Qing, R. Wu, H. Zou, Chem. Commun. 12 (2010) 2271.

45) S. Wang, Y. Shi, X. Ma, J. Gong, ACS Appl. Mater. Interfaces, 3 (2011) 2154.

46) V. Zeleňak, V. Hornebecq, S. Mornet, O. Schäf, P. Llewellyn, Chem. Mater. 18 (2006) 3184.

47) T. Kamegawa, Y. Masuda, N. Suzuki, Y. Horiuchi, H. Yamashita, Appl. Mater. Interfaces 3 (2011) 4561.

48) J. C. Hernández-Garrido, K. Yoshida, P. L. Gai, E. D. Boyes, C. H. Christensen, P. A. Midgley, Catal. Today 160 (2011) 165.

49) P. Linton, J. C. Hernandez-Garrido, P. A. Midgley, H. Wennerström, V. Alfredsson, Phys. Chem. Chem. Phys. 11 (2009) 10973.

50) E. Doren, P. Temmerman, M. Francisco, J. J. Mast, J. Nanobiotechnol. 9 (2011) 17.

51) K. Yoshida, M. Makihara, N. Tanaka, S. Ayoagi, E. Nishibori, M. Sakata, E. Boyes, P. Gai, Microsc. Microanal. 12 (2011) 264.

52) S. Li, C. Chang, C. Lin, Y. Lin, C. Chang, J. Yang, M. Chu, C. Chen, J. Am. Chem. Soc. 133 (2011) 11614.

53) M. Okuda, M. Takeguchi, Y. Zhu, A. Hashimoto, N. Ogawa, M. Tagaya, S. Chen, N. Hanagata, T. Ikoma, Surf. Interface Anal. 42 (2010) 1548.

54) S. Sueda, K. Yoshida, N. Tanaka, Ultramicroscopy 110 (2010) 1120.

55) K. J. Batenburg, S. Bals; J. Sijbers, C. Kübel, P. A. Midgley, J. C. Hernández, U. Kaiser, E. R. Encina, E. A. Coronado, G. Van Tendeloo, Ultramicroscopy 109 (2009) 730.

56) J.M. Thomas, P.A. Midgley, T.J.V. Yates, J.S. Barnard, R. Raja, I. Arslan, M. Weyland, Angew. Chem. Int. Ed. 43 (2004) 6745.

57) M. Thommes, B. Smarsly, M. Groenewolt, P.I. Ravikovitch, A.V. Neimark, Langmuir 22 (2006) 756.

58) Y. V. Lim, H. Fan, Z. Shen, C. H. Kang, Y. Feng, S. Wang, Appl. Phys. A 95 (2009) 555.

59) A. I. Kontos, I. M. Arabatzis, D. S. Tsoukleris, A. G. Kontos, M. C. Bernard, D. E. Petrakis, P. Falaras, Catal. Today 101 (2005) 275.

60) Laurie, Improvements related to the preservation of stone, U.K. Patent Office, 6-9-1923.

61) European Council Directive 1999/13/EC, 11-3-1999.

62) E. Wendler, D. D. Klemm, R. Snethlage, Proceedings of the 5th International Conference on Durability of Building Materials and Components. Brighton (UK), 1991.

63) I. J. González, G.W. Scherer, Environ. Geo. 46 (2004) 364.

64) E. Ruiz-Agudo, C. Rodriguez-Navarro, E. Sebastián-Pardo, Cryst. Growth Design 6 (2006) 1575.

65) G. Scherer, G. Wheeler, Key Engineering Materials, 391 (2009) 1.

66) I. O. Slavid, N. R. Weiss, Method for Consolidating and Protecting Calcareous Materials, United States Patent and Trademark Office, 28-10-1999.

67) A. F. Pinto, J. Delgado Rodrigues, S. Bracci, B. Sacchi, in João Mimoso, José Delgado Rodrigues (Eds.) Stone consolidation in cultural heritage, research and practice: proceedings of the international conference, Lisbon, 2008, 71.

68) G.W. Scherer, J. Non-Cryst. Solids 147&148 (1992) 363.

69) G.W. Scherer and G.E. Wheeler, in A. Moropoulou et al. (Eds), Proceedings of 4th International Symposium on the Conservation of Monuments, Rhodes, 1997, 355.

70) M. J. Mosquera, J. Pozo, L. Esquivias, T. Rivas, B. Silva, J. Non-Cryst. Solids 311 (2002) 185.

71) M. J. Mosquera, J. Pozo, L. Esquivias, J. Sol-gel Sci. Tech. 26 (2003) 1227.

72) C. Miliani, M. L. Velo-Simpson, G. W. Scherer J. Cult. Herit. 8 (2007) 1.

73) M. J. Mosquera, M. Bejarano, N. de la Rosa-Fox, L. Esquivias, Langmuir 19 (2003) 19.

74) L. Esquivias, N. de la Rosa-Fox, M. Bejarano, M. J. Mosquera, Langmuir 20 (2004) 3416.

75) C.T. Kresge, M.E. Leonowicz, W.J. Roth, J.C. Vartuli, Nature 359 (1992) 710.

76) J. S. Beck, J. C. Vartuli, W. J. Roth, M. E. Leonowicz, C. T. Kresge, K.D.Schmitt, C. T. Chu, D. H. Olson, E. W. Sheppard, S. B. McCullen, J. B. Higgins, J. L. Schenker, Journal of American Chemical Society 114 (1992) 10834.

77) P. Tanev, T. Pinnavaia, Science 267 (1995) 865.

78) A. Prado, C. Airoldi, J. Mat. Chem. 12 (2002) 3823.

79) M. J. Mosquera, D. M. de los Santos, A. Montes, L. Valdez-Castro, Langmuir 24 (2008) 2772.

80) M. J. Mosquera, A. Montes, D. M. de los Santos, Method of Strengthening Stone and Other Construction Materials, United States Patent and Trademark Office, 15-2-2007.

81) H. Schmidt, J. Non-Cryst. Solids 73 (1985) 73, 681.

82) J. D. Mackenzie, Y. Hu, J. Mater. Sci. 27 (1992) 4415.

83) J. D. Mackenzie, Y.J. Chung, Y. Hu, J. Non-Cryst. Solids 147&148 (1992) 271.

84) M. J. Mosquera, D. M. de los Santos, T. Rivas, Langmuir 26 (2010) 6737.

85) M. J. Mosquera, D. M. de los Santos, T. Rivas, P. Sanmartin, B. Silva, Journal of Nano Research 8 (2009) 1.

86) M. J. Mosquera, D. M de Los Santos, Procedimiento para hidrofugar y consolidar rocas y otros materiales de construcción, Oficina española de Patentes y Marcas, 26-02-2010.

87) J. F. Illescas; M.J. Mosquera, ACS Appl. Mat. Interfaces 4 (2012) 4259.

88) M.J. Mosquera, J. F. Illescas, Producto consolidante, hidrofugante y repelente de manchas para rocas carbonatadas y otros materiales de construcción, Oficina Española de Patentes y Marcas, 21-3-2011.
89) J. F. Illescas, M. J. Mosquera, J. Phys Chem. C 115 (2011) 14624.
90) M. J. Mosquera, J. F. Illescas, D. Facio, Producto para protección y restauración de rocas y otros materiales de construcción, Oficina Española de Patentes y Marcas. 16-02-2012.
91) P. Baglioni, L. Cassar (Eds.), Proceedings of international RILEM symposium on photocatalysis, environment and construction materials ; Florence, 2007, 315.
92) A.J. Fonseca, F. Pina, M. F. Macedo, N. Leal, A. Romanowska-Deskins, L. Laiz, A. Gómez-Bolea, C. Saiz-Jimenez, Int. Biodet. Biodegr. 64 (2010) 388.
93) M. V. Diamanti, M. Ormellese, M. Pedeferri, Cement Concrete Res. 38 (2008) 1349.
94) M. Lackhoff, X. Prieto, N. Nestle, F. Dehn, R. Niessner, Appl. Cat. B 43 (2003) 205.
95) I. Poulios, P. Spathis, A. Grigoriadou, K. Delidou, P. Tsoumparis, J. Environ. Sci. Health A 34 (1999) 1455.
96) D. Pinna, A.M. Lega, V. Mazzotti, Arkos 21 (2009) 18.
97) K. Rao, M. Subrahmanyam, P. Boule, Apply. Catal. B Environ. 49 (2004) 239.
98) E. Quagliarini, F. Bondioli, G. Goffredo, A. Licciuli, P. Munafò, J. Cult. Herit. 13 (2012) 204.
99) E. Quagliarini, F. Bondioli, G. Goffredo, A. Licciuli, P. Munafò, J. Cult. Herit. 2012, doi: 10.1016/j.culher.2012.02.006
100) G. Potenza, A. Licciulli, D. Diso, S. Franza, A. Calia, M. Lettieri, G. Ciccarella, in P. Baglioni, L. Cassar (Eds.), Proceedings of international RILEM symposium on photocatalysis, environment and construction materials ; Florence, 2007, 315.
101) L. Luvidi, G. Laguzzi, F. Gallese, A.M. Mecchi, G. Sidoti, in A. Ferrari (Ed.), Proceedings of 4th International Congress on Science and Technology for

the Safeguard of Cultural Heritage in the Mediterrean Basin, Vol. II, Cairo, 2010, 495.

102) A. Liciulli, A. Calia, M. Lettieri, D. Diso, M. Masieri, S. Franza, R. Amadelli, G. Casarano, J. Sol-gel. Sci. Technol 60 (2011) 437.

103) E. Quagliarini, F. Bondioli, G. Goffredo, C. Cordoni, P. Munafò, Constr. Build. Mater. 37 (2012) 51.

104) M. Noorjahan, M. P. Reddy, V. D. Kumari, B. Lavédrine, P. Boule, M. Subrahmanyam J. Photochem. Photobiol. A 156 (2003) 179.

105) M. F. La Russa, S. A. Ruffolo, N. Rovella, C. M. Belfiore, A. M. Palermo, M. T. Guzzi; G. M. Crisci, Prog. Org. Coat. 74 (2012) 186.

106) A. Rachel, M. M. Subrahmanyam, P. Boule, Apply. Catal. B Environ. 37 (2002) 301.

107) H. Yang, C. Li, H. Gu, T. Fang, J. Colloid Interf. Sci. 236 (2001) 69.

108) P. O. Vasiliev, B. Faure, J. B. S. Ng, L. Bergström, J. Colloid. Interf. Sci. 319 (2008) 144.

109) P. Mikulasek, R. J. Wakeman, J. Q. Marchant, Chem. Eng. J. 67 (1997) 97.

110) X. Zhang, B. Xia, H. Ye, Y. Zhang, B. Xiao, L. Yan, H. Lv, B. Jiang, J. Mater. Chem. 22 (2012) 13132.

111) J. Widegren, L. Bergström, J. Am. Ceram. Soc. 85 (2002) 523.

112) M. Kosmulski, P. Prochniak, J. B. Rosenholm, J. Phys. Chem C. 113 (2009) 12806.

113) K. Suttiponparnit, J. Jiang, M. Sahu, S. Suvachittanont, T. Charinpanitkul, P. Biswas, Nanoscale Res. Lett. 6 (2011) 1.

114) N. T. Boncagni, J. M. Otaegui, E. Warner, T. Curran, J. Ren, M. M. F. Cortalezzi, Environ. Sci. Tecnhol. 43 (2009) 7699.

115) E. Beyers, P. Cool, E. Vansant, J. Phys Chem. B 109 (2005) 10081.

116) D. Siwinska, A. Kołodziejczak-Radzimska, A. Krysztafkiewicz, T. Jesionowski, Appl. Surf. Sci. 255 (2009) 7337.

117) B. Erdem, E. D. Sudol, V. L. Dimonie, M. S. El-Aasser, J. Polym. Sci. Polym. Chem. 38 (2000) 4419.

118) C. Yu, H. Chu, Y. Wan, D. Zhao, J. Mater. Chem. 20 (2010) 4705.

119) M. J. Mosquera, D. M. de los Santos, L. Valdez-Castro, L. Esquivias, J. Non-Cryst. Solids 354 (2008) 645.
120) H. Shibata, T. Ohkubo, H. Kohno, P. Rangsunvigit, H. Sakai, M. Abe, J. Photochem. Photobiol. A 181 (2006) 357.
121) A. Mirabedini, S. M. Mirabedini, A. A. Babalou, S. Pazokifard, Prog. Org. Coat. 72 (2011) 453.
122) M .Kruk, M. Jaroniec, Chem. Mater. 13 (2001) 3169.
123) E. P. Barret, L. G. Joyner, P. P. Halenda, J. Am. Chem. Soc. 73 (1951) 373.
124) M. Thommes, B. Smarsly, M. Groenewolt, P.I. Ravikovitch, A.V. Neimark, Langmuir 22 (2006) 756.
125) Y. V. Lim, H. Fan, Z. Shen, C. H. Kang, Y. Feng, S. Wang, Appl. Phys. A 95 (2009) 555.
126) Y. Yamauchi, F. Takeuchi, S. Todoroki, Y. Sakka, S. Inoue, Chem. Lett. 37 (2008) 72.
127) Z. Demjén, B. Pubánsky, E. Foldes, J. Nagy, J. Colloid. Interface Sci. 190 (1997) 427.
128) M. Sekine, S. Katayama, M. Mitomo, J. Non-Cryst. Solids 124 (1991) 199.
129) C. H. Weigel, R. Kellner, Fresen Z. Anal. Chem. 335 (1989) 663.
130) P. Innocenzi, J. Non-Cryst. Solids 316 (2003) 309.
131) S. W. Verbruggen, K. Masschaele, E. Moortgat, T. E. Korany, B. Hauchecorne, J. A. Martens, S. Lenaerts, Catal. Sci. Technol. 2 (2012) 2311.
132) F. Babonneau, Polyhedron 13 (1994) 1123.
133) P.T. Tanev, T. Pinnavaia, J. Chem. Mater. 8 (1996) 2068.
134) A. P. Ferreira Pinto, J. Delgado Rodrigues, J. Cultural Heritage 9 (2008) 38.
135) G. Wheeler, Alkoxysilanes and the consolidation of stone, The Getty Conservation Institute: Los Angeles CA, 2005.
136) A. Sdiri, T. Higashi, T. Hatta, F. Jamoussi, N. Tase, Environ. Earth Sci. 61 (2010) 1275.
137) M. Drdácký, J. Lesák, S. Rescic, Z. Slížková; P. Tiano, J. Valach, Mater. Struct. 45 (2012) 505.

138) E. Zendri, G. Biscontin, I. Nardini, S. Riato, Const. Build. Mat. 21 (2007) 1098.

139) A. Mills, J. Wang, J. Photochem. Photobiol. A, Chem. 127 (1999) 123.

140) P. Chou, Q. Zhang, B. Russo, G. E. Fryxell, G. Cao, J. Phys. Chem. C 111 (2007) 6296.

141) Z. Zhang, C. Wang, R. Zakaria, J. Ying, J. Phys. Chem. B 102 (1998) 10871.

142) T. Carneiro, A. R. Almeida, J. A. Moulijn, G. Mul, Phys. Chem. Chem. Phys. 12 (2010) 2744.

143) Y. Li, Z. Liu, J. Am. Chem. Soc. 133 (2011) 15743.

144) C.Rodríguez-Navarro, E. Doehne, E. Sebastián, Cement Concrete Res. 30 (2000) 1527.

8. Annexes

Patent

Producto autolimpiante y consolidante para rocas y otros materiales de construcción

Oficina Española de Patentes y Marcas, 24/6/2011

UNIVERSIDAD DE CÁDIZ
BENITO PÉREZ GALDÓS, S/N
11002 CÁDIZ
CADIZ

Madrid, a 15 de noviembre de 2011

Continuación de Procedimiento de la solicitud de Patente Nacional 201100741

La Oficina Española de Patentes y Marcas (OEPM) le notifica, en relación con la tramitación de su solicitud de patente 201100741, que dicha solicitud ha superado el examen previsto en los artículos 31 de la Ley 11/1986, de Patentes y 17 de su Reglamento de Ejecución (RD 2245/1986).

Esta notificación se publicará en el Boletín Oficial de la Propiedad Industrial (BOPI) en fecha 25/11/2011. El BOPI puede consultarse en la Web de la OEPM.

Atentamente,

A. Amaro

Fdo.: Alicia Amaro Roldan
Técnico Superior Examinador

UCA Universidad de Cádiz

Vicerrectorado de Investigación y Transferencia
OTRI

C/ Benito Pérez Galdós, S/N
11002 Cádiz.
Tel. 956015171. Fax. 956015746
http://www.uca.es/otri/
otri@uca.es

El Vicerrector de Investigación y Transferencia de la Universidad de Cádiz,
D. Manuel Bethencourt Núñez

INFORMA: De la veracidad de los datos que aparecen a continuación, relativos a la solicitud de Patente de Invención "PRODUCTO AUTO-LIMPIANTE Y CONSOLIDANTE PARA ROCAS Y OTROS MATERIALES DE CONSTRUCCIÓN", cuya titular es la Universidad de Cádiz.

INVENTORES: **María Jesús Mosquera Díaz y Luis Miguel Faria Soares da Silva.**

TÍTULO: **Producto auto-limpiante y consolidante para rocas y otros materiales de construcción.**

Nº DE SOLICITUD: **P201100741**

FECHA DE SOLICITUD: **24/06/2011**

DESCRIPCIÓN BREVE DE SU CONTENIDO Y OBJETIVOS

La invención se refiere a un material composite constituido por partículas de titanio integradas en un gel de sílice, que posee actividad fotocatalítica. Este nuevo material origina un efecto auto-limpiante sobre sustratos pétreos y otros materiales de construcción de naturaleza porosa.

En concreto, se trata de un producto capaz de: (1) dotar a la superficie tratada de capacidad auto-limpiante por simple exposición a la luz solar. (2) mejorar su resistencia mecánica superficial (3) formar un recubrimiento cohesionado capaz de adherirse al sustrato pétreo tratado.

PAIS DE PRIORIDAD: **España**

Nº DE PATENTE: **Aún no publicada**

FECHA DE CONCESIÓN: **Aún en trámite**

ENTIDAD TITULAR: **Universidad de Cádiz.**

PAISES A LOS QUE SE HA EXTENDIDO:

EMPRESA(S) QUE LA ESTÁ(N) EXPLOTANDO o en las que existe un contrato de cesión o licencia: **Acuerdo de opción de licencia con empresa SILICALIA, S.L.**

Y para que así conste y a petición del interesado, firmo la presente en Cádiz a 14 de marzo de 2012.

Fdo. Manuel Bethencourt Núñez

PRODUCTO AUTO-LIMPIANTE Y CONSOLIDANTE PARA ROCAS Y OTROS MATERIALES DE CONSTRUCCIÓN

SECTOR DE LA TÉCNICA.

En la actualidad, la mayor parte de edificios en los núcleos urbanos exhiben un alto grado de suciedad originado por contaminación ambiental, residuos orgánicos de aves, pintadas, grafitis, etc. La limpieza de estos edificios y más concretamente, de sus zonas altas y de difícil acceso es complicada y requiere la contratación de personal y maquinaria especializada para este fin. Por tanto, la protección de los materiales de construcción mediante aplicación de productos con capacidad auto-limpiante supone un gran avance para la conservación y mantenimiento de los edificios y resto de los elementos arquitectónicos.

El producto, objeto de esta patente, es capaz de dotar a las rocas y otros materiales de construcción de propiedades auto-limpiantes por su simple exposición a la luz solar. Además, es capaz de incrementar la resistencia mecánica del sustrato pétreo tratado. Finalmente, mencionar que genera un recubrimiento hidrófobo sobre la roca que impide la penetración del agua líquida, principal vehículo de los agentes de deterioro.

ESTADO DE LA TÉCNICA ANTERIOR A LA FECHA DE PRESENTACIÓN.

En 1972, Honda y Fujishima descubrieron el efecto como fotocatalizador del dióxido de titanio (Fujishima, A y Honda, K Nature, 238, 37, 1972). Cuando el fotocatalizador es irradiado con fotones, su absorción promueve un salto de un electrón de la banda de valencia a la de conducción, generando pares electrón-hueco de acuerdo con la siguiente ecuación:

$TiO_2 + hv \rightleftharpoons e^- + h^+$ (ecuación 1)

En contacto con agua, se generan radicales libres:

$$h^+ + H_2O_{ads} \rightleftharpoons H^+_{ads} + OH^{\bullet}_{ads}$$ (ecuación 2)

$$h^+ + OH^-_{ads} \rightleftharpoons OH^{\bullet}_{ads}$$ (ecuación 3)

Los radicales libres formados son capaces de oxidar la materia orgánica, originando agua y dióxido de carbono como residuos de la reacción.

Como consecuencia de su eficacia como fotocatalizador y su reducido coste, el dióxido de titanio ha sido utilizado con múltiples aplicaciones, que incluyen la purificación del aire y del agua, como bactericida y como agente autolimpiante.

La aplicación de dióxido de titanio sobre los materiales de construcción se inicia a comienzos de los años 90. La versatilidad del titanio en cuanto a su actividad fotocatalítica combinada con su posible aplicación como material estructural en los edificios ha generado su rápida aplicación sobre sustratos de diversa naturaleza, incluyendo vidrios, morteros de cemento, azulejos y materiales de PVC. (Chen J y Poon, CS Build. & Environ. 44, 1899, 2009).

El dióxido de titanio se puede obtener a partir de alcóxidos de titanio mediante un simple proceso sol-gel que finaliza con la sinterización del recubrimiento de titanio sobre el sustrato por un proceso de calcinación. Esta última etapa de calentamiento a elevadas temperaturas (superior a 450ºC) promueve el crecimiento de cristales de rutilo y anatasa que poseen actividad fotocatalítica. Además, favorece la adhesión del gel al sustrato (Houmard M et al Surf. Sci. 602, 3364, 2008).

No obstante, el fotocalizador de TiO_2 más popular es, sin lugar a dudas, el producto comercial Aeroxide TiO_2 P25, comercializado por Evonik (Corma A et al. Phys. Chem. Chem. Phys. 10, 769, 2008). El producto P25 está constituido por partículas coloidales de dióxido de titanio con un diámetro de poro en torno a 21 nm y una superficie específica de 50 m^2/g. Después de la aplicación de

P25 sobre un sustrato se suele someter a calcinación para lograr la sinterización de las partículas y en consecuencia, la formación de enlaces covalentes que originan un recubrimiento estable desde el punto de vista térmico y mecánico.

En lo que concierne a la aplicación de dióxido de titanio sobre piedra, existen pocos trabajos en la literatura en los que no se han alcanzado resultados excesivamente satisfactorios. En concreto, Polious I et al. (J. Environ. Sci. Health, 34, 1455, 1999) han utilizado partículas P25 disueltas en agua para evitar procesos de sulfatación en mármoles y lograr un efecto antibacteriano sobre estos materiales pétreos. El gran inconveniente de este procedimiento fue la formación de un recubrimiento completamente fracturado. Por otra parte, Rachel A et al. (Catalysis Com. 3, 165, 2002) han aplicado P25 sobre lavas volcánicas de elevada porosidad como tratamiento de purificación de aguas. Como informaron estos autores, la escasa adherencia del titanio a las rocas produjo una significativa reducción de su efectividad con el tiempo. Finalmente, Romero-Sánchez MD et al (*Book of Abstracts 5th Eur. Conference on Solar Chem. & Photo.: Environ. Apply. (SPEA 5)* Palermo, Italy, 2008), presentaron, recientemente, resultados preliminares sobre la eficacia auto-limpiante de las partículas de titanio coloidal sobre dos tipos de roca. No obstante, en este trabajo no se ofrecieron datos sobre forma de aplicación del producto, su adherencia a la roca y efectos negativos del tratamiento, como formación de fracturas, cambio de color de la roca…

En los últimos años, Nuestro grupo de investigación ha diseñado una estrategia para evitar fracturas en los geles de silicio que ha sido objeto de una patente (Nº P200501887/2) y de una reciente publicación (Mosquera MJ, de los Santos Valdez-Castro, L, Montes, A, Langmuir, 24, 2772, 2008). Esta síntesis se basa en la adición de un surfactante que actúa como plantilla de los poros del material, creando un nanomaterial con tamaño de poro uniforme. Esta ruta permite obtener geles monolíticos debido a dos razones:

(1) el surfactante aumenta el radio de poro del gel, reduciendo la presión capilar responsable de la fractura del material.

(2) La reducción de la tensión superficial originada por el surfactante también reduce el valor de la presión capilar.

Posteriormente, nuestro equipo investigador ha modificado este proceso de síntesis con objeto de obtener otros productos con nuevas aplicaciones. En concreto, hemos diseñado un producto consolidante/hidrofugante por adición de un polidimetilsiloxano (PDMS) al precursor polimérico de silicio (TEOS) en presencia de n-octilamina. Este producto ha sido también objeto de una patente de invención (Nº P200702976). Además, hemos desarrollado un producto específicamente diseñado para rocas carbonatadas, capaz de incrementar la resistencia mecánica de la roca, hidrofugar y aumentar su resistencia al manchado (Nº solicitud de patente P201100339).

De acuerdo con los antecedentes expuestos, el objetivo de nuestro trabajo, que ha originado la presente patente de invención, se centró en el desarrollo de un nanomaterial compuesto silicio-titanio con actividad fotocatalítica, capaz de adherirse al sustrato pétreo y formar un recubrimiento libre de fracturas, ejerciendo además, un efecto auto-limpiante y consolidante sobre la roca tratada.

Partiendo de nuestros conocimientos previos, la síntesis se realizó en presencia de n-octilamina para evitar la formación de fracturas en el recubrimiento.

La adhesión al sustrato se consiguió mediante la integración de partículas coloidales de dióxido de titanio en una red de sílice. De acuerdo con la literatura y nuestro propio conocimiento, para lograr la adherencia y estabilidad del recubrimiento de partículas de titanio resulta imprescindible realizar un proceso de sinterización por calcinación. En nuestro caso, el calentamiento a altas temperaturas debe ser evitado porque muchas rocas son inestables a

dichas temperaturas y además no puede realizarse cuando el producto tiene que ser aplicado in situ en los propios edificios.

EXPLICACIÓN DE LA INVENCIÓN.

La presente invención se refiere a un material composite constituido por partículas de titanio integradas en un gel de sílice, que posee actividad fotocatalítica. Este nuevo material origina un efecto auto-limpiante, consolidante sobre sustratos pétreos y otros materiales de construcción de naturaleza porosa.

En concreto, se trata de un producto capaz de: (1) dotar a la superficie tratada de capacidad auto-limpiante por simple exposición a la luz solar. (2) mejorar la resistencia mecánica superficial de la roca tratada y (3) formar un recubrimiento cohesionado capaz de adherirse al sustrato pétreo tratado.

El producto que se puede aplicar sobre el sustrato pétreo por pulverización, brocha, rodillo, inmersión, ascenso capilar u otro método es capaz de polimerizar espontáneamente en su superficie y sus poros, formando un gel compuesto silicio-titanio con capacidad auto-limpiante.

El sol de partida contiene un oligómero de silicio, partículas coloidales de titanio y una amina primaria en una proporción, respecto al precursor del silicio, superior a su concentración micelar crítica (cmc).

Esta síntesis presenta varios aspectos innovadores respecto a nuestras patentes anteriores. En primer lugar, se desarrolla un material compuesto silicio-titanio a partir de un precursor polimérico de silicio y partículas de titanio coloidal. En segundo lugar, la concentración de la amina se ha aumentado diez veces con respecto a la concentración propuesta en patentes anteriores. Dos razones han originado este aumento:

(1) La inestabilidad de las partículas de titanio en el sol de partida obliga a acelerar el proceso de gelificación, incrementando la cantidad de n-octilamina, que actúa como catalizador en la transición sol-gel.

(2) En trabajos anteriores, el surfactante se añadía a una concentración muy inferior (por debajo de su cmc) porque se producía una rápida evaporación del etanol presente en el sol, incrementándose, de forma significativa, la concentración del surfactante. En este caso, la evaporación del sol es mínima porque no se han añadido disolventes, requiriéndose, por tanto, una concentración superior de n-octilamina para lograr una reducción de la presión capilar hasta un valor que evite la formación de fracturas.

En tercer lugar, es importante resaltar que el material objeto de esta patente no contiene ningún disolventes orgánico volátil (VOCs). Por tanto, se evita la contaminación ambiental que produce la evaporación de estos compuestos durante la fase de aplicación en el edificio pétreo.

DESCRIPCIÓN DE LAS FIGURAS

FIGURA 1.- Esquema de las síntesis realizadas en el laboratorio.

FIGURA 2.- Perfiles de difracción de Rayos X de los xerogeles objeto de estudio.

FIGURA 3.- Espectros FTIR de los xerogeles objeto de estudio.

FIGURA 4.- Isotermas de adsorción-desorción de nitrógeno de los xerogeles objeto de estudio.

FIGURA 5.- Distribución de diámetro de poros, según modelo BJH, para los geles evaluados.

FIGURA 6.- Imágenes de Microscopía Electrónica de Barrido de las películas objeto de estudio.

FIGURA 7.- Imágenes de Microscopía Electrónica de Barrido de la superficie pétrea antes y después de los tratamientos.

FIGURA 8.- Imágenes de Microscopía Electrónica de Barrido de la superficie pétrea después del test de adhesión. La parte izquierda de cada superficie corresponde a la parte no ensayada y la parte derecha a la superficie donde se realizó el test. Los espectros EDX son incluidos en el lateral de cada una de las superficies evaluadas.

FIGURA 9.- Valores medios de resistencia a la perforación de la roca sin tratar y después de la aplicación de los productos seleccionados, en función de la profundidad de penetración.

FIGURA 10.- Evolución de la variación de color de las manchas de azul de metileno sobre superficies pétreas tratadas en función del tiempo de exposición a la luz ultraviaoleta.

MODO DE REALIZACIÓN DE LA INVENCIÓN.

La síntesis del producto, objeto de la presente invención, incluye las siguientes etapas: En primer lugar, el oligómero de silicio se mezcla con la amina primaria, añadiéndose a continuación las partículas coloidales de dióxido titanio. Todo el proceso de mezcla se realiza mediante agitación ultrasónica, manteniéndose dicha agitación durante diez minutos. El oligómero de silicio puede ser TES40 WN (Wacker) y la amina utilizada en la síntesis, n-octilamina. Respecto a las concentraciones requeridas de cada componente en el sol de partida, mencionar que si el precursor polimérico es TES 40 WN de Wacker y la amina primaria n-octilamina, la concentración de surfactante en el sol inicial debe ser 0.22 M o superior, siendo la concentración micelar crítica de dicho surfactante en torno a 0.0065 M. Para concentraciones inferiores de n-octilamina, se produce la agregación de P25 antes que la transición sol-gel ocurra.

En el caso del dióxido de titanio, si las partículas son Aeroxide P25 de Evonik, su proporción en el sol debe ser igual o inferior al 2% p/v. Para concentraciones superiores se produce un incremento significativo de viscosidad que impide la penetración del sol en la estructura porosa de la roca.

La siguiente etapa del proceso, es la impregnación del material a tratar con el sol preparado. El producto puede penetrar en el sustrato por impregnación de la superficie mediante pulverización o bien, por aplicación mediante un cepillo o brocha. En el caso de objetos de tamaño reducido, por inmersión en un tanque que contenga el sol, o bien por ascenso capilar mediante el contacto superficial del producto y la cara inferior del objeto. Tras la impregnación, se produce la polimerización por condensación del oligómero de silicio, originándose un composite silicio-titanio.

A continuación, y con objeto de ilustrar con más detalle, las ventajas del producto objeto de patente frente a otros materiales, se describen resultados obtenidos en un nuestro laboratorio de investigación. En concreto, en el ejemplo 1 se describe el procedimiento de síntesis y se realiza la caracterización de los materiales sintetizados, en los que se varió la proporción de partículas coloidales de titanio respecto al sol entre 0 y 2% p/v.

En el ejemplo 2, los mismos materiales son aplicados sobre una roca caliza, realizándose una evaluación de su capacidad de adherencia al sustrato y su eficacia como consolidante, auto-limpiante e hidrofugante.

Con objeto de establecer comparaciones con otros productos, se sintetizó otra serie de geles compuestos silicio/titanio, utilizando ácido fosfórico como catalizador. Además, se prepararon dispersiones en agua de las partículas de titanio. En ambos casos, se utilizaron las mismas proporciones de titanio (0, 0.5, 1 y 2% p/v)

EJEMPLO 1

Se mezcló TES40 WN (en adelante “TES40”), fabricado por Wacker y constituido por oligómeros de silicio con la amina primaria, n-octilamina. La proporción de octilamina respecto a TES40 fue 0.37% (v/v). A continuación, se añadieron las partículas de dióxido de titanio coloidal Aeroxide TiO_2 P25, comercializadas por Evonik (en adelante “P25”). Su diámetro medio de partícula es 21 nm y su superficie específica es 50±15 m^2/g. La proporción de P25 respecto a TES40 se varió de acuerdo con las siguientes proporciones: 0, 0.5, 1 y 2% (p/v). Los cuatro soles preparados fueron sometidos a agitación por ultrasonidos (potencia 125 W/cm^3) durante 10 minutos. Estos productos fueron denominados UCATiO seguido por un número que indica la proporción de titanio en el sol.

Con objeto de establecer comparaciones con otros materiales con propiedades auto-limpiantes, se prepararon otras dos series de soles en las que se varió la concentración de titanio en la misma proporción que en la serie UCATiO.

En concreto, en la primera serie se prepararon dispersiones de P25 en agua, variando la proporción de titanio entre 0 y 2% (p/v). La mezcla se realizó por simple agitación manual.

Por último, se sintetizó otra serie de soles que contienen TES40 y ácido fosfórico como catalizador en una relación del catalizador respecto al sol de 0,18% (v/v). La proporción de P25 se varió en la misma proporción que en síntesis anteriores y la mezcla fue sometida a agitación por ultrasonidos. Estos productos se denominaron UCATiP.

En La Figura 1 se incluye un esquema resumiendo las síntesis realizadas en nuestro laboratorio.

Con objeto de comprobar si la viscosidad de los soles sintetizados es adecuada para su aplicación sobre rocas, se realizó su medida utilizando un viscosímetro rotacional de Brookfield (modelo DV-II+ con adaptador UL/Y). La temperatura

del experimento fue 25ºC. Además, se midió la viscosidad de las diferentes dispersiones de P25 en etanol. En la Tabla 1 se presentan los valores de viscosidad obtenidos.

Según la literatura (Fujishima A et al J. Photochem. Photobiol. C: Photchem. Rev. 1, 1, 2000), las dispersiones de partículas de titanio coloidales en agua presentan un comportamiento pseudo-plástico. Sin embargo, las tres dispersiones de P25 preparadas en nuestro laboratorio muestran una conducta newtoniana, como consecuencia de su baja concentración en titanio (entre 0 y 2% p/v). No obstante, es importante mencionar que las tres dispersiones de P25 evaluadas experimentaron agregación y posterior floculación de las partículas coloidales después de 1 o 2 horas, confirmando la inestabilidad de las dispersiones de partículas P25.

Tabla 1

Sample	Viscosity (mPa·s)	S_{total} (m^2/g)	V_{pore} (cm^3/g)	Pore size (nm)
P25-0.5	2.70			
P25-1	2.73	59	0.39	28.0
P25-2	2.75			
UCATIP-0	5.25	267	0.22	3.8
UCATiP-0.5	5.32	220	0.23	3.8
UCATiP-1	5.45	259	0.23	3.8
UCATiP-2	5.50	249	0.18	3.8
UCATiO-0	5.30	231	0.39	6.3
UCATiO-0.5	5.54	255	0.31	7.6
UCATiO-1	5.68	180	0.69	13.4

UCATiO-2	5.82	220	0.59	13.0

Respecto a los soles UCATiO y UCATiP, ambas series mostraron una conducta newtoniana en el rango evaluado. Por tanto, los valores de viscosidad fueron, en todos los casos, calculados como pendiente de la curva esfuerzo cortante frente al gradiente de velocidad. En las dispersiones P25 se observó un ligero incremento en el valor de viscosidad según aumenta la concentración de partículas P25. En las dos series de soles silicio-titanio, se produjo un incremento lineal de viscosidad al aumentar la proporción de partículas en el sol. No obstante, los valores de viscosidad, incluso para concentraciones de 2%p/v, no superaron los valores obtenidos para típicos consolidantes comerciales (2-6 mPa.s). Este hecho sugiere que todos los soles sintetizados en este estudio penetran, de forma similar a los productos comerciales, en la estructura porosa de las rocas tratadas. A este respecto mencionar que no se evaluaron soles con mayor proporción titanio/silicio, observándose un aumento significativo de la viscosidad del sol que impide su penetración en la estructura porosa de la roca. Como ejemplo, mencionar que la viscosidad de un sol con 3%p/v de P25 presenta una viscosidad de 11 mPa·s y la viscosidad de un sol con 4%p/v de las mismas partículas asciende a 14 mPa·s.

A continuación, todos los soles preparados en el laboratorio se depositaron como una película, mediante una pipeta pasteur, sobre placas Petri de plástico. La gelificación, que ocurrió en un tiempo aproximado de 24 horas, originó, en todos los casos, geles homogéneos. La formación de geles compuestos silicio-titanio homogéneos confirma que las partículas de dióxido de titanio se mantienen estables en el sol de TES40 durante el tiempo que dura el proceso de transición sol-gel. Nosotros explicamos esta estabilidad como una consecuencia de un fenómeno de repulsión electrostática entre las partículas coloidales. La adición de un catalizador ácido (ácido fosfórico) en la serie UCATiP o de un catalizador básico (n-octilamina) en la serie UCATiO origina un cambio en el pH de los soles hacia valores alejados del punto isoeléctrico de

las partículas P25 (6.5 en agua). Por esta razón, se producen repulsiones electrostáticas entre partículas que evitan su floculación. En un trabajo previo, Kosmulski M et al. (J. Phys. Chem. C, 113, 12807, 2009) estabilizaron partículas P25 en diferentes disolventes orgánicos por adición de un ácido (ácido fosfórico) o de una base (trietilamina).

Los geles se secaron en condiciones de laboratorio (20ºC y 60% de humedad), realizándose su caracterización mediante los ensayos descritos en los párrafos siguientes.

La presencia de dióxido de titanio cristalino en los xerogeles, responsable de la actividad fotocatalítica, se determinó mediante difracción de rayos X (XRD), utilizando un difractómetro Bruker D8 advance. Los perfiles de difracción obtenidos (Figura 2) muestran la presencia de silicio amorfo sin estructura ordenada y de titanio cristalino en forma anatasa (Bickey R et al., J. Solid State Chem., 92, 178, 1991). Como cabría esperar, la intensidad de los picos de anatasa se incrementa, para las dos series de geles evaluadas, al aumentar el porcentaje de partículas de titanio.

Para identificar los enlaces presentes en los geles, se realizaron ensayos de Espectroscopía de Infrarojo por transformadas de Fourier (FTIR), mediante un equipo Vertex 70 de Bruker en modo reflectancia total atenuada (ATR). Los espectros se muestran en la Figura 3. Con objeto de evaluar la presencia de octilamina residual en los geles UCATiO, se obtuvieron FTIR espectros a dos intervalos de tiempo diferente después de la síntesis: 1 mes (t1) y 8 meses (t2). Todos los espectros obtenidos presentan las bandas características de los geles de silicio. En concreto, se identifican los enlaces Si-O-Si, localizados a 800 y 1080 cm^{-1} y la banda típica de Si-OH (960 cm^{-1}). Además, se identifica una banda ancha (3400 cm^{-1}) que corresponde a la interacción, por puentes de hidrógeno, entre grupos silanoles y agua molecular. Finalmente, aparece un pico a 1300 cm^{-1} que puede ser asociado a la vibración de CH_2 (Fidalgo A & Ilharco L M, J. non-Cryst. Solids, 347, 128, 2004). La presencia de grupos CH_2 en las dos series de geles evaluadas, se explica por la presencia de grupos

etoxi, procedentes del oligómero de silicio sin hidrolizar. La mayor intensidad de este pico en los geles de octilamina podría explicarse por la presencia de CH_2 de la octilamina en esta serie de geles. Finalmente, mencionar que la intensidad de las bandas Si-O-Si, significativamente mayor en los geles de octilamina, pone de manifiesto un mayor grado de gelificación en estos materiales que en los que contienen ácido fosfórico. Las imágenes de Microscopía de Barrido comentadas en un párrafo posterior constatan esta hipótesis

Por otra parte, mencionar que en los espectros de UCATiO, obtenidos un mes después de la síntesis, se aprecian tres picos asociados a la presencia de octilamina. En concreto, 1400 cm^{-1} correspondiente al enlace C-N, 2800 y 1440 cm^{-1} asociados a la vibración del enlace C-H (Mosquera MJ et al. Langmuir, 26, 6737, 2008). Después de 8 meses, estos picos desaparecen, prácticamente, en todos los espectros obtenidos. Este hecho constata que la n-octilamina se ha eliminado por simple exposición de los geles a las condiciones de laboratorio.

Respecto a los enlaces Si-O-Ti que podrían aparecen en los materiales como consecuencia de un proceso de co-condensación entre el gel de sílice y las partículas de dióxido de titanio, mencionar que dicho pico, que debería situarse a 930 cm^{-1}, no puede ser visible en el espectro por un posible solapamiento con la banda correspondientes al enlace Si-OH, localizada a la misma longitud de onda (Tellez L et al. J. Mater. Sci. 38, 1773, 2003).

Las propiedades texturales de los geles se evaluaron mediante fisisorción de nitrógeno, utilizando un aparato Autosorb IQ de Quantacrome Instruments. En la Figura 4 se muestran las isotermas de adsorción-desorción y en la Figura 5, las distribuciones de diámetro de poro obtenidas, utilizando el modelo BJH. Los datos de superficie específica, volumen poroso y diámetro de poro se muestran en la Tabla 1. Con objeto de establecer una discusión sobre el efecto de las partículas de P25 en las propiedades texturales de los geles, se realizó el ensayo de fisisorción de nitrógeno sobre el producto comercial P25,

obteniéndose una isoterma tipo IV con histéresis H1, típica de un material formado por agregación de partículas coloidales (diámetro de poro de 28 nm).

La adición de partículas P25 a los geles de silicio produce una reducción significativa de su diámetro de poro respecto al que posee P25, como consecuencia de la integración de las partículas en el gel sílice. En el caso de los geles UCATiP, el volumen poroso disminuye mientras los geles UCATiO aumentan su volumen poroso como consecuencia de la acción de la n-octilamina, como se comenta en el párrafo siguiente.

Respecto a la estructura porosa de estos materiales, mencionar que los geles que contienen ácido fosfórico (UCATiP) presentan isotermas tipo I, correspondiente a materiales microporosos, con una ligera histéresis, característica de una isoterma tipo IV (material mesoporoso). Según se aprecia en la Figura 5, estos materiales muestran una distribución de poros localizada en el límite entre zona micro- y mesoporosa. Todos los geles UCATiO muestran isotermas tipo IV, típicas de materiales porosos según la clasificación IUPAC, exhibiendo una histéresis tipo H1, caracterizada por ramas de adsorción y de desorción prácticamente verticales y paralelas entre sí. En general, este tipo de histéresis es asociada a materiales formados por partículas esféricas, con una distribución de poro uniforme y elevada conectividad entre poros (Kruk, M & Jaroniec M, Chem. Mater., 13, 3169, 2001).

Respecto al volumen poroso, mencionar que es inferior, en toda la serie UCATiP, a los volúmenes obtenidos para los geles de octilamina, confirmando el papel desempeñado por este surfactante en la formación de la red porosa del gel. Además, la octilamina origina un incremento de tamaño de poro respecto a los geles que no contienen este surfactante.

La inclusión de P25 en los geles UCATiP no produjo diferencias significativas, respecto al gel sin partículas, en su volumen y distribución de poros mientras en los geles UCATiO, se aprecia un incremento en su volumen poroso y su diámetro de poro, según se aumenta la proporción de dióxido de titanio coloidal

en los geles correspondientes a esta serie, no observándose diferencias entre los dos geles con proporciones superiores de P25 (1 y 2%) de titanio coloidal. Estos resultados nos permiten constatar que la n-octilamina genera poros con un diámetro en torno a 6 nm, que se duplica (13 nm) cuando las partículas P25, que poseen un diámetro de 21 nm, se integran en la estructura del gel. La forma de la histéresis de las isotermas, tipo H1, para toda la serie, pone de manifiesto la formación de un gel de sílice ramificado y formado por una red de párticulas en el que se integran, de forma homogénea, las partículas de dióxido de titanio.

La Figura 6 muestra imágenes de Microscopía electrónica de Barrido de las películas de los geles objeto de estudio, obtenidas mediante un Microscopio Quanta 200 de JEOL. A la magnificación evaluada, se aprecian significativas diferencias en la morfología de las dos series de geles sintetizados. En concreto, los geles de octilamina forman una película continua y homogénea mientras los geles de ácido fosfórico forman una especie de agregado particular en el que se aprecia una clara discontinuidad en los geles sintetizados. Los espectros de FTIR (Figura 3), que muestran una mayor intensidad de los picos Si-O-Si en los geles de octilamina y por tanto un mayor grado de gelificación, confirman esta hipótesis.

EJEMPLO 2

Los productos sintetizados y caracterizados en el ejemplo 1 se aplicaron sobre una roca caliza de elevada pureza (98.5% de carbonato cálcico) con objeto de evaluar la eficacia consolidante y auto-limpiante de los materiales objeto de estudio. Los productos fueron aplicados por pulverización hasta alcanzar la saturación sobre probetas de la roca con dimensiones 5X5X2 cm. Los valores de consumo y materia seca obtenidos se reúnen en la Tabla 2.

Tabla 2

Muestra	Sin tratar	P25-0.5	P25-1	P25-2
Consumo (%w/w)	------	2.09±0.44	2.30±0.59	2.55±0.54
Residuo (%w/w)	------	0.04±0.02	0.05±0.03	0.05±0.02
Muestra	UCATiP-0	UCATiP-0.5	UCATiP-1	UCATiP-2
Consumo (%w/w)	1.31±0.29	1.43±0.39	1.28±0.24	1.15±0.36
Residuo (%w/w)	0.89±0.17	1.13±0.31	1.07±0.20	0.93±0.30
Muestra	UCATiO-0	UCATiO-0.5	UCATiO-1	UCATiO-2
Consumo (%w/w)	1.43±0.09	2.48±0.32	1.58±0.19	1.70±0.29
Residuo (%w/w)	1.05±0.06	1.78±0.23	1.15±0.14	1.31±0.23

El porcentaje de materia seca de las dispersiones de P25 en agua es significativamente inferior al que poseen los soles sintetizados en nuestro laboratorio. Este comportamiento se asocia a la sedimentación de las partículas P25 sobre la superficie pétrea mientras los soles penetran en la estructura

porosa de la roca, gelificando en sus poros, e incrementando por tanto, el porcentaje final de materia seca. Desde un punto de vista comparativo entre geles, el residuo de los geles UCATiO fue ligeramente superior que el obtenido para los geles UCATiP.

La Figura 7 muestra fotografías, obtenidas mediante Microscopía Electrónica de Barrido (Microscopio Quanta 200 de JEOL), de las superficie pétrea antes y después de la aplicación de los productos. Las dipersiones P25 y los geles con ácido fosfórico forman películas completamente fracturadas sobre las rocas pétreas mientras los geles con octilamina originan películas homogéneas y libres de fracturas que se integran en la estructura porosa de la roca. Este hecho confirma que la octilamina es capaz de disminuir la presión capilar del gel durante su etapa de secado hasta un valor suficientemente bajo para evitar la formación de fracturas. Esta reducción de la presión capilar se debe a dos razones: (1) disminución de la tensión superficial del sol. (2) Aumento del radio de poro del gel, como se demuestra en los resultados obtenidos por fisisorción de nitrógeno. El papel desempeñado por la n-octilamina para evitar la formación de fracturas, se discute con más detalle en publicaciones anteriores de nuestro grupo (Mosquera, M J et al. Langmuir 2008, *24*, 2772; Mosquera, MJ et al. Langmuir 2010, *26*, 6737).

El grado de adhesión de los productos sobre el sustrato pétreo se determinó mediante un test de adherencia, utilizando una cinta Scoth Magic (3M), según metodología previamente descrita por otros autores (Ling L et al. Langmuir, 25, 3260, 2009; Ding, Z et al. Langmuir, 25, 9648, 2009). Las superficies pétreas tratadas fueron sometidas en una mitad de su superficie al test de adherencia mientras la otra mitad se mantuvo sin cambios. Dicho test consistió, simplemente, en la colocación de la cinta sobre la superficie pétrea para, a continuación, ser extraída de forma manual, ejerciendo en todos los casos una presión similar. Los cambios en la superficie de la roca, se evaluaron por visualización al Microscopio Electrónico de Barrido (Quanta 200 de JEOL), operando en modo de bajo vacío. Además, se registraron los correspondientes espectros de rayos X (EDX) en las zonas visualizadas. Las imágenes obtenidas

y sus correspondientes espectros EDX se muestran en la Figura 8. Como Rao K et al. (Appl. Catal. B Environ. 49, 248, 2004), las películas de partículas P25, prácticamente, desaparecen después del test de adhesión. Los datos de EDX confirman esta hipótesis ya que no se observan los picos correspondientes al titanio, después del test de adhesión, en los espectros de P25-0.5 y P25-1. En el caso de la película P25-2, la intensidad del pico se reduce significativamente después del test.

La adherencia de los geles de UCATiP es superior a las partículas P25. No obstante, los resultados de EDX muestran una significativa reducción del porcentaje de titanio después del test. Respecto a la proporción de calcio (procedente del sustrato pétreo) se observa un significativo incremento después del test debido a la desaparición de la película superficial de gel que no contiene calcio. En el caso de las dispersiones de P25 la proporción de calcio no aumenta después del test de adhesión porque las partículas de titanio no forman un recubrimiento homogéneo sobre la superficie y por tanto, el carbonato cálcico presenta en la roca puede ser, perfectamente, identificado antes del test de adhesión.

En las superficies tratadas con geles UCATiO, la proporción de titanio, prácticamente, no es modificada por el test de adherencia. Además, en las imágenes de microscopía electrónica no se observan cambios significativos de la morfología superficial después del test de adherencia mientras los cambios experimentados por las superficies tratadas con P25 y geles UCATiP después de dicho test resultan evidentes. Por tanto, estos resultados nos permiten concluir que los geles sintetizados en presencia de octilamina presentan una adherencia al sustrato pétreo que no existe en los otros productos evaluados.

La eficacia consolidante de los productos sobre el sustrato pétreo se evaluó utilizando un microtaladro, capaz de determinar la resistencia de la roca en función de la profundidad de perforación, denominado “drilling resistance measurement system (DRMS)”, suministrado por Synth Technology. En este estudio, se emplearon brocas de 4.8 mm de diámetro con una velocidad de

rotación de 200 rpm y velocidad de penetración de 10 mm/min. Los perfiles de perforación obtenidos se muestran en la Figura 9. Las dispersiones de P25 y los geles de ácido fosfórico no produjeron ningún incremento en la resistencia mecánica de la roca. En el caso de los geles de octilamina, se aprecia un incremento significativo de dicha resistencia hasta 4 mm de penetración. Estos datos ponen de manifiesto que los geles UCATiO gelifican en la estructura porosa de la roca, incrementando su resistencia mecánica. Desde un punto de vista comparativo entre los geles con octilamina, mencionar que la adición de partículas de dióxido de titanio, en diferentes proporciones al sol, no modifica el efecto consolidante del producto, excepto en los geles con mayor proporción de titanio que se aprecia una ligera reducción de la resistencia mecánica de la roca. Por tanto, se puede concluir que es el gel de silicio, en el que se integran las partículas de titanio, responsable del efecto consolidante del producto. En el caso de los geles que contienen ácido fosfórico, la formación de un gel discontinuo constituido por agregados evita, con toda probabilidad, que posea efecto consolidante.

La eficacia auto-limpiante de los productos fue evaluado mediante un test diseñado y aplicado, previamente por Tatsuma T et al. (J. Phys. Chem. B 103, 8033, 1999) y por Fretwell R & Douglas P (J. Photochem Photobiol. A: Chem 143, 229, 2001). Para ello, 1 ml una de disolución de azul de metileno en etanol (10 mM) fue depositado sobre las superficies pétreas mediante una pipeta pasteur. Las manchas se dejaron secar, en condiciones de laboratorio, hasta peso constante. A continuación, las probetas fueron irradiadas con luz ultravioleta a 365 nm en una cámara Vilber Lourmat CN1.5.CL que contiene dos tubos de 15 Watios de potencia cada uno. La distancia entre muestras y tubos fue de aproximadamente 20 cm. Las variaciones de color experimentadas por las superficies pétreas fueron registradas, a diferentes tiempos, hasta que el cambio de color se mantuvo constante. Los cambios de color se determinaron utilizando un espectrofotómetro de reflexión para sólidos de Hunterlab con las siguientes condiciones: iluminante C, observador 10º y estándar CIEL*a*b*. La variación de color fue cuantificada mediante el

parámetro diferencia de color total (ΔE^*), utilizando el color de la superficie tratada como referencia (Berns R.S., 2000 Billmeyer and Saltzman's Principles of Color Technology. Wiley and Sons, Wiley-Interscience Eds. New York, USA). La Figura 10 muestra la evolución del parámetro ΔE^* frente al tiempo de exposición a la luz ultravioleta para las superficies pétreas tratadas con los productos objeto de estudio.

Las superficies tratadas con partículas P25 muestras una cinética de degradación de las manchas de azul de metileno significativamente más rápidas que las obtenidas en los geles silicio/titanio. La reducción de color de la mancha se produce en las primeras 120 horas de exposición a la luz ultravioleta, presentando una cinética similar para las diferentes concentraciones de partículas evaluadas. En el caso de las dos series de geles objeto de estudio, la cinética de degradación es más lenta, alcanzándose la estabilidad después de 620 horas de exposición a la radiación ultravioleta. Esta reducción de la cinética fotocatalítica se asocia a la menor proporción de titanio en estos recubrimientos que en las películas constituidas sólo por P25. Además, la inclusión de dichas partículas en una red de silicio podría, también, reducir dicha actividad. Desde un punto de vista comparativo entre geles, mencionar que la serie UCATiO presenta una velocidad de degradación superior a la que poseen los geles UCATiP. Los valores más altos de superficie específica y diámetro de poro que presentan los geles UCATiO respecto a los valores obtenidos para la serie UCATiP (ver datos de fisisorción de nitrógeno) podrían ser responsables de su mayor eficacia como fotocatalizadores.

Respecto a la reducción final de color de la mancha, mencionar que los geles UCATiO presentan valores similares a los obtenidos con las partículas P25, siendo significativamente superiores a los alcanzados por los geles UCATiP. Estos resultados ponen de manifiesto que los productos con octilamina muestran una eficacia autolimpiante superior a la que presentan los geles sintetizados en presencia de ácido fosfórico. Los datos obtenidos nos permiten concluir que los geles compuestos silicio/titanio obtenidos poseen una cinética de degradación del azul de metileno más lenta que la obtenida para rocas

tratadas con partículas de óxido de titanio. No obstante, la variación de color final de la mancha de azul de metileno es similar en las superficies pétreas tratadas con P25 que en las que contienen geles UCATiO.

Finalmente, mencionar que existe una ligera reducción de la mancha de azul de metileno en muestras sin tratar como consecuencia de la propia degradación que experimenta este colorante a radiaciones en el rango de radiación 350-520 nm (Mrowetz M et al. J. Phys. Chem. B 45, 17269, 2004). En el caso de los geles de silicio sin partículas de titano, en los que se aprecia una reducción de la mancha ligeramente superior a la observada en las muestras sin tratar, mencionar que esta desaparición de la mancha puede ser originada por un efecto combinado de un posible efecto hidrofugante del tratamiento (evaluado en el siguiente párrafo de la memoria) que evita la extensión y absorción de la disolución del colorante por parte de la superficie pétrea. la degradación del colorante asociazul del metileno y el efecto hidrofugante de los geles

Con objeto de comprobar el comportamiento de las rocas tratadas frente al agua, se realizaron medidas del ángulo de contacto estático utilizando un equipo de videomedición modelo OCA 15plus, suministrado por Datsphysic Instruments. Los resultados obtenidos se muestran en la Tabla 3. Teniendo en cuenta que las partículas de dióxido de titanio muestran un carácter hidrófilo y el agua es el principal vehículo de los agentes de deterioro de las rocas (sales solubles, biodeterioro..), la formación de una posible película hidrófila sobre la superficie pétrea, que favorezca la penetración de agua líquida en la estructura porosa de la roca, no es deseable.

Tabla 3

Muestra	Sin tratar	P25-0.5	P25-1	P25-2
Ángulo Contacto (º)	60±9	70±12	65±16	23±4
Absorción Capilar (%w/w)	2.72±0.08	----	----	----
ΔE*	----	0.66 ±0.21	1.57 ±0.85	1.59 ±0.83
Muestra	UCATiP-0	UCATiP-0.5	UCATiP-1	UCATiP-2
Ángulo Contacto (º)	93±2	92±6	98±2	96±5
Absorción Capilar (%w/w)	0.08±0.01	0.08±0.01	0.07±0.01	0.09±0.01
ΔE*	3.66± 0.49	2.68 ±0.31	2.27 ±0.31	1.72 ±0.25
Muestra	UCATiO-0	UCATiO-0.5	UCATiO-1	UCATiO-2
Ángulo Contacto (º)	121±1	118±6	101±6	100±3
Absorción Capilar (%w/w)	0.10±0.00	0.09±0.0	0.11±0.00	0.10±0.02
ΔE*	5.92±1.24	5.34±0.32	4.40±0.19	3.51 ±0.40

Como cabría esperar, la superficie pétrea es hidrófila. Las partículas P25 producen, también, superficies hidrófilas con valores de ángulos estáticos similares a la muestra sin tratar, excepto la película con mayor proporción de P25 que presenta una significativa reducción del ángulo de contacto (en 30º). Esta reducción permite suponer que sólo la dispersión con mayor proporción de partículas origina una película continua sobre la superficie pétrea. Además, estos datos ponen de manifiesto el conocido carácter hidrófilo de las películas de P25.

En el caso de los geles UCATiP y UCATiO, los valores de ángulos de contacto estático obtenidos muestran un comportamiento hidrófobo, siendo superiores los valores obtenidos para los geles de octilamina. Como demostrado previamente, los geles UCATiO forman películas homogéneas, continuas y libres de fracturas sobre la superficie pétrea mientras los geles de ácido fosfórico muestran cierta discontinuidad y fracturas que, obviamente, reducen la hidrofobicidad de la película. Desde un punto de vista comparativo entre los geles con octilamina, mencionar que el incremento gradual de partículas P25 produce una reducción progresiva en el valor de ángulo de contacto obtenido.

Estos resultados ponen de manifiesto que la adición de partículas de óxido de titanio a un precursor de silicio produce un gel compuesto silicio-titanio que dota a la roca de carácter hidrofugante, impidiendo la penetración de agua líquida en la estructura porosa de la roca. A este respecto, mencionar que la rugosidad de la roca caliza evaluada contribuye a incrementar los valores de los ángulos de contacto de las superficies pétreas tratadas (Illescas, JF & Mosquera MJ J. Phys Chem C, aceptado 2011).

Con objeto de corroborar este comportamiento hidrófobo, se determinó el porcentaje de absorción de agua por capilaridad, según procedimiento estandarizado (UNE-EN 1925; Natural *Stone test methods. Determination of water absorption coefficient by capillarity*. AENOR, 1999). Los valores máximos de agua absorbida se muestran en la Tabla 3. En el caso de las superficies pétreas tratadas con P25 no fue posible realizar este ensayo de absorción porque el agua arrastra las partículas P25. Los resultados obtenidos (próximos a cero) confirman que las superficies tratadas con los geles evitan la penetración de agua líquida en el interior de los poros de la roca.

Finalmente, se evaluaron los posibles cambios cromáticos inducidos por los por los tratamientos mediante medida del parámetro ΔE^*, de acuerdo con el procedimiento comentado previamente. Como se aprecia en la Tabla 3, los valores de ΔE^* obtenidos para las películas P25 y las formulaciones UCATiP fueron inferiores o iguales a 3, y por tanto no perceptibles al ojo humano. En el

caso de los geles UCATiO, los valores fueron ligeramente superiores, reduciéndose, de forma progresiva, según se incrementa la proporción de óxido de titanio en la mezcla, hasta alcanzar un valor en torno a 3 para el gel que contiene la máxima proporción de partículas. La explicación para este cambio de color se asocia al alto contenido de octilamina en el sol que amarillea ligeramente la roca caliza evaluada, que posee, antes del tratamiento, un color blanco intenso. El aumento de titanio en el gel origina un efecto blanqueante sobre la superficie pétrea que reduce la diferencia cromática observada.

MANERA QUE LA INVENCIÓN ES SUSCEPTIBLE DE APLICACIÓN INDUSTRIAL

El producto de la presente invención presenta aplicación industrial como tratamiento de protección de rocas y en general, para protección de cualquier material de construcción de naturaleza porosa. En concreto, el nuevo producto es capaz de incrementar la resistencia mecánica de la roca y formar un recubrimiento cohesionado que se adhiere al sustrato pétreo. Dicho recubrimiento posee actividad fotocalítica y en consecuencia, presenta efecto auto-limpiante en presencia de luz. Además, este producto es capaz de crea una superficie hidrófoba sobre la roca que impide la penetración de agua líquida en su estructura porosa.

REIVINDICACIONES.

1. Producto auto-limpiante, consolidante e hidrofugante para el tratamiento de rocas u otros materiales de construcción de naturaleza porosa que comprende:

   - Un oligómero de silicio o un alcoxisilano hidrolizado.
   - Partículas de dióxido de titanio coloidal.
   - Un tensioactivo no iónico en una concentración superior a su concentración micelar crítica.

2. Producto según reivindicación 1 donde el tensioactivo no iónico es una amina primaria, preferentemente n-octilamina.

3. Producto según reivindicaciones 1 y 2, donde la concentración de n-octilamina en el sol de partida debe ser 0.22 M o superior.

4. Producto según reivindicación 1, donde la concentración de partículas coloidales de dióxido de titanio en el sol, para un diámetro de partícula comprendido entre 20-25 nm, debe ser igual o inferior al 2% p/v.

5. Procedimiento para la obtención del producto según reivindicaciones 1 a 4 que consiste en mezclar un oligómero de silicio o un alcoxisilano hidrolizado, con n-octilamina y partículas coloidales de dióxido de titanio, sometiéndo la mezcla a agitación de ultrasonidos.

6. Uso del producto según reivindicaciones 1 a 5 para protección de cualquier material de construcción de naturaleza porosa.

7. Uso del producto según reivindicaciones 1 a 5 para la protección de rocas.

8. Uso del producto según reivindicaciones 1 a 5 para incrementar la resistencia mecánica de rocas y otros materiales de construcción de naturaleza porosa y formar un recubrimiento cohesionado que se adhiere al sustrato pétreo.

9. Uso del producto según reivindicaciones 1 a 5 para proporcionar un efecto auto-limpiante en presencia de luz a rocas y otros materiales de construcción de naturaleza porosa.

10. Uso del producto según reivindicaciones 1 a 5 para crea una superficie hidrófoba sobre rocas y otros materiales de construcción de naturaleza porosa, que impide la penetración de agua líquida en su estructura.

11. Uso del producto según reivindicaciones 1 a 5 para la consolidación, auto-limpieza e hidrofugación de rocas y otros materiales de construcción de naturaleza porosa.

RESUMEN

La presente invención se refiere a un material composite constituido por partículas de titanio integradas en un gel de sílice, que posee actividad fotocatalítica. Este nuevo material origina un efecto auto-limpiante sobre sustratos pétreos y otros materiales de construcción de naturaleza porosa.

En concreto, se trata de un producto capaz de: (1) dotar a la superficie tratada de capacidad auto-limpiante por simple exposición a la luz solar. (2) mejorar su resistencia mecánica superficial (3) formar un recubrimiento cohesionado capaz de adherirse al sustrato pétreo tratado.

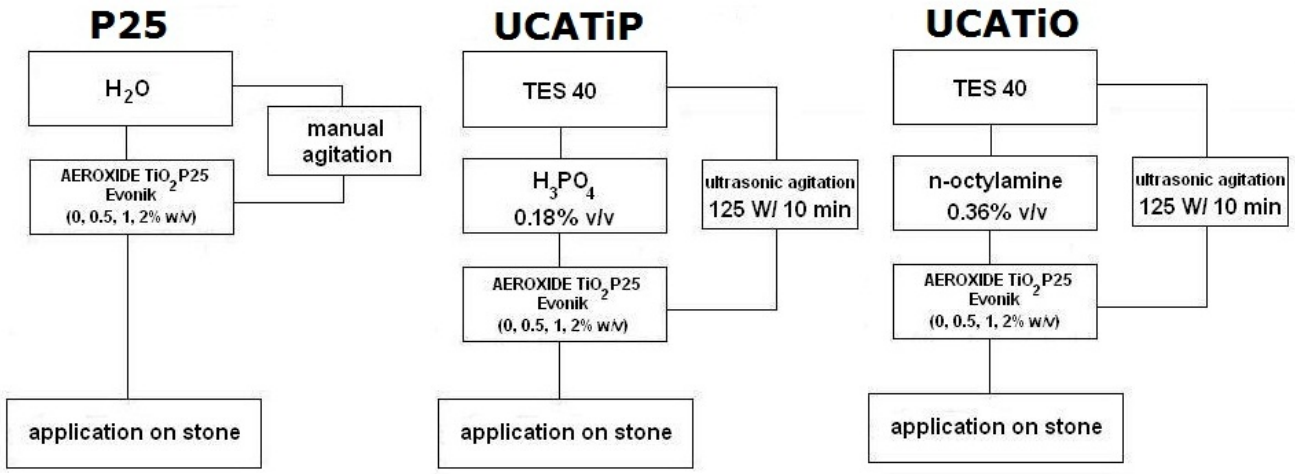
P25
H2O
manual agitation
AEROXIDE TiO2 P25 Evonik (0, 0.5, 1, 2% w/v)
application on stone
UCATiP
TES 40
H3PO4 0.18% v/v
ultrasonic agitation 125 W/ 10 min
AEROXIDE TiO2 P25 Evonik (0, 0.5, 1, 2% w/v)
application on stone
UCATiO
TES 40
n-octylamine 0.36% v/v
ultrasonic agitation 125 W/ 10 min
AEROXIDE TiO2 P25 Evonik (0, 0.5, 1, 2% w/v)
application on stone

FIGURA 1

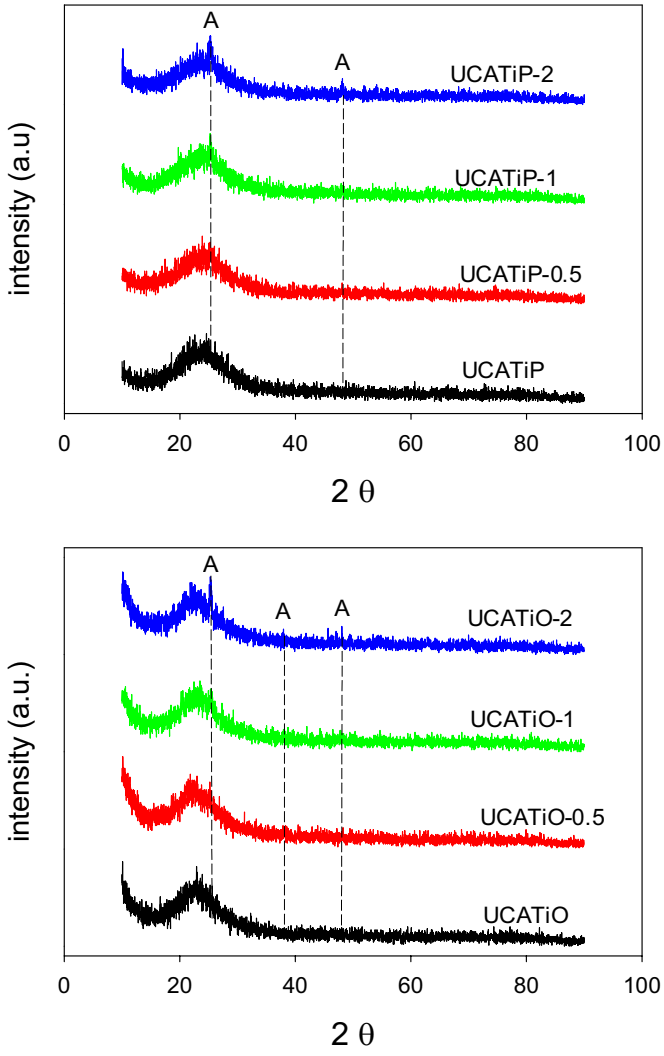
A
A
UCATiP-2
UCATiP-1
UCATiP-0.5
UCATiP
intensity (a.u)
0
20
40
60
80
100
2 θ
A
A
A
UCATiO-2
UCATiO-1
UCATiO-0.5
UCATiO
intensity (a.u.)
0
20
40
60
80
100
2 θ

FIGURA 2

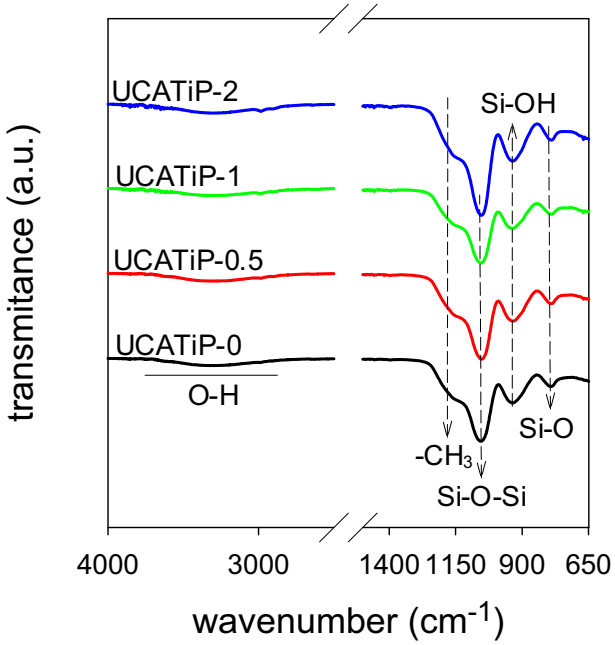
UCATiP-2
UCATiP-1
UCATiP-0.5
UCATiP-0
O-H
Si-OH
Si-O
-CH3
Si-O-Si
transmitance (a.u.)
4000
3000
1400
1150
900
650
wavenumber (cm-1)

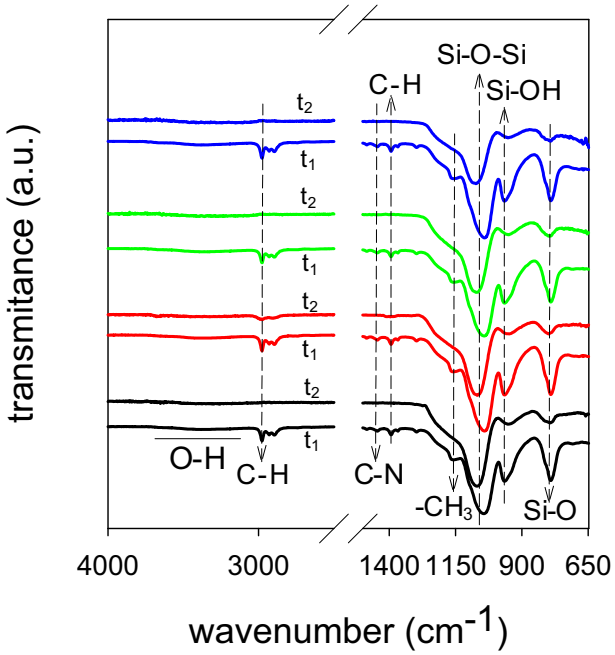
t2
t1
O-H
C-H
Si-O-Si
C-H
Si-OH
C-N
-CH3
Si-O
transmitance (a.u.)
4000
3000
1400
1150
900
650
wavenumber (cm-1)

FIGURA 3

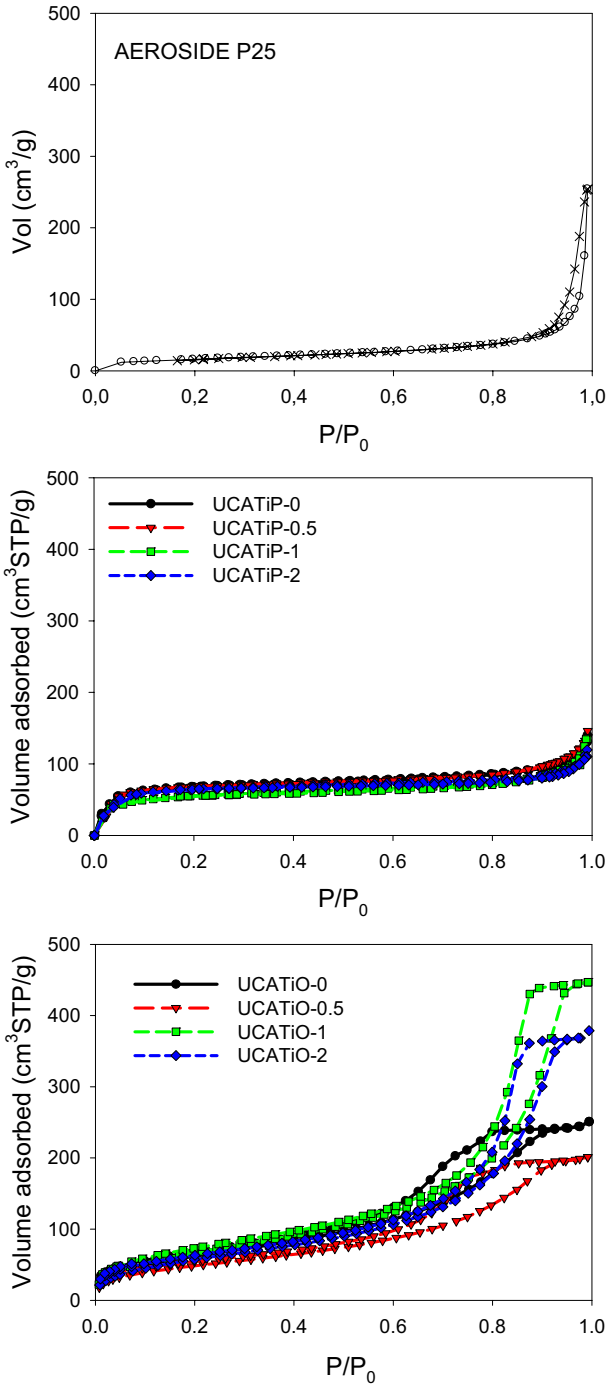
AEROSIDE P25
Vol (cm3/g)
P/P0
Volume adsorbed (cm3STP/g)
UCATiP-0
UCATiP-0.5
UCATiP-1
UCATiP-2
UCATiO-0
UCATiO-0.5
UCATiO-1
UCATiO-2

FIGURA 4

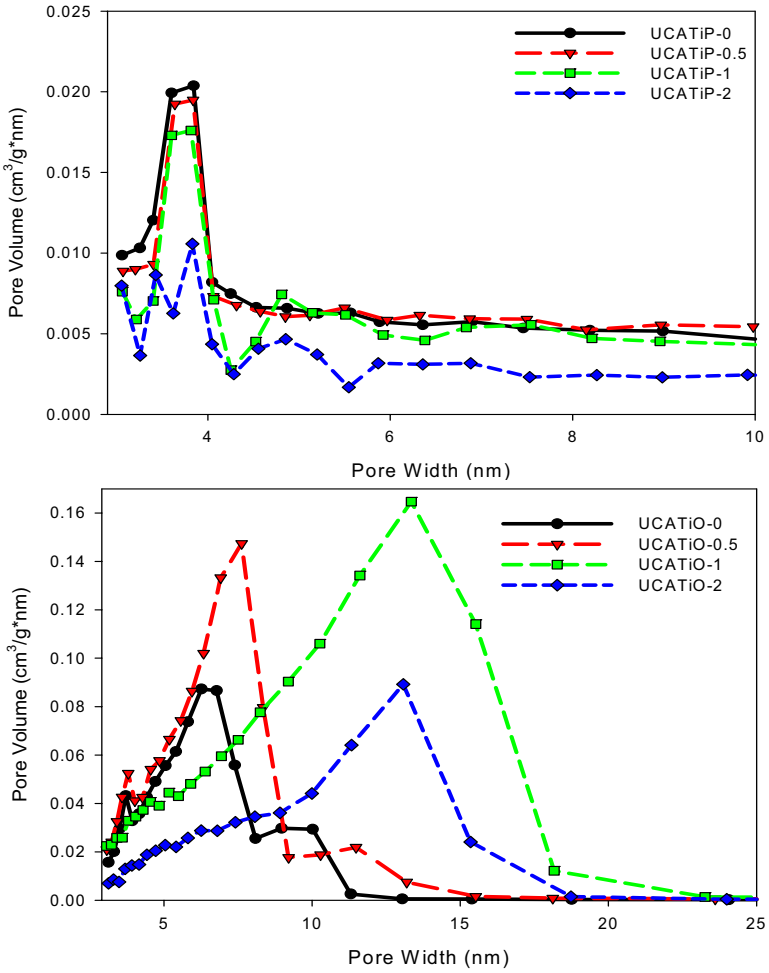
UCATiP-0
UCATiP-0.5
UCATiP-1
UCATiP-2
Pore Volume (cm3/g*nm)
Pore Width (nm)
UCATiO-0
UCATiO-0.5
UCATiO-1
UCATiO-2
Pore Volume (cm3/g*nm)
Pore Width (nm)

FIGURA 5

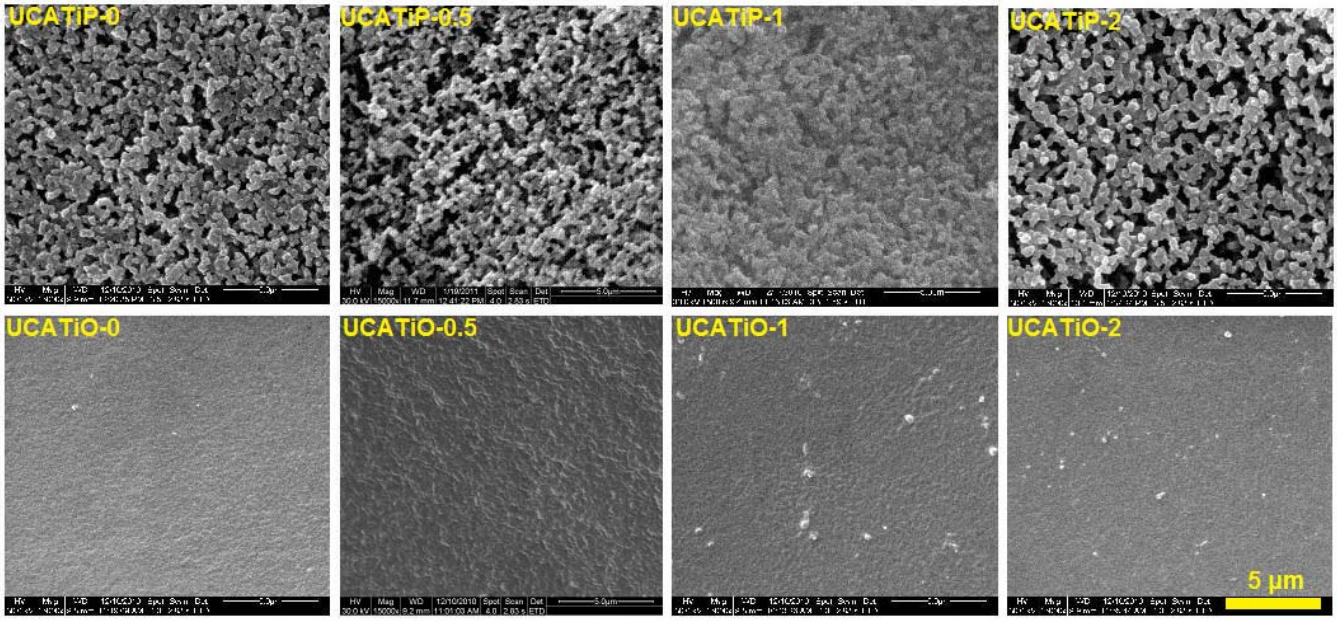
UCATiP-0
UCATiP-0.5
UCATiP-1
UCATiP-2
UCATiO-0
UCATiO-0.5
UCATiO-1
UCATiO-2
5 µm

FIGURA 6

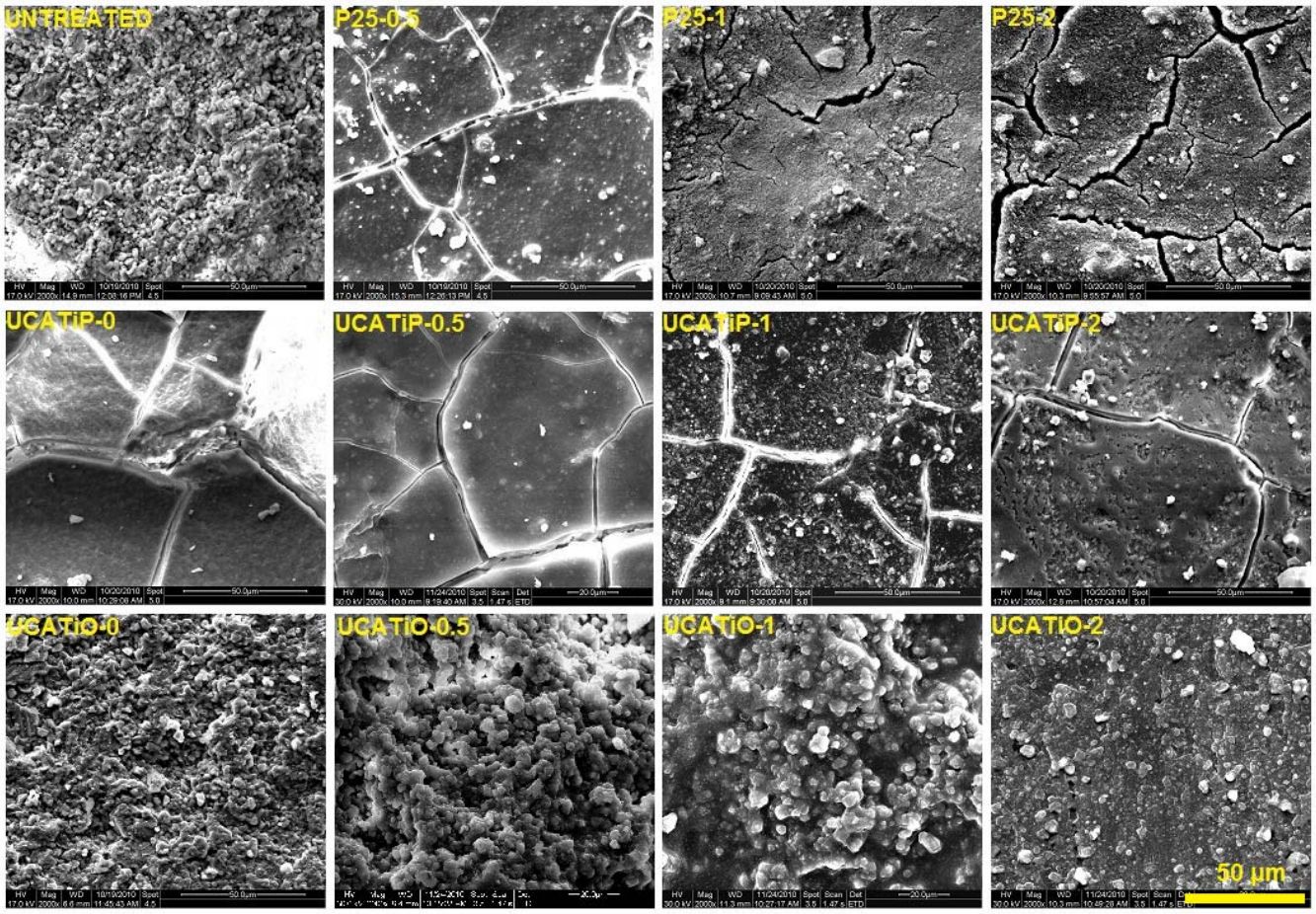
UNTREATED
P25-0.5
P25-1
P25-2
UCATiP-0
UCATiP-0.5
UCATiP-1
UCATiP-2
UCATiO-0
UCATiO-0.5
UCATiO-1
UCATiO-2
50 µm

FIGURA 7

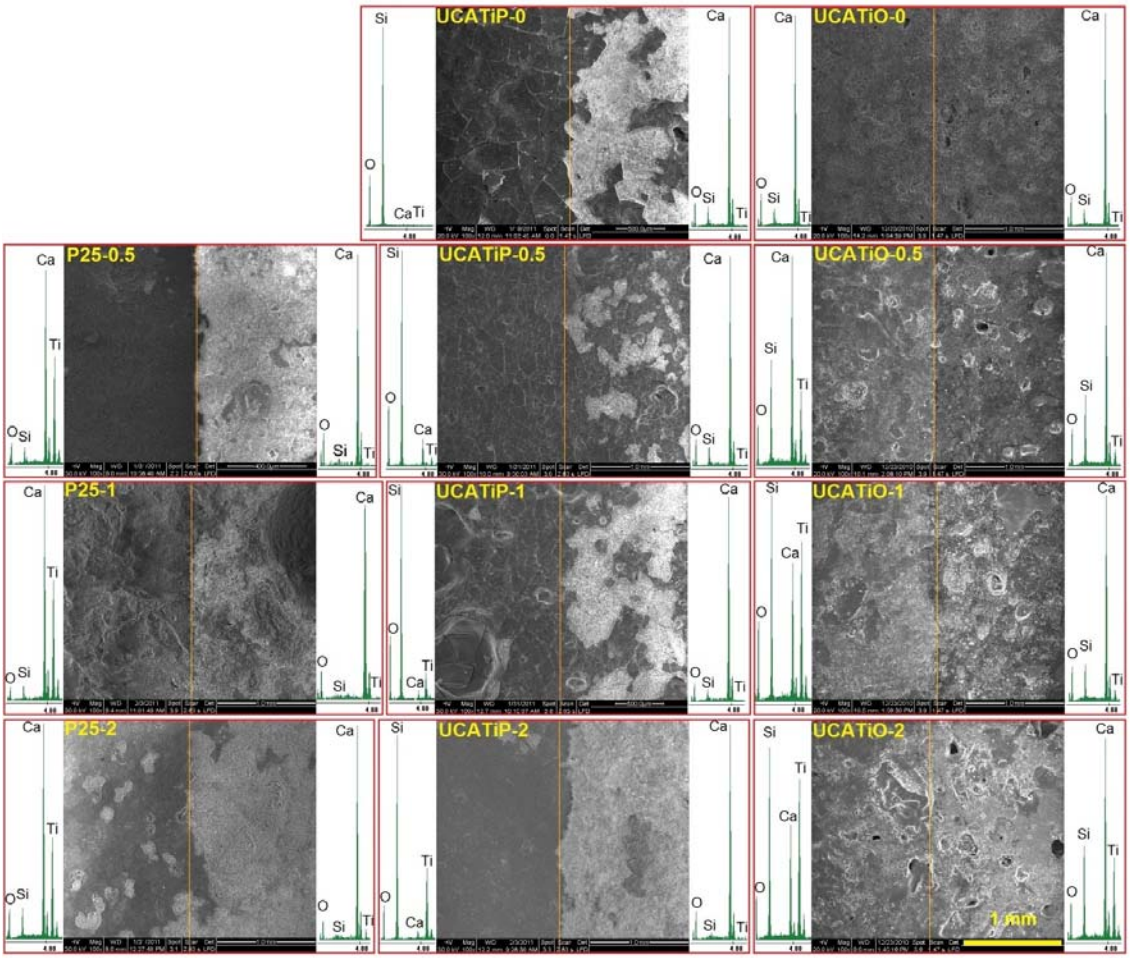
UCATiP-0
UCATiO-0
P25-0.5
UCATiP-0.5
UCATiO-0.5
P25-1
UCATiP-1
UCATiO-1
P25-2
UCATiP-2
UCATiO-2
1 mm

FIGURA 8

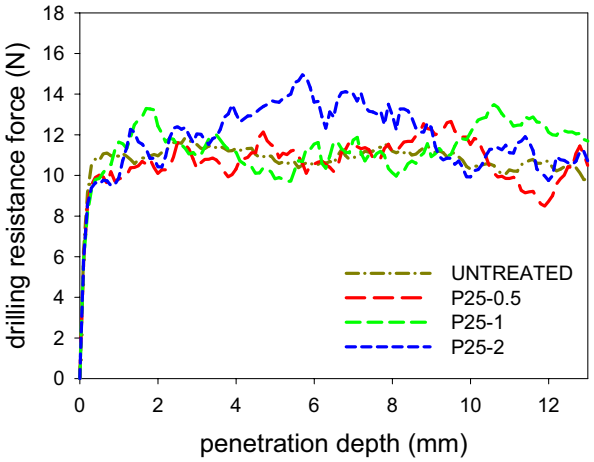
drilling resistance force (N)
penetration depth (mm)
UNTREATED
P25-0.5
P25-1
P25-2

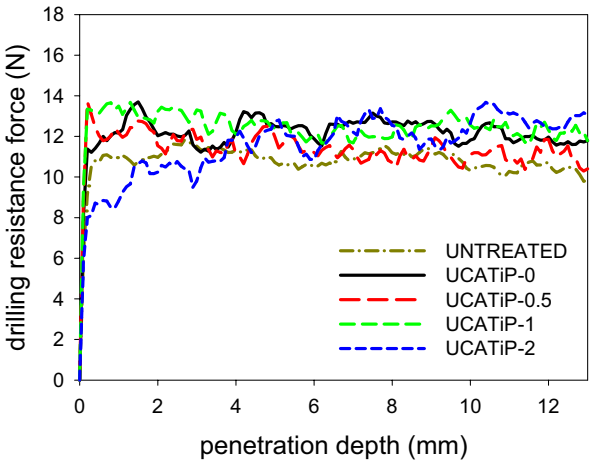
drilling resistance force (N)
penetration depth (mm)
UNTREATED
UCATiP-0
UCATiP-0.5
UCATiP-1
UCATiP-2

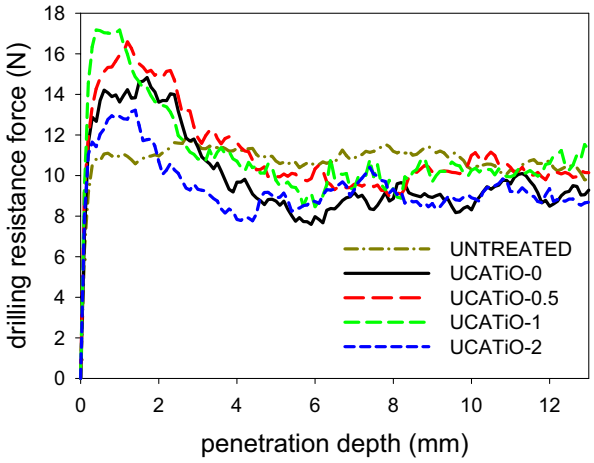
drilling resistance force (N)
penetration depth (mm)
UNTREATED
UCATiO-0
UCATiO-0.5
UCATiO-1
UCATiO-2

FIGURA 9

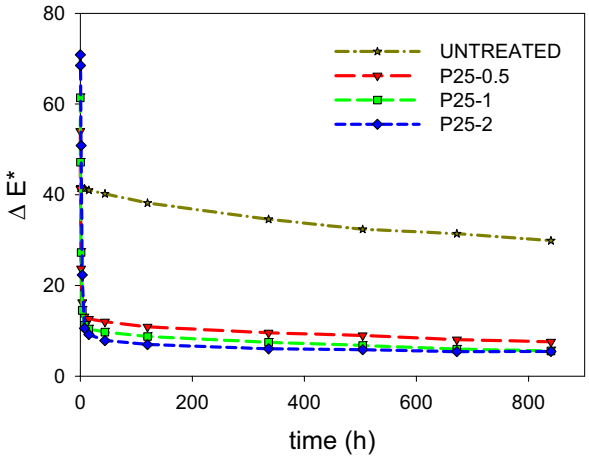
80
60
40
20
0
Δ E*
0
200
400
600
800
time (h)
UNTREATED
P25-0.5
P25-1
P25-2

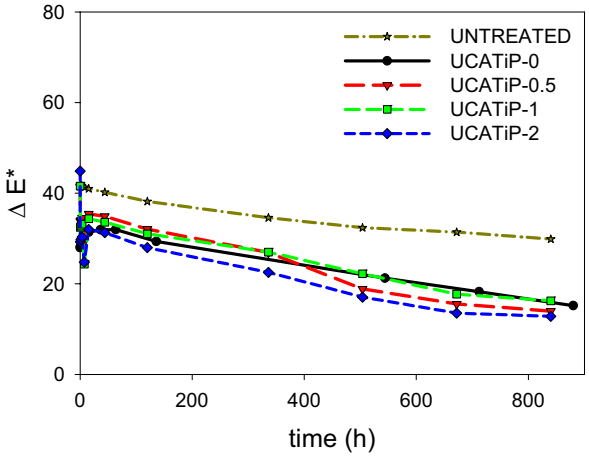
80
60
40
20
0
Δ E*
0
200
400
600
800
time (h)
UNTREATED
UCATiP-0
UCATiP-0.5
UCATiP-1
UCATiP-2

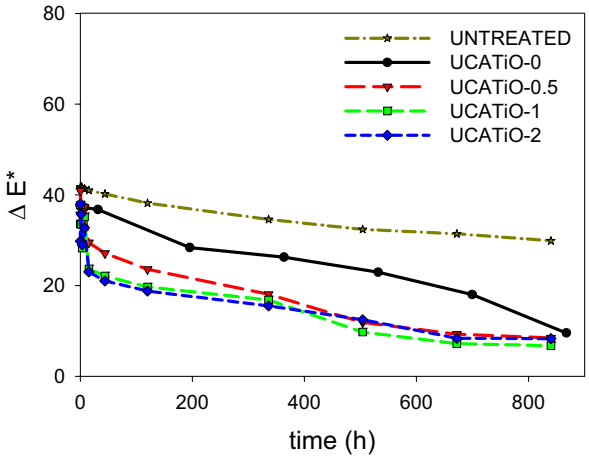
80
60
40
20
0
Δ E*
0
200
400
600
800
time (h)
UNTREATED
UCATiO-0
UCATiO-0.5
UCATiO-1
UCATiO-2

FIGURA 10

Conferences

- International congress Science and Technology for the Conservation of Cultural Heritage, October 2012, Santiago de Compostela (Spain)
- International Conference on Surfaces, Coatings and Nanostructured Materials, March 2012, Tampa (USA)
- 5th International Congress "Science and Technology for the safeguard of Cultural Heritage in the Mediterranean Basin", November 2011, Istambul (Turkey)
- 5th International Meeting on developments in Materials, Processes and applications of emerging technologies, June 2011, Portimão (Portugal)
- I Congreso Internacional "El Patrimonio Cultural y Natural como motor de desarrollo: Investigación e Innovación", January 2011, Jaén (Spain)

CURSOS E CONGRESOS

Research Advances for the Conservation of Cultural Heritage

International Congress on Science and Technology for the Conservation of Cultural Heritage

Santiago de Compostela, Spain, 2-5 October 2012

Book of Abstracts

Edited by
Massimo Lazzari
Sophie Rochette

UNIVERSIDADE DE SANTIAGO DE COMPOSTELA
publicacións

Titania-silica nanocomposite photocatalyst: application for stoneware self-cleaning

Claudia Mirabelli,[1] Luis Pinho,[1] Federica Fernandez,[2] Maria J. Mosquera[1]

[1]Physical-Chemistry Department, University of Cadiz.
PO BOX 40 11510 Puerto Real, Spain, e-mail: mariajesus.mosquera@uca.es
[2]Polo Universitario della Provincia di Agrigento, Via Quartararo, 6.
92100 Agrigento, Italy

Titania-silica composites are promising materials considering self-cleaning properties. Nowadays, they are widely available as commercial glass coatings. Our objective in this paper is to optimize these composites in order to be used as restoration materials. Recently, we have synthesized a mesoporous titania-silica composite with photocatalytic activity by mixing silica oligomers and titanium dioxide nanoparticles in the presence of *n*-octylamine [1].

In this study, this product was applied on stoneware tiles from a building of the 60's in the city centre of Palermo. This stoneware is a vitrified ceramic building material, consisting mainly of kaolin and feldspar. It is extensively used as floor pavement and wall covering in indoor and outdoor applications. The stoneware selected has low water absorption (<0.5%) and high bending strength (>35 MPa).

The treatment was performed on 2x2x3 cm samples by brushing. For comparison, other stoneware specimens were treated with a popular commercial photocatalytic product, E-503 (Nanocer), under the same conditions.

The adherence to stoneware was evaluated by performing a peeling test, adapted from the literature [2], combining a conventional test with SEM imaging and EDX analyses. We also investigated self-cleaning effectiveness of the coatings by studying the total colour change (ΔE^*) of stones stained with methylene blue and orange and exposed to UV irradiation (365 nm).

Our nanomaterial gave self-cleaning properties to the stoneware under study. In addition, this coating presented effective adhesion and was free of cracks. The commercial material produced a cracking coating with a poor adhesion on the stoneware. Concerning to self-cleaning test, the two products evaluated showed a significant reduction of the stain.

From the results obtained, we can conclude that the new coating material developed in our laboratory is capable of: (a) adhering firmly to the stoneware to ensure that the conservation and self-cleaning properties of the coating have a long-term effect; (b) providing self-cleaning properties to the stoneware surface. We have also shown that the commercial product do not create an effective coating that adheres to the substratum; therefore, such product is of no practical use for protecting stonework.

References:

[1] Pinho, L., Mosquera, M.J. 2011. Titania-silica nanocomposite photocatalysts with application in stone self-cleaning. *Journal of Physical Chemistry C*, 115: 22851-22862

[2] Ling, X.Y., Phang, I.Y., Vancso, G.J., Huskens, J., Reinhoudt, D.N. 2009. Stable and transparent superhydrophobic nanoparticle films. *Langmuir*, 25: 3260-3263

New nanomaterials for stone restoration

Maria J. Mosquera, Juan F. Illescas, Dario S. Facio, Luis Pinho, Farid Elhaddad

Physical-Chemistry Department, University of Cádiz.
11510 Puerto Real (Cádiz), Spain
e-mail: mariajesus.mosquera@uca.es

The sol-gel process has been found to be successful when applied to the protection and conservation of stones and other building materials. However, a well-known drawback of sol-gel materials is their tendency to crack while drying. Our research group has developed a novel synthesis [1-3] in which the sol-gel transition occurs in the presence of a surfactant. This provides an efficient means of preventing cracking of the gel in two ways: (1) by increasing gel pore radius; (2) by reducing solvent surface tension. Recently, we modified the process in order to avoid the use of volatile organic components (VOCs) in the starting sol [4,5]. The synthesis is simply carried out by mixing a silica oligomer and an aqueous solution of *n*-octylamine under ultrasonic agitation. With this procedure, we prepared materials with different applications: (1) stone consolidants; (2) hydrophobic products by adding an organic component (polydimethylsiloxane) to the starting sol; (3) self-cleaning materials by mixing a photocatalyst (TiO_2) with the silica precursor; (4) superhydrophobic materials by adding colloidal silica particles to the hybrid sol.

References:

[1] Mosquera, M.J., de los Santos, D.M., Montes, A., Valdez-Castro, L. 2008. New materials for consolidating stone. *Langmuir*, 24: 2772-2778

[2] Mosquera, M.J., de los Santos, D.M., Rivas, T., Sanmartín, P., Silva, B. 2008. New nanomaterials for protecting and consolidating stone. *Journal of Nano Research*, 9: 1-12

[3] Mosquera, M.J., de los Santos, D.M., Rivas, T. 2010. Surfactant-synthesized ormosils with application to stone restoration. *Langmuir*, 26: 6737-6745

[4] Illescas, J.F., Mosquera, M.J. 2011. Surfactant-synthesized PDMS/Silica nanomaterials improve robustness and stain resistance of carbonate stone. *Journal of Physical Chemistry C*, 115: 14624-14634

[5] Pinho, L., Mosquera, M.J. 2011. Titania-silica nanocomposite photocatalysts with application in stone self-cleaning. *Journal of Physical Chemistry C*, 115: 22851-22862

NANOSMAT USA

NANOSMAT-USA | Conference & Exhibition

Technical Programme

Venue: Embassy Suites Tampa - USF

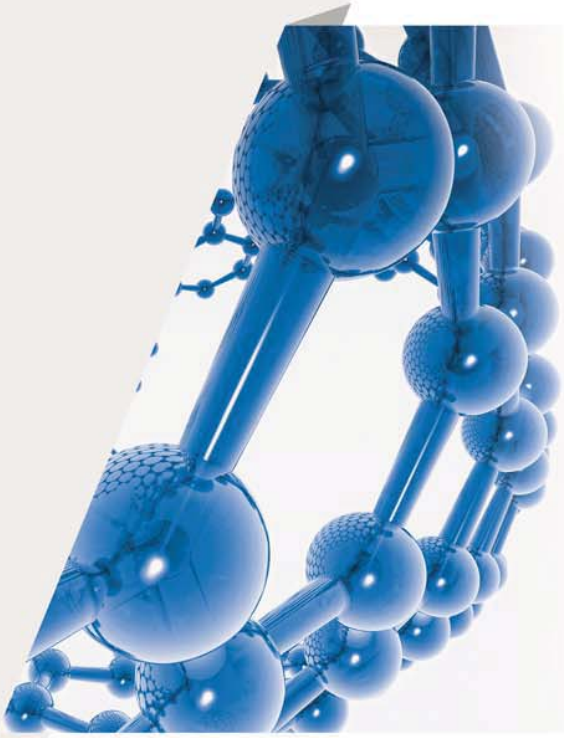

USA International Conference on Surfaces, Coatings and Nano-Structured Materials

- 27-30 March 2012
- Tampa, Florida, USA.

Friday
30th March

TIME	*Symposium:* NANOMAGNETISM ***Chairperson:*** *Professor Andrei Stanishevsky (USA)* ***Room:*** *Salon FG*
09:00 - 09:20	**NANO-33: Shavkat Yuldashev,** Dongguk University, Korea *"Critical behavior of Ga1-xMnxAs thin films near the Curie temperature"*
09:20 - 10:00	**INVITED-4: PROFESSOR David J. Sellmyer,** University of Nebraska, USA *"Physics and Assembly of Magnetic Nano-Objects and Nanomaterials"*
10:00 - 10:20	**NANO-113: Ovidiu Pana,** National Institute for Research and Development of Isotopic and Molecular Technologies, Romania *"Core-Shell Nanoparticles with Targeted Magnetic Properties"*
10:20 - 10:40	**REFRESHMENT BREAK**
TIME	***Symposium:*** *NANOMAGNETISM & RELATED PHENOMENA* ***Chairperson:*** *Professor D. J. Sellmyer (USA)* ***Room:*** *Salon FG*
10:40 - 11:10	**INVITED-14: Professor Steven C. Tidrow,** The University of Texas Pan American *"Electrical and Structural Properties of Ba(Y3+, Sb5+)0.05Ti0.90O3, a Dipole-Like B-Site Substituted Ferroelectric Perovskite"*
11:10 - 11:30	**NANO-131: Devajyoti Mukherjee,** University of South Florida, USA *"Dual Laser Ablation: A Novel Technique for the In-situ Growth of Epitaxial Multiferroic Heterostructures of Ultra-thin Films"*
11:30 - 11:50	**NANO-204: Maneesha Gupta,** Z.H.C.E.T, AMU. Aligarh. INDIA *"Effect of Ni doping on magnetic properties of La2/3Sr1/3Mn0.95Ni0.05O3 nano and micron perovskite"*
11:50 - 12:10	**NANO-13: Mojgan Ahmadrezaei,** Universiti Kebangsaan Malaysia, Malaysia *"Thermal expansion behaviour of nanomaterial Ba0.2Sr0.8Co0.8Fe0.2O3−δ (BSCF) with Sm0.2Ce0.8Ox (SDC)"*
12:10 - 13:30	**LUNCH**

TIME	*Symposium:* NANO & ELECTROMAGNETIC PROPERTIES ***Chairperson:*** *Professor Anirudha V. Sumant (USA)* ***Room:*** *Salon E*
09:00 - 09:20	**NANO-132: Kaya Wei,** University of South Florida, USA *"High performance thermoelectric properties via nano-scale enhancement of nanocomposite materials"*
09:20 - 10:00	**INVITED-13: PROFESSOR Daryush ILA,** Fayetteville State University, USA *"Pseudo-crystals consisting Nanomaterials for Thermoelectric Applications"*
10:00 - 10:20	**NANO-109: G.K. Strukova,** Russian Academy of Sciences, Russia *"With No Color and Scent: Microstructures of Metals and Alloys - Copies of Natural Objects"*
TIME	***Symposium:*** *NANO & INDUSTRY* ***Chairperson:*** *Dr Nasar Ali (UK)* ***Room:*** *Salon E*
10:40 - 11:10	**NANO-54: M.J. Mosquera,** University of Cádiz, Spain *"New Nanomaterials for Building Materials Protection"*
11:10 - 11:30	**NANO-80: Md Abu Nasser Nayeem,** Louisiana Tech University, USA *"In Situ Electrokinetic Polymer Formation to Prevent Reinforcement Corrosion in Concrete"*
11:30 - 11:50	**NANO-158: P. Anadão,** University of São Paulo, Brazil *"A study on the chemical resistance of polysulfide-clay nanocomposite membranes"*
11:50 - 12:10	**NANO-53: D.S. Facio,** University of Cádiz, Spain *"Producing a Nanocomposite for Stone Protection with Super-hydrophobic Properties"*

New Nanomaterials for Building Materials Protection

M.J. Mosquera, J.F. Illescas, D.S. Facio, L. Pinho, F. Elhaddad

Physical-Chemistry Department, University of Cádiz, 11510 Puerto Real (Cádiz), Spain

The sol-gel process has been found to be successful in applications for the protection and conservation of stones and other building materials. However, a well-known drawback of sol-gel materials is their tendency to crack during its drying. In this paper, we present an overview of our current research centred on producing crack-free gels with application on building materials [1-5]. We develop a novel synthesis in which the sol-gel transition occurs in the presence of a surfactant. This provides an efficient means of preventing cracking of the gel, as the result of coarsening of the gel network and decreasing of surface tension. The synthesis is carried out by mixing a silica oligomer and an aqueous solution of n-octylamine under ultrasonic agitation, being volatile organics components (VOCs) prevented in the starting sol. This procedure has several advantages for commercial purposes: (1) simple and low-cost synthesis; (2) Sol stability is above 6 months; (3) Sol-gel transition and drying occur by simple exposure to environment humidity; (4) Sol can be applied in situ, on the building surface, since gel transition spontaneously occurs. From this procedure, we prepare materials with different applications: (1) Stone consolidants; (2) Hydrophobic and water-repellent products by adding an organic component (polydimethylsiloxane) to the starting sol; (3) Self-cleaning materials by mixing a photocatalyst (TiO_2) with the silica precursor.

[1] M.J. Mosquera, D.M. de los Santos, A. Montes and L. Valdez-Castro, Langmuir, *24*, 2772 (2008).

[2] M.J. Mosquera, D.M. de los Santos, T. Rivas, P. Sanmartín, B. Silva, J. NanoR., 8, 1 (2009).

[3] M.J. Mosquera, D.M. de los Santos and T. Rivas, Langmuir, *26*, 6737 (2010).

[4] J.F. Illescas and M.J. Mosquera, J. Phys. Chem. C, *115*, 14624 (2011).

[5] L. Pinho and M.J. Mosquera, J. Phys. Chem. C, 115, 22851 (2011).

T.C. KÜLTÜR VE TURİZM BAKANLIĞI

İSTANBUL BÜYÜKŞEHİR BELEDİYESİ

İstanbul Üniversitesi

KUMID
KÜLTÜREL MİRASIN DOSTLARI DERNEĞİ

Consiglio Nazionale delle Ricerche
Istituto di Metodologie Chimiche

Association Investing in Culture

5th International Congress
on
"Science and Technology for the Safeguard of Cultural Heritage in the Mediterranean Basin"

Istanbul, Turkey
22 – 25 November 2011

TITANIA-SILICA COMPOSITE PHOTOCATALYSTS FOR SELF-CLEANING APPLICATION ON STONE: IMPROVING ADHESION AND CONSOLIDATION PROPERTIES

Luís Pinho[1], María J. Mosquera[1]

[1]Physical-Chemistry Department, University of Cádiz, 11510 Puerto Real (Cádiz), Spain,
e-mail: mariajesus.mosquera@uca.es

Keywords: Self-cleaning, titanium dioxide, stone, consolidant.

Titania-silica composites are promising materials considering self-cleaning properties (1). Nowadays, they are widely available as commercial glass coatings. Our objective in this paper is to optimize these composites in order to be used as restoration materials.

Our group has developed new products by adding an organosiloxane to silica precursors in presence of n-octylamine (2,3). Recently, we have synthesized titania-silica composites with self-cleaning properties in presence of the same surfactant (4). In this study, a mesoporous titania-silica composite that has photocatalytic activity has been synthesized by mixing silica oligomers and titanium dioxide nanoparticles in the presence of n-octylamine. For purposes of comparison, a simple dispersion of titania nanoparticles in water has also been tested. Both materials were sprayed on pure limestone (98% calcium carbonate) samples.

Since one significant drawback of titania particles applied on stone has been associated with a reduction in photocatalytic efficiency during long-term use due to the elimination of TiO_2 from the stone surface (5), we have investigated the degree of adhesion of these coatings synthesized in our laboratory on stone, by performing a peeling test adapted from the literature, combining a conventional test with SEM imaging and EDX analyses.We also investigated whether the mechanical resistance of a stone surface is improved after application of the coatings; this was done by measuring the drilling resistance of the untreated limestone and its treated counterparts. Hydrophobic properties of the coatings were evaluated through a capillary water uptake test. Finally, we investigated self-cleaning effectiveness of the coatings by studying the total colour change (ΔE^*) of stones stained with methylene blue and exposed to UV irradiation (365 nm).

Our nanomaterial gave self-cleaning properties to stone and improved its mechanical resistance. In addition, this coating presented effective adhesion and was free of cracks when applied on stone. Finally, the coating also presented hydrophobic properties. P25 material produced a cracking coating with a poor adhesion on the stone; furthermore, it does not increase the mechanical resistance of the stone. Considering the hydrophobic behavior of the titania-silica coating, the capillary water uptake values obtained are very low and significantly lower than those obtained for P25 treatment and the untreated counterpart. Concerning to self-cleaning test, all the materials showed a significant reduction of the stain, evaluated by the colour change (ΔE^*). ΔE^* values for aqueous dispersion of P25 resulted low and close to those corresponding to the titania-silica coating.

From the results obtained, we can conclude that the new coating material developed in our laboratory is capable of: (1) adhering firmly to the stone surface to ensure that the conservation and self-cleaning properties of the coating have a long-term effect; (2) increasing the mechanical resistance of the stone; (3) providing proven self-cleaning properties to the stone surface; and (4) providing hydrophobic properties to the stone surface. We have also shown that P25 commercial titania particles applied as a water dispersion on stone do not create an effective coating that adheres to the substratum; therefore, such dispersion is of no practical use for protecting stonework.

References:

(1) Fujishima, A.; Rao, T.; Tryk, D. *J. Photochem.Photobiol. C, 1*, **2000**, 1-21.
(2) Mosquera, M. J.; De los Santos, D.; Rivas T., *Langmuir, 26*, **2010**, 6737-6745.
(3) Illescas, J.F.; Mosquera, M.J. *J. Phys. Chem. C*, *30*, **2011**,14624-14634.
(4) Pinho, L., M. J. Mosquera, *J. Phys. Chem. C*, **2011** (accepted with changes)
(5) Rao, K.; Subrahmanyam, M.; Boule P. *Apply. Catal. B: Environ., 49*, **2004**, 239-249.

mpatech
NANOTECH CONFERENCE

5th International Meeting on Developments in Materials, Processes and Applications of Emerging Technologies

Technical Programme

mpa 2011

- 27-29 June 2011
- Alvor, Portugal.

Tuesday 28th June

TIME	**Session:** Applied Bionanotechnology & Nanomedicine **Chairperson:** J.Y. Ljubimova (USA) **Room:** Sala Brasil	**Session:** Surface Science and Technology **Chairperson:** Jas Pal S. Badyal (UK) **Room:** Sala Madeira
11:30 - 11:50	**MPA-40** **M.K. Gilmanov,** M.A. Aytkhozhin's Institute of Molecular Biology and Biochemistry, Kazakhstan *"The Phosphatidylinositol Nanocapsules For Therapy Severe Diseases"*	**MPA-52** **H. Fakhouri,** Université Pierre et Marie Curie, France *"Influence of RF reactive sputtering on the nitrogen chemical state in Nitrogen doped TiO2 thin films"*
11:50 - 12:10	**MPA-47** **N. Durán,** IQ-Universidade Estadual de Campinas, Brazil *"Biogenic Silver Nanoparticles and its Antifungal Activity on Tricophyton rubrum"*	**MPA-95** **Vyshnavi Narayanan,** Ghent University, Belgium *"Chemical solution deposition of novel, thick and dense lattice matched single buffer layers for YBCO coated conductors: Preparation and characterization"*
12:10 - 12:30	**MPA-204** **Tao Dong,** Vestfold University College, Norway *"High-sensitive detection of waterborne pathogens using NiHCF nanoparticle-based sensor"*	**MPA-219** **K. Grigoras,** Aalto University, Finland *"Aluminum oxide by Atomic Layer Deposition: influence of annealing"*
12:30 - 12:50	**MPA-188** **S. C. Tjong,** City University of Hong Kong, Hong Kong *"Bioactivity of Polypropylene Composites Filled with Hydroxyapatite Nanorods"*	**MPA-288** **L. Pinho,** Universidad de Cádiz, Spain *" Titania-silica Photoactive Coatings with Application in Stone Self-cleaning"*
12:50 - 13:10	**MPA-64** **A.B. Seabra,** Universidade Federal de São Paulo, Brazil *"New Strategy for Controlled Release of Nitric Oxide in Alginate/Chitosan Nanoparticles"*	**MPA-213** **X.D. Wang,** Taiyuan University of Technology, China *"Synthesis of Highly b-Oriented Ge-ZSM-5 Films on a-Al2O3 Substrates "*
13:10 - 14:10	**LUNCH**	

discharge and electrochemical impedance spectroscopy (EIS). Materials characterization shows that the carbons prepared in this work replicate the ordered mesoporous structure of the SBA-15 and possess tailored crystalline structure with graphene layers perpendicular to the axial of pore walls. The carbons both display preferable anode performance for LIBs. However, C-2 with thicker pore wall exhibits better properties than C-1 with larger pore size. Possible reasons for different properties are the influence of the pore structure and wall thickness of as-prepared mesoporous carbons.

MPA-288
Titania-silica Photoactive Coatings with Application in Stone Self-cleaning

L. Pinho, M. J. Mosquera
[1]Departamento de Química-Física, Facultad de Ciencias, Universidad de Cádiz, Campus Universitario Río San Pedro, 11510 Puerto Real, Cádiz, Spain,

Titania-silica composites are promising materials considering self-cleaning properties. Nowadays, they are widely available as commercial glass coatings. Our objective in this paper is to optimize these composites in order to be used as building materials. Three different strategies were used: (1) an aqueous dispersion of titania nanoparticles (Aeroxide P25) (2) sols containing a pre-hydrolized tetraethoxysilane (TES 40) mixed with P25 in the presence of phosphoric acid (H_3PO_4) (3) substituting phosphoric acid for a non-ionic surfactant (*n*-octylamine) in the previous mixture. The sol composition and P25 concentration played a significant role in the texture of the composite. Next, the sols under study were sprayed on limestone samples. We carried out a simple peeling test on stone surfaces. SEM images and their corresponding EDX analysis, carried out after the tests, showed that all the coatings were removed from stone surface, except for those prepared with *n*-octylamine. Finally, we investigated self-cleaning effectiveness of the coatings by studying the total colour change (ΔE*) of stones stained with methylene blue and exposed to UV irradiation (365 nm). All the titania materials showed a significant reduction of the stain, evaluated by the colour change (ΔE*) with respect to the coated samples. ΔE* values for aqueous dispersion of P25 resulted low and close to those corresponding to coatings containing n-octylamine. In the case of H_3PO_4 coatings, ΔE* values were higher. From these results we can conclude that the route using n-octylamine is the only effective self-cleaning coating for the limestone under study.

[1] A. Fujishima, T. Rao, D. Tryk, J. Photochem. Photobiol. C: Photochem Rev. 1, 1 (2000).
[2] M. J. Mosquera; D. De los Santos; T. Rivas, Langmuir 26, 6737 (2010).

MPA-289
Photosensitization of $BiNbO_4$ with Cationic Dye by Adsorption Method

D. J. L.S. Maia[1], L. A. Silva [1,2]
[1]Institute of Chemistry and [2]National Institute of Science and Technology – Energy and Environment, Federal University of Bahia, Salvador, 40170-290, Bahia, Brazil.

In the last decades a lot of attention was devoted to study bismuth niobates and tantalates, due to their excellent microwave dielectric properties and low sintering temperatures. These materials are also envisaged as interesting photocatalysts for eliminating organic pollutants from domestic or industrial effluents, as well as for producing H_2 by the photocatalytic decomposition of water under UV light irradiation. In order to improve the utilization scope of $BiNbO_4$, we used the photosensitization process to extend the photoresponse of $BiNbO_4$ into a visible region. In this direction, it was performed a previous study about hydrolysis reactions on the $BiNbO_4$ surface suspended in water. In general, hydroxyl groups on the metal oxide surface are involved in the follow acid-base equilibrium: $>MOH_2^+ = >MOH + H^+$ and $>MOH = >MO^- + H^+$ The pH of zero point of charge, pHzpc, was determined by solid addition method. In very simple terms, a pHzpc of 7 for $BiNbO_4$ implies that interactions with cationic dye will be favored for adsorption at high pH (9,7), while anionic dye will be favored at low pH (5). In order to accomplish the photosensitization, cationic dyes, such as rhodamine B and methylene blue, have been employed as photosensitizers. Photoacoustic spectra of photosensitized $BiNbO_4$ show clearly the absorption band of the dyes in each case.

I CONGRESO INTERNACIONAL

EL PATRIMONIO CULTURAL Y NATURAL COMO MOTOR DE DESARROLLO: INVESTIGACIÓN E INNOVACIÓN

JAÉN, 26, 26 Y 28 DE ENERO 2011

PROGRAMA Y DIRECTORIO DE COMUNICACIONES PRESENTADAS

cei
proyecto campus
de excelencia
internacional
en patrimonio
cultural y natural

Nuevos Nanomateriales para Restauración de Rocas Monumentales.

Maria J. Mosquera, Juan F. Illescas, Dario F. Silva y Luis M. Pinho
Grupo TEP243 Tamices Moleculares y otros Nanomateriales. Dto. de Química-Física.
Facultad de Ciencias, Universidad de Cadiz

Palabras clave: nuevos nanomateriales, consolidación, hidrofugación, autolimpieza, roca monumental

Resumen:
El proceso sol-gel se utiliza habitualmente en la conservación y restauración de roca. No obstante, estos materiales presentan un gran inconveniente: forman fracturas durante su secado en el interior de los poros de la roca tratada. En este congreso, presentamos un resumen de la investigación actual de nuestro grupo de investigación, dedicada a desarrollar materiales libres de fractura, obtenidos mediante ruta sol-gel, con aplicación en la consolidación y protección de rocas monumentales. Nuestra investigación se centra en el desarrollo de una nueva síntesis en la que un surfactante actúa como plantilla de los poros del material, aumentando su tamaño. El nuevo material es monolítico y no presenta fracturas.
Considerando que el agua es el principal vehículo de los agentes de deterioro de los edificios monumentales, dotar a dichos productos de propiedades como hidrofugantes presenta un interés añadido. Por esta razón, nosotros también hemos desarrollado productos en los que se añade un componente orgánico al precursor polimérico, para reducir energía superficial y en consecuencia proporcionar al material de propiedades hidrofugantes. En concreto, sintetizamos un ormosil (organically modified silicate) mediante co-condensación de tetraetoxisilano (TEOS) y polidimetilsiloxano (PDMS) con hidroxilos terminales en presencia de un surfactante no-ionico (n-octilamina).
Finalmente, nuestro grupo de investigación también ha desarrollado nanomateriales con un efecto combinado consolidante y auto-limpiante, capaces de eliminar manchas, suciedad o graffitis de las superficies pétreas, sin tratamientos posteriores. Con este objetivo, se añadió un monómero de titanio al precursor de silicio (TEOS) en presencia del surfactante. El producto obtenido es un composite silicio-titanio con propiedades auto-limpiantes, como consecuencia del efecto fotocatalítico e hidrofílico del óxido de titánico incorporado a la matriz. El nuevo producto presenta interesantes aplicaciones como anti-graffiti.

Abstract:
The sol-gel process has been found to be successful in applications for the conservation and restoration of stone. However, a well-known drawback of the materials obtained by this process is their tendency to crack during drying inside the pores of the treated stone. In this congress, we present an overview of our current research centred on producing crack-free sol-gel materials for consolidating and protecting building stone. A novel synthesis, in which a surfactant acts as a template to make the pore size of the gel network coarser and more uniform, is shown to provide an effective alternative for preventing the cracking of consolidants.
Hydrophobicity is also a valuable property for such products; it is important to prevent the penetration of water because it is the main vehicle by which the agents of decay enter the pore structure of the stone. Therefore, we also highlight an alternative pathway in which we add an organic component to the silica precursor in the presence of the surfactant. Specifically, an organically modified silicate (ormosil) has been synthesized by co-condensation of tetraethoxysilane (TEOS) and hydroxyl-terminated polydimethylsiloxane (PDMS) in the presence of a non-ionic surfactant (n-octylamine). We also prepare superhydrobhobic products by increasing surface roughness. It is obtained by adding silica particles to the starting sol.
Finally, we have also synthesisized nanomaterials that have both consolidant and self-cleaning properties that enable the "automatic" elimination of dirt, graffiti, etc. on the restored monument, without further treatment. To achieve this, we add a titanium monomer to the TEOS, in the presence of the surfactant, which result in a silicon-titanium composite gel presenting self-cleaning properties, as a consequence of the photocatalytic and hydrophilic effect of the titanium incorporated in the silica network. It shows an interesting application as antigraffiti products.

Declarations of conformity

La abajo firmante, co-autora del artículo titulado *Titania-silica Nanocomposite Photocatalysts with Application in Stone Self-Cleaning*, publicado en la revista The Journal of Physical Chemistry C el 08-10-2011 y del artículo titulado *Photocatalytic activity of TiO_2–SiO_2 nanocomposites applied to buildings: influence of particle size and loading*, enviado para publicación a la revista Applied Catalysis B: Environmental, el 10-10-2012, DECLARA que:

D. Luís Miguel Faria Soares Pinho da Silva ha realizado, a los mencionados artículos, las aportaciones que se relacionan a continuación:

1) La síntesis de los materiales y la mayor parte de los estudios experimentales incluidos en dicho artículo.

2) Ha recopilado y analizado la mayor parte de la bibliografía que aparece recogida en la publicación.

3) Ha colaborado en el análisis e interpretación de los datos experimentales anteriormente mencionados.

4) Ha colaborado en la discusión, redacción y preparación del contenido gráfico presente en el manuscrito.

La abajo firmante se compromete también a no presentar estos artículos como parte de otras tesis doctorales.

Esta declaración se realiza a solicitud de D. Luís Miguel Faria Soares Pinho da Silva, con el fin de dar cumplimiento a la normativa de la Universidad de Cádiz para la elaboración de tesis doctorales.

Puerto Real, 10 de Octubre del 2012

Dra. María Jesús Mosquera

Los abajo firmantes, co-autores del artículo titulado *2D and 3D characterization of a surfactant-synthesized TiO_2-SiO_2 mesoporous photocatalyst obtained at ambient temperature*, enviado para publicación a la revista Physical Chemistry Chemical Physics el día 29-7-2012. DECLARAN que:

D. Luís Miguel Faria Soares Pinho da Silva ha realizado, al mencionado artículo, las aportaciones que se relacionan a continuación:

1) La síntesis de los materiales y los estudios experimentales incluidos en dicho artículo, con excepción de los estudios de tomografía.

2) Ha recopilado y analizado la mayor parte de la bibliografía que aparece recogida en la publicación.

3) Ha colaborado en el análisis e interpretación de los datos experimentales anteriormente mencionados.

4) Ha colaborado en la discusión, redacción y preparación del contenido gráfico presente en el manuscrito.

Los abajo firmantes se comprometen también a no presentar este artículo como parte de otras tesis doctorales.

Esta declaración se realiza a solicitud de D. Luís Miguel Faria Soares Pinho da Silva, con el fin de dar cumplimiento a la normativa de la Universidad de Cádiz para la elaboración de tesis doctorales.

Puerto Real, 14 de Septiembre del 2012

Dra. María Jesús Mosquera

Dr. Juan Carlos Hernández

Prof. José J. Calvino

Los abajo firmantes, co-autores del artículo titulado *A novel TiO_2–SiO_2 nanocomposite converts a very friable stone into a self-cleaning building material*, enviado para publicación a la revista Applied Surface Science el día 2-10-2012, DECLARAN que:

D. Luís Miguel Faria Soares Pinho da Silva ha realizado, al mencionado artículo, las aportaciones que se relacionan a continuación:

1) Ha colaborado en la síntesis de los materiales y en los estudios experimentales incluidos en dicho artículo.

2) Ha recopilado y analizado la mayor parte de la bibliografía que aparece recogida en la publicación.

3) Ha colaborado en el análisis e interpretación de los datos experimentales anteriormente mencionados.

4) Ha colaborado en la discusión, redacción y preparación del contenido gráfico presente en el manuscrito.

Los abajo firmantes se comprometen también a no presentar este artículo como parte de otras tesis doctorales.

Esta declaración se realiza a solicitud de D. Luís Miguel Faria Soares Pinho da Silva, con el fin de dar cumplimiento a la normativa de la Universidad de Cádiz para la elaboración de tesis doctorales.

Puerto Real, 2 de Octubre del 2012

Dra. María Jesús Mosquera

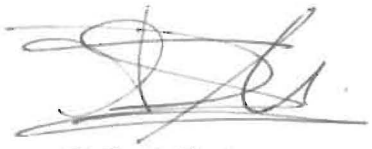

D. Darío Facio

D. Farid Elhaddad